PolyPublie
Polytechnique Montréal

POLYTECHNIQUE MONTRÉAL
UNIVERSITÉ D'INGÉNIERIE

Titre: Title:	An Off-Design Mean-Line Methodology to Predict the Missing Data of Single-Stage Transonic Axial Compressor Tests
Auteur: Author:	John Kidikian
Date:	2019
Type:	Mémoire ou thèse / Dissertation or Thesis
Référence: Citation:	Kidikian, J. (2019). An Off-Design Mean-Line Methodology to Predict the Missing Data of Single-Stage Transonic Axial Compressor Tests [Thèse de doctorat, Polytechnique Montréal]. PolyPublie. https://publications.polymtl.ca/4152/

Document en libre accès dans PolyPublie
Open Access document in PolyPublie

URL de PolyPublie: PolyPublie URL:	https://publications.polymtl.ca/4152/
Directeurs de recherche: Advisors:	Marcelo Reggio
Programme: Program:	Génie mécanique

Ce fichier a été téléchargé à partir de PolyPublie, le dépôt institutionnel de Polytechnique Montréal
This file has been downloaded from PolyPublie, the institutional repository of Polytechnique Montréal

https://publications.polymtl.ca

POLYTECHNIQUE MONTRÉAL

affiliée à l'Université de Montréal

An Off-Design Mean-Line Methodology to Predict the Missing Data of Single-Stage Transonic Axial Compressor Tests

JOHN KIDIKIAN

Département de génie mécanique

Thèse présentée en vue de l'obtention du diplôme de *Philosophiæ Doctor*

Génie mécanique

Décembre 2019

© John Kidikian, 2019.

POLYTECHNIQUE MONTRÉAL

affiliée à l'Université de Montréal

Cette thèse intitulée :

An Off-Design Mean-Line Methodology to Predict the Missing Data of Single-Stage Transonic Axial Compressor Tests

présentée par **John KIDIKIAN**

en vue de l'obtention du diplôme de *Philosophiæ Doctor*

a été dûment acceptée par le jury d'examen constitué de :

Jean-Yves TRÉPANIER, président

Marcelo REGGIO, membre et directeur de recherche

Huu Duc VO, membre

Dimitri MAVRIS, membre externe

DEDICATION

To my two boys, Oliver and William, who at their young age reminded me on how to remain a loving dad and to do the most important task during this academic endeavour; to play with them.

And to my wife, Carla, who gracefully supported and reminded me on how to remain a loving husband and to do the most important task during this academic endeavour; to do the endeavour.

Thank you for your love and your support.

"Son, for every problem there is a solution.
The art is to understand what is the problem." – Gerard Kidikian

ACKNOWLEDGEMENTS

The author would like to convey his heartfelt thanks to his supervisor, Dr. Marcelo Reggio, for his assistance and participation with this work. He set in motion this entire endeavor the day he called me and said "*you will teach the bachelor course*", and then one day, a few years later, with a simple, straight faced phrase of *"there must be a PhD in all of this research you do."* It was his confidence that inspired and ignited the inner courage and grit to execute such an undertaking.

I would also like to express sincere gratitude to Arthur Wennerstrom, USAF retired, who accepted to answer questions on transonic axial compressors from a complete stranger; answers which proved that "*the more things change, the more they stay the same."*

Many thanks for all my friends, colleagues, and acquaintances from near and far, who, in one form another, have participated with me on this journey with hallway conversations, coffee anecdotes, and lunch-and-learns. To Marco Beaulieu, Guillaume Godbout, Steve Arvanitis, and André Montpetit to name a few, the coffees were much appreciated.

Additionally, a special thank you is passed on to Eddy Petro and Alain Robidoux, who both shared their knowledge and supported the CFD aspect of this thesis. Not only did I benefit from their knowledge transfer, so did our masters students.

Finally, much thanks and gratitude are due to the countless cited authors who prepared the fields of knowledge to be harvested by this humble researcher. There are no better words to describe them than those stated by Sir Isaac Newton; *"If I have seen further than others, it is by standing upon the shoulders of giants."*

REMERCIEMENTS

L'auteur tient à exprimer ses sincères remerciements aux diverses générations d'étudiants du cours AER4270. Leurs questions et leur intérêt pour la recherche de nouvelles connaissances dans le domaine des turbines à gaz ont permis à l'auteur d'enrichir ce document.

En particulier je voudrais remercier mes étudiants pour avoir utilisé et poussé MDIDS-GT jusqu'à ses limites. Le logiciel qui est le visage informatique des idées et notions présentées dans cette thèse.

RÉSUMÉ

Le domaine de l'ingénierie est plein de théories, d'hypothèses et de nombreuses approches de conception. En outre, la conception et l'analyse techniques reposent sur de nombreuses procédures développées, perfectionnées et héritées d'une génération d'ingénieurs à l'autre. Cet héritage de conception a des vertus et de inconvénients.

D'une part, chaque génération d'ingénieurs bénéficie des connaissances et des compétences acquises dans les approches et procédures de conception et d'analyse qu'elle a été chargée d'apprendre et de prendre en charge. Les nouvelles générations bénéficient du fait que d'autres ont « compris » et mis au point des formules, des règles empiriques, des modèles, des scripts et même des logiciels. Il suffit d'apprendre et d'appliquer ces éléments et ingrédients pour pouvoir créer un design qui réponde aux besoins de connaissances et d'expérience conservateurs de leurs pairs, de leurs ingénieurs seniors et de la direction.

D'autre part, dans l'environnement de travail actuel du 21e siècle, l'ingénieur est guidé par des modèles et des logiciels et des espaces de conception conservateurs. Cela est dû au fait que les détenteurs de connaissances d'origine souvent ne sont plus actifs dans l'entreprise ; et pour les philosophies et pratiques de gestion où la productivité et la performance sont les paramètres dominants.

L'industrie des turbines à gaz ne fait pas exception. Des approches de conception 1D à 3D, associées à une vaste liste de meilleures pratiques, de pratiques standard et de règles empiriques, font que l'ingénieur devienne une centrale de manipulation de données, de dessins et de communication entre pairs. Chaque génération hérite au mieux la majorité des connaissances de la génération précédente. Dans cette passation du relais, certaines connaissances sont considérées comme acquises et la phrase « nous l'avons toujours fait ainsi » se glisse dans le lexique de l'ingénierie.

Aujourd'hui, avec les avancées annuelles dans les techniques et les méthodologies informatiques en matière de dynamique des fluides, ainsi que la capacité et les capacités accrues de la CPU, du GPU et du stockage des informations, CFD est devenu un puissant outil de conception. Cependant, malgré ses vastes atouts pour les turbines à gaz, une analyse CFD repose toujours sur le bon développement de la méthodologie d'analyse de ligne de moyen unidimensionnelle.

Pendant plus de six décennies, la méthodologie unidimensionnelle de la ligne de moyenne a joué un rôle essentiel dans les phases de conception, de conception détaillée et du cycle de vie d'une turbine à gaz. Cette méthodologie a été utilisée dans la majorité, sinon dans toutes les turbines à gaz développées pour des applications industrielles et aérospatiales.

En outre, la méthodologie unidimensionnelle de la ligne de moyenne a été la pierre angulaire de la conception et de l'analyse des turbines à gaz ; contestée par d'autres méthodologies, telles que l'analyse en flux méridien bidimensionnel ou l'analyse en équilibre radial, et les diverses manifestations de la simulation numérique (CFD). Après plus de six décennies d'utilisation, la méthodologie de la ligne de moyenne joue encore un rôle vital, sinon dominant, dans l'industrie des turbines à gaz.

Malgré le pedigree historique et le rôle fondamental de cette méthodologie unidimensionnelle, la plupart des modèles de prédiction hors le point nominal (ou de design) publiés, des compresseurs axial transsonique testés, présentent trois faiblesses communes: 1) la méthodologie ne permet pas de prédire correctement la début de la condition blocage sonique dans les conditions de débit massique élevé et de faible rapport de pression, 2) la méthodologie ne permet pas de prédire correctement la naissance du décrochage ou une ligne de pompage dans les conditions de faible débit massique et de forte rapport de pression, et 3) prédire correctement les tendances des performances de la ligne de vitesse hors conception en termes de taux de pression sur l'étage et d'efficacité totale - totale par rapport au débit.

Sur la base de l'énoncé du problème mentionné ci-dessus, et parmi les nombreux « toujours fait ainsi » que l'on trouve dans l'industrie des turbines à gaz, il y a la méthodologie de mise à l'échelle des cartes de performances utilisée pour les compresseurs axial. Cette méthodologie prend les résultats d'une carte de compresseur générée par un modèle 1D ou 2D et utilise une mise à l'échelle et des ajustements pour s'adapter aux données des tests. Cela est dû au fait qu'il est « connu » que les modèles 1D et 2D ne représentent pas ou n'ont pas été calibrés pour produire ou prédire avec confiance les résultats des tests.

En général, les modèles 1D sont bien calibrés pour réaliser des calculs pour le point nominal ou de design, mais pas pour des opérations en mode hors design. Le but de cette thèse est de présenter une approche révélant qu'il est possible d'utiliser la méthodologie simple de ligne de moyen hors design ou « off-design » pour prédire des données manquantes de tests de compresseur axial

transsonique. L'approche proposée offre à l'ingénieur deux avantages : i) une mise à jour étroitement couplée entre la prédiction et les données de test et ii) une base pour collecter des données de résultats de tests afin de pouvoir créer de nouvelles règles empiriques, de nouvelles formules et de nouvelles connaissances.

Ce document vise à décrire des méthodes fondées sur l'ingénierie et les critères qui permettent de résoudre les faiblesses de la méthodologie ligne de moyen « off-design » mentionnés ci-dessus. En particulier, nous décrirons deux méthodologies et deux critères d'ingénierie.

La première méthodologie convertit les données des tests expérimentaux en facteurs d'ajustement de la modélisation des pertes de ligne de moyen. Nous allons montrer que l'analyse basée sur la ligne moyenne hors design nécessite l'incorporation d'un ensemble de facteurs de blocage d'entrée et de sortie et des angles de déviation qui varient en fonction des conditions de performance du compresseur. Cette approche diffère des hypothèses procédurales fondées sur la littérature (ou règle générale) de facteurs de blocage d'entrée et de sortie fixes d'environ *0,98* et de l'utilisation d'un angle de déviation unique basé sur la règle de Carter.

La deuxième méthodologie est une approche généralisée permettant de créer des corrélations pour les pertes de charge totales du rotor et du stator, les angles de déviation et les facteurs de blocage d'entrée et de sortie de l'aube. Nous montrerons que pour tenter de prédire correctement les performances hors conception, le modèle de perte du rotor doit non seulement tenir compte des modifications physiques et des variations de débit dues à une modification du RPM, mais également pour le modèle de perte du stator nous avons besoin de prendre en charge des modifications physiques et une modification des RPM. Cette approche unique et nouvelle capture implicitement l'interaction couche de limite entre le rotor et stator, et capture implicitement les interactions jeu entre le rotor et stator.

De plus, deux critères basés sur l'ingénierie seront introduits, décrivant la condition de blocage sonique du compresseur axial transsonique et l'apparition du décrochage ou une ligne de pompage. Le critère pour le condition blocage sonique basé sur l'ingénierie peut être utilisé à la place de l'hypothèse procédurale de la condition de flux de masse verticale, ou « stone wall », qui a été utilisée tout au long de l'histoire de la méthodologie de la ligne de moyenne. En outre, un critère d'ingénierie relativement simple, nouveau et efficace pour le début du décrochage ou une ligne de pompage sera introduit.

Les méthodologies de ligne de moyen et les critères basés sur l'ingénierie sont ensuite incorporés et testés dans un logiciel de conception spécialisé, développé pour la conception et l'analyse d'un moteur à turbine à gaz complet. Ce logiciel, qui inclut un modèle intégré de ligne de moyen hors conception de compresseur axial, est utilisé pour obtenir les données de performances manquantes et pour prédire le condition blocage sonique et le début décrochage ou une ligne de pompage de quatre compresseurs axiaux transsoniques bien documentés par la NASA.

Les méthodologies de ligne de moyen hors design et les critères basés sur l'ingénierie révèlent une conclusion commune. Pouvoir obtenir une correspondance adéquate des performances hors conception d'un compresseur axial transsonique d'un étage (ce qui conduit ensuite à une meilleure prévision de la tendance des performances hors conception), y compris les conditions blocage et pompage, requiert un ensemble complet de données de test de compresseur axial et un modèle de ligne de moyenne correctement ajusté qui tient compte des modifications du rapport de pression du rotor et de l'étage, des variations du rapport de température du rotor et des facteurs de blocage qui changent selon les conditions hors design.

La méthodologie de modélisation généralisée des pertes en ligne de moyen, ainsi que les critères d'ingénierie qui l'accompagnent, permettront au concepteur de compresseurs de déclasser l'utilisation des techniques de mise à l'échelle des cartes de performances pour les compresseurs à un étage. A sa place, la méthodologie prédictive généralisée estimera avec précision les performances hors conception des compresseurs axial transsoniques et peut être utilisée pour prédire et compléter les données de performances manquantes.

Il faut juste imaginer les possibilités.

ABSTRACT

"*I would rather have questions that can't be answered than answers that can't be questioned*." - Richard Feynman

With yearly advances in computational fluid dynamics (CFD) techniques and methodologies, and the increased capacity and capabilities of computer CPU, GPU, and information storage, CFD has become a powerful design tool. However, despite its vast strengths for gas turbines, a CFD analysis is still based on the sound development of the one-dimensional mean-line analysis methodology.

For more than six decades, the one-dimensional mean-line methodology has played a vital role in the preliminary, detailed design, and production phases of the gas turbine life-cycle. This methodology has been used in all gas turbines developed for both industrial and aerospace applications.

Furthermore, the one-dimensional mean-line methodology has been a cornerstone for gas turbine design and analysis; challenged by other methodologies, such as the two-dimensional meridional through-flow, or radial equilibrium analysis, and the various manifestations of three-dimensional computational fluid dynamics, after more than six decades of use, the one-dimensional mean-line methodology still plays a vital, if not dominant, role in the gas turbine industry.

Despite the historical pedigree, and the fundamental and foundational role of the one-dimensional mean-line methodology, most published off-design prediction models, of tested transonic axial compressors, suffer from three common weaknesses[1]: 1) the methodology does not properly predict the onset of the choking condition at the high mass flow rate and low pressure ratio conditions, 2) the methodology does not properly predict the onset of stall or surge at the low mass flow rate and high pressure ratio conditions, and 3) the methodology does not properly predict the off-design speed-line performance trends in terms of stage pressure ratio and total-to-total efficiency versus the mass flow rate of an axial compressor.

---

[1] Which is the overall problem statement to be resolved within this investigation

This document endeavors to describe engineering-based methodologies and criteria that resolve the off-design mean-line methodology weaknesses mentioned above. In particular, we will describe two methodologies and two engineering-based criteria.

The first methodology converts experimental test data into mean-line loss modeling tuning factors. It will be shown that the off-design mean-line analysis requires the incorporation of a set of inlet & exit blockage factors and deviation angles that vary with the compressor performance conditions. This approach differs from the literature-based procedural assumptions (or rule-of-thumb) of fixed inlet and exit blockage factors of approximately *0.98*, and the use of a unique deviation angle based on Carter's rule.

The second methodology, which is a generalized methodology to create correlations for the rotor and stator total pressure losses, deviation angles, and blade row inlet and exit blockage factors, is used to convert the mean-line model tuning factors into specific axial compressor stage loss models. It will be shown that to be able to attempt a proper prediction of the off-design performance, not only does the rotor loss model must cater for both physical and flow changes due to a change in RPM, the stator loss model must also cater for both physical and flow changes due to a change in RPM. This unique and novel approach implicitly captures the rotor-stator boundary layer interaction and the rotor-stator clearance interactions.

Additionally, two engineering-based criteria will be introduced that best describes the transonic axial compressor choking phenomenon, and the onset of the stall conditions. The engineering-based criterion for choke, which is based on a static pressure ratio between the stator exit and the rotor inlet and exit static pressures, can be used in lieu of the literature-based procedural assumption of the vertical, or *stone-wall*, mass flow condition which has been used throughout the mean-line methodology's history. Furthermore, a relatively simple, novel, and effective engineering-based criterion for the stall onset will be introduced, which is based on a 1D off-design mean-line model ratio comparing the rotor exit absolute tangential velocity against the rotor exit and the stator inlet absolute axial velocity.

The mean-line methodologies and engineering-based criteria are then incorporated and tested in a specialized gas turbine design software, developed by the present author for the design and analysis of a whole gas turbine engine. This software, which includes an embedded axial compressor off-

design mean-line model, is used to obtain the missing performance data, and predict the choke and the onset of the stall conditions of four well-documented NASA transonic axial compressors.

The off-design mean-line model methodologies and engineering-based criteria reveal a common threaded conclusion. To be able to obtain a proper and successful match of the off-design performance of a single-stage transonic axial compressor (which then leads to an improved trend prediction of the off-design speed-line performance), including the choke and surge conditions, requires a complete set of axial compressor test data and a properly tuned mean-line model that caters for both the rotor and stage pressure ratio changes, its accompanying rotor temperature ratio variations, and blockage factors that change per off-design condition.

The generalized mean-line loss modelling methodology, and its accompanying engineering-based criteria, will allow the compressor designer to decommission the use of the performance map scaling techniques for single-stage compressors. In its place, the tuned-to-predictive methodologies will accurately estimate the off-design performance of transonic axial compressors, and can be used to predict and complete the missing performance data.

Let us note that this document contains elements of two ASME 2018 TurboExpo conference papers [1, 2].

Imagine the possibilities.

TABLE OF CONTENTS

LIST OF TABLES

LIST OF FIGURES

NOMENCLATURE

List of symbols and abbreviations

1D	One Dimensional
2D	Two dimensional
3D	Three dimensional
A	Annulus area
AF1	1st airfoil blade row
AF2	2nd airfoil blade row
AF3	3rd airfoil blade row
AR	Aspect ratio
B.E.J.	Best Engineering Judgement
CFD	Computational Fluid Dynamics
C_D	Blockage factor
C_p	Specific heat in constant pressure
CPU	Central Processing Unit
C_v	Specific heat in constant volume
DCA	Double Circular Arc
DP	Design Point
f	Correction factor (loss)
GE	General Electric
GPU	Graphics Processing Unit
Δh	Specific work
i	Incidence angle (alternative)
inc	Incidence angle
LBM	Lattice-Boltzmann Methodology
MCA	Multiple Circular Arc
$\dot{m}$	Mass flow rate
M	Mach number
MAMF	Maximum Attainable Mass Flow
MCA	Multiple Circular Arc
MLM	Mean-Line Methodology
NASA	National Aeronautics and Space Administration
NTRS	NASA Technical Report Server
OD	Off-design
P	Pressure
PR	Pressure Ratio
PWA	Pratt and Whitney America
r	Radius
R&D	Research and Development

RANS	Reynolds Average Navier-Stokes
Re	Reynolds number
Rg	Gas constant
T	Temperature
TipClr	Tip Clearance
TR	Temperature Ratio
U	Peripheral speed
UI	User interface
U_m	Mean-radius angular velocity
USAF	United States Air Force
V	Velocity
W	Velocity (alternative)
W	Loss bucket width
Y	Loss parameter

Greek Letters

α	Absolute flow angle
β	Relative flow angle
γ	Gamma, C_p / C_v
δ	Deviation Angle
χ	Correction factor (alternative)
λ	Reaction
ω	Loss parameter (alternative)
ω	Rotational speed in Eq. 27
ϖ	Average loss
ζ	Loss parameter (alternative)

Subscripts

1,2,3,4	Calculation plane number
abs	Absolute quantity
absT	Absolute tangential component
absX	Absolute axial component
ANN	Annulus loss
AR	Aspect ratio
CL	Clearance loss
COR	Corrected loss
DEV	Deviation angle
EW&TC	End Wall and Tip Clearance loss
ew	End wall
ex	Exit plane
in	Inlet plane
inc	Incidence

INC	Incidence (alternative)
m	Mid-section or mean-radius
M	Mach number
Ma	Mach number (alternative)
Mach	Mach number (alternative)
min	Minimum loss
O	Total (stagnation) flow quantity
P	Profile loss
PS	Part Span
P&TE	Profile and Trailing Edge loss
Re	Reynolds Number
r	Rotor
rel	Relative quantity
relT	Relative tangential component
relX	Relative axial component
s	Stator
S	Static flow quantity
S	Secondary loss
SH	Shock loss
SPAN	Part span shrouds
SR	Airfoil surface roughness
X	Axial component

LIST OF APPENDICES

CHAPTER 1 INTRODUCTION

"The most dangerous phrase in the language is, 'We've always done it this way.'" - Rear Admiral Grace Murray Hopper

With yearly advances in CFD techniques and methodologies, and the increased capacity and capabilities of computer CPU, GPU, and information storage, this computational avenue has become a powerful and integral part of the gas turbine design process [3]. CFD has been used to reduce the time and cost associated with aerodynamic design and optimization [4], it has reduced the number of calibration and validation experiments [5], and most importantly, if applied judiciously, it can lead to the discovery of design parameter trends which would have been considered too expensive to run experimentally [5], and too difficult to measure with instrumentation [5]. This methodology can also be considered as an approach to supplement missing information when experimental data is not readily available [6]. However, despite its vast strengths, a CFD analysis still requires the time and effort to create, run, and understand the simulated flow physics. Within these optics, the engineer will need to create the *3D* geometry, converge to a multi-disciplinary design compromise (which includes stress & dynamics, aerodynamics, performance, weight, and internal air systems), create and refine the mesh that will represent the discrete computational domain, and perform the flow simulation using various models (inviscid, viscous, steady-state, and transient). This CFD-related process will provide a detailed insight of the assessed flow physics, and, when enhanced through the post-processing of the computational results, will yield extremely useful information for the aerodynamic design.

To even begin the journey of a CFD analysis, especially for a turbine or compressor stage of a gas turbine, a *1D* mean-line design, based on well-understood empirical data, assumptions, and experience, is still required as a prerequisite in the overall integrated design optimization life-cycle. As stated by Horlock & Denton in 2005,

> "*Simple methods with empirical input are still needed for the mean-line design, and it is often emphasized by experienced designers that if the one-dimensional design is not correct then no amount of CFD will produce a good design*" [5].

The primary use of the *1D* mean-line methodology (which is but one of many steps and analytical approaches used throughout the gas turbine product life-cycle) is to assess, or predict, the design-point stage efficiency or, as termed by Koch & Smith, the *efficiency potential* of a stage [7]. Within the design life-cycle of a gas turbine, and dependent on an institution's particular proprietary design methodology and philosophy, the *1D* mean-line methodology may also support the activities involved with the generation of preliminary airfoil boundary conditions[2], the prediction or assessment[3] of the off-design performance [8], and may be used to support preliminary stress analysis [9] and internal air system modeling. From just a set of blade-row velocity triangles, using simple trigonometric relationships, the mean-line methodology is capable of defining the general behavior of gas turbine compressor and turbine stages [10].

The simplicity of the *1D* mean-line methodology remains attractive as the initial approach to converge to a feasible gas turbine design, execute parametric studies [11], either manually or by specialized optimization software, and may be used for test-cell performance data reduction and analysis by creating off-design performance maps to calibrate the differences between test data and predicted data. In terms of use, the mean-line methodology has been used to improve or augment the overall design life-cycle. For example, Denton recently proposed a gas turbine design system, for small to medium sized companies, that couples a mean-line methodology, a blade profile generator, and 3D CFD [12]. Whereas Klein et al. introduced a methodology that integrated a mean-line analysis with the component simulation results obtained by CFD for a compressor fan stage [13].

1.1 Compressor design life-cycle

From improved procedures and integrated software, to advanced manufacturing techniques and materials, each gas turbine company spends time and money, either their own or through government funding, to innovate and improve the overall gas turbine life-cycle. The purpose is to achieve a competitive product, bringing value to their stakeholders and shareholders. Any

---

[2] Inlet and exit boundary conditions of total temperatures, and total & static pressures, used for 2D throughflow or 3D CFD.

[3] In turbomachinery literature, the term component performance "assessment" or "prediction" is used interchangeably.

improvement in the lead-time of the various disciplines, axial compressor design as an example, brings that company, or country, a few paces ahead of the competition. Figure 1-1 is a generic axial compressor design life-cycle that may take a few months to a year to complete. Any improvement or innovation in the design life-cycle can make the difference of controlling the market or sharing it with the competition.

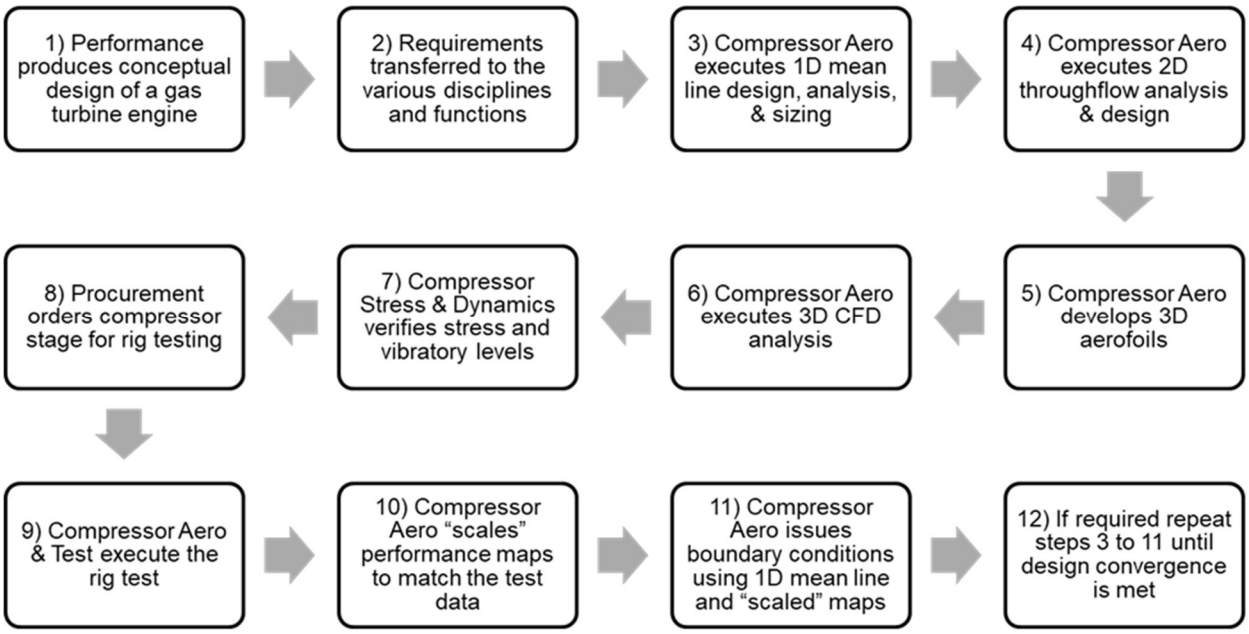

Figure 1-1: Generic axial compressor design life-cycle

During the compressor design optimization activity, the various supporting disciplines require inlet and exit boundary conditions to progress their particular designs and analysis. The *1D* mean-line methodology gives the opportunity to provide preliminary inlet and exit boundary conditions, scaled or adjusted to the appropriate performance condition of interest, until the CFD results have been obtained[4], and furthermore, if the mean-line code functionality is properly developed, it can be used in a multi-disciplinary integrated environment.

Within a generic iterative design life-cycle of an axial compressor, the *1D* mean-line methodology will be used to create the design-point conceptual cross section of a single- or multi- stage

[4] Depending on the organization's particular design system, the mean-line model based data may be the only boundary conditions available until test data has been gathered.

compressor. This cross-section development is achieved by using design rules-of-thumb and past experience.

This conceptual design will then be transferred to the various compressor specialists for further refinement and optimization with respect to design parameters (such as axial chord, blade count, aspect ratio) and blade profile shapes (such as DCA, MCA, diffusion controlled, or other shapes particular to the institution's experience).

The compressor specialist will then extract the inlet and exit flow conditions to be transferred to higher fidelity analysis, such as *2D* through-flow and *3D* CFD analysis. The results of the higher fidelity analysis may be used to tune, or correct, the mean-line analysis results. Furthermore, the results stemming from the design-point and off-design mean-line codes may be used as inlet and exit boundary conditions for other disciplines such as internal air systems, stress, performance, and even turbine cooling.

When the iterative design has been converged, accepted, and released to manufacturing, the compressor stage is procured. Once received, the compressor stage will undergo a rig test to produce the off-design compressor performance map. The results of the rig test will then be used to further tune the analytical maps produced by the mean-line analysis; either the map scaling [14] or the map warping methodology [15] may be used to achieve this. Finally, the resultant mean-line map tuning factors are then stored (either in a database or in the mean-line code itself) and used for subsequent compressor designs.

The importance of the *1D* mean-line methodology may be considered as two-fold. At one end of the spectrum, the *1D* mean-line methodology is used to size the single- or multi- stage axial compressor. Various geometric parameters are iterated upon to find an optimal, or an *engineering compromise*, between such aspects as cost, weight, and performance. Through the use of engineering grit, geometric parameters such as airfoil count, blade type, stage count, and the multi-stage distribution of work and reaction (or other pairs of parameters based on an institution's particular proprietary design process) may be either manually iterated upon, or grinded through an optimization routine. It should be noted that the results from a mean-line model design are used to create the preliminary engine design which is then used in the bidding process. Since the performance specifications are guaranteed during the bidding process, it becomes extremely important that the mean-line model results are as accurate and realistic as possible.

At the other end of the spectrum, the *1D* mean-line methodology is used to define the boundary conditions of other higher fidelity analysis, such as the *2D* meridional through-flow analysis, and *3D* computational fluid dynamics (CFD) which currently stands on the Reynolds Average Navier-Stokes (RANS) model; and perhaps one day on emerging models as the lattice Boltzmann method (LBM) [16]. The results of these various *1D* to *3D* methodologies are meticulously converged upon, maintaining a consistent thread of performance and loss assessment.

1.2 Axial compressor performance map or chart

Figure 1-2 represents a generic axial compressor performance chart. It is decomposed in the following manner:

- The abscissa describes the Q value of $\dot{m}\sqrt{T_0}/P_0$, where $\dot{m}$ is the mass flow rate, T_o is the inlet total temperature and P_o is the inlet total pressure
    - The Q value is "corrected" for the reference pressure and temperature to be able to use the performance data of different inlet total temperature and total pressure conditions which normally vary with altitude. This corrected mass flow rate is useful for actual altitude based off-design condition calibration or prediction.
    - The ordinate (dimensionless) is the total pressure ratio, *PR*, of the compressor stage or rotor, depending on the analysis of interest.
    - The oval shapes (blue) are isolevels of total-to-total efficiency. The inner most oval represents the highest efficiencies, and each oval stemming from that is a lower, decreasing efficiency value.
- The performance chart is further enriched by lines, also known as *speed-line*s, representing constant speed. These speed-lines capture the *PR*-vs-mass flow rate behavior. From these speed-lines two important compressor conditions are identified:
    - Compressor **Choke**: A compressor is considered choked when the speed-line becomes vertical. Once the speed-line becomes vertical there is no change in the mass flow rate through the compressor.
    - Compressor **Rotating Stall**: The instability phenomenon of compressor rotating stall is found at the opposite end of the constant speed-line. The stall point is the

performance condition where the compressor will exhibit a breakdown in the axisymmetric flow leading to a non-uniform rotating flow cell. This rotating cell, if left to grow in size, will lead to a compressor pressure ratio drop which may then lead to an adverse backflow and finally surge.

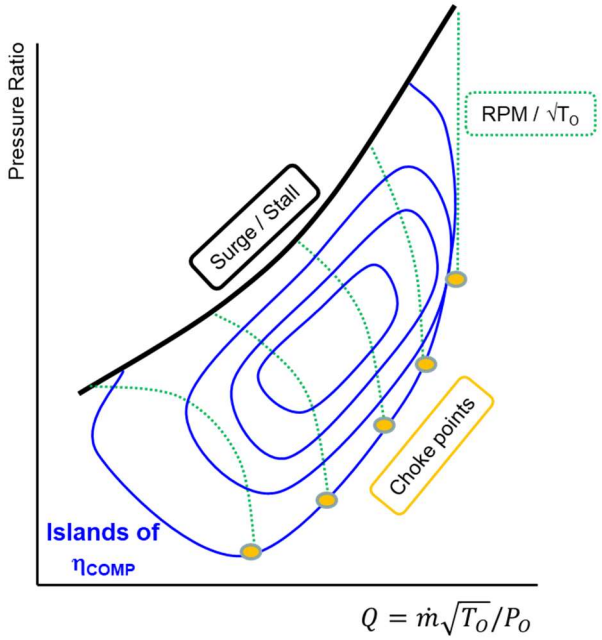

Figure 1-2: Generic axial compressor performance map

1.3 Problem statement and research questions

The *1D* mean-line methodology, despite being useful and versatile, suffers from a major limitation; with the available published loss models it cannot accurately predict the off-design behavior of transonic axial compressors. Most published off-design prediction models, of tested transonic axial compressors, suffer from three common weaknesses: 1) the methodology does not properly predict the onset of the choking condition at the high mass flow rate and low pressure ratio conditions, 2) the methodology does not accurately predict the onset of stall or surge at the low mass flow rate and high pressure ratio conditions, and 3) the methodology does not suitably predict the off-design speed-line performance trends in terms of stage pressure ratio and total-to-total efficiency versus the mass flow rate of an axial compressor off-design performance chart. Figure 1-3 shows the predictive results of independent off-design mean-line codes as found in literature [8, 17].

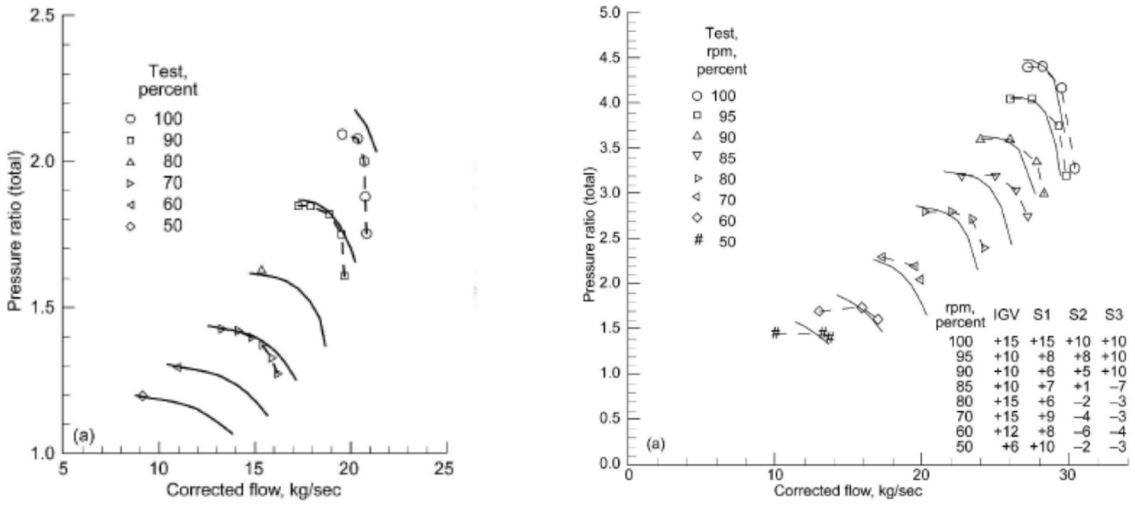

a) Veres - Stage-37 [8] b) Veres - Stage 74-A [8]

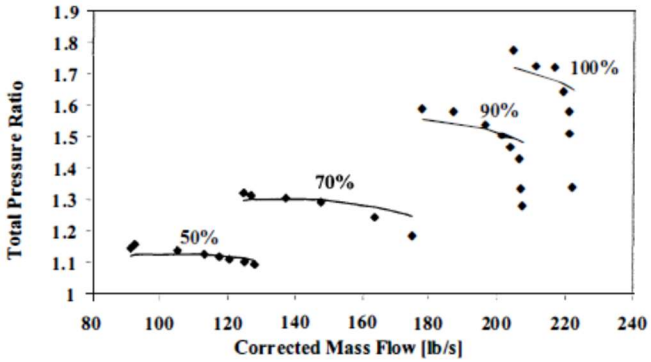

c) Smith - Rotor 1-B [17]

Figure 1-3: Independent mean-line code results

Figure 1-4, based on the axial compressor performance chart of Figure 1-2, represents a consolidated image of the various literature based model predictions versus that of experimental test data. In terms of the speed-line predictions, two main behaviors are encountered: 1) either the speed-lines do not properly represent the level of mass flow rates (which is seen as parallel speed-lines shifted by a certain amount), or 2) the speed-lines cross over the experimental data. These behaviors indicate that the specific loss model employed does not correctly cater for the mass flow rate predictions. Additionally, with respect to loss and work (which is represented by the total pressure ratio value) the speed-line trends are not properly represented. With respect to the choking condition, it is found that the majority of models grossly under predict the PR level when choking occurs. As shown in Figure 1-4, there is an actual (orange dots) versus a theoretical (red dots)

choking line. Most predictive models calculate choke within a numerical region which is based on the identification of a constant mass flow rate or a mean-line code solution divergence. Finally, in terms of the stall or surge onset, most predictive models employed either under- or over- predict the onset of the surge line.

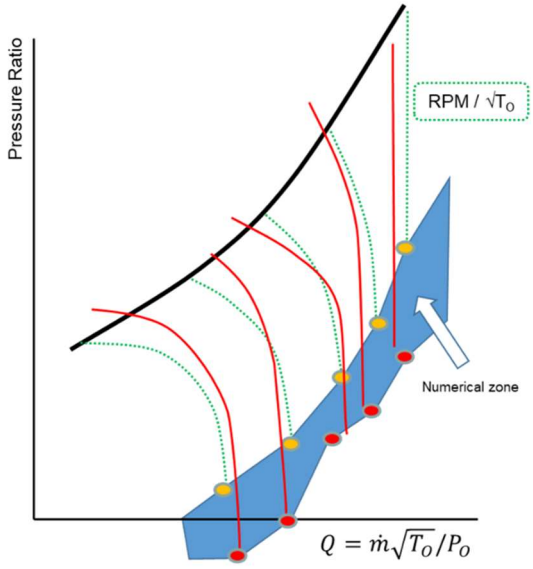

Figure 1-4: Pictorial problem statement of an axial compressor map
(red solid speed-line = prediction, green dotted speed-line = experimental)

This research attempts to answer the four underlying questions raised in Figure 1-5. The specific objectives of this investigation is to establish the set of assumptions, formulas, and methodologies that will predict a single-stage transonic axial compressor performance to within ±0.5% to ±1.0% of the measured and calculated total-to-total compressor rotor and stage efficiencies.

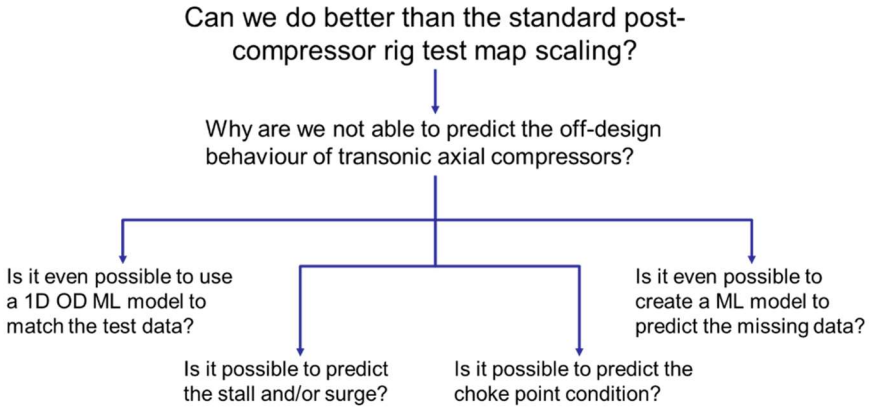

Figure 1-5: Transonic axial compressor research questions

To do so, a new transonic axial compressor mean-line loss modelling methodology, and accompanying engineering-based criteria, will be introduced that will predict the off-design performance of four NASA transonic axial compressors. This new methodology can then be used to replace the map scaling methodologies.

1.4 Organization of thesis

This thesis document has been divided into the following sections:

- Chapter 1 Introduction

  This present chapter describes the overall problem statement of the research investigation. An overview of the axial compressor design process and that of the axial compressor performance map was presented.

- Chapter 2 Literature Review

  In this chapter the various aspects of axial compressor modelling are discussed. The axial compressor mean-line methodology will be described, followed by axial compressor loss modeling, with specific short discussions with respect to the rotor inlet shock structure, the treatment of the deviation angle, the choke condition, and the onset of stall.

- Chapter 3 Methodology

  In this section, a systematic approach to developing an off-design mean-line model and accompanying loss model will be described. First, the selection of candidate axial compressors to investigate will be discussed. This is followed by the description of the off-design mean-line model used, and a high-level overview in correlation creation approach. Following this, a brief discussion of the CFD results of Rotor 37 will be presented. The qualitative observations described will implicitly contribute to the loss model development.

  The remainder of the chapter will describe two methodologies and two engineering-based criteria. The first methodology is an approach on tuning the off-design mean-line model parameters of deviation, blockage factors, and loss to match the experimental test data. This is then followed by a methodology that converts said tuning factors into specific axial compressor loss models for the purposes of predicting the missing speed-line data.

The chapter concludes with the description of two engineering-based criteria that are used to identify the choking condition and the onset of axial compressor stall.

- Chapter 4 Results

Chapter 4 presents the results of the two methodologies and engineering-based criteria. The chapter also includes the comparison of selected stall criteria for comparative purposes.

- Chapter 5 Conclusion and Recommendations

This chapter encapsulates the conclusions, future work, and the limitations and constraints of the various methodologies presented.

- Appendices

In this section, several appendices have been provided to supplement and support the information and discussions presented in this thesis.

CHAPTER 2 LITERATURE REVIEW

> *"A mean line efficiency prediction method is the sum of a large number of loss components. While some of them may prove to be quantitatively imperfect, the manner in which they are combined may cause errors to cancel. The final proof of a loss system must be its ability to correctly predict the efficiencies of well documented turbines [or compressors]*"- Kacker & Okapuu [18]

Since 1946 it has been known that axial compressors could reach transonic speeds [19]. However, the understanding of the flow physics, the prediction of the losses, and the required blade profile shapes to produce acceptable performance were not yet established. In North-America, NACA / NASA, various companies (such as General Electric and Pratt and Whitney), and the USAF undertook the design and testing of both linear cascades and annular stages. The goal was to better understand the loss mechanisms found within such designs, and to create a set of correlations to be used in a mean-line model to be able to predict or assess the compressor performance.

2.1 Off-design axial compressor mean-line methodology

The *1D* gas turbine mean-line analysis methodology (MLAM), also referred to as a mean-line model (MLM) or a mean-line code (MLC), is a relatively simple and versatile engineering design & analysis tool. The axial compressor mean-line model is the simplest of analytical tools available to the gas turbine engineer. The mean-line model, in itself, is a gross one-dimensional approximation and simplification of the geometry, the physics, and the formulae pertaining to a gas turbine engine and its components. A mean-line model is developed on the basis of 14 fundamental assumptions that have various nuances (refer to Appendix A for details), and its numerical structure involves a *1D* matching process of the various compressible flow equations, with internal models to predict the airfoil (or *aerofoil*) geometry and its associated losses.

A mean-line model is categorized into two distinct modes of Design-Point (DP) and Off-Design (OD) analysis as follows:

Design-Point (DP) Analysis Mode: The design-point mean-line model is used to define the geometry and performance at a selected singular design-point condition. This condition, for an axial compressor, is usually defined at the 100% speed-line max thrust requirement for a turbo-jet

or turbo-fan engine. The objective of design-point mean-line is two-fold: 1) to predict or assess the losses (or efficiency) of an axial compressor stage which is based on the limits of the model's design space, and 2) to predict the preliminary airfoil camber based on the velocity triangles for each blade row.

Off-Design (OD) Analysis Mode: The off-design mean-line is used to define the off-design behavior of the design-point stage design at varying speeds and inlet conditions. In doing so, a variation in incidence and deviation is calculated, which in turn is used in loss models that cater for such differences.

Table 2-1: Parameter differences between a DP & OD mean-line

Parameter	Design-Point	Off-Design
Inlet Temperature	Fixed	Fixed
Inlet Pressure	Fixed	Fixed
Inlet mass flow rate	Fixed	Varied
Inlet flow angle	Fixed	Fixed
Clearances (hub or shroud)	Fixed	Fixed
Stage Reaction	Imposed or Calculated	Calculated
Stage pressure ratio	Imposed or Calculated	Calculated
Stage temperature ratio	Imposed or Calculated	Calculated
Stage work	Imposed or Calculated	Calculated
Rotor RPM	Fixed	Varied
Losses	Calculated	Calculated
Geometry (metal angles)	Calculated	Fixed / Adjusted
Geometric area	Calculated	Fixed / Adjusted

Between the two modes of DP and OD of a mean-line methodology, there are slight differences in the imposed boundary conditions and stage characteristics, as shown in Table 2-1. The design-point mean-line is considered to be a *well-defined* solution since all the stage characteristics are

imposed, and all that remains to calculate are the velocity triangles and their related losses. Of the four stage parameters identified, only two are required to be imposed while the others will be resolved. The off-design mean-line, as a minimum, requires the rotor RPM and stage mass flow rate to vary for a series of speed-lines (percentages of the design-point RPM). It is usually assumed that the inlet temperature, pressure, flow angles, and clearances remain constant. For axial compressors with variable stator settings and Inlet Guide Vanes (IGV), the internal geometry is adjusted to mimic the changes in the blade row metal angles and the inlet and exit geometric areas. The geometry that is stored in the off-design mean-line is the geometry that was predicted by the design-point mean-line.

The use of the off-design mean-line methodology, which stems from the design-point mean-line model, is dependent on the assumptions employed to describe such a model (as outlined in Appendix A). Based on a combination of literature review, the author's experience, and one-on-one conversations with peers, it was found that, in academia and industry, a so called procedural *recipe* is followed. This recipe, which employs simplifying modeling assumptions, is as follows:

1) It is assumed that the off-design deviation angle does not vary significantly. To be more specific, Carter's rule is the main dominant deviation angle formulation employed in various mean-line models. This rule calculates a singular deviation angle and remains constant throughout the off-design performance excursion.

2) The off-design blade row inlet and exit blockages (C_{Din} and C_{Dex} respectively) do not vary significantly. It was found that the blockage factors are first initialized during the development of the design-point mean-line model. The majority of the blockage factors fall within a range of 0.98 down to 0.96. The actual value for blockage is a combination of both past experience and an aerodynamicist's initial assumptions.

3) The two main industry-based published loss models are those of Koch & Smith [7] and of Wright & Miller [20]. These models are implicitly considered to be the *gold standard* to benchmark against.

4) The clearance values (tip for rotors and, if any, hub for stators) are inherited directly from the design-point mean-line model clearance assumptions. Despite the fact that it is common knowledge that the thermal and centrifugal forces of a rotating rotor-disk system will produce a change in the clearance value, most if not all off-design mean-line models do not

cater for this change. There is no known model in public literature that has explicitly varied the axial compressor clearance values during an off-design condition, for the specific use of performance calculations.

5) The consideration to include a shock loss model depends on the particular loss model employed. Corrections for shock losses, if any at all, are mainly based on the normal shock model stemming from Schwenk et al [21]. However, the use of the normal shock model under predicts the resultant back pressure. Hence, the shock loss value is reduced by the square of the inlet Mach number [21, 22].

6) The prediction of the choke point is mainly achieved through a numerical divergence of the solution or when a constant mass flow is converged upon.

7) The onset of stall or surge point prediction is considered in literature to be one of the more challenging aspects in axial compressor modelling. Most mean-line methodology stall or surge models are based on proprietary approaches, test data, or the use of CFD as a predictive tool. The true stall point is most often validated by the compressor test rig.

8) And finally, all mean-line codes are based on and use the non-linear *bladed mass flow equation*. This equation is derived from the formulas found in Table 2-2.

$$\frac{\dot{m}\sqrt{T_o}}{P_o C_D A_{axial} \cos\beta} = M\sqrt{\gamma/R_g}\left[1+\frac{\gamma-1}{2}M^2\right]^{-(\gamma+1)/2(\gamma-1)}$$

Table 2-2: Bladed mass flow equation composition

From	Formula
Compressible isenthalpic flow	$\frac{T_o}{T} = \left(1+\frac{\gamma-1}{2}M^2\right)$
Compressible isentropic flow	$\frac{P_o}{P} = \left(1+\frac{\gamma-1}{2}M^2\right)^{\gamma/\gamma-1}$
Mass flow equation	$\dot{m} = \rho A V$
Perfect (ideal) gas equation	$P = \rho R_g T$

From within the *bladed mass flow equation*, the Area (A) is one of the terms that must be well understood. The mass flow equation, $\dot{m} = \rho AV$, defines the mass flow rate ($\dot{m}$) as a function of the Area (A) and the Velocity (V). It should be noted here that A and V are through a control surface, and that the control surface is perpendicular to the flow velocity. If the velocity vector has a tangential component, then the actual flow area is adjusted from the axial direction by the cosine of the flow vector.

$$A_{flow} = A_{axial} \cos \beta$$

For the *bladed mass flow equation*, depending on the compressor or turbine flow assumptions employed, the angle β is usually taken to be the mid-span relative flow angle, or metal angle, of a mean-line model solution.

Furthermore, if one is considering the flow defect caused by the boundary layer growth generated by the airfoil surfaces and by the annulus end walls, then a blockage term, C_D, is usually incorporated to reduce the *geometric* or *physical* flow area to a *true* or *effective* flow area.

The blockage factor C_D is used at both the inlet and exit planes of each blade row. Three different uses for C_D have been determined:

- The blockage factor is used to mimic the boundary layer growth thickness.
- It is used to compensate for the thin camber airfoil assumption. The blockage factor may be used as a proxy for the leading edge and trailing edge airfoil thickness.
- And, the blockage factor may be used as an overall *go-to* or loss correction parameter to adjust the total pressure value.

2.2 Off-design axial compressor mean-line loss model

The flow physics in any transonic axial compressor, as shown by Yu et al [23] and presented as Figure 2-1, is quite complex. Between incidence and deviation changes, vortex structures developed by clearance flows, vortex structures developed by the end wall-airfoil interface, the laminar to turbulent boundary layer growth, strong shock structures, corner stall separations, and the rotor-stator boundary layer interactions, defining a set of simplified loss equations should not be considered a trivial task.

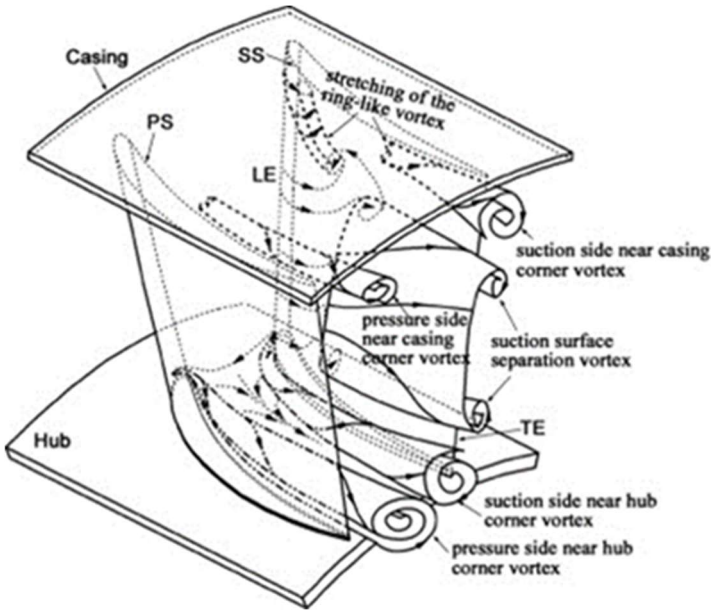

Figure 2-1: 3D flow structure, Yu et al [23]

The flow in an axial compressor blade-row is highly three-dimensional. It envelops a multitude of flow mechanisms creating losses (entropy increase) that will impact the overall efficiency of a compressor stage. For simplification purposes, as shown in Figure 2-2, the loss structure of an axial compressor blade-row may be decomposed into four interdependent loss zones as follows:

- **ZONE 1** may be considered as the flow incidence zone, which may also include shock structures and leading edge bow waves.
- **ZONE 2** is considered to be the boundary layer growth zone, which may include extensions of the shock structures. This region will be dominated by the profile (friction or boundary layer) loss, and depending on the aspect ratio of the blade row, the secondary vortex structures.
- **ZONE 3** represents that portion pertaining to changes in flow deviation angle and the trailing edge wakes.
- **ZONE 4** may be considered that portion pertaining to span effects; vortex generation caused by either the casing-to-airfoil interaction (commonly known as secondary flow or vortices) or by the vortex structures generated by the clearance space between the casing and airfoil extremities.

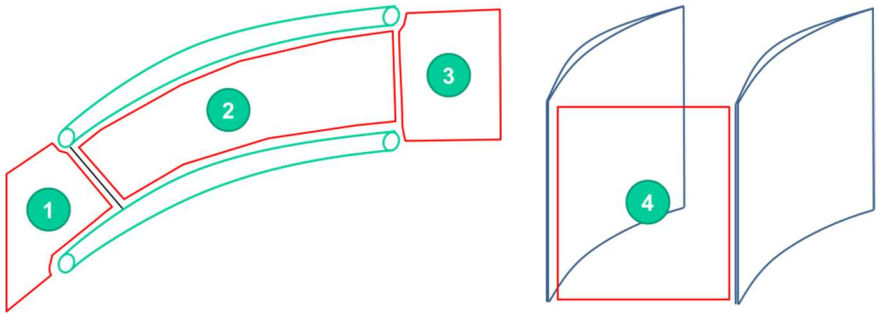

Figure 2-2: Simplified compressor loss zone model

A review of more than sixty years' worth of axial compressor loss modelling literature (refer to Table 2-3 for details) has shown that there are many parameters that drive the axial compressor losses. These parameters may also include various correction factors and adjustments, introduced throughout the compressor modelling history, to better match a particular set of compressor designs. The literature shows that the axial compressor blade row total loss may be considered to be a function of the following four dominating loss components:

- Profile Loss Y_P
- Secondary (Vortex) Loss Y_S
- Clearance Loss Y_{CL}
- Shock Loss Y_{SH}

Furthermore, these loss components may be corrected for the following flow characteristics or parameters, where the letter *f* signifies correction factor:

- Aspect Ratio f_{AR}
- Mach number f_{Mach}
- Reynolds number f_{RE}
- Incidence f_{INC}
- Deviation f_{δ}
- Airfoil surface roughness f_{SR}
- Part Span Shrouds f_{SPAN}
- Annulus (End wall) f_{ANN}

The literature has shown that each cited author in Table 2-3 has presented an independent loss model different from each other. The majority of the authors have quoted the classic authors such as Lieblein for the diffusion factor and the diffusion ratio formulae, as described in NASA's SP-36 [24], and Carter for his deviation rule [25]. Furthermore, some authors have cited, as part of their literature survey, the industry-based loss models of Koch & Smith from General Electric [7], and that of Wright & Miller from Rolls-Royce [20]. Beyond that, each author has applied a different set of references and formulae to build their unique loss model. The combination and form of these losses are dependent upon the individual researcher's background, scope, design limitations, knowledge, and biases.

Loss modeling may be considered to be based on two major contributing factors[5]:

- **History**: any engineering discipline will contain a wealth of historical methodologies, classic contributing authors, and a wealth of design knowledge, that in today's world of digitized graphs and powerful computers, is taken for granted and not properly understood or appreciated.
- **Theory**: within the history of the engineering discipline, much theory would exist that strives to describe the physics, behaviours, and interpretations of that engineering discipline. These theories, based on the at-the-time availability of experimental data and analysis methodologies, would have set the foundation of others to build from.

Creating an off-design mean-line loss formulation for transonic axial compressors, which encompasses all of the major loss components and correction factors listed above, would require quality test data that includes systematic permutations of the various flow and geometric parameters; this data must then be analyzed, intertwined, and interconnected with theory and physical observations. Furthermore, it would be difficult to discretize these losses into linearized stand-alone components, since each of these loss components could have dominant interdependencies with other loss components.

---

[5]Beyond the facts and data, "opinion" still drives the approach of understanding, accepting, and even challenging the theory and history behind loss model development

Table 2-3: Chronological view of axial compressor mean-line loss models

Author	Total Loss	Formula
Lieblein (1953) [24]	Profile	$\omega_{TOTAL} = \omega_P$
Koch & Smith (1976) [7]	Profile & Trailing Edge + End wall & TipClr + Shock + Part span shrouds	$\omega_{total} = \omega_{P\&TE} + \omega_{EW\&TC} + \omega_{shock} + \omega_{PS-shrouds}$ *(interpreted formula from reference)*
Barbosa (1987) [26]	Profile + Secondary + Shock Corrected for • Re	$\omega_{TOTAL} = \omega_P f_{Re} + \omega_S + \omega_{SH} + \omega_{COR}$
Wright & Miller (1991) [20]	Profile + Endwall & TipClr + Shock Corrected for • Re	$\omega_{total} = \left(\omega_p\|_{Re=10^6} + \omega_{EW\&TC}\right) f(Re) + \omega_{shock}$ *(interpreted formula from reference)*
Bloch, Copenhaver, O'Brien (1997) [27]	Profile + Shock	$\bar{\omega} = \omega_{profile} + \omega_{shock}$
Cahill (1997) [28]	Profile + Secondary + Shock	$\omega_{TOTAL} = \omega_P + \omega_S + \omega_{shock}$
Lynette Smith (1999) [17]	Profile + Shock Corrected for: • incidence	$\omega = (\varpi_{min} + \varpi_M)\left[1 + \left(\frac{i - i_{min}}{W}\right)^2\right]$
Ramakdawala (2001) [29]	Profile + Endwall & TipClr + Shock	$\omega_{TOTAL} = \omega_{Profile} + \omega_{EW\&TC} + \omega_{Shock}$
Boyer (2001) [30]	Profile + Shock + Secondary (tip & hub) Corrected for: • incidence	$\omega = \left(\varpi_{min} + \varpi_M + \varpi_{tip} + \varpi_{hub}\right)\left[1 + \left(\frac{i - i_{min}}{W}\right)^2\right]$
van Antwerpen (2007) [31]	Profile + Secondary + Annulus Corrected for: • Incidence • Reynolds, • Ma	$\omega = \omega_p^* \left(\frac{\omega}{\omega_i}\right)_{inc} \left(\frac{\omega}{\omega_i}\right)_{Re} \left(\frac{\omega}{\omega_i}\right)_{Ma} + \omega_s \left(\frac{\omega}{\omega_i}\right)_{Re} + \omega_a$, for i>$i_{min}$ $\omega = \omega_p^* \left(f\left(\frac{\omega}{\omega_i}, \Phi\right)\right)_{inc} \left(\frac{\omega}{\omega_i}\right)_{Re} + \omega_s \left(\frac{\omega}{\omega_i}\right)_{Re} + \omega_a$, for i<$i_{min}$
Falck (2008) [32]	Profile + End wall	$\omega_{TOTAL} = \omega_P + \omega_{ew}$ NOTE: simplified version of the Wright & Miller model
Intentionally left blank		

Veres (2009) [8]	Profile + Shock	$\omega_{TOTAL} = \omega_P + \omega_{shock}$
Benini (2010) [33]	Basic loss + shock + secondary + tip clearance + off design correction	$\zeta = \zeta_{(M=0)}\chi_R\chi_M + \zeta_{shock} + \zeta_S + \zeta_\delta + K_M\left(i - i_{ref}\right)^2$

Another challenging aspect of using the OD mean-line modelling methodology is the decision towards which loss model to use. The literature has shown that there is no one *golden standard* or unique model to be based on. As shown in Table 2-3, a compressor aerodynamicist has a multitude of loss models to choose from. From Lieblein's model introduced in 1953, to Benini's in 2010, each model has its own set of assumptions, approaches, and accompanying results. Furthermore, as a researcher investigates the various citations they may uncover the stage stacking model of Steinke from NASA [34] which references the stage stacking methodology as described by Howell & Calvert [35] from the National Gas Turbine Establishment of England; then, there is the theoretical model as described by Schobeiri [36, 37], and let us not forget the description of turbomachinery loss mechanisms written by Denton [38]. Additionally, we may find the loss model comparison executed in the 1987 AGARD report [39], and Aungier's ASME text on compressor design [40].

2.2.1 Treatment of the inlet shock structure

Modern axial compressor stages are capable of running at conditions where a shock is sustained at the leading edge of the rotor blade row. Starting with a weak shock near the relative inlet Mach number of 1.0, and continuing on as high as 1.4 or more, the inlet shock structure will contribute to the sum of the rotor blade row losses. The question then arises as to how best to capture the loss contribution due to an inlet shock structure on a compressor rotor blade row.

Let us recall that a shock (normal) structure will cause the static pressure, static temperature, and the gas density to increase *instantaneously*[6] across it. Since there is no work done across the shock, and if assumed that it is adiabatic, the total enthalpy and the total temperature remain constant. However, because of the entropy increase across the shock, the total pressure downstream of the

[6] With respect to the thickness of the shock wave structure

shock will be less than the total pressure upstream of the shock. Another important feature of the normal shock structure is that the Mach number will decrease across the shock. The normal shock structure physics is a very enticing approach to attempt to explain axial compressor inlet shock phenomenon. Table 2-4 presents the normal shock equations for reference.

Table 2-4: Normal shock equations [41]

$$M_1^2 = \frac{(\gamma-1)M_0^2 + 2}{2\gamma M_0^2 - (\gamma-1)}$$

$$\frac{P_{S1}}{P_{S0}} = \frac{2\gamma M_0^2 - (\gamma-1)}{(\gamma+1)}$$

$$\frac{T_{S1}}{T_{S0}} = \frac{\left[2\gamma M_0^2 - (\gamma-1)\right]\left[(\gamma-1)M_0^2 + 2\right]}{(\gamma+1)^2 M_0^2}$$

$$\frac{\rho_{S1}}{\rho_{S0}} = \frac{(\gamma+1)M_0^2}{(\gamma-1)M_0^2 + 2}$$

$$\frac{T_{O1}}{T_{O0}} = 1$$

$$\frac{P_{O1}}{P_{O0}} = \left[\frac{(\gamma+1)M_0^2}{(\gamma-1)M_0^2 + 2}\right]^{\frac{\gamma}{\gamma-1}} \left[\frac{(\gamma+1)}{2\gamma M_0^2 - (\gamma-1)}\right]^{\frac{1}{\gamma-1}}$$

Since the late 1950's, various researchers have attempted to either explain or define the physics and modeling approaches to capture the loss contribution of the compressor inlet shock.

- In 1957, Schwenk, Lewis, & Hartmann introduced a preliminary analysis of the magnitude of shock losses in transonic compressors [21]. The results of double-circular-arc (DCA) blades showed that the inlet shock may contribute between 35 to 55% of the overall blade row loss [21]. They proposed to approximate the complex compressor blade row shock structure through the use of the normal shock model, repeated here as Figure 2-3 [21].

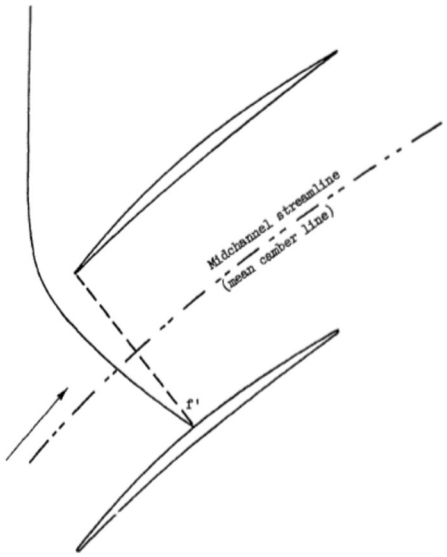

Figure 2-3: Schwenk, Lewis, & Hartmann normal shock model [21]

- In 1961, Miller, Lewis, & Hartmann published the work done at NASA in 1957 by Schwenk, Lewis, & Hartmann [42].
- In 1982, Puterbaugh & Wennerstrom released a report containing results of attempts to improve the shock loss estimation of an in-house axial compressor design code by introducing a three-dimensional shock surface [43]. The document also reported the shock structure findings of Prince, represented as Figure 2-4. Two specific shock structures were described. The first shock structure described is that which occurs when the blade row back pressure is at the design point condition. It was shown that the shock structure stretches axially across the blade row, from the leading edge to a portion behind the trailing edge, Figure 2-4a. The second structure, Figure 2-4b, which occurs at very high back pressures, resembles a normal shock [43].

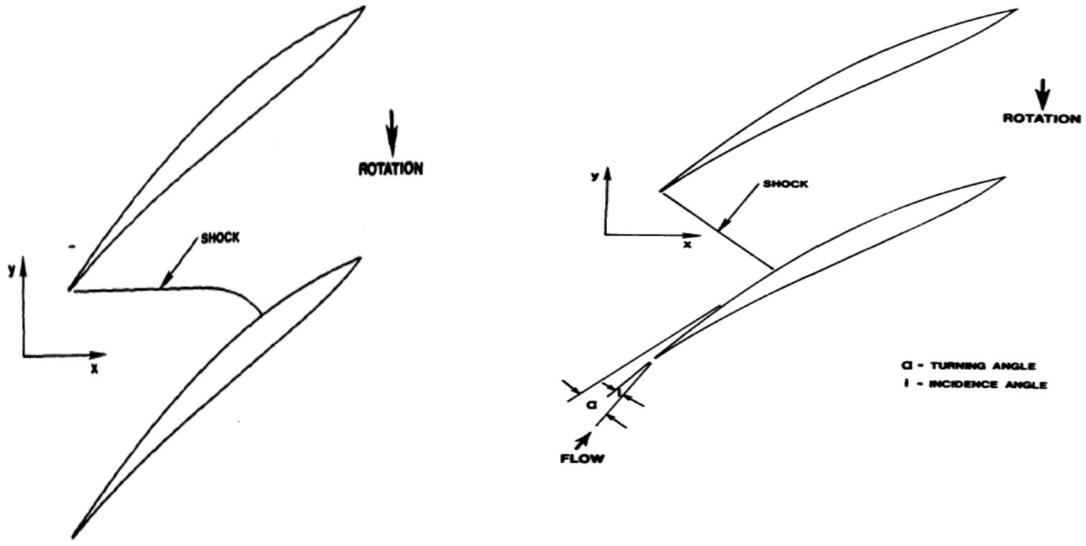

a) Design point b) High back pressure

Figure 2-4: Puterbaugh & Wennerstrom shock model description [43]

- In 1989, Freeman & Cumpsty stated that "*many features of the flow can be predicted with the simple one-dimensional approach*" [44]. With respect to the inlet shock structure, they used an approach known as the *unique incidence*. Additionally, they calculated the combination of the mass flow, the stagnation enthalpy, and the momentum of an inlet control volume [44]. Despite being relatively complex, their predictive approach was significantly deviating from the rotor experimental measurements
- In 1994, Wadia & Copenhaver issued a paper describing that the transonic compressor rotor performance was highly sensitive to the variations in cascade area ratios [45]. They demonstrated the effects of how the shock structure may vary due to changes in cascade throat area, internal contraction, and trailing edge effective camber [45]. Furthermore, their report showed that a transonic axial compressor may have a dual shock system, as shown in Figure 2-5 [45].

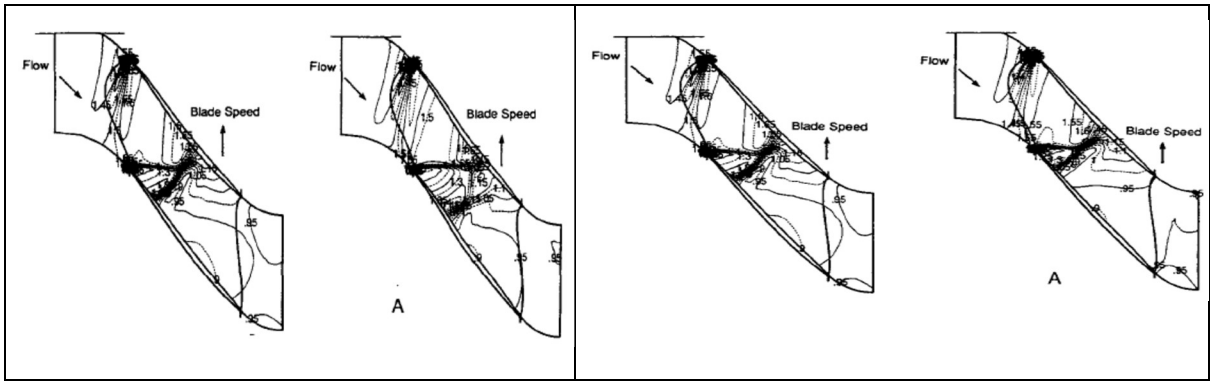

Figure 2-5: Wadia & Copenhaver dual shock patterns [45]

- In 1996, Puterbaugh et al described the use of a three-dimensional shock loss model [46]. The paper was an extension of the 1982 report by Puterbaugh & Wennerstrom [43], mentioned above. Their computational results, when compared to their experimental results, showed a parallel trend with respect to adiabatic efficiency, and an under prediction of the pressure ratio at the 100% speed-line.
- In 1997, Bloch, Copenhaver & O'Brien presented an *engineering* shock loss model [27]. There formulation was based on the Prandtl-Meyer equation coupled with the bladed mass flow equation. They also considered the detached shock wave physics as reported by Moeckel (1949). Their results showed that at a Mach number of 1.20 their model had a reasonable match to the experimental data. However, at inlet relative Mach numbers of 1.12 and 1.10 significant differences were seen.

One of the issues encountered in the use of the normal shock equations is the fact that the resultant exit Mach number does not represent the exit Mach numbers encountered in an axial compressor. For example, at a gas flow with γ=1.4, for a normal shock with an inlet relative mid-span Mach number of 1.4 should produce an exit Mach number of approximately 0.7397. For four NASA axial compressors under investigation (Stage 35 to 38), with relative inlet mid-span Mach numbers of 1.3 to 1.39, will produce a mid-span relative exit Mach number of 0.67 to 0.82, which definitely does not follow the classical normal shock table results. Figure 2-6 shows the comparison between the normal shock model and the predicted mean-line model results (based on a calibrated loss model to be described in Chapter 3) of four NASA transonic axial compressor rotors. What can be seen is that the resultant mean-line model pressure ratio and exit Mach numbers do not coincide with the normal shock model. In terms of Mach numbers, the NASA rotors have a completely

different distribution than the normal shock model. More significantly, the rotor exit relative Mach numbers are less than the normal shock model.

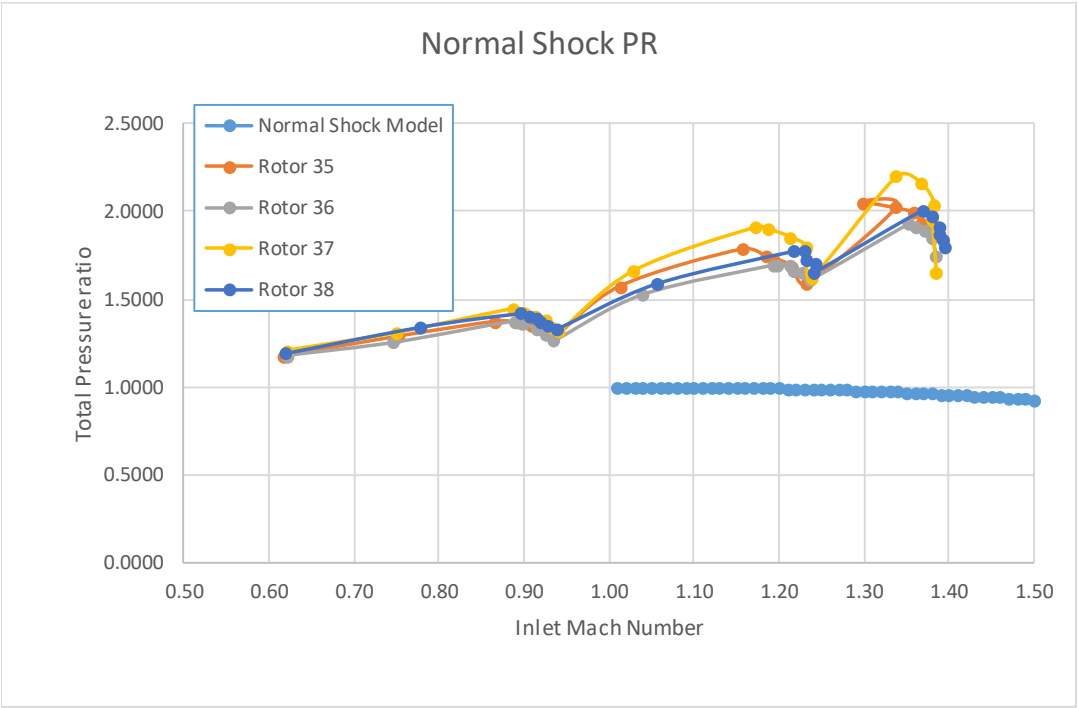

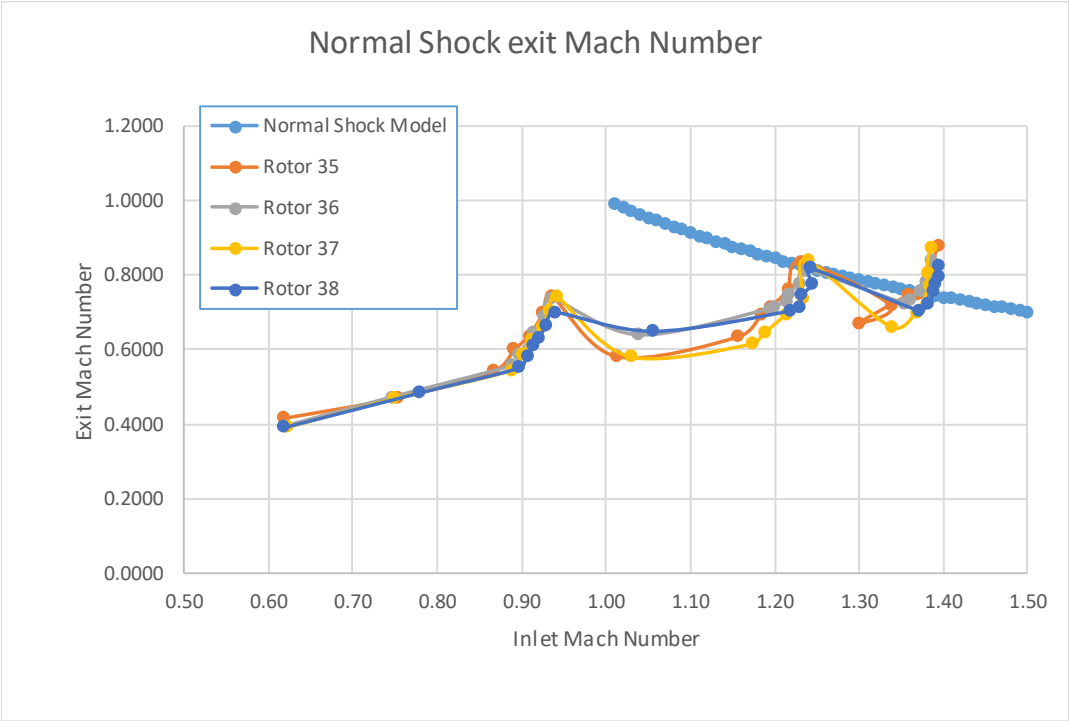

Figure 2-6: Comparison of normal shock model and NASA rotors

2.2.2 Treatment of the deviation angle

One of the challenging aspects of compressor loss modeling is the understanding and prediction of flow deviation. Flow deviation is most commonly considered as the difference between the exit flow angle, which varies due to the off-design performance excursion, and that of the compressor blade metal angle, which is considered fixed in space.

$$\text{Deviation Angle, } \delta = \beta_{ex-flow} - \beta_{ex-metal}$$

The deviation angle, represented by the Greek symbol of δ (delta), or sometimes ε (epsilon), is the difference between $\beta_{ex\text{-}flow}$, which is the flow angle from the axial direction (in degrees) and $\beta_{ex\text{-}metal}$, which is the blade trailing edge metal angle from the axial direction (in degrees). Figure 2-7 is a representation of this concept.

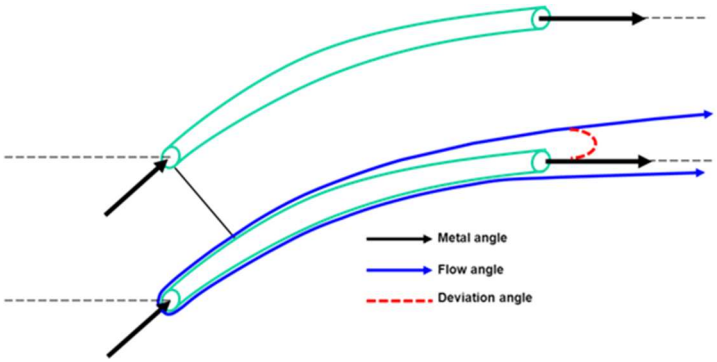

Figure 2-7: Simplified diagram representing compressor blade deviation

The development of flow deviation may be assumed to commence in **ZONE 1**, and progress until the exit boundary of **ZONE 3**. As the flow passes through the diverging channel of an axial compressor blade row, the flow is compressed and, in the meantime, a boundary layer is formed over the blade surface. This boundary layer formation and growth will cause the average bulk flow to change angle, since the boundary layer will *push* the bulk flow away from the blade surface. The main driving parameters of boundary layer growth are the incidence angle, inlet Mach number (including any shock structures due to high Mach numbers), airfoil camber, and airfoil blade count.

In 1996, AGARD held a conference proceeding where the main topic regarded turbomachinery losses [47]. With respect to compressors, there were discussions on loss models and CFD analysis. The main take-away is from Dunham's key note address. Dunham explained that the prediction of the compressor temperature ratio and efficiency were sensitive to small changes in the calculated

deviation. He also quoted the following sensitivity requirements to obtain accurate efficiency and loss assessments: i) the loss coefficient needs to be within ±0.01 to obtain an efficiency accuracy of less than 1% and ii) the deviation angle needs to be within ±0.5° to obtain a temperature ratio accuracy, which represents work, to less than 2% [47].

Table 2-5: Consolidated list of various formulations for deviation prediction

Author	Formula
Carter (1946)	$\delta = m\theta\sqrt{1/\sigma}$
NASA SP-36 [24] (1965)	$\delta = (K_\delta)_{sh}(K_\delta)_t\left(\delta_0^\circ\right)_{10} + m \cdot \theta$
Crouse & Gorrell [22] (1981)	Applies a correction to Carter's "m" value based on a figure plotting non-circular arc chord ratio and blade chord angle.
Wright & Miller [20] (1991)	$\delta_{opt} = 1.13m\left(\varphi\sqrt{\frac{s}{c}+3}\right) + m_1(\Omega - 1) + m_2\left(\frac{t_{max}}{c} - 0.05\right) + 0.8$
Cahill [28] (1997)	$\delta = \delta^* a(i - i^*)^2 + b(i - i^*) + c$
Boyce [48] (2006)	$\delta_f = m_f\theta\sqrt{1/\sigma} + 12.15\frac{t}{c}\left(1 - \frac{\theta}{8.0}\right) + 3.33(M_1 - 0.75)$
Benini [33] (2010)	$\delta = \frac{1}{K}\left[(K_\delta)_t(\delta_0)_{10} + \frac{(m)_{\sigma=1}}{\sigma^b}\vartheta\right] + \Delta\delta_{ref} + \left(\frac{d\delta}{di}\right)_{i_{ref}}\left(i - i_{ref}\right)$

With respect to deviation formulae, as shown in Table 2-5, NASA introduced the concept of the reference deviation angle [24], Crouse & Gorrell modified Carter's "*m*" value based on a figure which plotted the non-circular arc shapes ratio parameter versus the blade chord angle [22], Wright & Miller described an optimal deviation angle [20], Cahill presented an empirically based off-minimum-loss deviation angle prediction [28], Boyce modified Carter's formula through the addition of geometric parameters [48], and Benini described a deviation formula based on various geometric and flow parameters [33]. The raw data for these formulae were not available for validation or corroboration.

2.2.3 Treatment of the choke condition

One of the main aspects in creating an axial compressor performance map is the ability to capture the so called *choke* condition. Barbosa has defined this condition as the condition where the speed-lines become *vertical*, or when there is no change in the mass flow rate regardless of the pressure ratio [26]. However, there is a notional issue with this description of choke. In *1D* gas dynamics, choke is considered to be the condition where the minimum throat area has reached its maximum mass flow rate [41]. This occurs when the throat Mach number has achieved the unity value.

Related to the current subject title, we had introduced the draft notion of the *pseudo-choke*. This stemmed from the necessity of identifying a definition for compressor choke, to be used in an off-design mean-line model, since a mid-span Mach number of unity was neither found nor calculated (using the OD mean-line model to be described) throughout the off-design excursion. This notion stirred the following anonymous reviewer's comment: "*The authors' discussion of 'choke' draws attention to an ambiguity of terminology common in the field.*" [2] Inspired and motivated from this critique, this section attempts to 1) describe where the choke terminology ambiguity may rise from and 2) clarify the ambiguous compressor choke phenomenon.

To better describe the observed off-design behavior, the term *Maximum Attainable Mass Flow* (MAMF) was used [2]. Classically, choke pertains to the unique situation of when an isentropic flow reaches a maximum mass flow rate through the smallest constriction of a particular system, commonly known as the *throat area*. At this area, the Mach number becomes 1 (or *unity*), also known as the critical condition; it is for this reason that choke is synonymous with a Mach number of unity. To avoid confusion with this classical notion of isentropic choke, the generic use of MAMF better describes the impact of choke when losses are considered. Here, the term captures the notion of the maximum mass flow rate through a constriction for either isentropic and non-isentropic flow conditions, independently from the actual Mach number at which the mass flow rate has reached its maximum value.

The choke condition in an axial compressor is one of the conditions that needs to be properly identified. The other two important conditions to be identified on an axial compressor performance chart are 1) the onset of the stall or surge point and 2) the constant RPM speed-line behavior of mass flow rate versus the pressure ratio and efficiency. The identification of the choke condition plays a vital role in the overall performance of a gas turbine. Based on accumulated knowledge, it

is recognized that when a compressor is in the choke condition the mass flow cannot be further increased without a change in the compressor geometry. Furthermore, the notion of choke is classically defined as when the minimum geometric throat area reaches a Mach number of unity for an isentropic converging duct [41]; and this notion stems from the scholarly halls of our universities. The classical conclusion for adiabatic inviscid flows is that "*choke occurs at a Mach number of unity*".

This description of choke is used in axial turbine stages with much success. In an axial turbine, choke is assumed to occur at the minimum geometric throat area close to the trailing edge. The choke condition may be encountered in the stator and/or the rotor blade rows. Furthermore, the concept of axial turbine *limit loading* is defined as the condition when the axial exit Mach number of the rotor reaches a value of unity [49, 50]. Additionally, the choke phenomenon in axial turbines occurs at the trailing edge throat, and this condition is identified when the mean-line model based throat area, and accompanying loss model, achieves a Mach number of unity. This may lead to the incorrect conclusion that, for turbines, choke occurs for both isentropic and non-isentropic converging ducts.

Surely, with such successful applications in expanding flows as found in axial turbine stages, which seems to closely follow the classical definition, the choke condition explanation should be, or mistakenly be, applicable to an axial compressor stage; in other words, choke should be identified when the minimum geometric throat area, located at the leading edge of the compressor, has reached a Mach number of unity. If this definition of choke is pursued, it is quite difficult to find such a condition for all reported speed-lines found in the four NASA compressor stages under investigation.

A literature review of various sources was executed to pinpoint the potential root-cause or -causes to the ambiguity of the choke terminology. Table 2-6 shows a summary of the statements and models employed by other researchers to define choke in an axial compressor.

Table 2-6: Chronological view of axial compressor choke definition and models

Author	Choke criteria, description, or
DeHaller (1953)	No choking criteria mentioned
Creveling & Carmody (1968) [51]	**Choking criteria:** "*check for a choke margin of 5%*" (O/h* ≥1.05)
Koch & Smith (1976) [7]	No choking criteria mentioned
Howell & Calvert (1978) [35]	**Choking criteria (methodology):** It is based on a known choke point condition and then scaled
Greitzer (1980) - REVIEW PAPER	No choking criteria mentioned
Koch (1981) [52]	No choking criteria mentioned
Crouse & Goreell (1981) [22]	Uses minimum blade choke margin of (A/A*)-1, where A* "*is the area needed to pass the streamtube flow at a relative Mach number of 1.0*"
Steinke (1982) [34]	**Choking criteria (methodology):** It is based on a known choke point condition and then scaled. Based on the work of Howell & Calvert
Barbosa (1987) [26]	**Choke description:** "*The annulus or the throat is considered choked when an increase in axial velocity gives rise to a decrease in mass flow. This implies the possibility of choke whilst some of the stream-tubes remain un-choked to satisfy radial equilibrium.*"
Miller & Wasdell (1987) [53]	**Choking Incidence:** 3x minimum loss or capture the vertical characteristic
Freeman & Cumpsty (1989) [44]	**Choking Criteria:** when $P_{02}/P_{01} = P_2/P_1$ plotted against Vx/U.
Wright & Miller (1991) [20]	No choking criteria explicitly defined
Walsh & Fletcher (1998) [54] Textbook: Gas Turbine Performance 2nd edition	**Choke Description:** "*One key phenomenon for compressible flow is choking, where a Mach number of 1 is reached at the minimum area along a duct. Reducing downstream pressure further provides no increase in mass flow.*" "*For each referred speed line there is a maximum flow which cannot be exceeded, no matter how much pressure ratio is reduced. This operating regime is termed choke.*"
Hall & Dixon (1998) [55] Textbook: fluid mechanics, thermodynamics of turbomachinery	**Choke Description: "***The choked regions of both the compressor and turbine characteristics may be recognised by the vertical portions of the constant speed lines. No further increase in m√T01/p01 is possible since the Mach number across some section of the machine has reached unity and the flow is said to be choked.*"
Saravanamuttoo, Rogers, & Cohen (2001) [10] Textbook: Gas turbine theory 5th edition	No choking criteria explicitly defined
Hanlon (2001) [56] Textbook: compressor handbook	**Choke Description:** "*Stonewall, or choke, is a condition at which increased capacity (flow) results in a rapid decrease in head as flow is increased. This occurs because the Mach number is approaching 1.0.*"

Boyce (2002) [57] Textbook: Gas turbine engineering handbook 2nd edition	**Choke Description:** "*Flow rate cannot be increased, since at this point it is beyond Mach one at the minimum area of the compressor, or a phenomenon known as "stone walling" occurs, causing rapid drop in efficiency and pressure ratio.*"
Aungier (2003) [40]	**Choke Description:** "*Similarly, at flow rates greater than the design flow rate, the increase in loss will eventually result in no rise in pressure. This condition is commonly referred to as choke, although it may be caused by large losses due to off-design operation rather than a true aerodynamic choke condition.*"
Falck (2008) [32]	No choking criteria mentioned
Veres (2009) [8]	**Choke Criteria:** "*Choke is determined as the limit of flow where the code fails to converge on the rotor exit velocity triangles.*"
Barbosa & Figueiredo (2010) [58]	**Choking criteria:** Use of the Throat width / inlet mass flow ratio
Banjac, Petrovic, & Wiederman (2015) [59]	No choking criteria mentioned
Peyvan & Benisi (2016) [60]	**Choking criteria:** "*With a slight increase in mass parameter near choking condition, pressure drop increases sharply resulting the declination of pressure ratio.*"

The two main potential root-causes, that have been concluded from the literature research with respect to the choke terminology ambiguity, are 1) most of the off-design performance charts are based on the *vertical*, or *stone-wall*, mass flow condition and 2) choke has been repeatedly defined, if at all, as when the Mach number achieves unity.

With respect to the *vertical*, or *stone-wall*, phenomena Dixon best describes this as the condition where the speed-lines exhibit no change in the mass flow rate and becomes vertical [55]. This is implicitly observed in the compressor performance charts predicted by Howell & Calvert [35], Miller & Wasdell [53], Freeman & Cumptsy [44], Wright & Miller [20], Aungier [40], and Banjac et al [59].

In terms of defining choke as occurring when the Mach number becomes unity, we can identify the text of Walsh & Fletcher [54], Hanlon [56], and Boyce [57]. The remaining authors, cited in Table 2-6, refer to the choke term without providing an explicit definition. The reader is then left to their own devices to interpret that choke most likely occurs at a Mach number of unity, assuming that that definition is the only one that the reader is aware of.

The most recent discussion (2018) on mean-line model choke was by Cadrecha et al [61]. In this paper it was stated that the "*choked and critical conditions are equivalent only for isentropic flows.*" [61] It was further explained that, when losses are taken into account, the choking Mach

number becomes less than the critical Mach number of 1. In other words, compressor choke, when taking into account the blade row losses, does not necessarily occur at a Mach number of unity.

This phenomenon was independently corroborated by the 2-part paper presented in 2018 [2], which is part of this investigation. Unlike the formula to update the choke Mach number by Cadrecha et al [61], in this research it was decided to search for a pressure-based criterion to avoid the creation of semi-empirical formulas and complex numerical calculations.

2.2.4 Treatment of the onset of stall or surge

For more than six decades, models have been described with the potential to assess, or predict, the stall and surge condition through the use of the *1D* mean-line methodology. Even with the various near-successful attempts, each one presenting its own strengths and limitations, this portion of the axial compressor performance chart remains elusive to successful prediction. Based on Greitzer's review paper on stall phenomena [62], and Augnier's ASME textbook on axial compressors [40], one may be left to believe that it will be a near impossible task to discover either a physics-based or semi-empirical formulation for such a complex physical phenomenon. It is for this implicit reason that the compressor test rig is still required in the overall compressor design life-cycle; not just to validate the compressor performance, but to also properly identify the stall and surge line.

In terms of technical language, the word *surge* should not be used when talking about a stand-alone compressor. Surge is an instability that requires the presence of a large plenum volume downstream of the compressor (such as a combustor) and a valve (which is usually the 1st turbine vane). Surge occurs when the compressor can no longer sustain the pressure ratio to maintain the compressed air in the downstream plenum. For axial compressors, as mentioned in Greitzer [62], the compressor enters into a rotating stall before it triggers surge. It is due to this reason that the words *stall* and *surge* are interchangeably used. However, this is not the case for centrifugal compressors which may operate in rotating stall without triggering surge. Table 2-7 presents a chronological view of the various stall and surge models employed in a *1D* mean-line methodology. The models are summarized as follows:

1) **Velocity ratio:** this ratio stems from the classical de Haller value, where it is stated that the exit to inlet relative velocity ratio below 0.72 will introduce the onset of stall.

2) **Known stall point:** Howell & Calvert [35] and Steinke [34], following similar stage stacking methodologies, use a known efficiency value at the stall point and empirically scale the value to other compressor speed-line values.

3) **Stall pressure rise coefficient:** of the more substantial works, Koch presented the notion of the *stalling pressure rise coefficient* [52]. His formulation took into account parameters such as staggered spacing, Reynolds number, and rotor-stator axial distance.

4) **Stalling incidence:** Miller & Wasdell [53] and Wright & Miller [20] both used a stalling incidence formulation to find the stall point.

5) **Max static pressure ratio:** Freeman & Cumpsty used a maximum attainable pressure ratio approach to define the surge conditions [44].

6) **Equivalent relative velocity ratio:** Aungier, based on his research, introduced the *equivalent velocity ratio* [40] which takes into account parameters such as the ratio of maximum thickness to chord, solidity, camber and stagger angles. Since then, some authors have followed Aungier's model as part of their 1D mean-line methodology formulation.

In terms of text or handbooks used in the universities, such as Dixon & Hall [55], Walsh & Fletcher [54], Saravanamuttoo et al [10], Hanlon [56], and Boyce [57], we find that the authors cite the works of other authors, however they do not provide any particular model to work with.

Table 2-7: Chronological view of surge models

Author	Stall or Surge
DeHaller (1953)	**Stall criterion** $W_2 / W_1 < 0.72$ Where W is the relative velocity
Creveling & Carmody (1968) **[51]**	No stall or surge criteria mentioned
Koch & Smith (1976) [7]	No stall or surge criteria mentioned
Howell & Calvert (1978) **[35]**	**Stall criterion** Based on a known stall point condition and then scaled to other speed-lines
Greitzer (1980) **[62]**	**Review Paper** Literature of various surge concepts and explanations of

Author	Stall or Surge
Koch (1981) [52]	**Stalling pressure rise coefficient** $C_h = \frac{c_p t_1 \left[\left(\frac{p_2}{p_1}\right)^{\frac{\gamma-1}{\gamma}} - 1\right] - \frac{1}{2}(U_2^2 - U_1^2)}{\frac{1}{2}(V_{1rotor}'^2 + V_{1stator}^2)}$ The bladerow inlet pitchline free stream dynamic head was replaced by the effective dynamic head $\mathbf{F_{ef}}$ in the pressure coefficient $\mathcal{F}_{ef} = \frac{V_{ef}^2}{V_2} = \frac{V^2 + 2.5V_{min}^2 + 0.5U^2}{4V^2}$ $\frac{V_{min}^2}{V^2} = \sin^2(\alpha + \beta)$ If $(\alpha+\beta)\leq 90°$ and $\beta \geq 0°$ $\frac{V_{min}^2}{V^2} = 1$ If $(\alpha+\beta)>90°$ $\frac{V_{min}^2}{V^2} = \frac{U_2^2}{V^2}$ If $\alpha_1<0°$ for rotors If $\beta_1<0°$ for stators
Steinke (1982) [34]	**Stall criterion** Follows similar approach as Howell & Calvert
Barbosa (1987) [26]	**Stall criterion** Mentions that "*there are no practical correlations*" Uses the equivalent diffusion factor near a value of 2.20
Miller & Wasdell (1987) [53]	**Stalling Incidence** $i_s = A + \frac{B}{s/c} - C\Theta$ Where A, B, and C are coefficients obtained from graphs **Or** 2x the minimum loss
Freeman & Cumpsty (1989) [44]	**Surge Criterion** ∂(p2/p01)/∂Vx
Wright & Miller (1991) [20]	**Stall Criterion** As described by Miller & Wasdell [1987]
Cahill (1997) [28]	Benchmarks various mean-line loss models, and identified when each one stalls or surges
Dixon & Hall (1998) [55] Textbook: fluid mechanics, thermodynamics of turbomachinery	Mentions works from various authors
Walsh & Fletcher (1998) [54] Textbook: gas turbine performance 2nd edition	Describes surge in terms of engine performance perspective, does not provide a specific predictive model
Saravanamuttoo, Rogers, & Cohen (2001) [10] Textbook: Gas turbine theory 5th edition	Describes surge in terms of engine performance perspective, does not provide a specific predictive model
Hanlon (2001) [56] Textbook: compressor handbook	Describes an anti-surge methodology, and surge as a peak head for impellers

Author	Stall or Surge
Boyce (2002) [57] Textbook: Gas turbine engineering handbook 2nd edition	Mentions stall & surge, does not provide a specific predictive model
Aungier (2003) [40]	**Surge Criterion** $W_{RE} < \frac{(0.15 + 11t_{max}/c)/(0.25 + 10t_{max}/c)}{1 + 0.4[\theta\sigma/\{2\sin(\theta/2)\cos(\lambda)\}]^{0.65}}$ $W_{RE} < \left[(2.2/D_{eq})^{0.60}\right] \frac{(0.15 + 11t_{max}/c)/(0.25 + 10t_{max}/c)}{1 + 0.4[\theta\sigma/\{2\sin(\theta/2)\cos(\lambda)\}]^{0.65}}$ $\theta\sigma/[2\sin(\theta/2)\cos(\lambda)] \geq 1.1$
Falck (2008) [32]	**Surge criterion** Based on **Koch's** stalling pressure rise coefficient, explicitly mentions the following summarized process $C_{p,max} = C_{pD}\mathcal{F}_{ef}\left(\frac{C_p}{C_{pD}}\right)_{Re}\left(\frac{C_p}{C_{pD}}\right)_{\varepsilon}\left(\frac{C_p}{C_{pD}}\right)_{\Delta Z}$ $\mathcal{F}_{ef} = \frac{C_{ef}^2}{C_2} = \frac{C^2 + 2.5C_{min}^2 + 0.5U_2^2}{4C^2}$ Where C_{pD} is taken from a figure and corrected for Re, clearance, and axial spacing
Veres (2009) [8]	**Surge criterion** Rotor diffusion factor ≈ 0.60 **And** Rotor (tip to mid) relative velocity ratio $V_{REL,Tip\ Inlet}$ / $V_{REL,Mid\ Exit}$ ≈ 1.9
Barbosa & Figueiredo (2010) [58]	**Surge criterion** Diffusion Factor $D = \frac{(W_{max} - W_2)}{W_1} > 0.6$ **Or** Equivalent Diffusion Factor $D_{eq} = \frac{W_{max}}{W_2} > 2.2$
Benini (2010) [33]	Mentions stall and surge, provides general compressor charts for design selection
Banjac, Petrovic, & Wiederman (2015) [59]	Based on Aungier's (2003) cascade stall condition Writes formula as W_{Rmin} in lieu of W_{RE} Where $W_{R\,min} = (w_2/w_1)_{min}$ Also mentions impact and/or influence due to tip clearance, EWBL separation criterion, and Maximum pressure ratio criterion
Peyvan & Benisi (2016) [60]	Based on Aungier's (2003) surge criteria

Despite the richness of these aforementioned models, none is capable of predicting consistently or accurately the stall onset of a transonic axial compressor. Arguably, the only model that seems to produce interesting visual results is that of Wright & Miller [20]. With respect to the various publicly available off-design axial compressor performance charts, we encounter a variety of predicted versus experimental results. Figure 2-8 is a qualitative consolidated representation of the various prediction figures stemming from the cited publications of the stall and surge models.

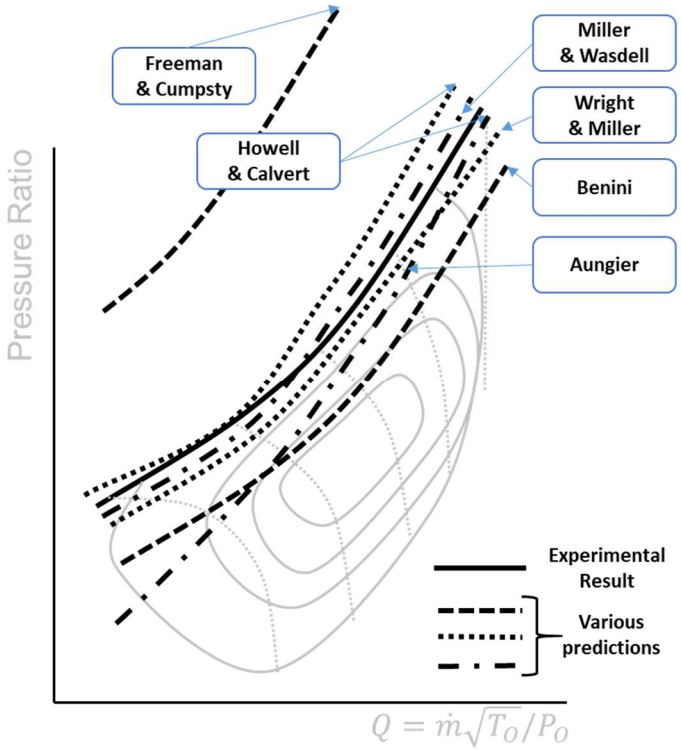

Figure 2-8: Qualitative comparison of various predicted versus experimental surge lines

For example:

- Howell & Calvert's stage stacking methodology of 1978 revealed four distinctive surge line predictive trends [35]. Their model respectively under- and over- predicted the NGTE based C135 and C141 axial compressors, Figure 2-9. For the NASA 2 Stage fan, their model showed a near trend prediction, whereas for a NACA 8-stage compressor their model revealed an over prediction of the surge line.

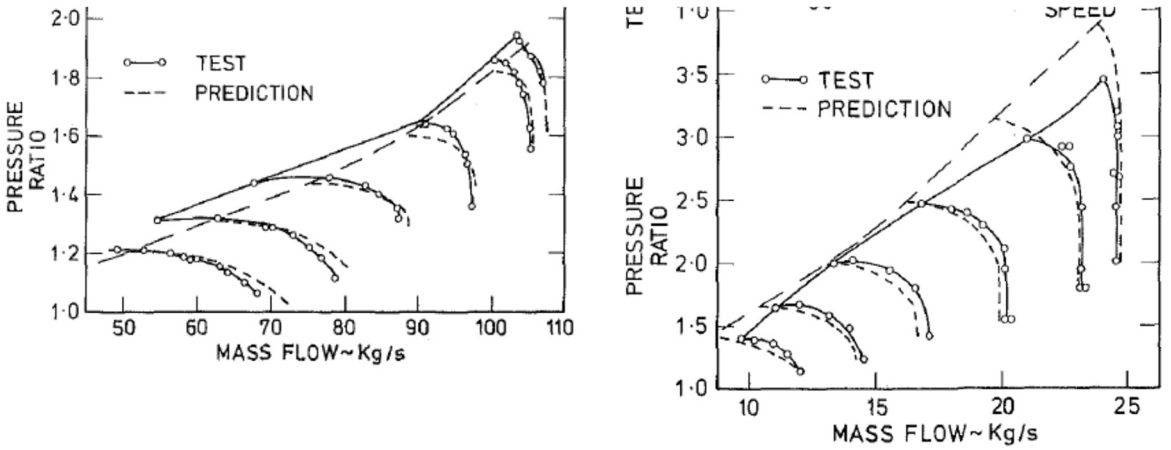

a) C135 compressor map b) C141 compressor map

Figure 2-9: Howell & Calvert's C135 and C141 compressor maps [35]

- In Miller & Wasdell's 1987 loss model paper [53], a 4-, 8-, and 10- stage experimental versus predicted comparison was shown, Figure 2-10. In their comparisons the surge line exhibited a cross-over point for all three compressor types.

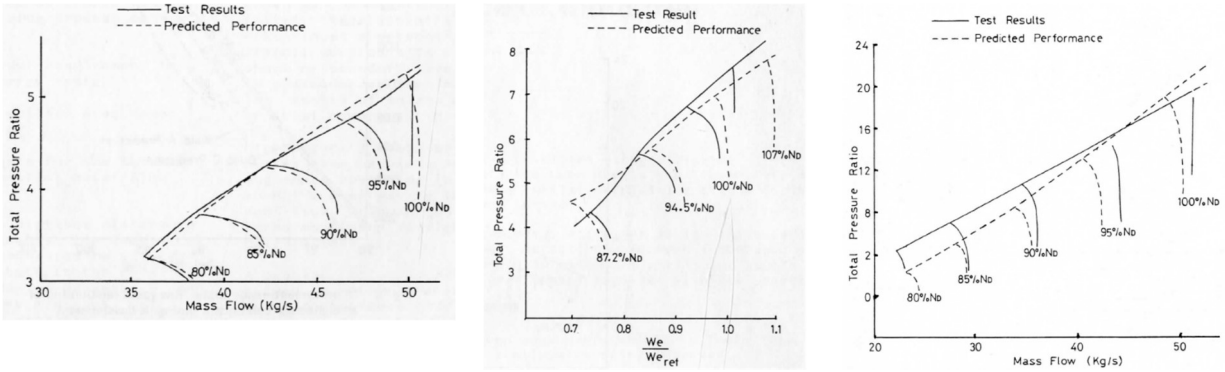

a) 4-stage b) 8-stage c) 10-stage

Figure 2-10: Miller & Wasdell's 4-,8-, and 10-stage compressor maps [35]

- In 1989, Freeman & Cumpsty introduced their version of a simplified mean-line loss model [44]. In their paper they reported the experimental versus predicted results of a Pratt & Whitney single stage compressor and an Aachen University axial compressor, Figure 2-11. The surge line for the Pratt compressor was dramatically overestimated, and that for the Aachen compressor was under predicted while maintaining a parallel trend behavior between the experimental and predicted results.

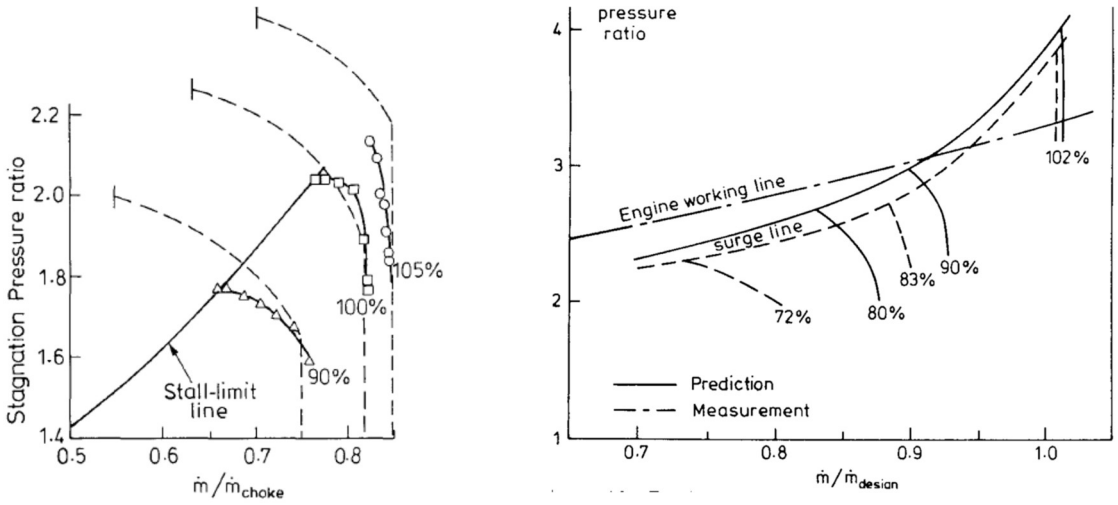

a) Pratt & Whitney compressor b) Aachen university compressor

Figure 2-11: Freeman & Cumpsty's PW and Aachen compressor maps [44]

- Wright & Miller's 1991 loss model publication [20], which is a modification of the Miller & Wasdell model [53], presented the off-design results of four NASA middle stages, Figure 2-12, two 6-stage compressors, and a 10-stage compressor. The surge line comparison between experimental and predictive results could be separated into two categories: i) the predicted surge line followed closely the experimental surge with a cross over point, or ii) the surge line was slightly under predicted while maintaining a parallel trend between the experimental and predicted results.

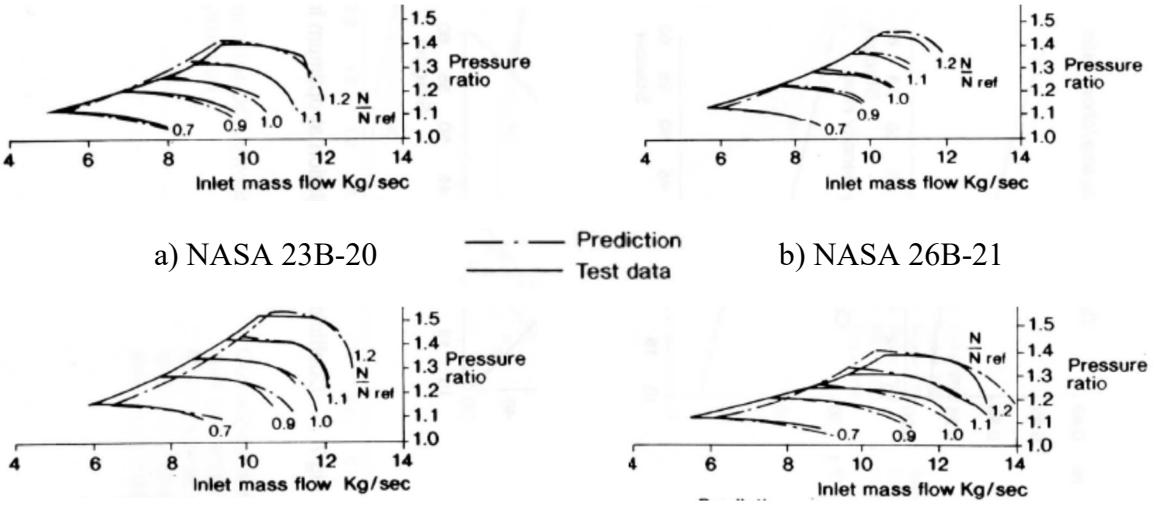

a) NASA 23B-20 b) NASA 26B-21

a) NASA 28B-22 b) NASA 26D-21D

Figure 2-12: Wright & Miller's selected 14 Middle Stages compressor maps [53]

- In Aungier's 2003 ASME text on axial compressor design [40], he showed the results of various multi-stage compressor analysis; three NACA stages and, 5-, 8-, and 10-stage compressors were compared. The experimental versus predicted performance chart comparisons revealed an interesting trend; as the number of stages increased the surge line was increasingly under predicted.
- In Veres' 2009 paper [8], the NASA compressor OD mean-line code *COMDES* showed slightly over predicted results for NASA Stage 37 and NASA Stage 74A, Figure 1-3a and 1-3 b. The observable variation in the performance charts were due to the differences in the level of mass flow rate and pressure ratio predictions which, for a few specific speed lines, created a difference between the mean-line based surge line prediction and the known experimental results.
- Benini's 2010 OD mean-line loss model visually showed an under prediction of the surge line for a Rolls-Royce HP-9 compressor, Figure 2-13 [33].

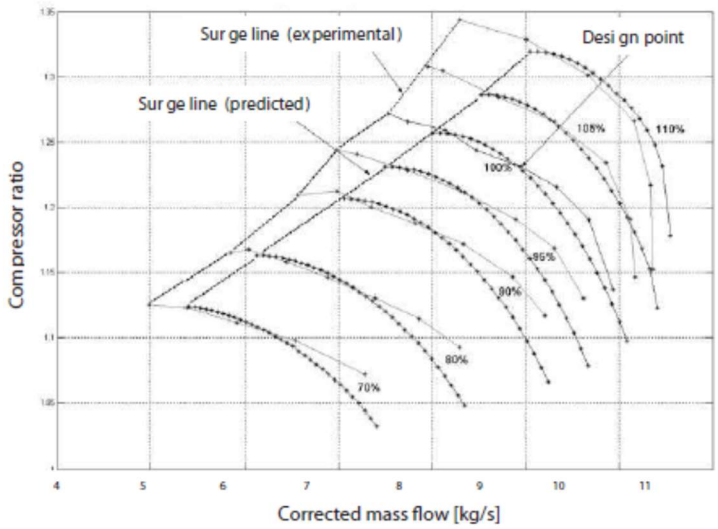

Figure 2-13: Benini's Rolls-Royce HP-9 compressor map [53]

- In Banjac et al's 2015 paper [59], they presented the experimental versus predictive results of eight different axial compressors. Their results, in general, showed under predicted surge lines.

CHAPTER 3 METHODOLOGY

"Essentially, all models are wrong, but some are useful."- George Box

The one-dimensional mean-line methodology (MLM) contains the accumulated knowledge of the successful and not so successful designs in a company's portfolio. Due to this particular proprietary knowledge, embedded and manifested in the form of mathematical models and digitized design charts, the one-dimensional mean-line methodology, as a whole, is considered a core competency and a trade secret. Since most of the axial compressor tests were conducted under proprietary conditions, the performance and/or the detailed measurements were not readily made available to the general public. NASA, as a public government institution, has made their internal reports available, and can be found on the NASA Technical Report Server (NTRS) using specific keyword search terms [63].

3.1 Selection of axial compressor geometries to investigate

Table 3-1 shows a snapshot of the various axial compressor cascade and stage reports obtained from the NTRS and other citations. The table indicates the name given to the compressor design, and includes a brief summary of the relevant information with respect to this work. The various airfoil types are highlighted in aqua for the classical NACA profile, green for the DCA type, and yellow for MCA blade profile shapes. Furthermore, those that were designed *with* dampers (part span shrouds) have been highlighted in orange. Finally, those stages that lack information have been labelled as *missing* in the comments section. The purpose of this table was to help identify candidate axial compressor stages for this thesis.

Table 3-1: List of potential validation cases

Compressor stage(s)	Memo ID	Comments
NACA 16-Stage compressor [64]	RM E52L03	stacked stages, subsonic, NACA airfoils **Missing**: Incidence, deviation, and radial profile data
NACA 10-stage compressor [65, 66]	RM E52B18 RM E52C04	stacked stages, subsonic, NACA airfoils **Missing**: Incidence, deviation, and radial profile data
NACA 8-stage compressor [67, 68]	RM E53I24 RM E53J06	stacked stages, subsonic **Missing**: Incidence, deviation, and radial profile data
NACA 6-Stage compressor [69]	TN 4253	stacked stages, transonic, NACA airfoils **Missing**: Incidence, deviation, and radial profile data
NACA 5-Stage compressor [70, 71]	RM E54F24 RM E54G01	stacked stages, transonic, Rotor DCA, Stator DCA and NACA **Missing**: Incidence, deviation, and radial profile data
Intentionally left blank		

NASA 2-Stage Fan [72]	TP 1314	Near complete set of data Rotor MCA, and Stator DCA; 60, 80, and 100% RPM
NASA 14-middle stages [73]	TP 1423	DCA airfoils, no dampers **Missing**: Incidence, deviation, and radial profile data
NASA Rotor 1 [74]	CR-54581	Mix of DCA and MCA airfoils, with rotor dampers **Missing**: Incidence, deviation, and radial profile data
NASA Rotor 2B [74, 75] NASA Rotor 2D NASA Rotor 2E	CR-54581 TN D-7662	Mix of DCA and MCA airfoils, with rotor dampers
NASA Rotor 3 [76]	TM X-2448	Mix of DCA and MCA airfoils, with rotor dampers
NASA Rotor 4 [77]	TM X-2449	Mix of DCA and MCA airfoils, with rotor dampers
NASA Rotor 5 [78]	TM X-2379	Mix of DCA and MCA airfoils, with rotor dampers
NASA Rotor 6 [79]	TM X-2697	Mix of DCA and MCA airfoils, with rotor dampers
NASA Stage 6-1 [80]	TM X-2731	MCA airfoils, with rotor dampers
NASA Stage 8-8 [81]	TM X-2926 TP 2049	MCA airfoils, with rotor dampers TP 2049 includes tip clearance impact
NASA Stage 11-04 [82]	TM X-2905	MCA airfoils, with rotor dampers
NASA Stage 12-05 [83]	TM X-2658	MCA airfoils, with rotor dampers
NASA Stage 14-10 [84]	TM X-2645	MCA airfoils, with rotor dampers
NASA Stage 16-11 [85]	TM X-2904	MCA airfoils, with rotor dampers
NASA Stage 17-12 [86]	TM X-2903	MCA airfoils, with rotor dampers
NASA Stage 18-13 [87]	TM X-3100	MCA airfoils, with rotor dampers
NASA Stage 35 [88, 89]	TP 1338	✓ Complete set of data, MCA airfoils, 50 to 100% RPM
NASA Stage 36 [89, 90]	TP 1974	✓ Complete set of data, MCA airfoils, 50 to 100% RPM
NASA Stage 37 [89, 91]	TP 1659	✓ Complete set of data, MCA airfoils, 50 to 100% RPM
NASA Stage 38 [89, 92]	TP 2001	✓ Complete set of data, MCA airfoils, 50 to 100% RPM
NASA Stage 51A [93]	TM X-3052	DCA airfoils, no dampers, 90% to 120% RPM
NASA Stage 51B [94]	TM X-3341	DCA airfoils, no dampers, 90% to 120% RPM
NASA Stage 51BR [95]	TM X-3451	DCA airfoils, no dampers, reversed flow
NASA Stage 52 [96]	TM X-3083	DCA airfoils, no dampers, 70% to 120% RPM
NASA Stage 53 [97]	TP 1299	DCA airfoils, no dampers, 70% to 120% RPM
NASA Stage 54 [98]	TM X-3430	MCA airfoils, no dampers, 80% to 120% RPM **Missing for stages 51 to 54:** low end speed lines
NASA Stage 55 [99, 100]	TM X-2837 TM X-3101 TM X-3338 TM X-3342 TM X-3349	Rotor DCA, Stator NACA, no dampers **Missing:** low end speed lines, only 80% and above **For stages 51 to 55:** Near complete set of data
NASA Stage 57 [101, 102]	TP 1502 TP 1510	no mention of airfoil shape, no dampers
NASA Stage 66 [103]	TM X-3345	Transonic, includes an IGV Rotor MCA, Stator DCA, no dampers **Missing**: speed lines, only 100% available
NASA Rotor 67 [72, 104]	TP 1314 TP 1493	(related to the NASA 2-Stage Fan)
NASA Stage 74A [105]	TP 2597	stacked stages, transonic, includes IGV Rotor 1 & 2 MCA, all Stators & Rotor 3 DCA, no dampers **Missing**: Geometry, Incidence, deviation, and radial profile data
NASA Stage 76 [8]	No report(s) issued	Designed, procured, never tested **Missing**: Report, incidence, deviation, and radial profile data
NASA / GE EEE (E^3) [106, 107]	CR-165558 CR-168245	stacked stages, General Electric design for HPC **Missing**: Incidence, deviation, radial profile data, and individual stage data

NASA / Pratt EEE (E^3) [108]	CR-180850	stacked stages, Pratt & Whitney design for HPC **Missing**: Incidence, deviation, radial profile data, and individual stage data
Pratt Compressor [109]	CR-72694	
NASA low speed compressor [110]	TM 4635	stacked repeating stages, includes IGV **Missing**: Incidence, deviation, radial profile data, and individual stage data
L030-4, and L030-6 [111]		Axial cascade tests, USAF design **Missing**: Incidence, deviation, radial profile data, and individual stage data
University Notre Dame compressors		No publicly available information
Purdue University three stage compressor		No publicly available information
Sharif University (Iran) Single stage axial compressor		No publicly available information

Figures 3-1, 3-2, and 3-3 show the comparisons of various NASA axial compressor stage performances. In Figure 3-1, we have the performance comparisons of the NASA axial compressor Stages 35 to 38 (MCA profiles) versus the NASA axial compressors Stages 51 to 54 (DCA profile). What we see is the performance differences of MCA versus DCA airfoil designs.

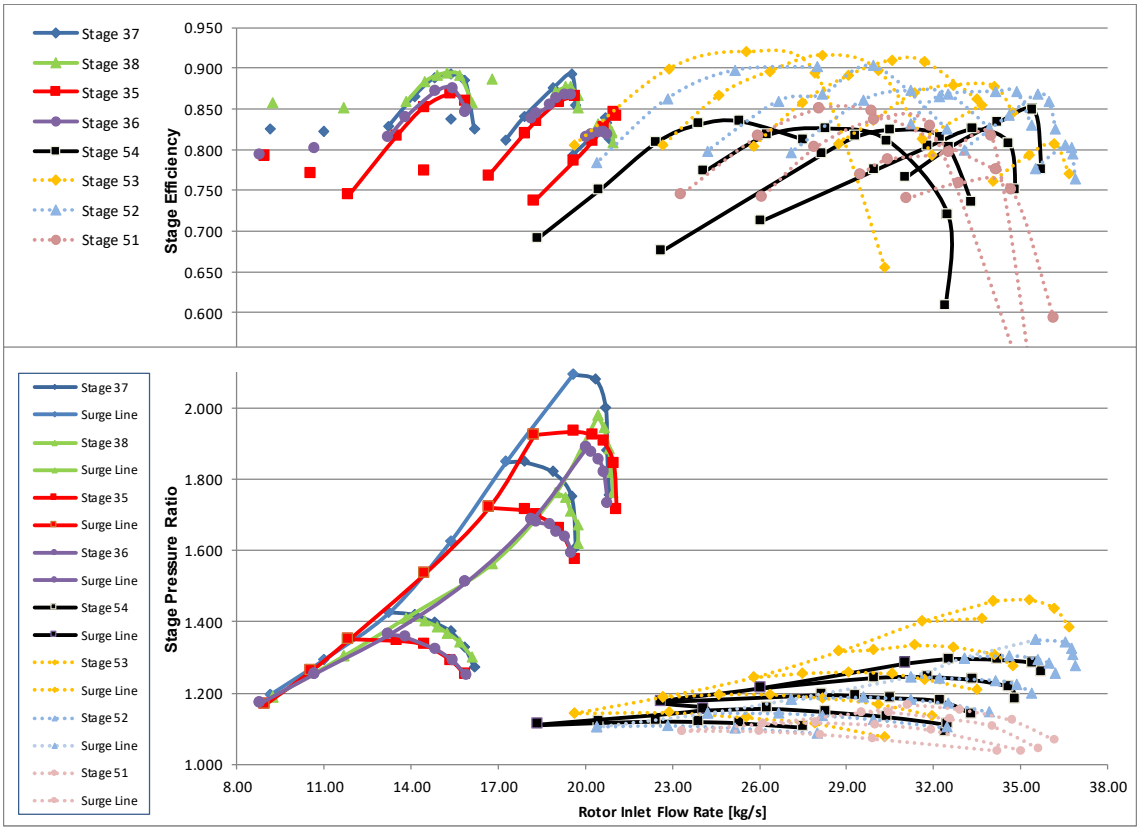

Figure 3-1: Off design performance comparison of Stages 35 to 38 vs Stages 51 to 54

Additionally, what can be seen in Figure 3-1 is the difference between the attainable peak pressure ratio of the various stages. Since Stages 35 to 38 were designed for a pressure-ratio of 1.82 to 2.05, we see that it towers above Stages 51 to 54 where the target pressure ratio was between 1.151 to 1.351. Table 3-2 shows the main design-point characteristics of these stages.

Table 3-2: Design point comparisons of Stage 35 to 38 versus 51 to 54

Stage #	35	36	37	38	51	52	53	54
Stage PR	1.82	1.82	2.05	2.05	1.151	1.251	1.351	1.201
Stage TR	1.225	1.227	1.270	1.269	1.047	1.074	1.100	1.061
Airflow [kg/s]	20.188	20.188	20.188	20.188	29.937	32.659	32.659	30.554
RPM	17188.700	17188.7	17188.7	17188.7	9167.3	9741.3	11459.2	8593.92

In Figure 3-2, we have plotted the 14 different combinations, also known as the NASA *14 middle stages*, of the NASA rotors 23 to 28 with stators 20 to 22. What these plots show is the impact of the various rotor and stator blade row combinations of different airfoil counts and aspect ratio.

Finally, Figure 3-3 shows the comparison between three selected NASA middle stages versus the performance results of Stages 35 to 38. This shows the relative difference in terms of performance impact of differing design-point characteristics.

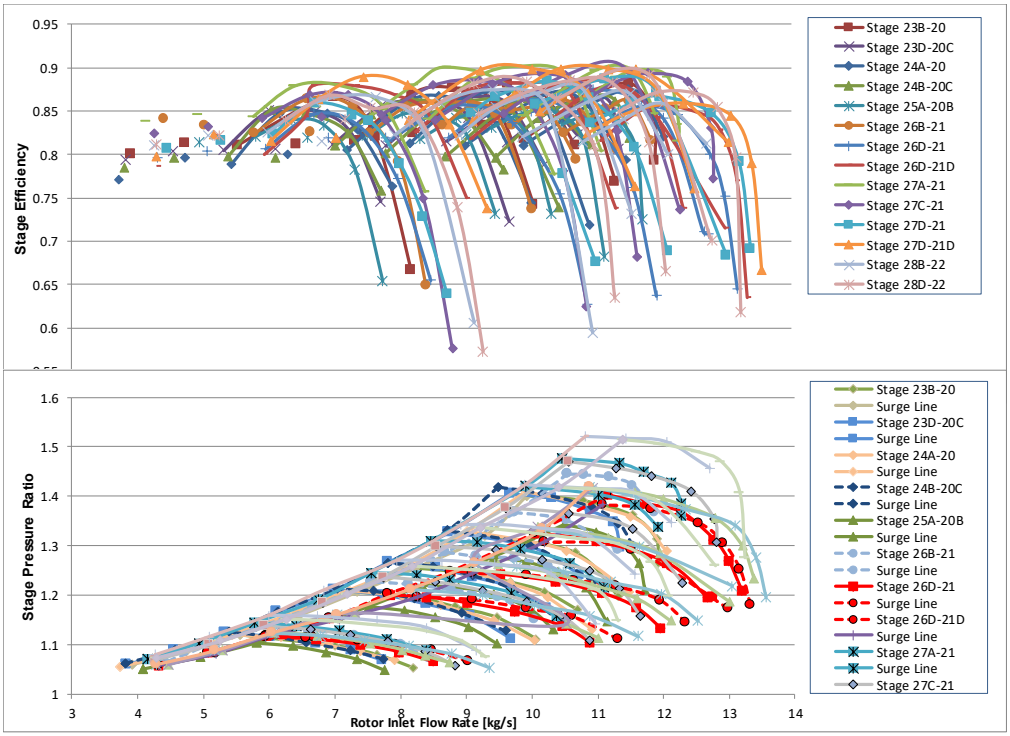

Figure 3-2: Off design performance comparison of the NASA 14 middle stages

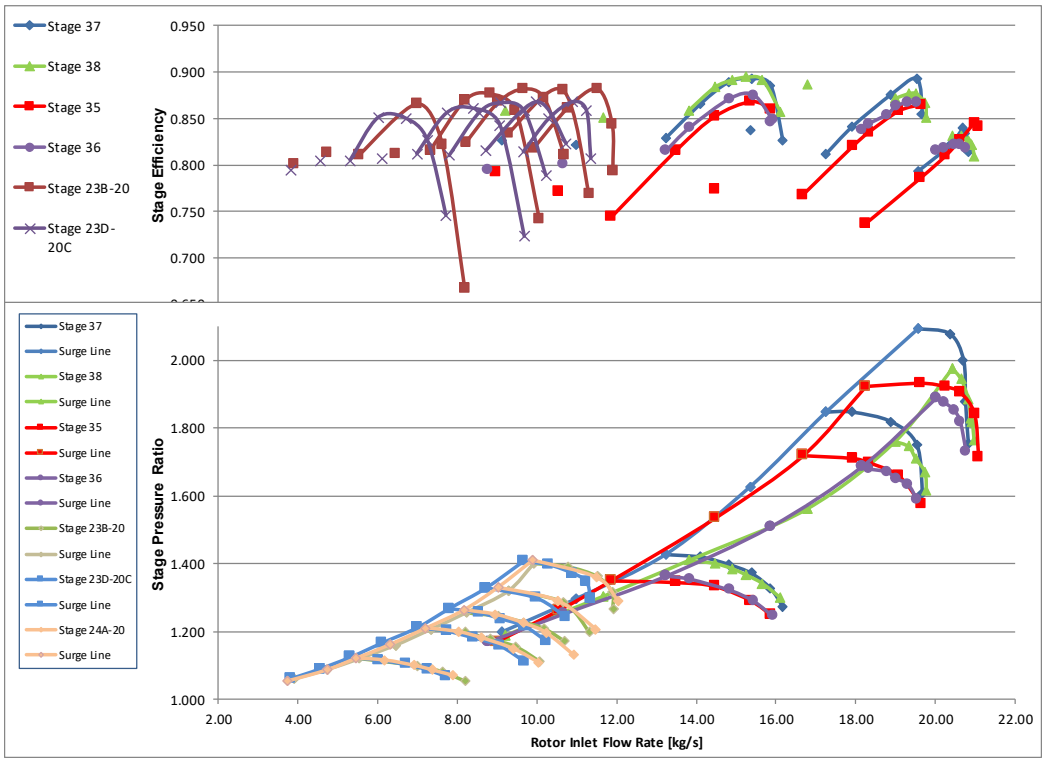

Figure 3-3: Off design performance of Stages 35 to 38 vs selected 14 Middle Stages

Based on the particular report or memo conclusions, and studying the various published axial compressor performance charts, a compressor aerodynamicist may be able to create tacit and deduced knowledge. With the information related to the geometric parameter variations tested, the compressor aerodynamicist may be able to surmise the theory or theories that dictate the off-design performance behavior that these variations create. For example, based on the observations and conclusions found in the report for the NASA 14 middle stages, one may infer the general behavior of rotor and stator count variations.

- "*At constant blade aspect ratio, rotors with more blades, and thus higher solidities, had lower mass flows than rotors with fewer blades and lower solidities. This reduction in flow is most likely caused by the greater blade blockage for the higher solidities.*" [73]
- "*Reducing rotor solidity also tended to increase the stall margin at all diffusion factors tested."* [73]
- "*No significant change in the minimum-efficiency difference occurred when stator solidity was lowered. Therefore, stator designs with fewer blades, and hence lower solidity, would mean lower fabrication cost without sacrificing performance.*" [73]

Freeman & Cumptsy also attempted to explain the performance characteristic of a two-stage compressor with a supersonic compressor [44]. Table 3-3 is an exercise in comparing the concluding remarks of Freeman & Cumpsty when applied to the plotted performance maps of the NASA transonic axial compressor Stage 35 to 38, shown in Figures 3-1 and 3-3. It should be noted that Freeman & Cumpsty's explanation was for a particular two-stage transonic axial compressor. Of the physical descriptions provided by them, i), iii), and iv) tend to fail when used to describe the four NASA transonic axial compressors investigated in this study.

Table 3-3: Freeman & Cumpsty explanations

	Freeman & Cumptsy conclusions	Conclusions when applied to the NASA compressor stages "35" to "38"
i.	*"As the speed is increased the pressure rise-flow rate characteristics become steeper and the range of flow between instability*	As the speed is increased the pressure rise-flow rate characteristics become slightly steeper only for Stages 36 and 38. Stages 35

	(leading to stall or surge) and choking narrows. At high rotational speed the flow range can vanish altogether." [44]	and 37, which have been described to having a relatively smaller aspect-ratio, do not show a steep behavior. *"At high rotational speed the flow range of Stages 35 and 37 are much more varied than Stages 36 and 38."* [89]
ii.	"*the maximum efficiency at each speed, which is often very good at part speeds, drops at or above the design speed.*" [44]	Explanation remains the same as per Freeman & Cumpsty
iii.	"*The line marking the boundary of stable operation, which is usually called the surge line, rises more steeply at high tip speeds*" [44]	The line marking the boundary of stable operation, which is usually called the surge line, does not seem to rise more steeply at high tip speeds.
iv.	"*At high speeds, when the rotor is choked, the peak efficiency is achieved at the highest pressure ratio achievable. As a result the range of pressure ratio between stall and the peak efficiency point narrows to vanish at high speed; to obtain reasonable efficiency it is necessary to operate near the stability limit.*" [44]	"*As a result the range of pressure ratio between stall and the peak efficiency point narrows to vanish at high speed; to obtain reasonable efficiency it is necessary to operate near the stability limit. This is true mainly for Stages 36 and 38. For Stages 35 and 37 it seems that the peak efficiency is more towards the choke than the stability limit.*" [89]

Despite having reported the consolidated performance maps, it was discovered that the majority of the cited documents did not contain the detailed radial measurements required to validate the proposed mean-line tuning methodology described in this investigation. Furthermore, these designs

span from the 1950's to the late 1990's, the design methodologies and analytical tools employed differed throughout the time period, and the airfoil shapes tested varied through the decades (from NACA series, to DCA, to MCA, and even diffusion controlled). Also, some of the compressor designs were designed for NASA research purposes by GE and PWA, thus introducing company-based design methodologies and biases using in-house analytical tools that have also evolved through the decades.

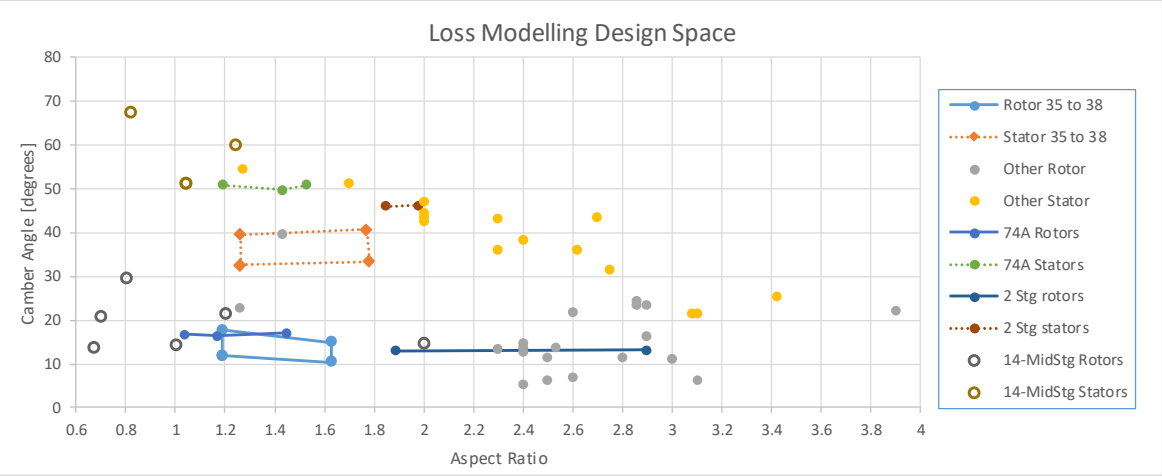

Figure 3-4: Comparison of compressor stage camber angle vs aspect ratio

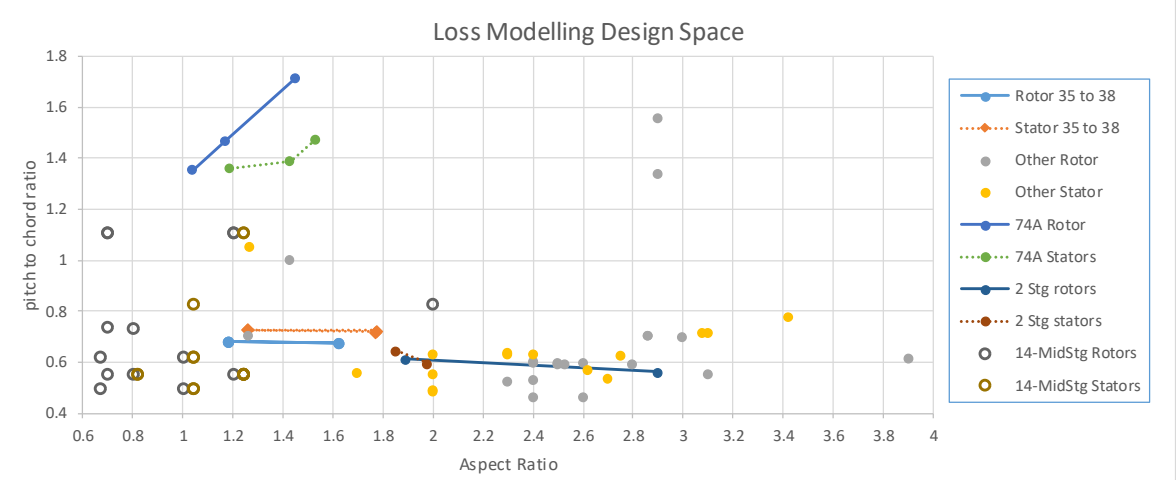

Figure 3-5: Comparison of compressor stage pitch-chord ratio vs aspect ratio

Another aspect to take note of with respect to the compressor test data, is the fact that it lacks the systemized approach, expected for design of experiment methodologies, to be able to ascertain which parameters are the dominant parameters for potential semi-empirical and physics-based loss formulations. Figures 3-4 and 3-5 represent the camber and pitch-to-chord ratio (respectively)

versus aspect ratio plots for both rotors and stators. As it can be seen, the tested axial flow compressors lack a systemized order of geometric variations.

Based on these facts, it was decided to focus on a set of compressor tests that were similar in regards of design and analysis methodologies, and represent, at best, modern compressor design[7]. To this end, four NASA-designed and tested single-stage transonic axial compressors were selected.

The four compressors identified as Stage 35 [14], Stage 36 [15], Stage 37 [16] and Stage 38 [17] were identified as the main focus of this investigation. These stages were selected due to the following facts:

- The four different rotors did not have any part-span shrouds, or *clappers*. This is a closer representation of modern engines as compared to earlier designs where the rotors required part-span shrouds to prevent vibratory issues. Also, compressor stages that employ part-span shrouds have a different blockage behavior when compared to their non-part-span shrouded counterpart.
- All compressor stages were designed and tested within the same 5-year time frame [89].
- The four compressors followed similar design and testing methodologies, design assumptions, and analytical tools [89].
- The rotor and stator blade rows were of MCA design [89]. Compared to NACA and DCA blade row profiles, MCA are considered to have better off-design performance for transonic conditions.
- Together, these compressors represent two pairs of design pressure ratio and aspect ratio. Based on Figures 3-1 and 3-3, we see that these stages have high pressure ratio (high work) capacity, and in terms of Figures 3-4 and 3-5, the design parameters are within the mapped design parameter space.

And finally, the experimental data was considered as extensive and complete, and included parameters such as: inlet and exit profiles for the various flow parameters, rotor and stator airfoil

[7] In terms of modern design, we wish to have blade row designs that have good off-design performance for transonic conditions, and do not have clappers, or part span shrouds, for vibratory damping.

geometry coordinates, and calculated performance parameters. Figure 3-6 shows the consolidated stage performance charts, and Figure 3-7 represents the geometric design space which is investigated. The reader is referred to the original NASA reports for images of the blade row designs.

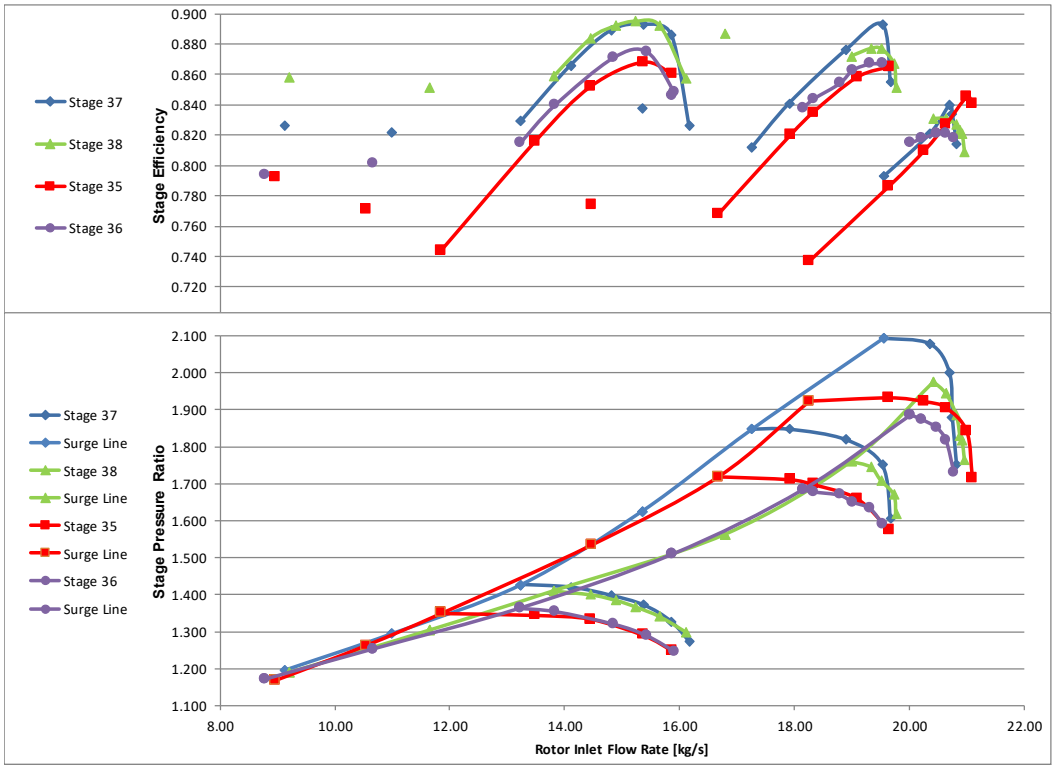

Figure 3-6: NASA stages 35 to 38 consolidated off-design stage performance charts

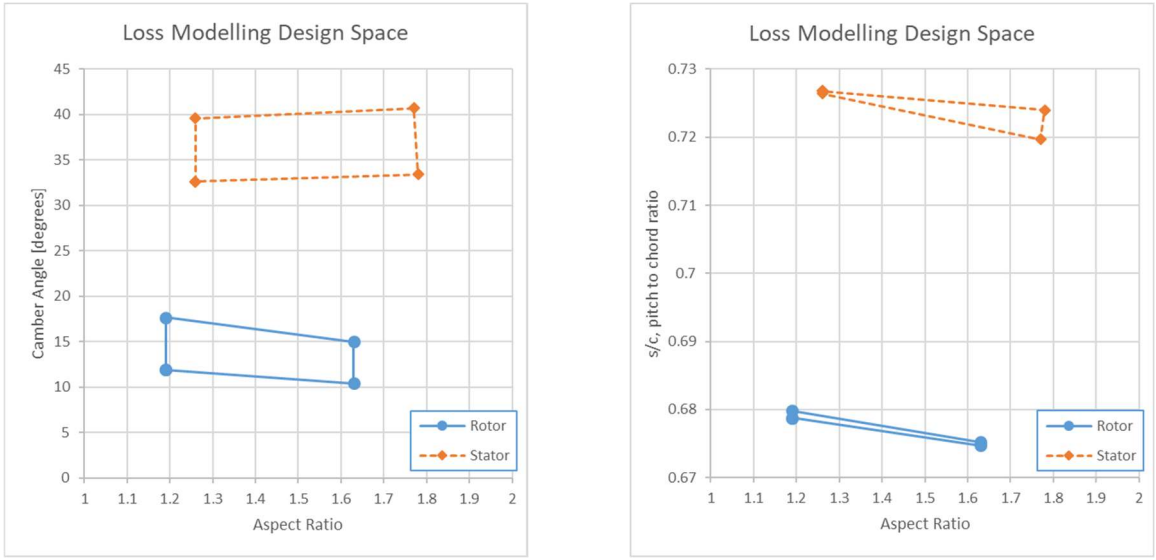

Figure 3-7: NASA stage 35 to 38 rotor and stator design space

In terms of the exact testing procedures, the following is a summary of the NASA reported procedures executed for Stages 35 to 38. The reader is referred to the original reports for complete details.

Rotor inlet measurements: the inlet mass flow was measured using a calibrated thin-plate orifice [89]. Two thermocouples were used to obtain the orifice temperature, and the orifice pressures were measured using calibrated pressure transducers [89]. An electronic speed counter with a magnetic pickup was used to measure the rotational speed of the rotor [89].

Radial measurements of total temperature, total pressure, and flow angle upstream of the rotor were taken by using a two-combination probe, and a wedge probe was used to measure the static pressure and flow angle [89]. Furthermore, static pressure taps were used on the inner and outer gas path walls at the rotor inlet [89].

Stator exit measurements: similar to the rotor inlet measurements, two-combination probes and wedge probes were used to measure the distributions of pressure, temperature, and flow angle [89]. The probes were traversed in both the circumferential and radial directions, and measurements were taken at nine radial positions [89]. Stator exit static pressure taps were also used on the inner and outer gas path walls [89].

Rotor exit values: no probes were used to measure the rotor exit flow parameters due to the close spacing between the rotor exit and the stator inlet [89]. The rotor exit temperatures, pressures, and flow angles were back-calculated from the stator exit along streamlines [89].

The rotor exit radial distribution of static pressure and flow angle were based on calculations using the continuity of mass flow and radial equilibrium formulas [89].

Flow measurements: for the various speed-line, the conditions measured were from the maximum mass flow rate to the near-stall conditions.

Finally, the NASA reports include the errors with respect to the test instrumentation as follows:

Parameter	**error**	**Unit**
Mass flow rate	± 0.3	Kg/sec
Rotative speed	± 30	RPM

Flow angle	± 1.0	Degrees
Temperature	± 0.6	Kelvin
Rotor-inlet (station 1) total pressure	± 0.01	N/cm^2
Rotor-inlet (station 1) static pressure	± 0.03	N/cm^2
Stator-outlet (station 3) total pressure	± 0.17	N/cm^2
Stator-outlet (station 3) static pressure	± 0.10	N/cm^2

These errors were taken into consideration when identifying target objectives for the various modelling approaches presented throughout this study.

3.2 Description of an axial compressor off-design mean-line model

To improve the multi-disciplinary nature of gas turbine design, NASA and various American gas turbine companies joined forces to create NPSS, the Numerical Propulsion System Simulation. In Europe, several companies, universities, and governments joined forces to create PROOSIS, the Propulsion Object Oriented Simulation Software. Inspired by these various programs and coupled with past experiences in industry, a modest initiative was undertaken by the present author to develop a Multi-Disciplinary Integrated Design System for Gas Turbines, MDIDS-GT[8], in which a design-point and an off-design mean-line model is found [112].

The axial compressor mean-line model used in this investigation, is an embedded software module that the author has developed as a R&D platform for gas turbine modeling. The software contains common User Interfaces (UI) for the design-point and off-design mean-line analysis modes for compressors and turbines (Figures 3-8a and 3-8b). Comparable mean-line codes have been developed at the University of Cincinnati [9], Lund University [32], and at NASA [8] .

[8] This specialized engineering software, which supports research and development in gas turbine modeling, design, and analysis, has also been used to teach the topic of gas turbines at both the bachelor and masters levels as part of Polytechnique Montreal's and Carleton University's engineering curriculum.

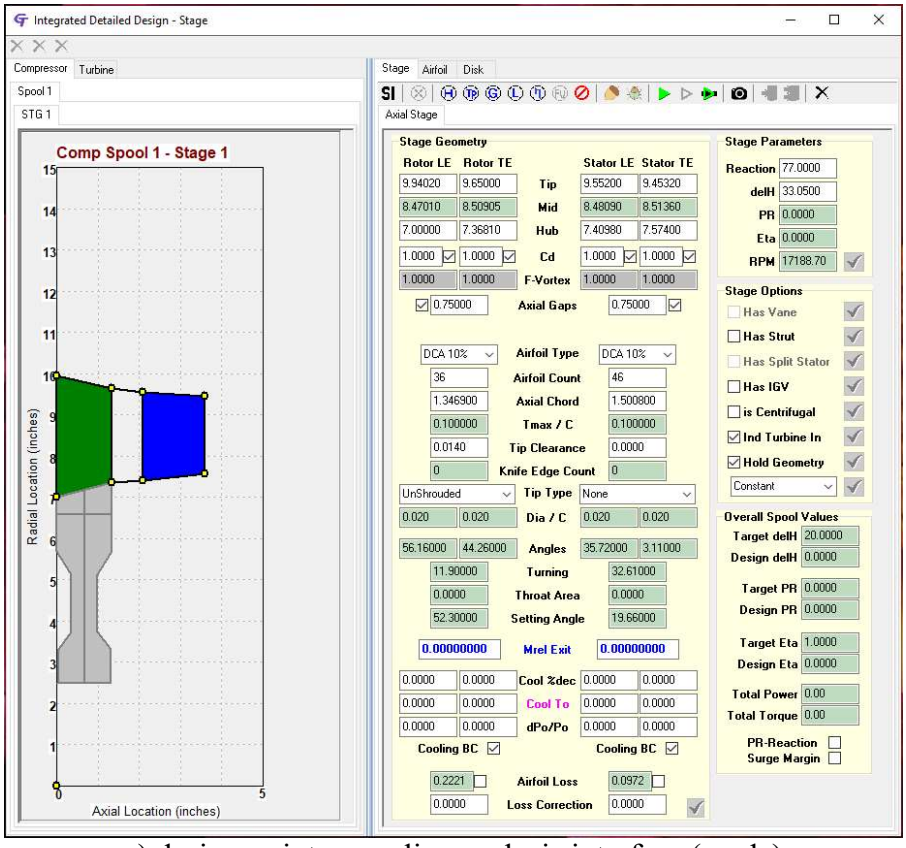

a) design-point mean-line analysis interface (mode)

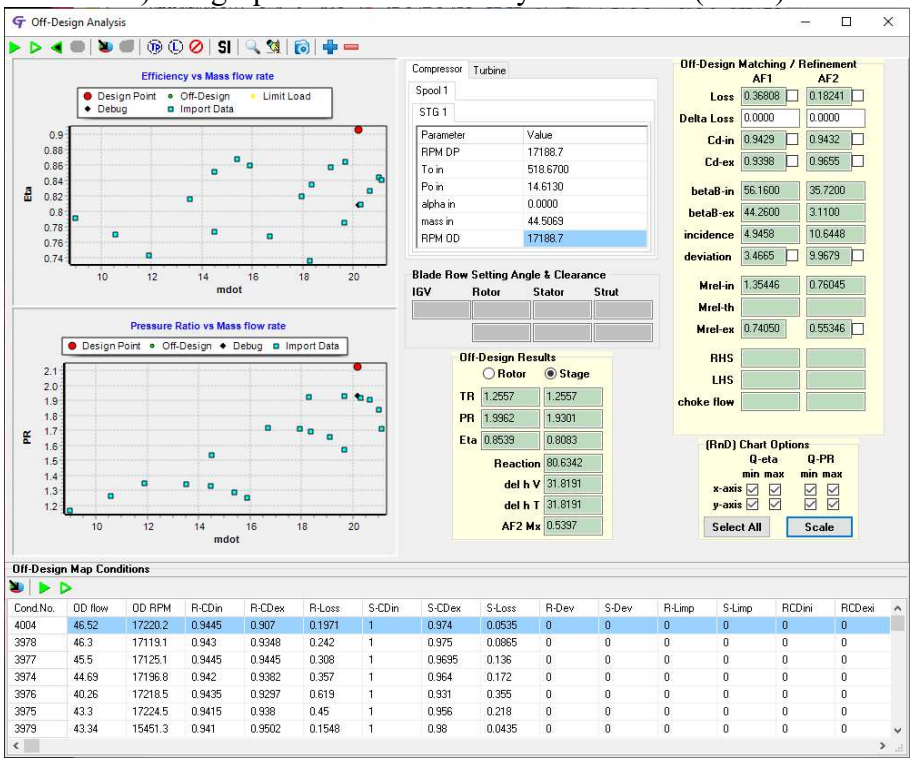

b) off-design mean-line analysis interface (mode)

Figure 3-8: MDIDS-GT mean-line module user interfaces [112]

Figure 3-9 describes the steps undertaken to create the various transonic axial compressor stage test cases. As part of the design-point mean-line preparation to execute the off-design compressor test case analysis, let us describe the main steps of the software which supports this investigation.

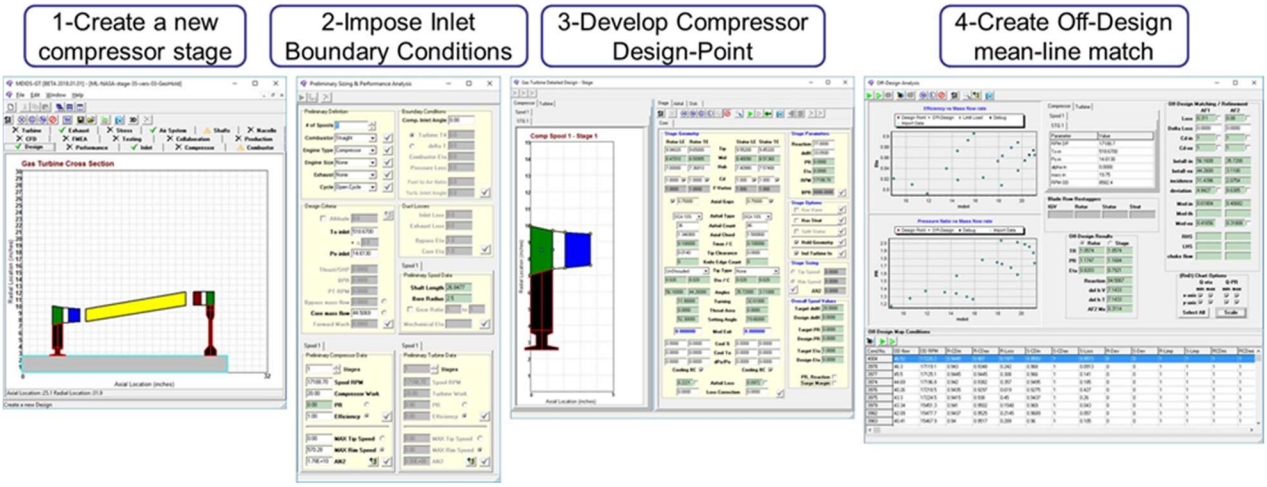

Figure 3-9: MDIDS-GT high-level design-point to off-design creation process

In all, there are three main steps in the process of creating a compressor validation case as follows:

1) The *new* button of the software executable creates the main design window. Then, the *engine type* is selected to be *compressor* and the values of the compressor inlet conditions, spool RPM, and basic geometric parameters are entered.

2) In *STEP 2: Design Point Analysis*, the details of the compressor stage such as blade row corner points, blockage factors, airfoil type, and loss correction are entered. The DP mean-line model can then be executed, where the resulting mean-line analysis flow field and loss decomposition are displayed in a tabular format. Appendix E describes the rotor and stator mean-line geometry and boundary conditions, extracted from the various NASA reports, used to develop the NASA Stages 35 to 38 mean-line models in MDIDS-GT.

3) Once the DP ML model is considered satisfactory, *STEP 3: Off-design analysis* can be executed. This step gives access to the standardized off-design window, as shown in Figure 3-10. Further details with respect to the software use and functionalities can be found in Refs. [112] and [113] as well as in

(https://sites.google.com/site/mdidsgt/home/softwareresources)

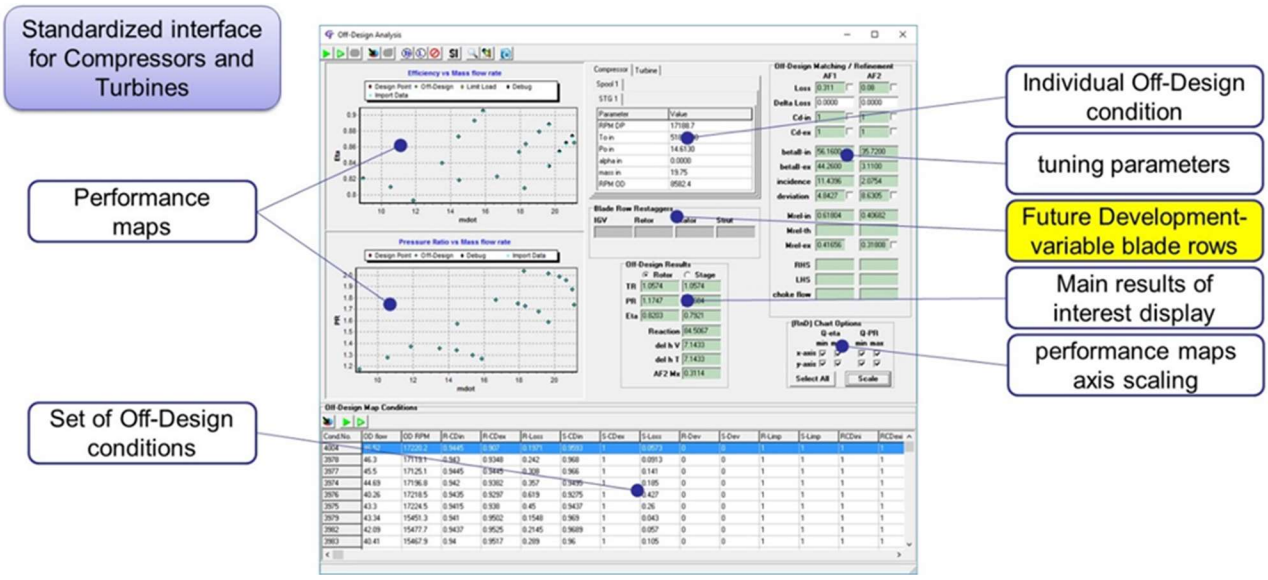

Figure 3-10: MDIDS-GT standardized off-design window

The off-design axial compressor mean-line model, which automatically and seamlessly inherits its geometry from the design-point mean-line, is run in either a *predictive* mode or a *tuned* mode based on the various options available. The interface includes an off-design conditions display section which loads a formatted file of off-design conditions, tuning values, and flags that control the use or not of the tuning values. These flags, shown in Figure 3-11, can be used to turn on or off the various loss components in the compressor loss model.

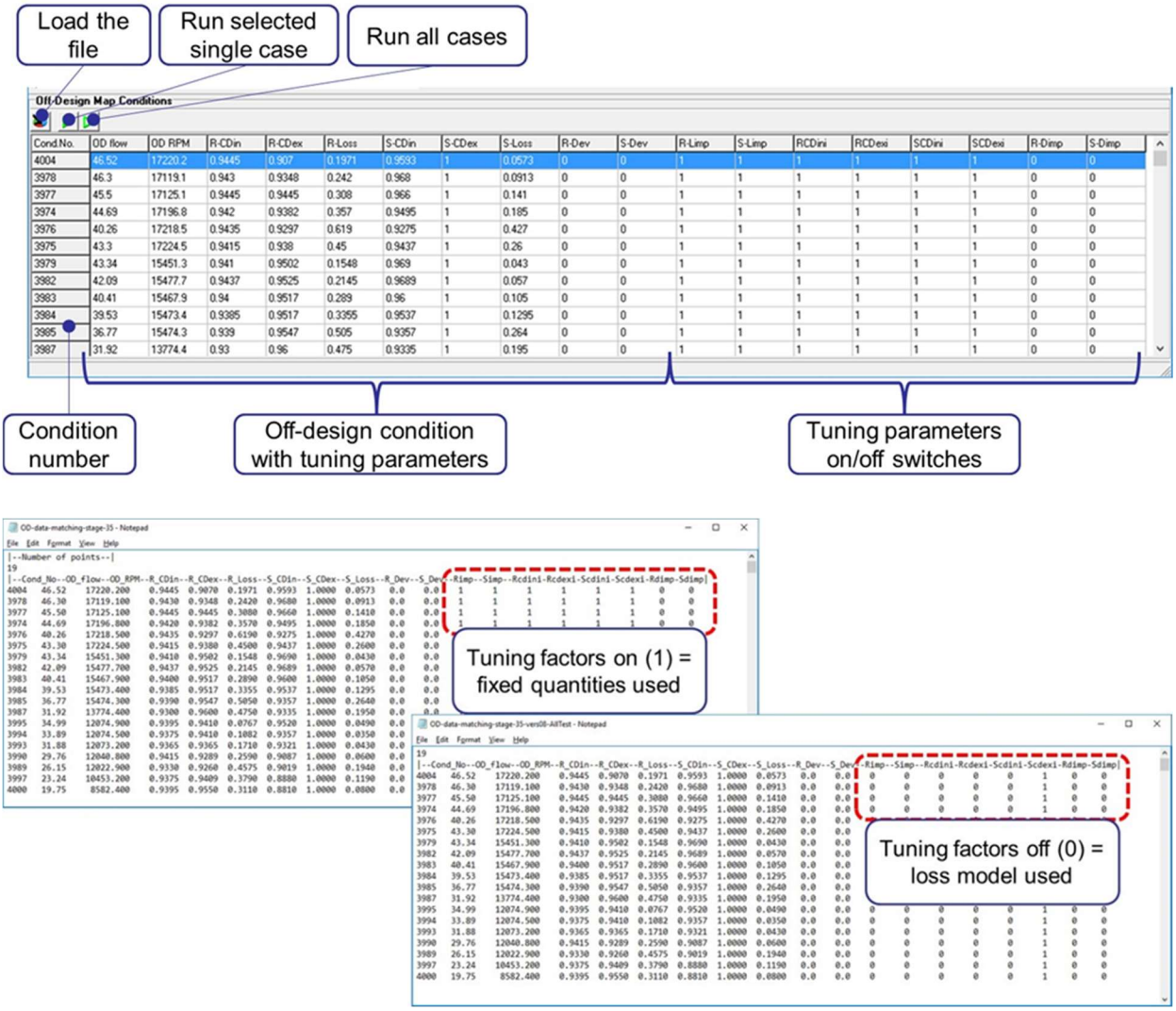

Figure 3-11: MDIDS-GT interface & formatted input file for off-design conditions

Figure 3-12 represents the generic axial compressor mean-line model nomenclature used in the software. The rotor is defined by the produced work, pressure ratio, and efficiency, whereas the stage is defined by the stage pressure-ratio and efficiency. The location of the inlet and exit

calculation planes are defined as 1 to 4 and are circled. At each calculation plane the absolute & relative velocity triangles and flow properties are calculated.

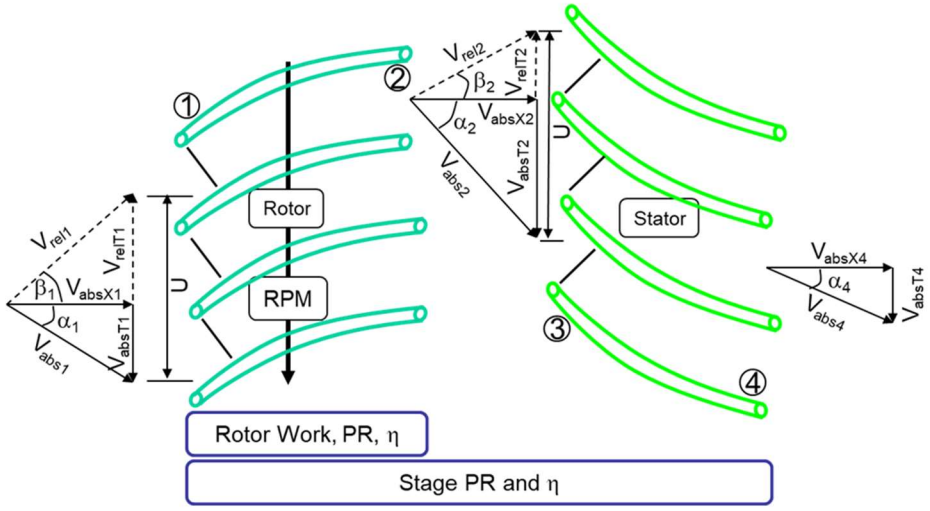

Figure 3-12: Axial compressor stage nomenclature

Figure 3-13 shows the mean-line model decomposition of an axial compressor stage. The stage is divided into three blade rows defined as:

- AF1 for the rotor
- AF2 for the stator
- and AF3 for the strut if any

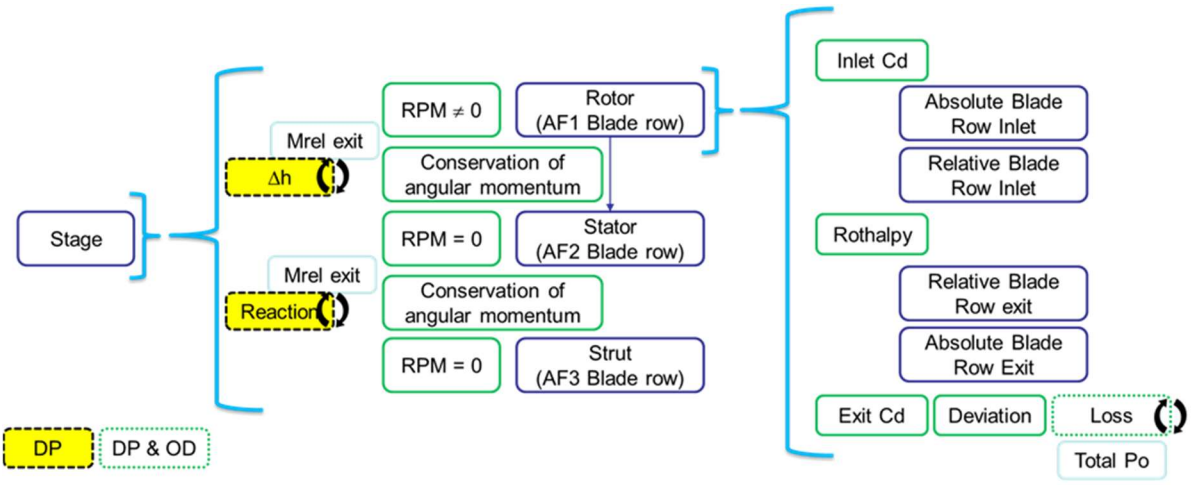

Figure 3-13: Mean-line stage blade-row nomenclature

The mean-line model uses a generic blade row definition for the three airfoil types. Each blade row is decomposed into inlet and exit planes. Each inlet and exit plane has a blockage factor C_D that may be imposed to tune the results, or use a predictive formula. The exit plane calculations additionally have the functionality to calculate the deviation angle based on a predictive formula or tuned by imposing a value.

As indicated in Figure 3-13, for the design-point analysis mode the blade row exit relative Mach numbers are iterated until the imposed rotor work and stage reaction are converged upon, and the blade row losses are iterated upon until an acceptable error difference is achieved. In the off-design analysis mode, only the blade row losses are required to be iterated until they converge to an imposed error difference. This is due to the fact that the off-design geometry is inherited from the final results of the design-point analysis, and it is held fixed. For both the design-point and off-design modes, the blade row pressure losses are calculated by an internal loss model or imposed to tune to existing test data.

Additionally, the following two major assumptions are employed in the axial compressor mean-line model: 1) the stator blade row is adiabatic with the absolute stagnation (total) temperature across the stator equal to that of the rotor exit condition, and 2) the compressor stage performance is represented by the velocity triangles measured at the geometric mid-span of the blade rows in-lieu of the *equal area* mid-section.

The off-design mean-line mode is considered to have constant inlet boundary conditions of total temperature, total pressure, and absolute flow angle. Furthermore, only a change in the inlet mass flow rate and rotor RPM are required to create the off-design performance behavior.

The off-design blade row inlet and exit conditions are calculated as follows:

Blade row inlet condition: The absolute total (stagnation) inlet flow properties are first solved. The inlet conditions are derived from either the stage inlet boundary conditions, or that of the preceding blade row exit conditions. Assuming that there are no bleed or purge flows at the inlet plane, and that there are no total pressure losses between the exit of a preceding blade row to the inlet of the current blade row, the inlet total (stagnation) temperature and pressure are defined as:

If the stage has inlet boundary conditions, then

$$T_{o1} = T_{inletBC} \quad \textbf{(1)}$$

$$P_{o1} = P_{inletBC} \quad \textbf{(2)}$$

Else, if the blade row has a preceding stage blade row then

$$T_{o1} = T_{o4}\text{, of previous stage} \quad \textbf{(3)}$$

$$P_{o1} = P_{o4}\text{, of previous stage} \quad \textbf{(4)}$$

Else, transfer the exit condition of the preceding blade row as the inlet conditions of the current blade row. Additionally, between the exit plane of one blade row to the inlet plane of the next blade row, the conservation of angular momentum must be satisfied. Taking into consideration bleed flows we will obtain the following 1D equation at steady state:

If the blade row has a preceding stage blade row, then

$$\dot{m}_1 r_{m1} V_{absT1} = \dot{m}_4 r_{m4} V_{absT4} \,|\text{of previous stage} \quad \textbf{(5)}$$

Else, if the blade row has a preceding blade row then

$$\dot{m}_3 r_{m3} V_{absT3} = \dot{m}_2 r_{m2} V_{absT2} \quad \textbf{(6)}$$

Where $\dot{m}$ is the mass flow rate, r_m is the mean geometric radius of the blade row span, and V_{absT} is the absolute tangential velocity. An inlet Mach number, referred to the absolute velocity, must be found to resolve the remaining inlet flow properties. Assuming an initial value for M_{abs1} we get

$$T_{s1} = \frac{T_{o1}}{\left[1 + \frac{(\gamma - 1)}{2} M_{abs1}^2\right]} \quad \textbf{(7)}$$

$$P_{s1} = \frac{P_{o1}}{\left[1 + \frac{(\gamma - 1)}{2} M_{abs1}^2\right]^{\gamma/(\gamma-1)}} \quad \textbf{(8)}$$

$$V_{abs1} = M_{abs1}\sqrt{\left(\gamma R_g T_{s1}\right)} \qquad \textbf{(9)}$$

$$V_{absX1} = \frac{\dot{m}_1 R_g T_{s1}}{C_D A_1 P_{s1}} \qquad \textbf{(10)}$$

Knowing that

$$V_{absT1}^2 = V_{abs1}^2 - V_{absX1}^2 \qquad \textbf{(11)}$$

a Newton-Raphson iterative scheme can be used to iterate on a value of M_{abs1} such that the velocity relationship of Eq. 11 is satisfied. To be more specific, the Newton-Raphson functions of F(x) and F'(x), where x = M_{abs1} in this research context, are as follows:

$$F(x) = V_{abs1}^2 - V_{absX1}^2 - V_{absT1}^2 \qquad \textbf{(12)}$$

$$\therefore F(x) = \left(\frac{\dot{m}_1 R_g T_{o1}}{P_{o1} C_D A_1}\right)^2 \left[1 + \frac{\gamma - 1}{2} x^2\right]^{\frac{2}{\gamma - 1}} + V_{absT1}^2 - \gamma R_g T_{o1} x^2 \Big/ \left[1 + \frac{\gamma - 1}{2} x^2\right] \qquad \textbf{(13)}$$

and its derivative will become

$$F'(x) = 2x\left(\frac{\dot{m} R_g T_{o1}}{P_{o1} C_D A_1}\right)^2 \left[1 + \frac{\gamma - 1}{2} x^2\right]^{\frac{3-\gamma}{\gamma - 1}} - \gamma R_g T_{o1}\left\{\frac{2x}{1 + \frac{\gamma - 1}{2} x^2} - \frac{(\gamma - 1)x^2}{\left(1 + \frac{\gamma - 1}{2} x^2\right)^2}\right\} \qquad \textbf{(14)}$$

Once F(x) has converged to a pre-established tolerance, equations (7) to (10) are repeated and the absolute inlet flow angle is found as

$$\alpha_1 = \tan^{-1}\left(V_{absT1} \Big/ V_{absX1}\right) \qquad \textbf{(15)}$$

NOTE: If the inlet flow angle is imposed, then a slightly modified formulation of Eq. 13 and 14 is used.

The absolute values are then converted to the relative flow values as follows:

$$V_{relT1} = V_{absT1} - U_{m1} \quad \textbf{(16)}$$

$$V_{rel1} = \sqrt{\left(V_{relT1}^2 + V_{absX1}^2\right)} \quad \textbf{(17)}$$

$$M_{rel1} = V_{rel1} \Big/ \sqrt{\left(\gamma R_g T_{s1}\right)} \quad \textbf{(18)}$$

$$\beta_1 = \tan^{-1}\left(V_{relT1} \Big/ V_{absX1}\right) \quad \textbf{(19)}$$

$$T_{orel1} = T_{s1}\left[1 + \frac{\gamma - 1}{2} M_{rel1}^2\right] \quad \textbf{(20)}$$

$$P_{orel1} = P_{s1}\left[1 + \frac{\gamma - 1}{2} M_{rel1}^2\right]^{\frac{\gamma - 1}{\gamma}} \quad \textbf{(21)}$$

The off-design incidence is then calculated as the difference between the relative inlet flow angle and the airfoil metal angle at the leading edge.

$$\boldsymbol{inc = \beta_{flow} - \beta_{metal}} \quad \textbf{(22)}$$

Blade row exit condition: following a similar pattern as that of the inlet flow calculations, the relative flow properties are first calculated. The mean-line code calculates the relative exit flow angle, which is based on the addition of the deviation angle and the fixed blade angle at the trailing edge as follows

$$\boldsymbol{\beta_{flow} = \delta + \beta_{metal}} \quad \textbf{(23)}$$

From the conservation of rothalpy the exit relative total (stagnation) temperature is found as follows, where C_p is the specific heat at constant pressure and T_{or} is the relative total (stagnation) temperature

$$C_{P2}T_{or2} - C_{P1}T_{or1} = \frac{1}{2}U_{m2}^2 - \frac{1}{2}U_{m1}^2 \qquad \textbf{(24)}$$

The mid-section peripheral speeds U_m are calculated as

$$U_{m1} = \left(2\pi r_{m1} RPM\right) \Big/ 60 \qquad \textbf{(25)}$$

$$U_{m2} = \left(2\pi r_{m2} RPM\right) \Big/ 60 \qquad \textbf{(26)}$$

Furthermore, if the inlet and exit mid-section radii are not equal, an isentropic pressure correction is used to find the modified pressure P_{0rel}' as follows

$$\left(\frac{P_{0rel1}}{P_{0rel}^{'}}\right) = \left\{1 + \frac{\gamma+1}{2}\frac{(\omega r_2)^2}{\gamma R_g T_{01}}\left[1 - \left(\frac{r_{m1}}{r_{m2}}\right)^2\right]\right\}^{\gamma/\gamma-1} \qquad \textbf{(27)}$$

Where $\omega = U_{m1}/r_{m1}$. The relative total exit pressure is calculated based on the corrected relative pressure and a loss value Y_{total}. The exit pressure is calculated by the following two formulas:

$$Y_{total} = \frac{P_{orel}^{'} - P_{orel2}}{P_{orel2} - P_{s2}} \qquad \textbf{(28)}$$

$$P_{orel2} = \frac{P_{orel}^{'}}{\left\{1 + Y_{total} - \dfrac{Y_{total}}{\left[1 + \dfrac{(\gamma-1)}{2}M_{rel2}^2\right]^{\gamma/(\gamma-1)}}\right\}} \qquad \textbf{(29)}$$

A relative exit Mach number must be found to resolve the remaining exit flow properties. Assuming an initial value for M_{rel2} we get

$$T_{s2} = \frac{T_{orel2}}{\left[1 + \frac{(\gamma - 1)}{2} M_{rel2}^2\right]} \quad \textbf{(30)}$$

$$P_{s2} = \frac{P_{orel2}}{\left[1 + \frac{(\gamma - 1)}{2} M_{rel2}^2\right]^{\gamma/(\gamma-1)}} \quad \textbf{(31)}$$

$$V_{rel2} = M_{rel2}\sqrt{(\gamma R_g T_{s2})} \quad \textbf{(32)}$$

$$V_{relX2} = V_{absX2} = \frac{\dot{m}_2 R_g T_{s2}}{C_D A_2 P_{s2}} \quad \textbf{(33)}$$

The Newton-Raphson scheme mentioned above is repeated (swapping absolute terms for relative terms) to iterate on a value of M_{rel2} such that the following relative velocity relationship is satisfied.

$$V_{relT2}^2 = V_{rel2}^2 - V_{absX2}^2 \quad \textbf{(34)}$$

Once M_{rel2} has converged to a pre-established tolerance, equations (30) to (33) are repeated, and the absolute flow properties are then calculated.

The set of inlet and exit blade row calculations are repeated for the stator, and strut blade row if any. Once all of the blade rows have been calculated, the rotor specific work (Δh) and stage reaction (λ) are calculated as follows

$$\Delta h = C_{P2} T_{o2} - C_{P1} T_{o1} \quad \textbf{(35)}$$

$$\lambda = \frac{P_{s2} - P_{s1}}{P_{s4} - P_{s1}} \quad \textbf{(36)}$$

As a final convergence check, the total enthalpy work is compared to Euler's turbomachinery work formula defined as

$$\Delta h = U_{m2} V_{absT2} - U_{m1} V_{absT1} \quad \textbf{(37)}$$

The mean-line model described contains four tuning parameters that can be either imposed or use an internal correlation. These tuning factors are the inlet and exit blockage factors (C_{Din} and C_{Dex}), the blade row loss (Y_{total}), and the deviation angle (δ).

3.3 Loss model development approach

Mean-line loss models are basically loss data plotted against various geometric parameters. Historically, with respect to axial compressors, the NACA series of cascade tests [114] were the first and only publicly available data that represented an attempt to develop performance curves of a particular compressor airfoil shape based on the systematic variation of geometric and flow parameters.

Additionally, the NACA series of tests were based on the NACA series of compressor blade shapes, which were tested in a linear, subsonic, cascade, of a particular span. As time passed, different shapes were introduced (for example DCA, MCA, and diffusion controlled) and different loss mechanisms were analyzed (for example shock structures, span effects, clearance effects, and rotor-stator wake interactions). Unfortunately, despite the myriad of tests, none were truly children of a particular parent. Due to time and cost constraints, most, if not all testing were constrained to the specific geometry of interest and qualitatively compared to previous tests.

The life-cycle of a loss model starts off with data. This data is created through two avenues 1) physical test data or 2) analytical data. Regardless of the approach taken, the backbone of the loss model is based on a variation of geometric and flow parameters. It is left to each individual engineer to attempt to describe how these parameters physically interact with respect to 1) a theoretical notion of the flow physics or 2) an interpretation of the flow physics from measured flow data. The end objective of the loss model life-cycle is to be able to predict the behavior of the particular test undertaken (this may be considered as calibration curves) and predict the behavior of compressors which have been designed within the loss model data boundaries (this may be considered as predictive curves). Since loss models are based on data, one will need to understand how this data is consumed and processed.

Loss models start off as a cloud of data on graphs, with an attempt to find visible trends by comparing the value of interest with either geometric and / or flow parameters. Figure 3-14 is an

example of the percent blade row loss (in decimal format) versus the ratio of inlet to exit blade row Mach Numbers. The next step is to interpret the trend of the data plotted, if any exist.

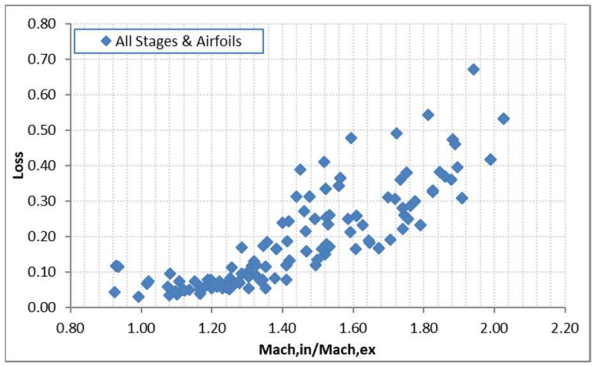

Figure 3-14: Sampling of blade row loss versus inlet to exit Mach number ratio

Data interpretation is both subjective and contentious. No one observer will see the same trend. The interpretation will depend on two fundamental factors with respect to data analysis:

1) The **depth** of the interpretation taken by the researcher; in other words, what level of data dissection the researcher will undertake to understand the data
2) The **bias** of the researcher; in other words, the subjective or opinionated nature of the selection and choice of parameters to execute the data dissection.

Figure 3-15 shows examples of the various potential interpretations of the data.

A) Simple curve fit: The simplest of all data reduction steps is to simply plot the data, based on a set of desired parameters, and pass the best fit curve through it. The weakness of this approach is that, except for the values used to plot the data, no true insight has been extracted from the data.

B) Bounded by curves: An improved version of the simple curve fit is to have the data bounded by two curve fits for the minimum and maximum sets of data that surrounds the cloud of data plotted. The weakness of this approach is similar to that of the simple curve fit. However, a minor improvement lies in the fact that one may be able to interpolate between the minimum and maximum values.

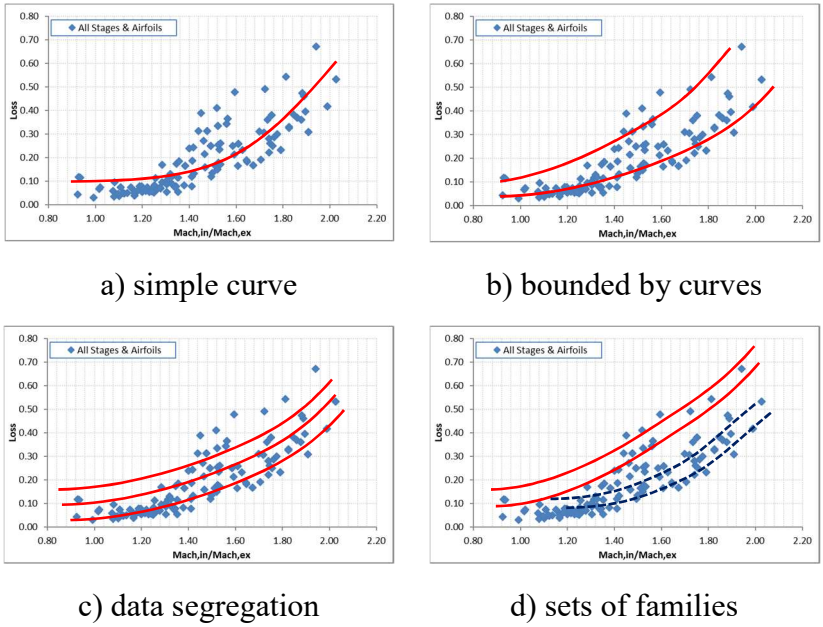

a) simple curve b) bounded by curves

c) data segregation d) sets of families

Figure 3-15: Trend analysis of blade row loss versus inlet to exit Mach number ratio

C) Data Segregation: At this point of the data reduction process, data segregation is an attempt to find a third parameter to better describe the data behavior. This is usually done between two or three sets of different graphs in an attempt to find which parameters collapse the data into sets of curves that may be individually distinguished. Plots that employ data segregation provide an improved insight into the behavior of the parameters.

D) Sets of families: Data segregation may be further improved by identifying a fourth parameter to distinguish further the data behavior into sets of families of segregated data

Once the data has been interpreted into trend curves, the next step is to be able to convert these trends into a physical explanation by creating formulas to be able to collapse the data into unique, identifiable curves. These curves are then used to create equations, either for hand calculations or for the digitized environment. For example, Microsoft Excel supplies various trend line options, from linear to exponential, and will also display the equation used to generate the trend line.

Curve fitting alone may not be sufficient to find, discover, or even uncover trends. Some data behaviors are not explicitly shown based on a simple set of parameter selection. The data itself needs to be processed to create the trends. With respect to a *2D* plot of **x** and **y**, both **x** and **y** data may be processed through equations to reveal trends. The goal of applying formulas to the data as pre-conditioners is to be able to collapse the data onto itself to further extract distinguishable data

behaviors. It is the choice of these pre-conditioned formulas that introduce the physics- or engineering- based notions of compressor aerodynamics. Any new formula introduced in this thesis is based on the data reduction methodology described above.

3.4 CFD results for Rotor 37 using ANSYS CFX 16.x

To aid in the development of correlations to describe flow mechanisms, *3D* CFD was executed for NASA Rotor 37. Appendix C shows the qualitative CFD results using ANSYS CFX, which were executed for this investigation. Both high and low mass flow rate results of the 100, 90, 80, 70, 60, and 50% speed-lines are shown. What can be observed per speed-line is as follows:

- **100% Speed-line:** at the low mass flow rate a resemblance of a typical normal shock is observable. At the high mass flow rate, we encounter a near axial shock line.
- **90% Speed-line:** at the low mass flow rate a resemblance of a normal shock is still observable. It may be argued that at the high mass flow rate the previous near axial shock line is diminishing, or changing its axial strength in terms of direction.
- **80% Speed-line:** at the low mass flow rate, the shock structure seems to be standing perpendicular to the airfoil surface. At the high mass flow rate, we encounter a dual shock system.
- **70% Speed-line:** at the low mass flow rate, as expected, we do not encounter an inlet shock. Surprisingly, what we encounter at the high mass flow rate is a potential dual shock system. A shock region at the leading edge, and a shock structure close to the trailing edge.
- **60% Speed-line:** at the low mass flow rate, as expected, we do not encounter an inlet shock. Surprisingly, what we encounter at the high mass flow rate is a shock structure close to the trailing edge.
- **50% Speed-line:** the results at this speed-line are similar to that of the 60% speed-line.

The CFD results, presented in Appendix C, illustrates how the axial compressor shock structure varies through the off-design conditions. This is, in itself, a subject that may be treated on its own. For the purposes and scope of this current mean-line loss modeling investigation, it was consciously decided to pursue the development of loss model correlations that implicitly caters for the rotor shock loss by using the mean-line model relative rotor inlet Mach number as a parameter.

Another aspect that was qualitatively reviewed was the blockage development at the trailing edge of the rotor. What can be observed per speed-line is as follows:

- **100% Speed-line:** at the low mass flow rate we see a zone of higher Mach number in the rotor tip clearance region. Additionally, we see low momentum flow (identified by the low Mach numbers in blue) at the rotor exit. At the high mass flow rate, we encounter a significant low Mach number region at the rotor exit, an indication of a change of blockage.
- **90% Speed-line:** at the low mass flow rate we still retain a zone of higher Mach number in the rotor tip clearance region. With respect to blockage, visually it seems that the high mass flow rate may have a slightly larger low Mach number region than its low mass flow rate condition.
- **80% Speed-line:** the results at this speed-line resembles that of the 90% speed-line
- **70% Speed-line:** at the low mass flow rate, there is a significant region of low Mach number. Whereas we find a much smaller low Mach number region in the high mass flow rate condition.
- **60% Speed-line:** the results at this speed-line resembles that of the 70% speed-line.
- **50% Speed-line:** the results at this speed-line resembles that of the 70% speed-line.

3.5 Off-design mean-line model tuning methodology

In the public literature, the off-design axial compressor is tuned to match test data by modifying the inlet and exit blockages. These values are usually based on experience stemming from the design-point modelling, and remain fixed for the off-design analysis at values of 0.97 or 0.98. Also, the off-design deviation angle remains fixed, and the main formula used is Carter's rule.

Based on the off-design mean-line model description and modelling recipe of the previous chapter, it was found that the results of the off-design mean-line model did not properly, or accurately, predict the off-design performance of four well documented NASA transonic axial compressors. A modified tuning approach, manually executed using trial-and-error data reduction, was created that was able to produce a *near-exact* match of the NASA-reported off-design performance maps.

The modified tuning process for a single-stage axial compressor, based on the off-design mean-line model mid-span based values, was executed as follows:

1) Adjust the rotor inlet blockage factor (imposed value) until the measured mid-span absolute inlet flow angle is matched.
2) Change the rotor deviation (imposed value) until the NASA reported back-calculated mid-span rotor exit flow angle is matched.
3) Modify the rotor loss (imposed value) until the rotor pressure ratio is matched.
4) Vary the rotor exit blockage factor (imposed value) until the rotor temperature ratio is matched.
5) Repeat steps 3 & 4 until the rotor pressure and temperature ratio converge to the test data.

NOTE: Steps 3 to 5 may also be achieved by matching the combination of pressure ratio and efficiency in lieu of the pressure and temperature ratio combination.

6) Adjust the stator inlet blockage factor (imposed value) until the NASA reported back-calculated mid-span stator inlet flow angle is matched.
7) Modify the stator deviation (imposed value) until the measured mid-span stator absolute exit angle is matched.
8) Change the stator loss (imposed value) until the stage efficiency, or the stage pressure ratio, is matched.
9) Vary the stator exit blockage factor (imposed value) to match the mid-span stator exit Mach number.

Tables D-1 to D-4, found in Appendix D, list the imposed values resulting from the modified tuning process. These tables have been provided for those researchers that are interested in recreating the results.

Rotor inlet blockage factor: The rotor inlet blockage factor was varied to be able to match the measured mid-span inlet flow angle. The imposed blockage factors fall within a range of approximately 0.92 to 0.94. This is clearly less than the value of 0.98 used by Veres [8].

Stator inlet blockage factor: The stator inlet blockage factor was adjusted to be able to match the back-calculated mid-span inlet flow angle. The stator inlet blockage factors required a significantly lower number than 0.98. For a few low-end speed-line conditions, the value of C_{Din} was less than 0.90 and had reached a low value of approximately 0.82.

Rotor and Stator deviation: Carter's deviation rule is based on the assumption that the deviation angle varies only slightly at off-design conditions [115]. A review of the rotor data at the mid-span tends to support this assumption. However, this assumption did not stand true for the measured stator deviation which varied for more than 8°.

While matching rotor blockage factors, it was discovered that an accurate match of the NASA calculated rotor deviation angle had a noticeable impact on the resulting rotor C_{Dex} values, despite the fact that a relatively small deviation variation existed. This will be further discussed in the next paragraph. The stator deviation angle was matched by imposing the measured mid-span value.

Rotor exit blockage factor: During the first round of data matching an interesting behavior was encountered. Adjusting the rotor loss produced a well matched rotor pressure ratio; however, the rotor efficiency was questionable since it was over predicted. The over-prediction was due to an incorrect temperature ratio prediction. This first round of data matching had fixed inlet and exit blockage factors of 1.0. The rule of thumb of 0.98 for C_{Din} and C_{Dex} was attempted with no improvement in the efficiency discrepancy. It was decided to dispose the fixed blockage factor rule, as used by Veres [8], and attempt non-constant blockage factors. It was found that the C_{Dex} value had a significant impact on the matching of the rotor temperature ratio, which in turn had an impact on the rotor efficiency; and furthermore, a change in C_{Dex} required adjustments in the rotor loss value. C_{Dex} and rotor loss were adjusted until the rotor pressure and temperature ratios were matched to the reported values.

When a second round of data matching refinement (using varying C_{Dex} and loss) was executed, it was discovered that the use of Carter's rule for deviation was under predicting the exit flow angles for the rotors and stators. It was decided to dispose of the unique deviation angle rule and impose a more accurate deviation angle as calculated or measured from the test data. This required further adjustment of the imposed rotor C_{Dex} values and rotor losses to realign the rotor pressure and temperature ratios.

Rotor losses: As mentioned above, the use of non-constant blockage factors and non-constant deviation angles had a noticeable impact on the rotor loss values. Since the majority of the cited loss models, in general, catered for subsonic to near sonic conditions, utilized Carter's rule for deviation, and did not have any off-design correction for inlet or exit blockage factors, it was decided to use imposed loss values in lieu of predicted values.

Stator losses: Unlike the rotor dilemma of concurrently adjusting the combination of deviation, blockage factor, and loss, the stator losses were simply modified to obtain the correct stage pressure ratio match.

Stator exit blockage factor: The stator exit blockage factor was adjusted to match the reported stator mid-span exit Mach number. Similar to the rotor analysis, a change in stator exit blockage factor required a modification in the stator loss.

3.6 Deviation, loss, and blockage factor correlations to predict missing data

Based on axial compressor literature and the various loss models presented in Chapter 2, the four NASA transonic axial compressor stages (identified as Stage 35, 36, 37, and 38) were separated into similar aspect ratio pairs. As shown in Figure 3-16a, these pairings lead to the following blade row sets:

- Rotor 35 and 37 with an AR of 1.19
- Rotor 36 and 38 with an AR of 1.63
- Stator 35 and 37 with an AR of 1.26
- Stator 36 and 38 with an AR of 1.78

Furthermore, these pairings, when coupled with the blade row camber angles as shown in Figure 3-16b, produce a bounded design space where a mean-line code loss model could interpolate within to resolve similar compressor stage designs.

Based on these pairings, a set of loss modelling correlations, based on physical parameters, were created for each blade row. These correlations were then used to convert the set of tuning factors used to define the inlet and exit blockage factors, deviation angles, and total loss. These correlations were then incorporated into the off-design mean-line code, described in the previous sections, to produce accurate off-design performance maps. The remainder of this chapter will describe the correlations. Each section will summarize the physical parameters used and present the formulae to support said parameters in terms of input parameters (x-axis) and coefficient formulation (y-axis).

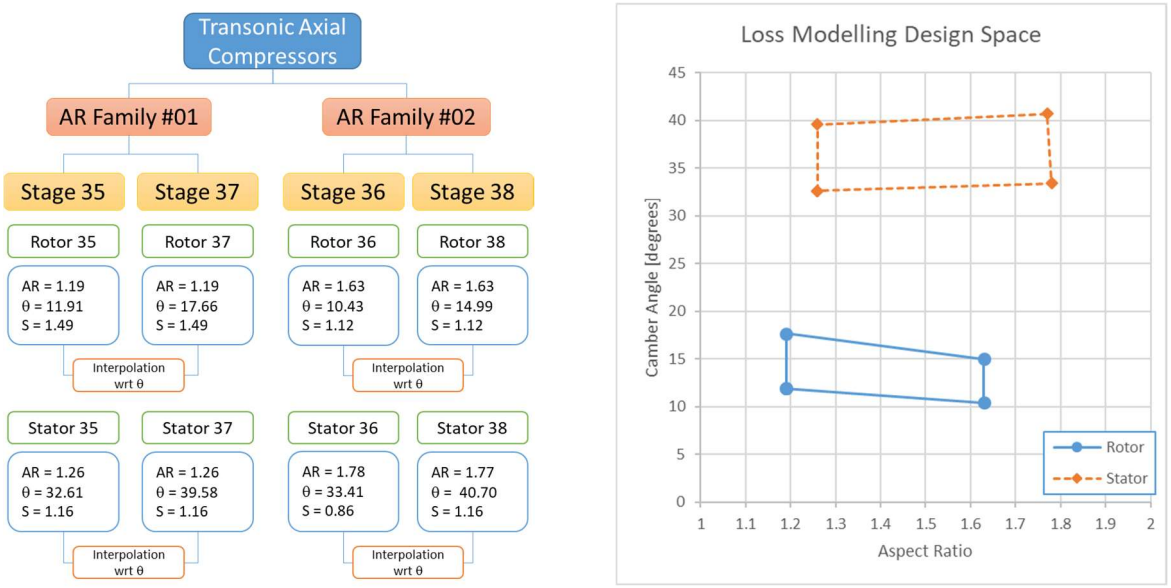

a) axial compressor blade row family sets b) parameter design space

Figure 3-16: Aspect ratio families for four NASA compressors

3.6.1 Deviation correlation

As described in Chapter 2, the main driving parameters of deviation angle are the incidence angle, inlet Mach number (including any shock structures due to high Mach numbers), airfoil camber, and airfoil blade count. Since the values of incidence, inlet Mach number, and deviation varied during the off-design excursion it was decided to plot the trend results of these values. Figure 3-17 represents the change in rotor deviation angle due to the rotor relative inlet Mach number and the rotor incidence angle, whereas Figure 3-18 represents the same set of parameters for the stator. Figure 3-19 is a consolidated view of all rotor and stator deviation angles. The plotted values are based on the NASA reports.

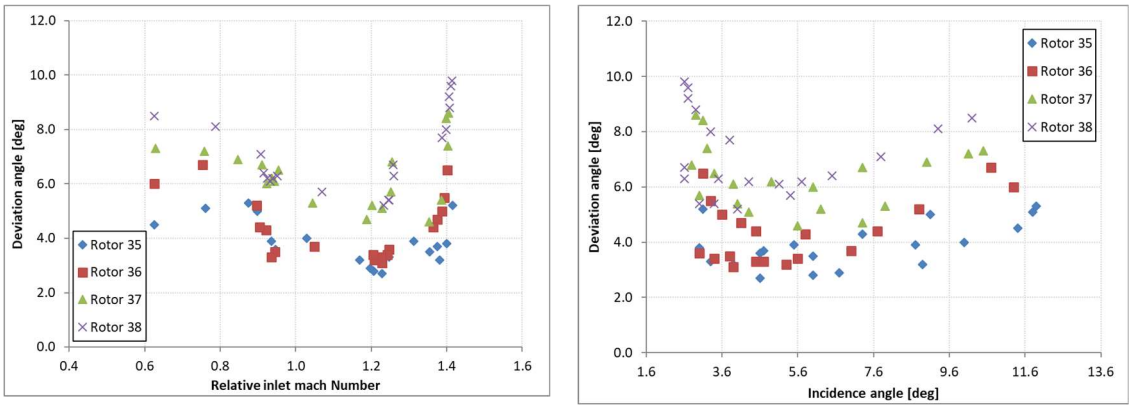

a) Inlet Mach number b) Incidence

Figure 3-17: Rotor deviation angle versus inlet Mach number and incidence

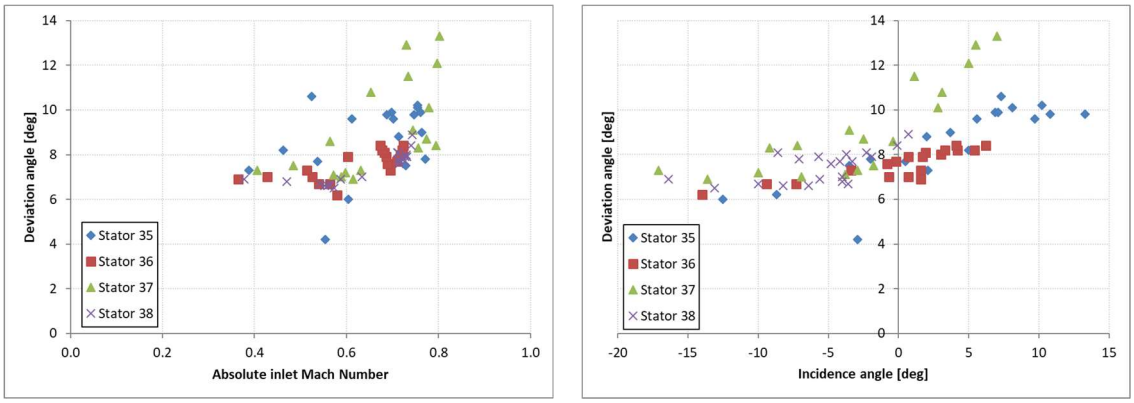

a) Inlet Mach number b) Incidence

Figure 3-18: Stator deviation angle versus inlet Mach number and incidence

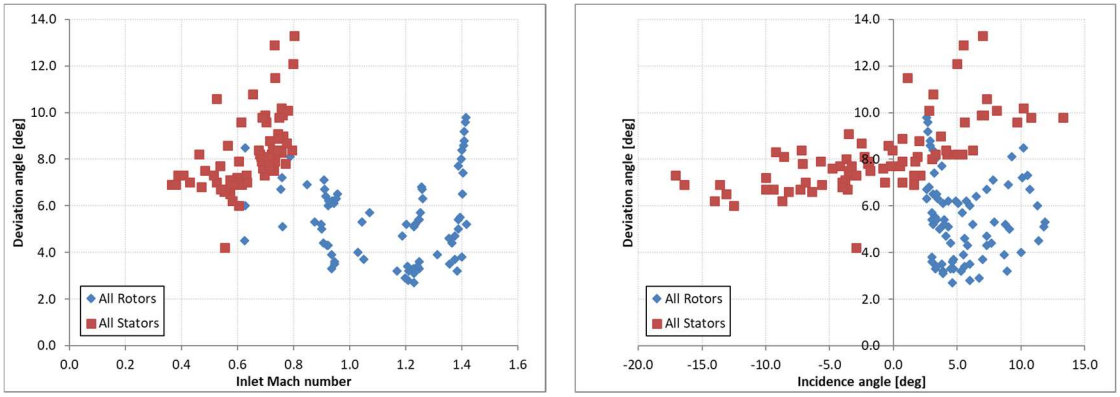

a) Inlet Mach number b) Incidence

Figure 3-19: All blade row deviation angle versus inlet Mach number and incidence

Based on Figures 3-17 to 3-19, the following observations can be made:

- All deviation values remain positive
- Since the rotor is the first airfoil blade row, and the measured inlet flow angle were not adjusted by inlet guide vanes, all rotor incidence values remain positive.
- The incidence angles for the stators range from a negative value to a positive value.
- With respect to inlet Mach number, the rotor data shows a skewed parabolic behavior, whereas the stators present a cloud of data. It may be argued that Stators 36 and 38 show a curved behavior.
- Furthermore, with respect to the rotor inlet Mach number, there is a maximum Mach number wall of 1.4. This is due to the fact that the NASA tests were not run at Mach conditions higher than 1.4. The 100% speed-line maintained an average inlet Mach number of approximately 1.4.
- With respect to incidence angle, the rotor data shows a skewed parabolic behavior, and the stators show a curved behavior.
- In general, with respect to the rotor data, four distinguishable rotors can be identified. Whereas for the stators, it resembles a cloud of data.

In the development of the deviation correlation, the input parameter (x-axis) for both the rotor and stator was casted in terms of the tangent of the inlet flow angle (relative for rotors and absolute for stators) to maintain a consistent approach. The inlet flow angle was used since it was found that different combinations of incidence and inlet Mach number may result in the same flow angle measurement. By trial-and-error data reduction, the y-axis was casted with the resultant deviation angle as an implicit parameter embedded in a *deviation angle correlation* term as presented below. The *0.005* term for the *rotor deviation angle correlation* is a numerical artifact introduced to avoid a zero value in the calculations.

input	**Rotor deviation angle correlation**
$\tan(\beta_1)$	$\frac{\tan(inc)}{\tan(\beta_1)}\tan(\beta_1 + inc - \delta) + 0.005$

input	**Stator deviation angle correlation**
$\tan(\alpha_3)$	$\tan(\alpha_3 + \delta)$

Figures 3-20a and 3-21a show the formula behavior, and Figures 3-20b and 3-21b show the error analysis. As it can be seen, the formulation produces an accuracy within ±1.0° for the majority of data points which is similar to the NASA test measurement error for the inlet and exit flow angles. These formulae, and related graphs, implicitly take into account the incidence angle and the inlet Mach number by the use of the inlet flow angle. Additionally, since the data was segregated in terms of blade rows to be able to interpolate for similar designs, the correlations implicitly account for aspect ratio and camber angle.

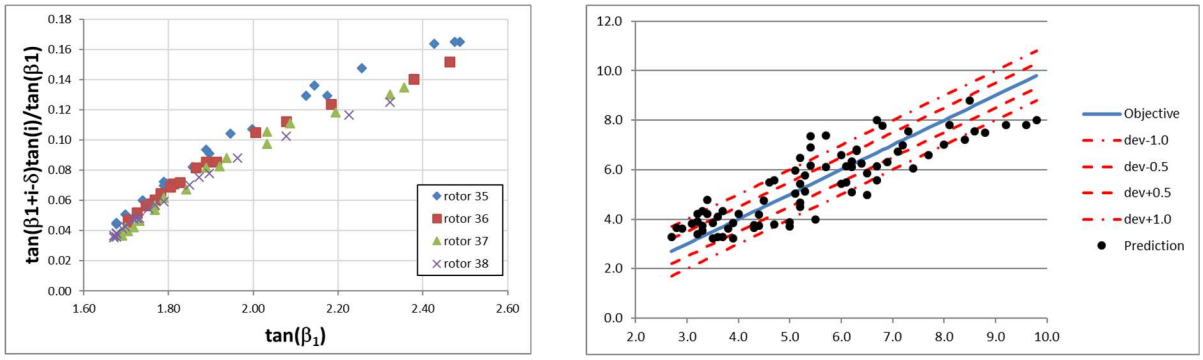

a) rotor deviation angle coefficient b) error analysis

Figure 3-20: Rotor deviation angle correlation formulation

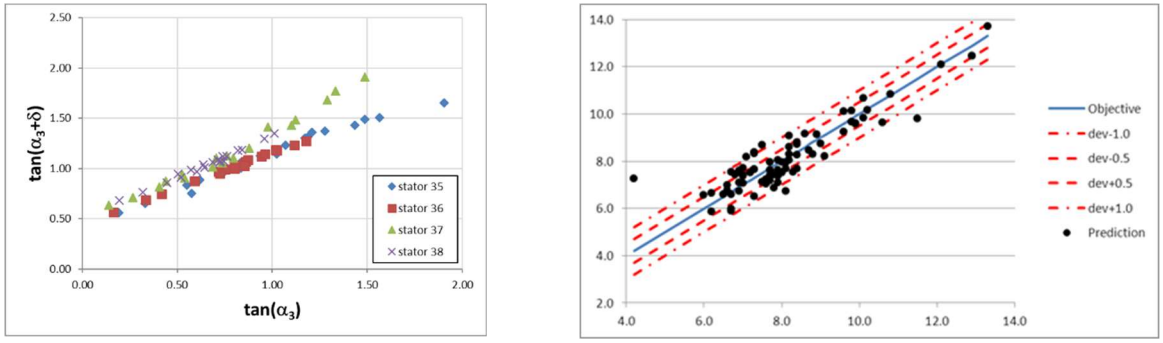

a) stator deviation angle coefficient b) error analysis

Figure 3-21: Stator deviation angle correlation formulation

3.6.2 Rotor inlet blockage factor

It should be duly noted that, despite being intuitively logical, there is no public literature that explicitly describes the use of a correlation to adjust the inlet or exit blockage factors, in a mean-line code, with respect to off-design performance conditions.

With respect to the inlet blockage factor, this loss modelling component is found in **ZONE 1** of the simplified loss zone model. It is known that during the off-design excursion, the dominant parameters that vary are the rotor RPM and the imposed mass flow rate. RPM has a direct impact on the change in the relative inlet flow angle, and the mass flow rate has a direct impact on the Mach number levels of the velocity triangles. From a subsonic to supersonic inlet condition, the main velocity component that remains subsonic is the axial velocity. This velocity component will still *sense* any changes in flow conditions due to changes in the rotor leading edge bow waves in terms of penetration and blockage. These variations stem from the detached shock wave physics as described by Moeckel [116]. In his report, he described an approximate method to calculate the distance of a detached shock bow ahead of a body. This calculated distance was based on the inlet Mach number.

The incorporation of the deviation correlations required an accurate assessment of the inlet flow angles. Based on the mean-line model assumption of a thin cambered airfoil, the inlet blockage factor was originally ignored. When the off-design mean-line model performance predictions were attempted, it was found that the mean-line based inlet angles did not equal those of the experiment. Since the deviation formulas were casted as a function of the experimentally measured inlet flow angles and calculated incidence angles, the thin cambered airfoil assumption did not support the incidence based deviation formulas. Based on the tuning methodology, it was found that a change in the inlet blockage factor produced an improved matching of the data.

Inspired by Moeckel's work, it was decided to cast the *inlet blockage factor (C_{din}) correlation* as a function of the inlet axial Mach number; since this velocity triangle component remained subsonic and would still *sense* any bow wave blockage. Furthermore, the data was segregated into the percent RPM speed-lines to implicitly capture the impact of the subsonic to supersonic inlet conditions of the rotor. Finally, to improve the predictive accuracy, the blockage coefficient utilizes

the pre-modified[9] (*pre*) axial inlet Mach number as calculated by the mean-line code. The resultant correlation is shown below, where the exponent values were discovered by trial-and-error data reduction.

input	**Rotor C_{din} correlation**
$1/preM_x^{0.5}$	$C_{din}^{0.25} preM_x^{0.5}$

The overall behavior of the inlet blockage factor correlation is shown in Figure 3-22.

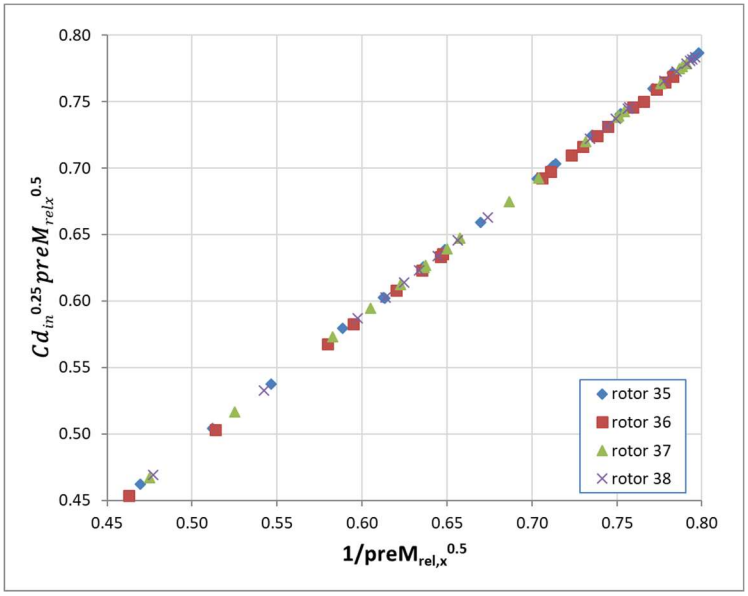

Figure 3-22: Rotor inlet blockage factor correlation formulation

3.6.3 Rotor total loss

The dominant profile and shock structure components are found in **ZONE 2** of the simplified loss zone model. It is well known that the blade row profile will produce a boundary layer growth creating frictional losses, which are then translated into pressure losses. Furthermore, the inlet shock structure will modify said boundary layer growth, changing the absolute level of the overall pressure losses. As the RPM and inlet mass flow rates change, the strength of the shock structure

[9]in this context "pre-modified" signifies values calculated before being modified by the inlet or exit blockage factors.

will follow suit, decreasing as the RPM decreases, and its contribution to the overall blade row loss will also decrease.

In **ZONE 3** the effects of the trailing edge wakes will be encountered, the strength of which is dependent on the trailing edge airfoil thickness of the rotor. In **ZONE 4** the rotor loss will be impacted by the rotor tip clearance penetration, the end-wall boundary layer growths, and the strong secondary (vortex) loss structures that are amplified as the rotor aspect ratio is decreased.

During the formulation of the rotor total loss a dilemma was encountered; which cited author's loss model to use? One of the issues related to loss modelling is which reference loss model is to be used to develop a modified loss description[10]. When a particular loss model does not match the test data, one will tend to apply correction factors to tune the model to attempt an improved prediction. These tuning values will differ from one loss model to another. Moreover, if researchers wish to recreate the results presented in this investigation, their particular loss model may not be aligned to the one used, complicating the benchmarking exercise. Additionally, if an institution's particular loss model is not published due to its proprietary nature, then the exercise of data matching might end as a futile attempt.

Due to these concerns and potential limitations, an overall rotor loss formulation was pursued. The benefits of doing so are two-fold: 1) The rotor loss model is independent from the use of a reference loss model and hence the benchmarking exercise is simplified, and 2) when more complete compressor off-design test data and geometries are found in the public domain, the overall loss model introduced can be further refined and decomposed into its classical loss constituents.

Based on the available data, the rotor total loss was casted as a function of the rotor incidence angle (noted by $\boldsymbol{i}$), relative inlet Mach number (M_{rel}), and total loss as shown below. To capture the effects of the rotor tip clearance[11] variation, the *total loss correlation* was separated into the

[10] Unlike turbine loss modelling which has the AMDCKO or CCC models, compressor loss models do not present a genealogical evolution from author to author.

[11] Except for rotor 37, no published values were available. One may implicitly account for this parameter by using the %RPM variation that directly translates into the centrifugal forces which cause the variation in clearances.

reported percent RPM speed-lines. The exponent values were discovered by trial-and-error data reduction.

input	**Rotor total loss correlation**
$\tan(i)$	$Loss \cdot \tan^3(i) \cdot M_{rel\cdot in}^2$

The formulation for the *rotor total loss correlation* is presented in Figure 3-23, where the increase in RPM is from the right-hand most speed-line (50%) towards the left-hand most speed-line (100%). The solid dots represent the values obtained from the tuned matching methodology, and the non-solid dots represent the results of plotting the *rotor total loss correlation*. These plots were created to observe if the tuned data would be properly predicted by the correlation.

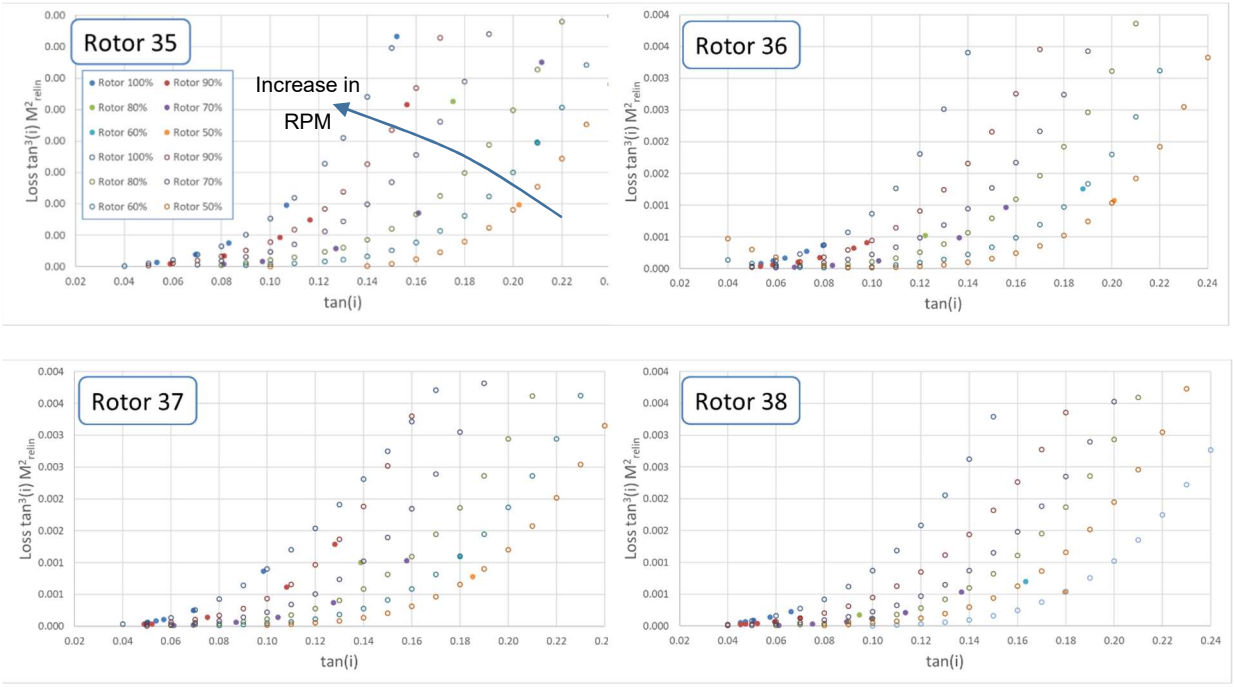

Figure 3-23: Rotor loss correlation formulation

3.6.4 Rotor exit blockage factor

Similar to the inlet rotor blockage, there is no public literature that explicitly describes the use of a formula to adjust the exit blockage factors with respect to the off-design performance conditions. It is known, however, that procedurally the exit blockage factor may be adjusted to tune the design-point mean-line analysis results to known test data. This value is then left fixed throughout the off-design performance analysis.

With respect to the exit blockage factor, this component begins is **ZONE 2** and continues on into **ZONE 3** of the simplified loss zone model. As the blade surface develops a boundary layer, the flow will create a blockage that will reduce the effective flow area. As the flow reaches the trailing edge, the impact of the trailing edge wakes and the mixing of the boundary layer will increase the local blockage. This can be seen in Lieblein's et al classic image [117], presented as Figure 3-24, which describes the boundary layer growth and trailing edge wake created by a compressor blade row.

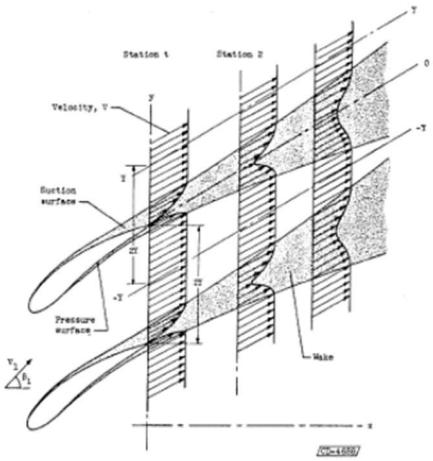

Figure 3-24: Development of boundary layers and wake about cascade blade sections [117]

The exit blockage factor will be dominated by those parameters described for the inlet blockage factor, mainly the RPM and the mass flow rate. As mentioned before, the RPM has a direct impact on the change in inlet flow angle, and the mass flow rate has a direct impact on the Mach number levels of the velocity triangles. The varying off-design conditions will produce differing boundary layer growths and trailing edge wake strengths. Furthermore, as mentioned for the rotor loss, the changing tip clearance, implicitly deduced from the change in RPM, will also have an impact on the overall exit blockage factor. As described by Khalid [118], a change in tip clearance will

contribute to the overall blade row blockage especially in the tip end wall region. For these various reasons, the exit blockage factor follows a similar formulation approach as that of the rotor loss. The incidence angle is used as an input, and an *exit blockage factor correlation* is created using both the incidence and relative inlet Mach number as the main flow parameters. The exponent values, except for blockage factor, were kept as those for the rotor loss correlation.

input	**Rotor C_{dex} correlation**
$\tan(i)$	$C_{Dex} \cdot \tan^3(i) \cdot M_{rel\cdot in}^2$

Figure 3-25 shows the segregation based on the percent RPM speed-lines, where the increase in RPM is from the right-hand most speed-line (50%) towards the left-hand most speed-line (100%). The solid dots represent the values obtained from the tuned matching methodology, and the non-solid dots represent the results of plotting the rotor correlation. These plots were created to observe if the tuned data would be properly predicted by the correlation.

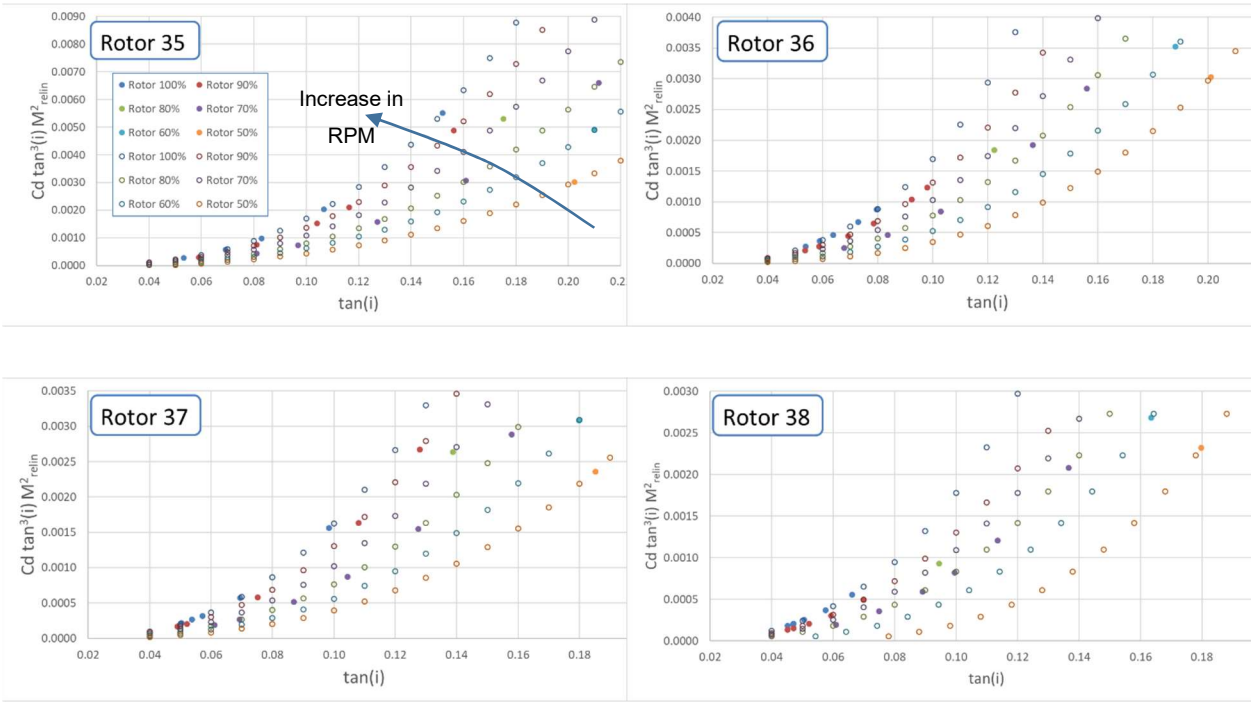

Figure 3-25: Rotor exit blockage factor correlation formulation

3.6.5 Stator inlet blockage factor

The stator inlet blockage formulation inherits the approach and description of the rotor loss and exit blockage factor coefficients. The stator inlet blockage commences in **ZONE 1**, however, unlike the rotor inlet condition, the stator will be exposed to the complex exit flow physics of the rotor. The stator will be subjected to the rotor boundary layers, the trailing edge wakes, and additionally the rotor tip clearance and secondary vortex flows. To be able to properly capture these effects and to produce accurate results, the input to the stator *inlet blockage factor correlation* utilizes a pre-modified inlet flow angle. Furthermore, the inlet blockage factor is casted as a coefficient coupled to the pre-modified[12] (*pre*) inlet flow angle and the pre-modified inlet Mach number, as shown below. The exponent values for the correlation, except for the blockage factor, were kept as those for the rotor loss correlation. The input and blockage exponent value was based on a trial-and-error data reduction.

input	**Stator C_{din} correlation**
$\tan^2(pre\ \alpha_{in})$	$Cd_{in}^{0.25} \tan^3(pre\ \alpha_{in})\, preM_{in}^2$

As shown in Figure 3-26, the stator inlet blockage factor coefficient was segregated into the percent RPM speed-lines of the rotor to implicitly capture the complex nature of the rotor exit conditions; where the increase in RPM is from the right-hand most speed-line (50%) towards the left-hand most speed-line (100%). The solid dots represent the values obtained from the tuned matching methodology, and the non-solid dots represent the results of plotting the stator correlation. These plots were created to observe if the tuned data would be properly predicted by the correlation.

[12] in this context "pre-modified" signifies values calculated before being modified by the inlet or exit blockage factors.

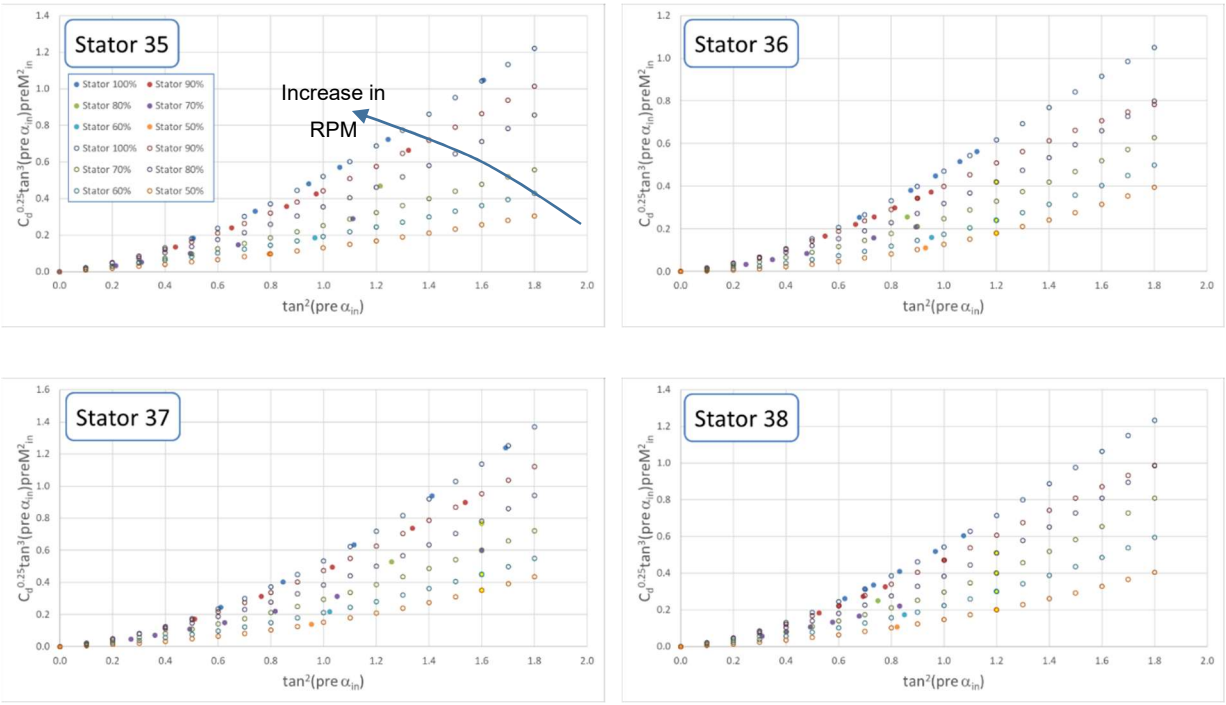

Figure 3-26: Stator inlet blockage factor correlation formulation

3.6.6 Stator losses

The stator total loss directly inherits the physics description of the rotor loss, and the formulation approach of the stator inlet blockage factor. The stator loss formulae, where the exponents were obtained from a trial-and-error data matching exercise, are shown below. Except for the input and loss exponents, which were obtained through a trial-and-error data correction, the correlation exponents were taken from that of the stator C_{din} correlation.

input	**Stator total loss correlation**
$\tan^4(pre\ \alpha_{in})$	$Loss^{0.20}\tan^4(pre\ \alpha_{in})\ preM_{in}^3$

Figure 3-27 shows the results of the above formula, and the segregation into the percent RPM speed-lines of the rotor, where the increase in RPM is from the right-hand most speed-line (50%) towards the left-hand most speed-line (100%). The solid dots represent the values obtained from the tuned matching methodology, and the non-solid dots represent the results of plotting the stator correlation. These plots were created to observe if the tuned data would be properly predicted by the correlation.

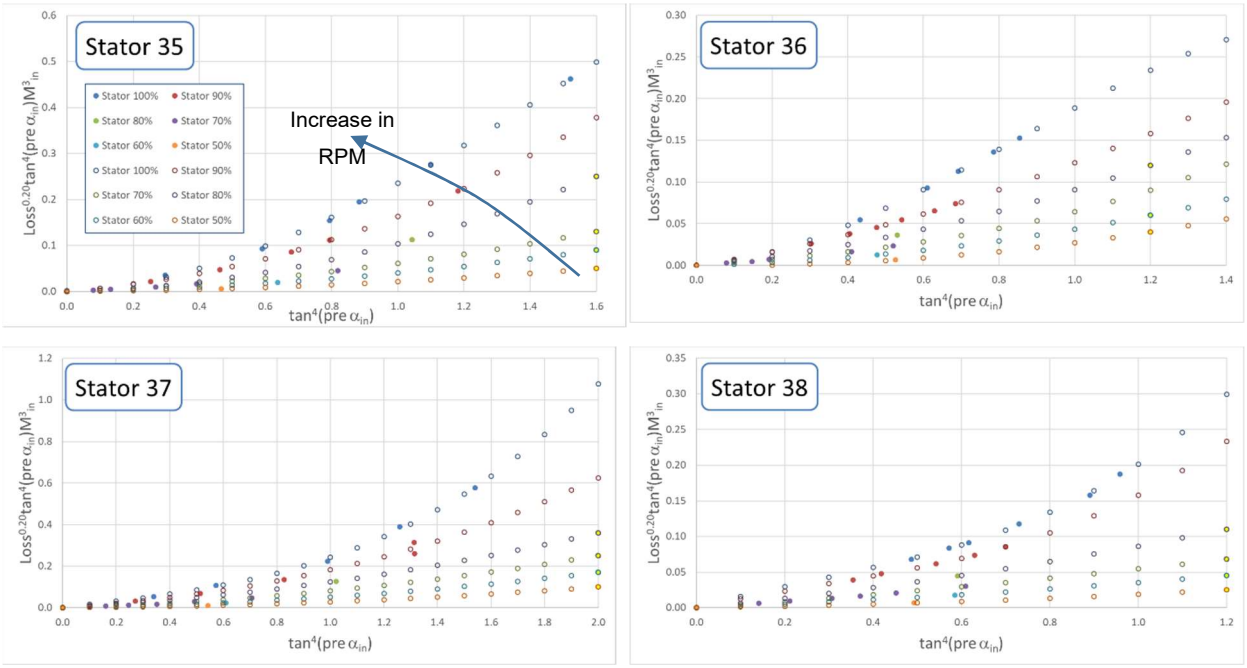

Figure 3-27: Stator loss correlation formulation

3.6.7 Stator exit blockage factor

The stator exit blockage factors were tuned to match the reported exit Mach number. The formulation for the stator exit blockage factor required a similar approach to the stator inlet blockage factor and total loss. The exit blockage factor requires the input of the pre-modified inlet flow angle, and is casted as a correlation of the pre-modified inlet angle and pre-modified Mach number. The exponents of the correlation were taken from the stator C_{din}, and the input and blockage exponents were obtained through a trial-and-error data reduction exercise.

input	**State Cdex correlation**
$\tan^3(pre\ \alpha_{in})$	$Cd_{ex}^{1.0} \tan^3(pre\ \alpha_{in})\, preM_{in}^2$

Figure 3-28 shows the results of the above formula, and the segregation into the percent RPM speed-lines of the rotor, where the increase in RPM is from the right-hand most speed-line (50%) towards the left-hand most speed-line (100%). The solid dots represent a mix of tuned data and added values to control the polynomial behaviour.

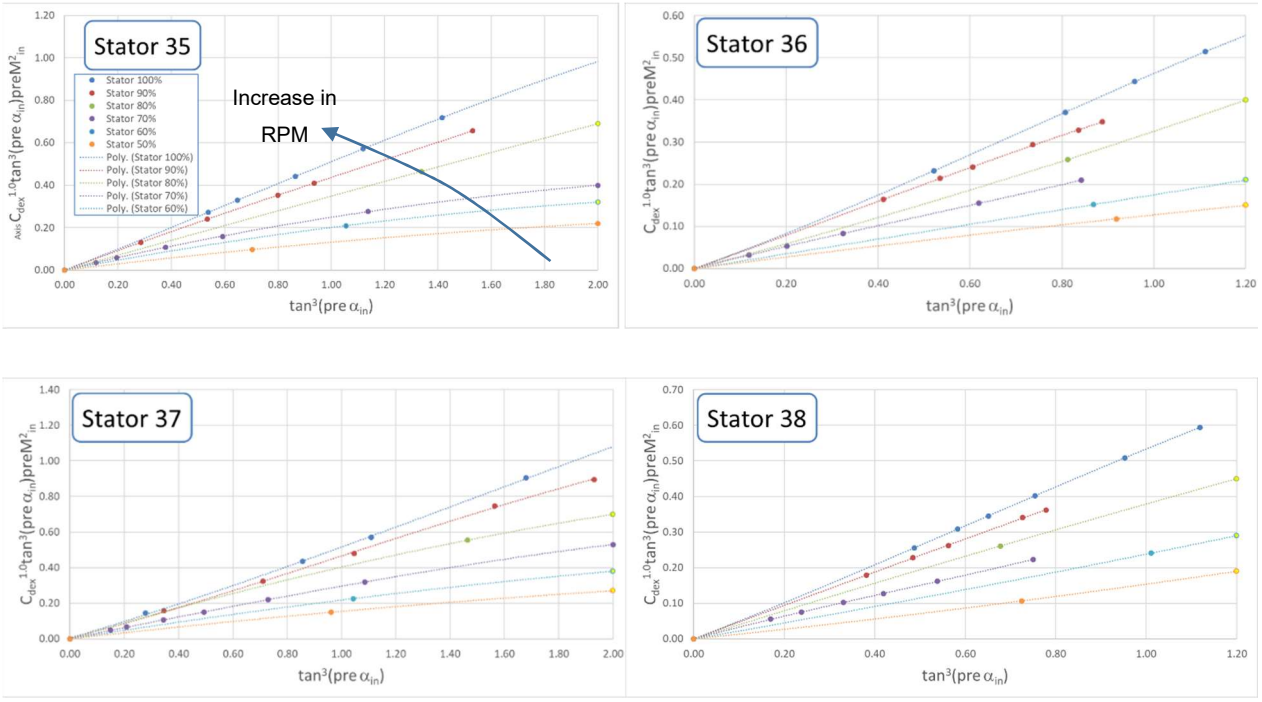

Figure 3-28: Stator exit blockage factor correlation formulation

3.7 Development of a choke criteria

Based on Chapter 2's description of choke, for the four NASA transonic axial compressors under investigation, it was quite difficult to find a condition for all reported speed-lines where the mid-span Mach number became unity. Except for the rotor which has a subsonic to supersonic inlet condition, the stator inlet does not achieve a Mach number of unity. Furthermore, the NASA experiments were executed by varying the exit throttle until the so called *choke* condition was achieved [88]. The reported performance charts by NASA show no indication of the *vertical choke line*, nor a constant mass flow, except for the 100% speed-line results. It was decided to search for an alternative approach to describe the choking condition of the four axial compressors under investigation. The main objectives that had to be satisfied was that the rule had to be a) relatively simple and b) independent of any semi-empirical formulas or correlations which would require the accounting of the various flow and geometric parameters encountered in a transonic axial compressor.

To meet the above mentioned objectives, it was chosen to search for a choke definition that differed from the three approaches described by the cited authors. These approaches are 1) the use of a

known efficiency for choke and scaling it to the appropriate speed-line values, as described by Howard & Calvert [35] and Steinke [34], 2) the use of a choke loss multiplier as per Miller & Wasdell [53], and 3) the use of a numerical approach of calculating a constant mass flow, either through a vertical line identification or a convergence error, as per Barbosa [26], Hanlon [56], Boyce [57], and Veres [8]. It should be duly noted that the analysis and conclusions made in the following section are strongly related to the *1D* nature of the mean-line modelling methodology

The approach taken to search for a choke criteria was based on the observations of the mean-line model flow field calculation of the compressor stage. Figure 3-29 shows the OD ML UI with the tabular flow field to the right. The UI mass increment (+ icon) and mass decrement (- icon) were used to change the mass flow rate in and around the measured choke data point until an observable trend was found.

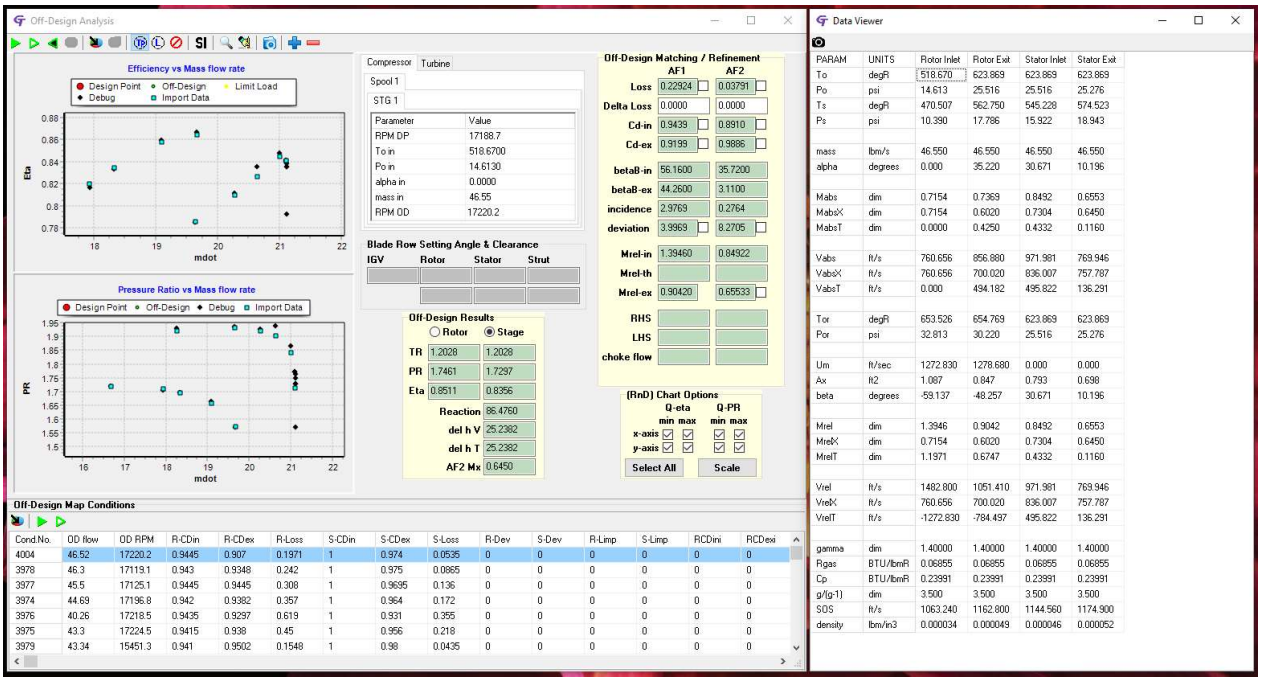

Figure 3-29: Choke criteria identification approach

What was discovered was that a rotor-stator system based rule, using a static pressure ratio, segregated in sets of rotor relative inlet Mach numbers, best described the MAMF condition of the four NASA transonic axial compressors under investigation.

High-Supersonic Mach numbers: It was found that, when the rotor relative inlet Mach number was greater than or equal to 1.2, four distinctive rotor-stator MAMF conditions may occur. It was

further discovered that there was a hierarchy in the order of the MAMF condition identification to be respected.

1) In the off-design mean-line model predictions, it was found that the rotor relative exit Mach number ($M_{r\text{-}rel\text{-}ex}$) was able to achieve a value of 1.0. This was considered to be the extreme form of the MAMF condition. When the rotor exit chokes, no further increase in mass flow can occur. Surprisingly, this situation is somewhat similar to the approach for axial turbine limit loading condition.

2) When the stator exit static pressure ($P_{S,ex}$) becomes less than the stator inlet static pressure ($P_{S,in}$), the stator has achieved its maximum diffusion potential and the rotor-stator system has achieved its MAMF condition. The stator cannot create an exit static pressure which is less than the stator inlet static pressure.

3) When the stator exit static pressure becomes less than the rotor inlet static pressure, independently from the stator inlet condition, then the stator has achieved its maximum diffusion and the rotor-stator system has achieved its MAMF condition. The stator cannot create an exit static pressure which is less than the rotor inlet static pressure.

4) When the stator inlet static pressure **and** the stator exit static pressure is less than the rotor exit static pressure, then the stator has achieved its maximum diffusion and the rotor-stator system has achieved its MAMF condition. The stator cannot create an exit static pressure which is less than the rotor exit static pressure.

Low to High Supersonic Mach numbers: For rotor relative inlet Mach numbers between 1.02 to 1.20, it was found that two of the four high-supersonic Mach numbers rules apply. The first rule (1) of the rotor relative exit Mach number reaching a value of one is verified. Then the third rule (3) of the stator exit static pressure becomes less than to the rotor inlet static pressure is verified.

High Subsonic to Low Supersonic Mach numbers: For rotor inlet relative Mach numbers between 0.92 and 1.02, it was found that only the third rule (3) of the stator exit static pressure becomes less than the rotor inlet static pressure was required.

Subsonic Mach numbers: for the remaining subsonic conditions, it is first verified if the stator inlet Mach number achieves unity. This is the closest behavior to the classically defined choke definition. Once verified, the third rule (3) of when the stator exit static pressure becomes less than

the rotor inlet static pressure and the first portion of the fourth rule (4) of when the stator inlet static pressure is less than the rotor exit static pressure are checked.

What these rules describe are the systematic variation of the potential choke locations of a rotor-stator system. To better visualize how these rules may come into existence, one must visualize the difference between two simplified models. In Figure 3-30a we have the rotor-stator system described as cylinders, with the inter-blade row spacing described as a slightly larger vertical span representing the annulus area excluding the reduction due to the rotor trailing edge thickness and the stator leading edge thickness. In Figure 3-30b we have a similar diagram, except the cylinders are replaced with diverging ducts to represent the compressor blade row passages. Figure 3-31 shows how Figure 3-30b was created.

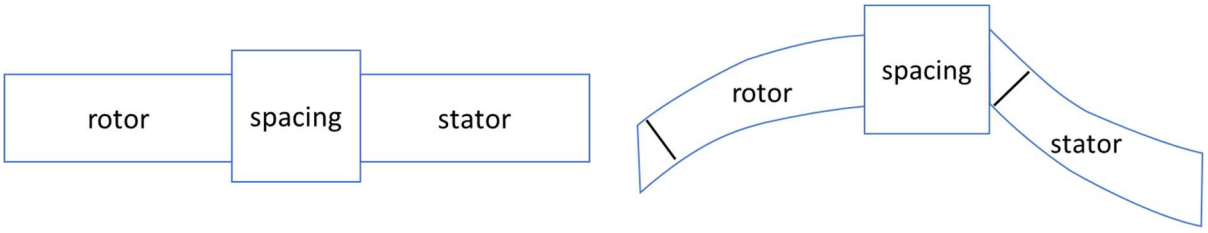

a) basic axial pipe system **b) modified diverging passage system**

Figure 3-30: Simplified pipe and duct representation of a compressor stage

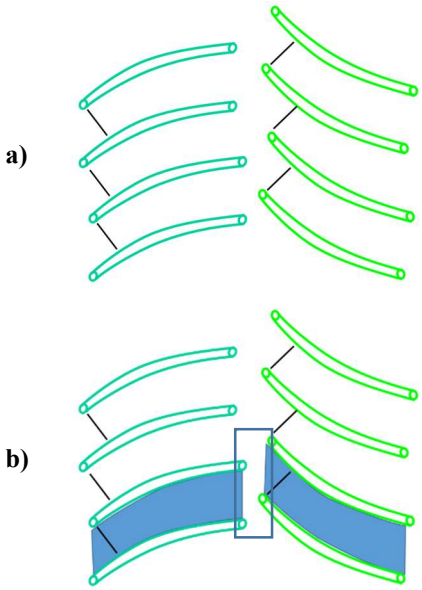

Figure 3-31: Obtaining the simplified duct representation

In Figure 3-30a one may be able to identify the choke location by inspecting the geometry of a converging-diverging passage. Assuming that we are not trying to produce a shock wave within the cylinders, the most likely location for choke to occur would be at the inlet to the stator cylinder. Here, we will find that the area of the inter-blade row spacing reduces to the area of the stator inlet, creating the minimum throat area; a simple yet deceiving concept.

In Figure 3-30b we have a different story. Unlike a constant diameter cylinder, we have two diverging passages laid out sequentially. Not only must we contend with the fact that we have changes in the rotor inlet conditions, variation of the boundary layer thickness, passage losses, and that the incidence & deviation values do not remain constant, we must also include one additional fact of axial compressors; as the mass flow increases the static pressure gradient will decrease across the blade rows. What the four MAMF criteria described above reveal is that there are three major choking phenomenon that may occur:

1) The stator passage chokes as the stator passage static pressure ratio becomes unity, before that of the rotor passage.

2) The stator passage chokes as the rotor-stator (inlet-exit respectively) static pressure ratio becomes unity, before the rotor exit and stator inlet could achieve a MAMF condition. This is due the variation of blockage, loss, and rotor exit to stator inlet geometry that sets up such a condition.

3) And finally, as an overall balancing act, the stator chokes when the stator inlet and exit conditions cannot diffuse lower than the rotor exit.

These rules show that the back pressure (or exit pressure) reduction is the physical phenomena that is driving the *Maximum Attainable Mass Flow* (MAMF). The rotor-stator system cannot produce a stator exit static pressure which is less than the rotor inlet, the rotor exit, or the stator inlet.

It is not at all surprising that, to avoid dealing with the complex flow physics interaction, one may be lead to believe that a Mach number of unity best describes the axial compressor MAMF condition; a simple yet deceiving concept.

3.8 Development of a stall criteria

Based on the literature review of Chapter 2, and publicly available comparisons between experimental and predictive model results of varying types, it begs the question *"is it even possible to find a simple methodology to consistently predict the stall or surge onset?"*

In the quest of answering the above question, it was initially decided to investigate the rotor speed-line extremities to observe any potential trends. Both loss and de Haller values were plotted. The first was an attempt to corroborate the stalling incidence approach, and the second was to look into any possible insight with respect to de Haller's stalling criteria. Figure 3-32 represents the loss and de Haller trends for the four NASA transonic axial compressors under investigation.

What is observed is that there is an inconsistent sinusoidal trend amongst the various plotted curves. The loss based curves show a semi-consistent trend between Rotor 36 and 38. However, an inverted trend is encountered for the Rotor 35 and 37 pairing.

With respect to the de Haller trend plot, a much more dramatic inversion between rotors are encountered. It may be argued that the rotor pairings of 35 & 37 and 36 & 38 are maintained. Nevertheless, an explanation for the mirror-like profiles escaped the author. Various attempts, not shown here, to collapse the loss and de Haller based data, into reasonable trend curves, were unsuccessful.

a) Loss based

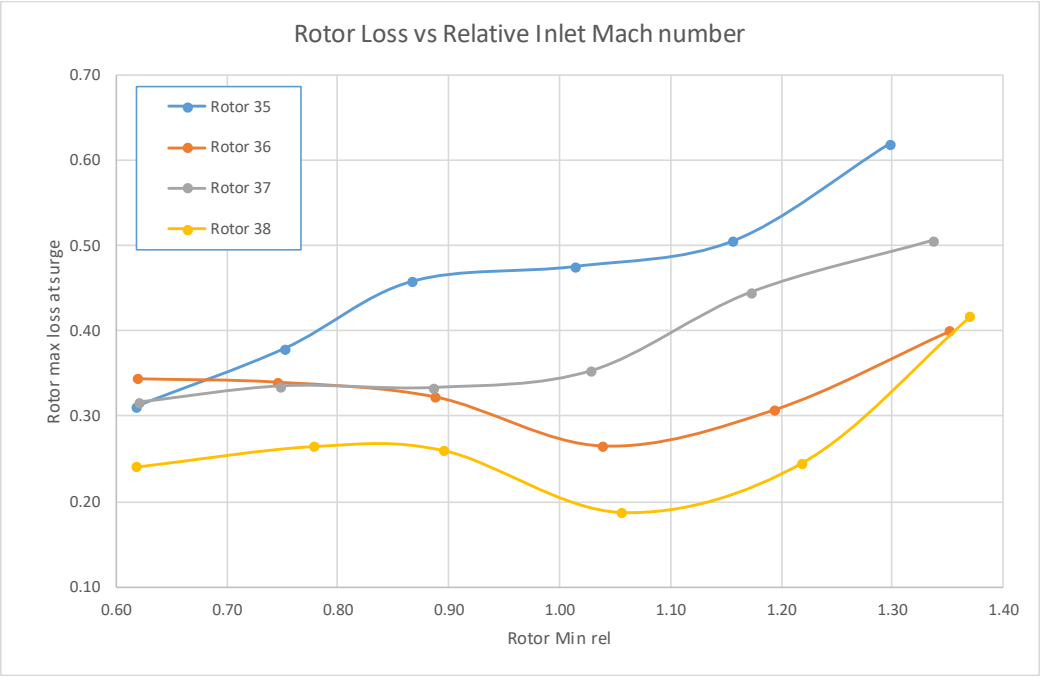

b) de Haller based

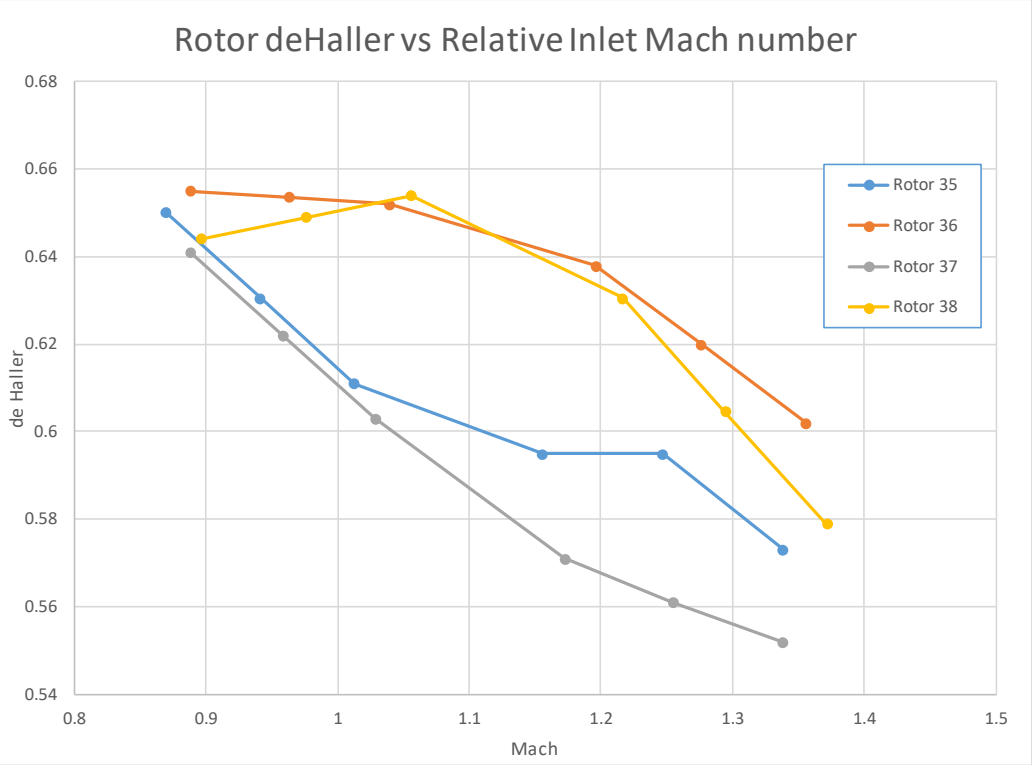

Figure 3-32: Initial surge model based on speed-line extremities

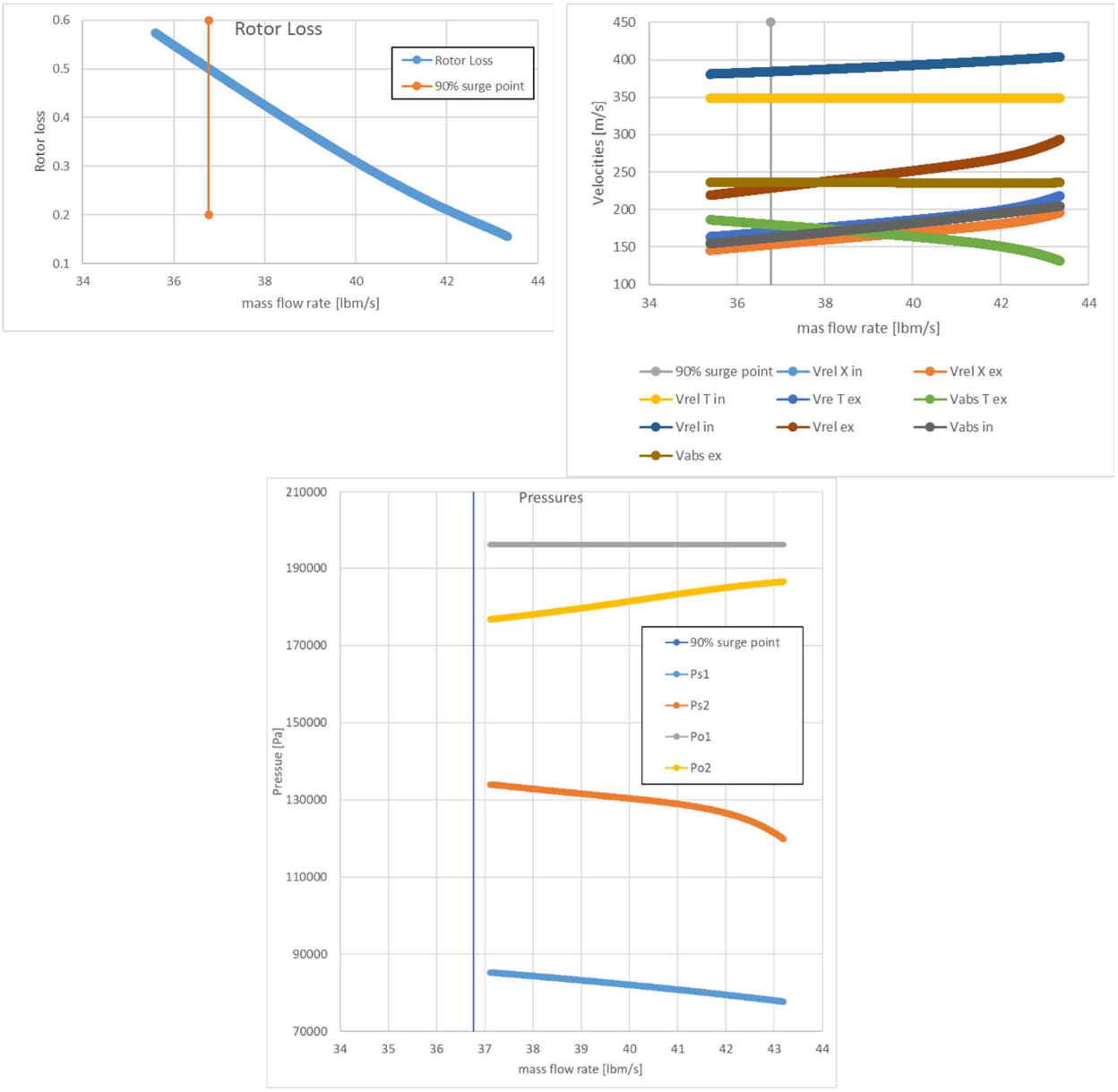

Figure 3-33: Stage 35, 90% speed-line off-design trend of various mean-line model values

It was then decided to, inspired by the models of past authors, to plot the main driving parameters presented in the various formulations. Figure 3-33 presents the variations of loss, pressure, and mean-line velocity components versus mass flow rate for Rotor 35 at the 90% speed-line. With respect to the off-design loss variation, no maximum loss value is detected. The off-design pressure variations did not reveal any interesting or identifiable trends; there were no maximum or minimum pressure value peaks to be observed. Interestingly, what can be observed from the velocity-based figure is that there is a cross over between the various rotor mean-line model based velocities.

Inspired by Professor Ivor Day's, of Cambridge University in England, quote[13] of "s*tall is a tangential phenomenon, while surge is an axial phenomenon*", the velocity component cross-over was chosen as a potential avenue in describing the stall or surge point. The mean-line model velocity-based figure was repeated for all stages and speed-lines (of 50, 60, 70, 80, 90, and 100%) to reveal any potential meaningful trends. Figures 3-34 to 3-37 show the resultant rotor absolute and relative velocity components plotted against the mass flow rate. For speed lines from 80 to 100% the stator inlet axial velocity has been included (dashed red line), for which the reasons for this inclusion will be explained shortly. The mass flow rate range is based on an identified M*aximum Attainable Mass Flow* (MAMF) value, using the static pressure ratio described in the previous section, up to a predicted stall value based on the simple stall criterion which will also be described shortly.

All four NASA compressor stages, with their respective data and mean-line models, were used to converge on a potential stall criterion for all speed-lines. This analysis led to the conclusion that the stall point may be described as the intersection of the axial and absolute tangential velocities between the rotor exit and stator inlet.

[13] This quote was found, during a literature research, in an on-line blog for compressors

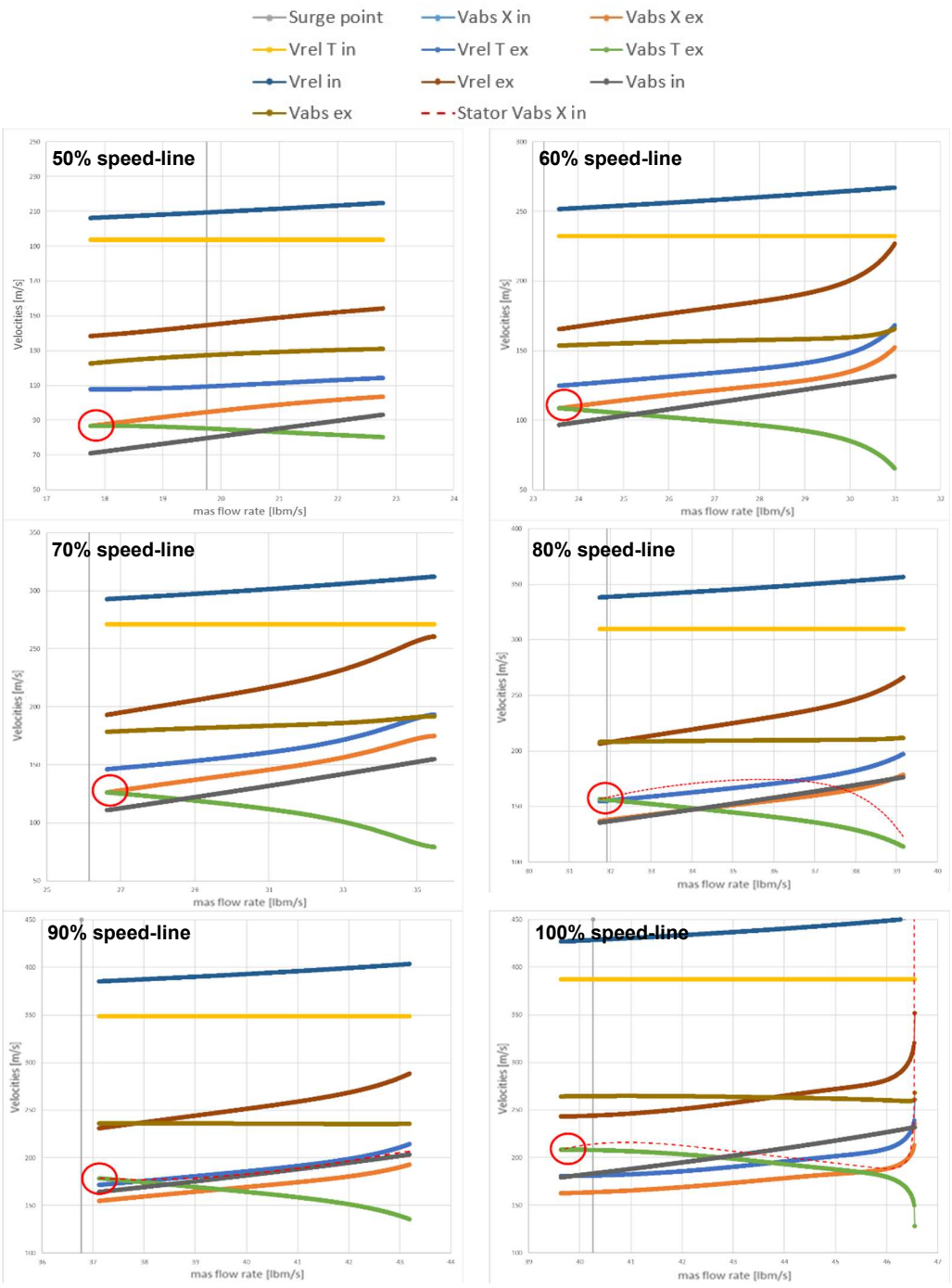

Figure 3-34: Stage 35 off-design velocity component variation

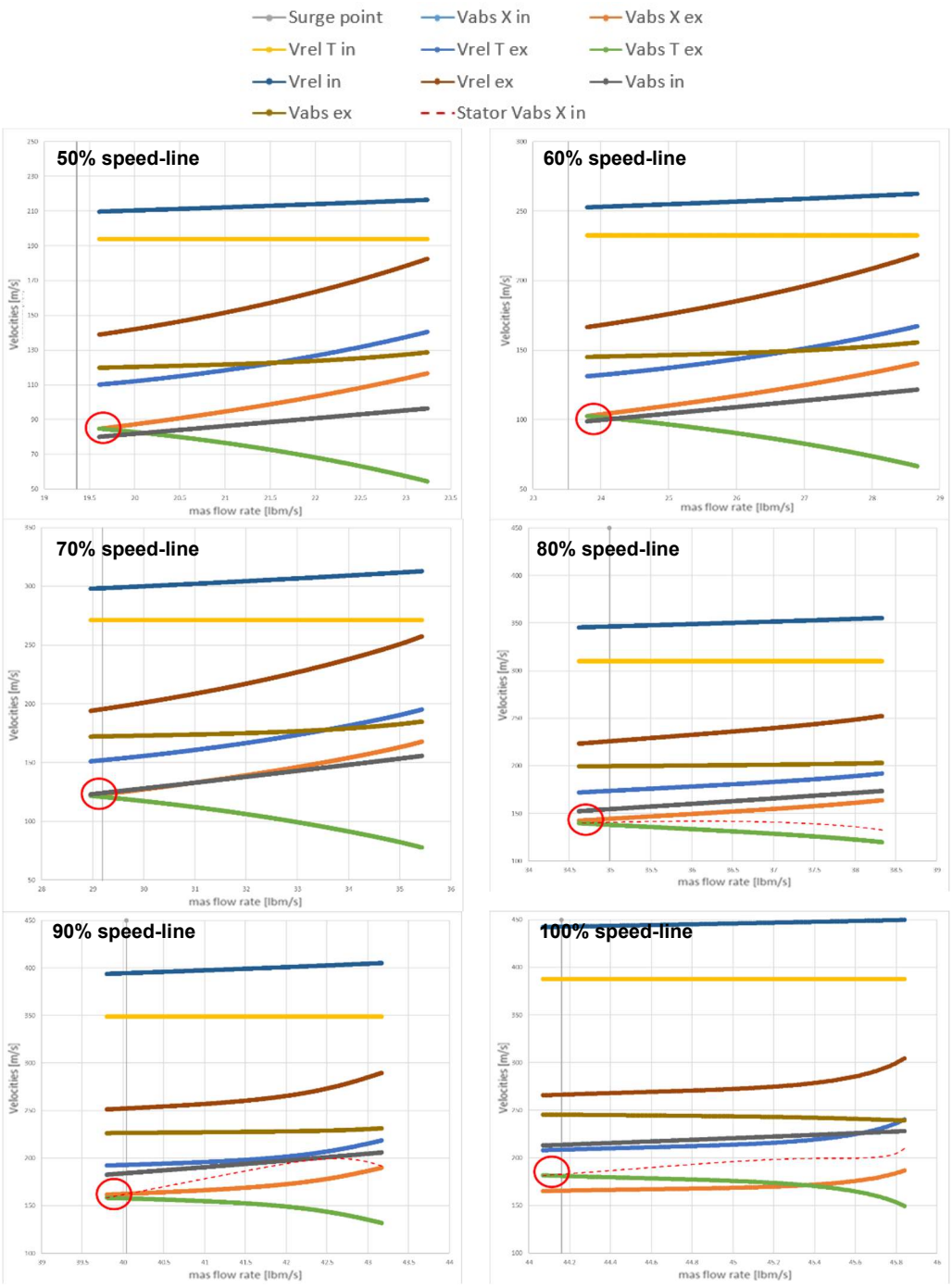

Figure 3-35: Stage 36 off-design velocity component variation

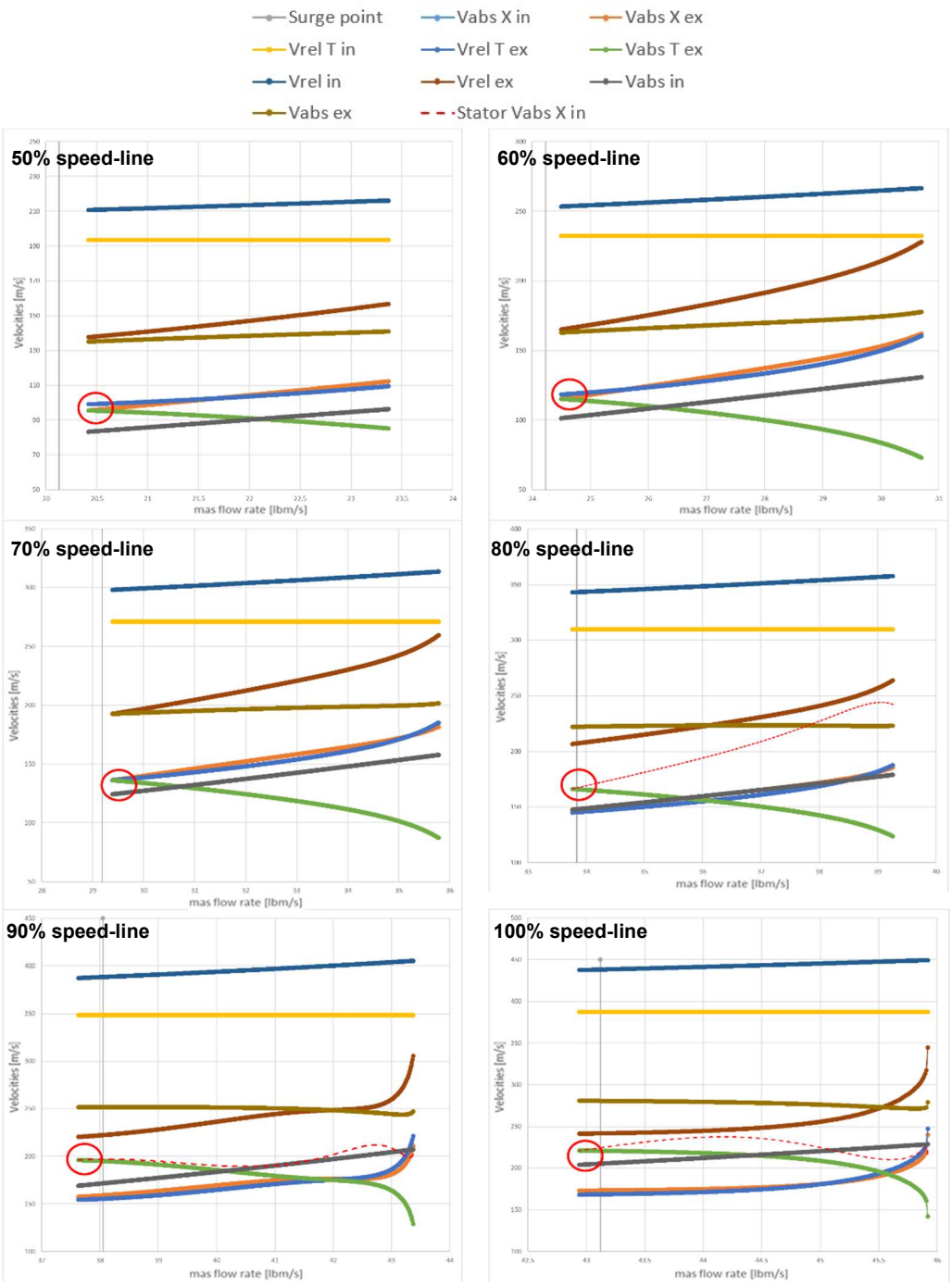

Figure 3-36: Stage 37 off-design velocity component variation

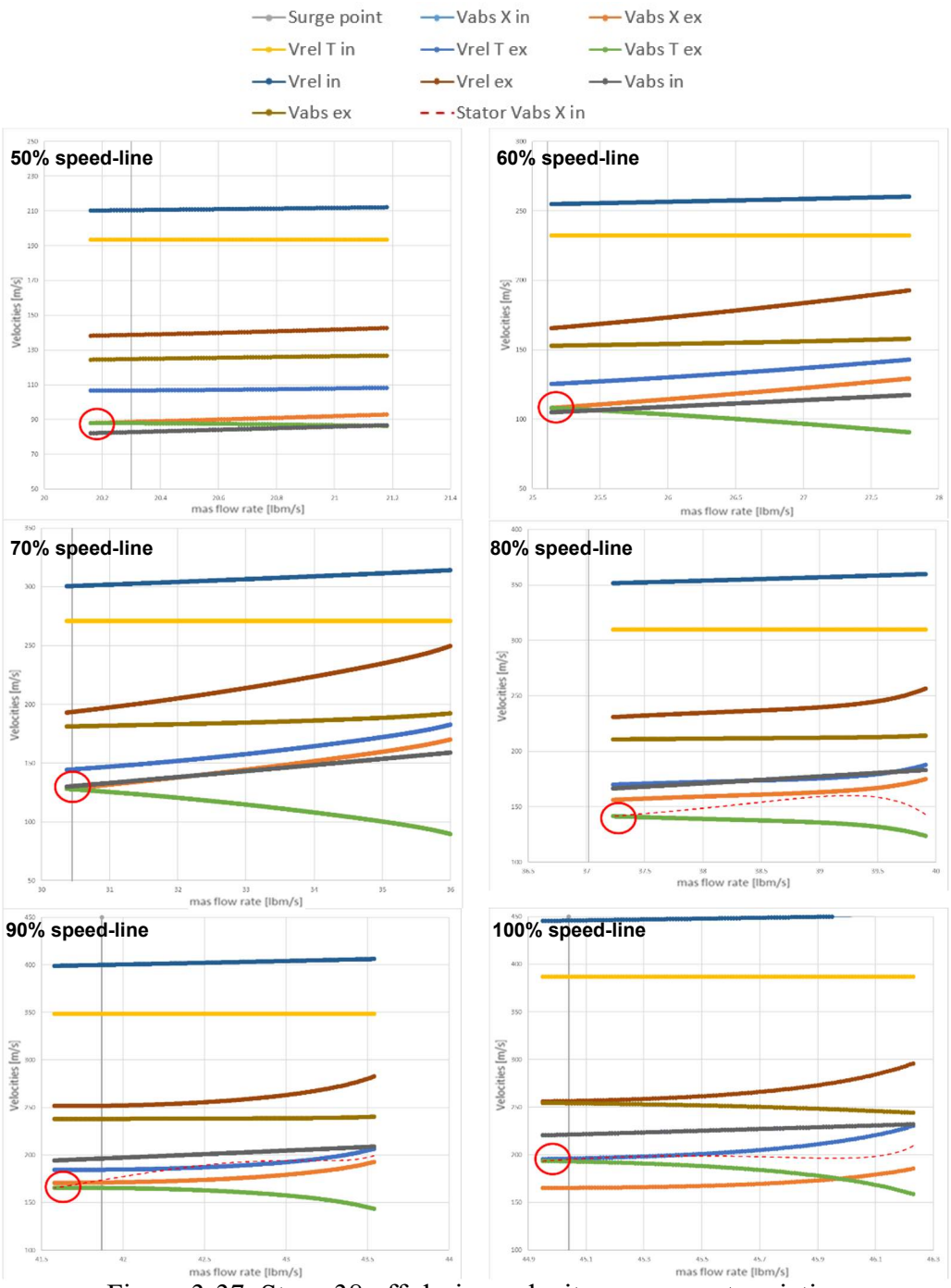

Figure 3-37: Stage 38 off-design velocity component variation

In terms of an engineering description, what can be observed from the majority of the images found in Figures 3-34 to 3-37, is that at the choke condition the axial velocity is the dominant flow parameter. As the mass flow rate decreases so does the difference between the absolute axial and tangential velocities. Finally, as the mass flow rate approaches that of the stall point, the absolute tangential velocity will become greater than the axial velocity. The idea of evolution of the velocity triangles from choke to stall is shown in Figure 3-38.

a) Velocity triangle at choke

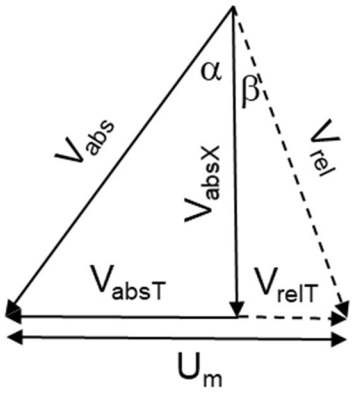

b) General velocity triangle

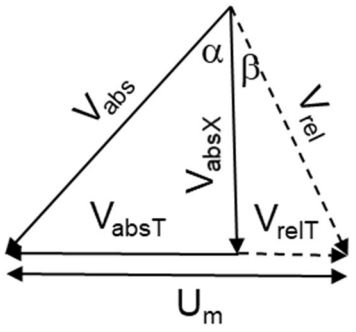

c) Velocity triangle at stall

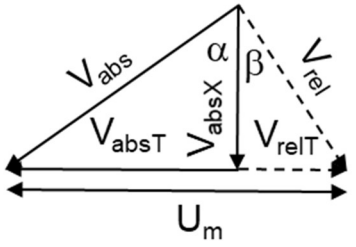

Figure 3-38: Changes in velocity triangles from choke to stall

One may be correct to argue that the axial velocity versus tangential velocity cross over is indicative of a swirl or deviation angle impact. However, defining a surge model based on angles

alone would require the creation of semi-empirical formulas to capture a peak or valley value, or even a cut-off point. Figures 3-39 and 3-40 show the off-design deviation of the various rotors.

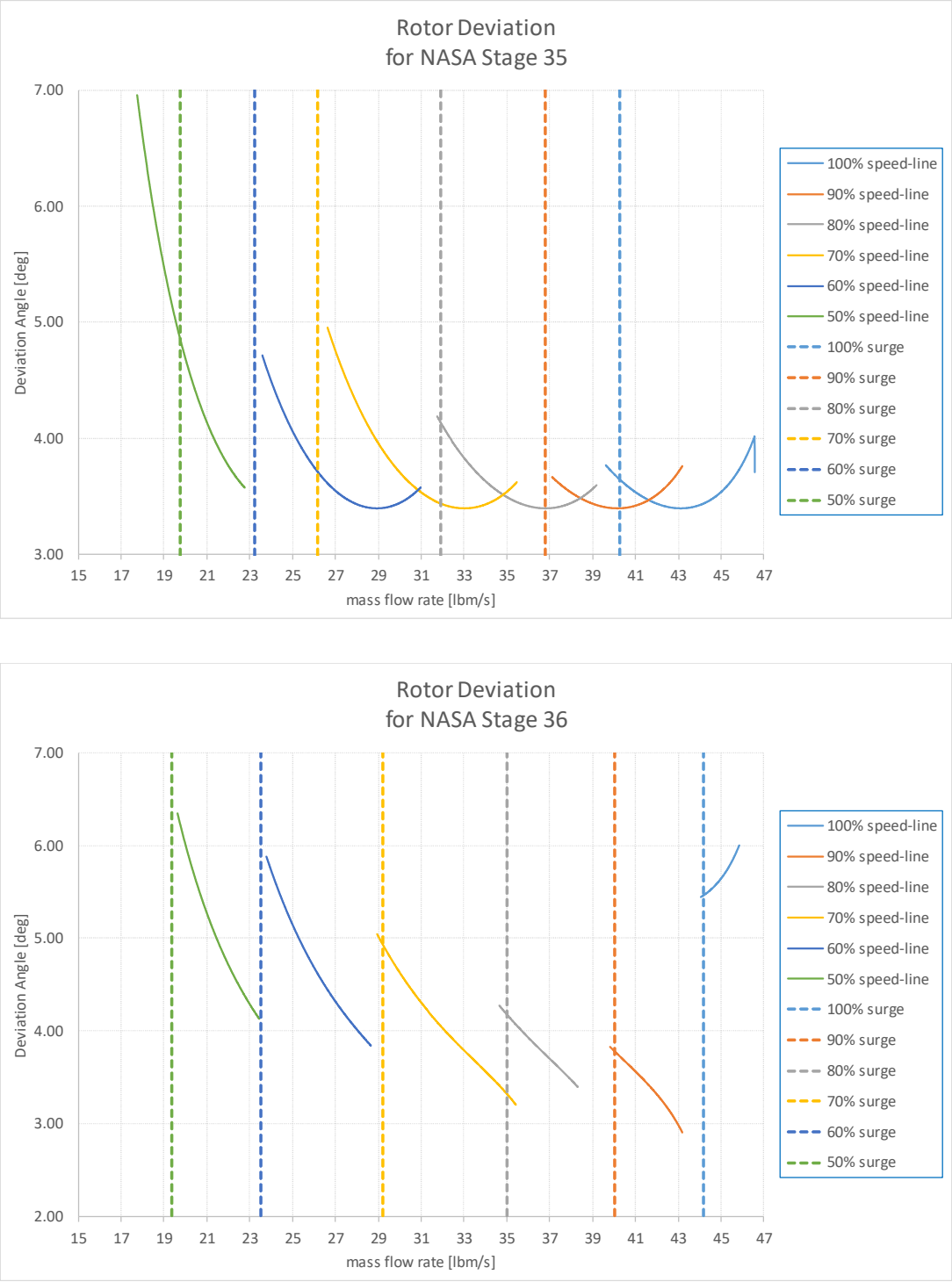

Figure 3-39: Off-design deviation variation for Rotor 35 and 36

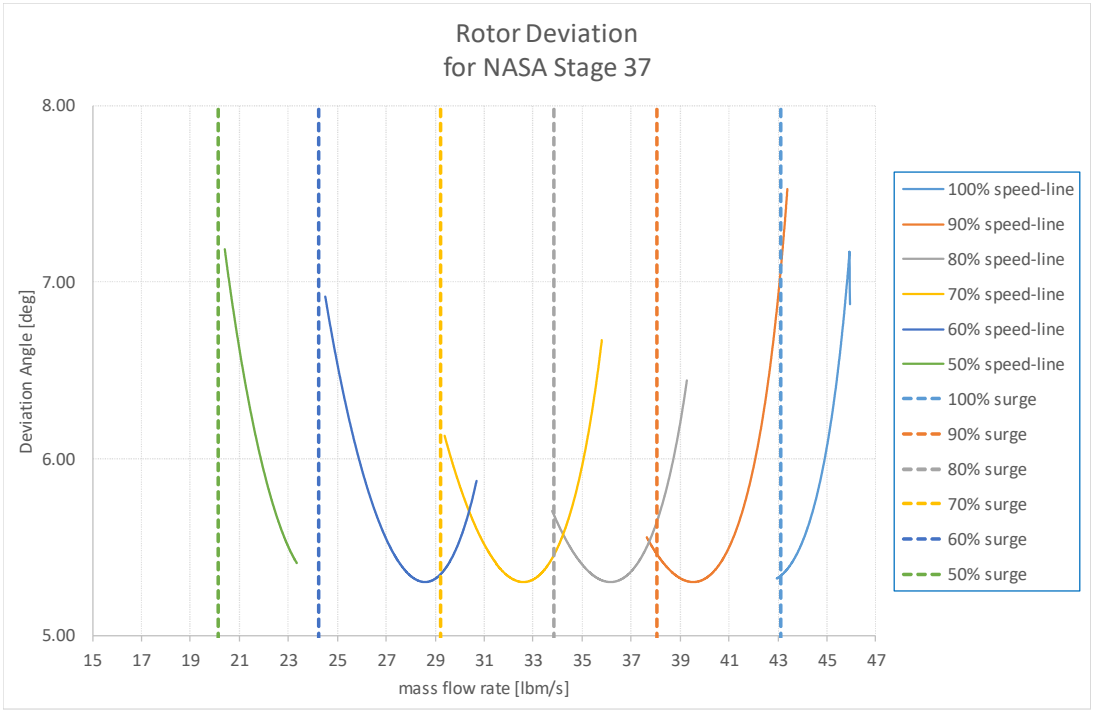

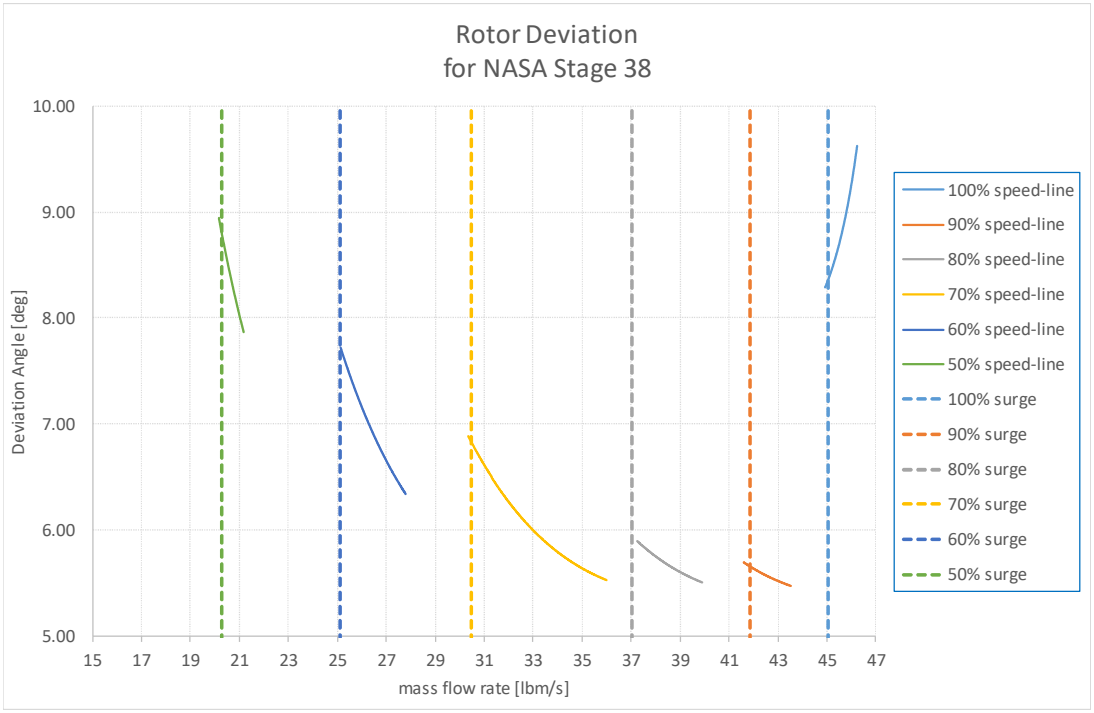

Figure 3-40: Off-design deviation variation for Rotor 37 and 28

Figures 3-39 and 3-40 show that there is no unique deviation angle to identify all of the stall points. The benefits of using a relatively simple ratio to capture physical phenomena is exactly that, being

simple. The onus of loss model complexity falls on the formulas that properly define the simultaneous interaction between deviation, blockage, and loss as presented in the previous sections.

Referring to the results obtained from Figures 3-34 to 3-37, the engineering-based surge criterion was segregated based on the rotor relative inlet Mach numbers. Two conditions were identified, subsonic inlet conditions and supersonic inlet conditions.

Subsonic Mach numbers: For the 50, 60, and 70% speed-lines, where the rotor relative inlet Mach number remains subsonic, it was found that stall identification occurred when the mid-span rotor exit absolute axial velocity ($V_{abs,X,ex}$) was less than or equal to the mid-span rotor exit absolute tangential velocity ($V_{abs,T,ex}$). It may be observed that, for some of the subsonic speed-lines, the rotor exit velocity components cross over occurred either before or after the experimental based stall conditions. This is due to the sensitivity of the overall loss model used to predict the missing speed-line data.

Supersonic Mach numbers: For the 80, 90, and 100% speed-lines, where the mid-span rotor relative inlet Mach number becomes unity or greater, and an inlet shock is encountered, it was found that stall occurs when the mid-span stator inlet absolute axial velocity ($V_{abs,X,in}$), identified as the dashed red curve, is less than the mid-span rotor exit absolute tangential velocity ($V_{abs,T,ex}$). Despite the fact that some of the supersonic based speed-lines revealed other velocity component cross-over, only that of the stator absolute inlet axial velocity ($V_{abs,X,in}$) versus the rotor absolute exit tangential velocity ($V_{abs,T,ex}$) showed a consistent behavior for stall identification for all of the above-mentioned speed-lines.

CHAPTER 4 RESULTS

"*It is common sense to take a method and try it. If it fails, admit it frankly and try another. But above all, try something.*" - Franklin D. Roosevelt

4.1 Off-design stage performance matching using tuned parameters

The results of the modified tuning process are shown in Figures 4-1 and 4-2. It can be seen that using imposed loss values, coupled with non-constant blockage factors and deviation angles, produced an alignment between the off-design mean-line results and the NASA reported off-design performance maps. With respect to a visual inspection, the off-design mean-line analysis masks the reported experimental test data, hence creating a near-exact match to the test data. Most importantly, the data in Appendix D reveals that there is a unique combination of blade row blockage factors and losses. This leads to a potential procedural improvement by automating the tuning process.

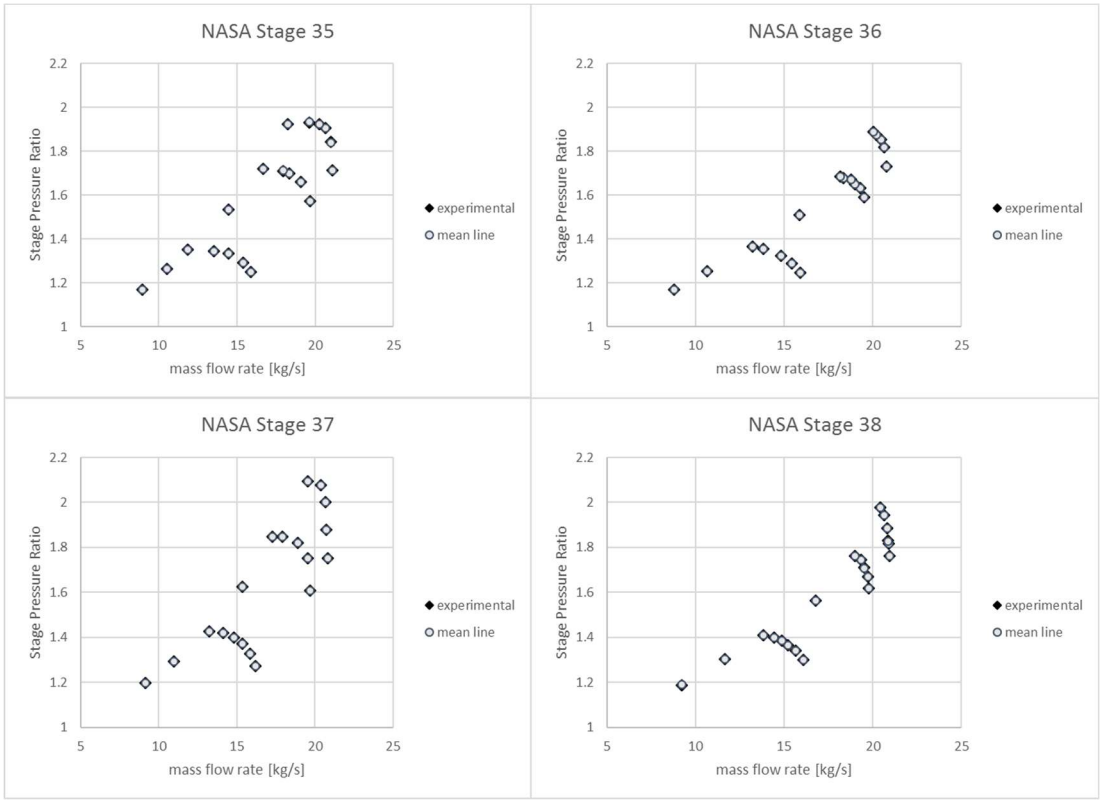

Figure 4-1: Stage Pressure Ratio, off-design mean-line analysis versus experimental results

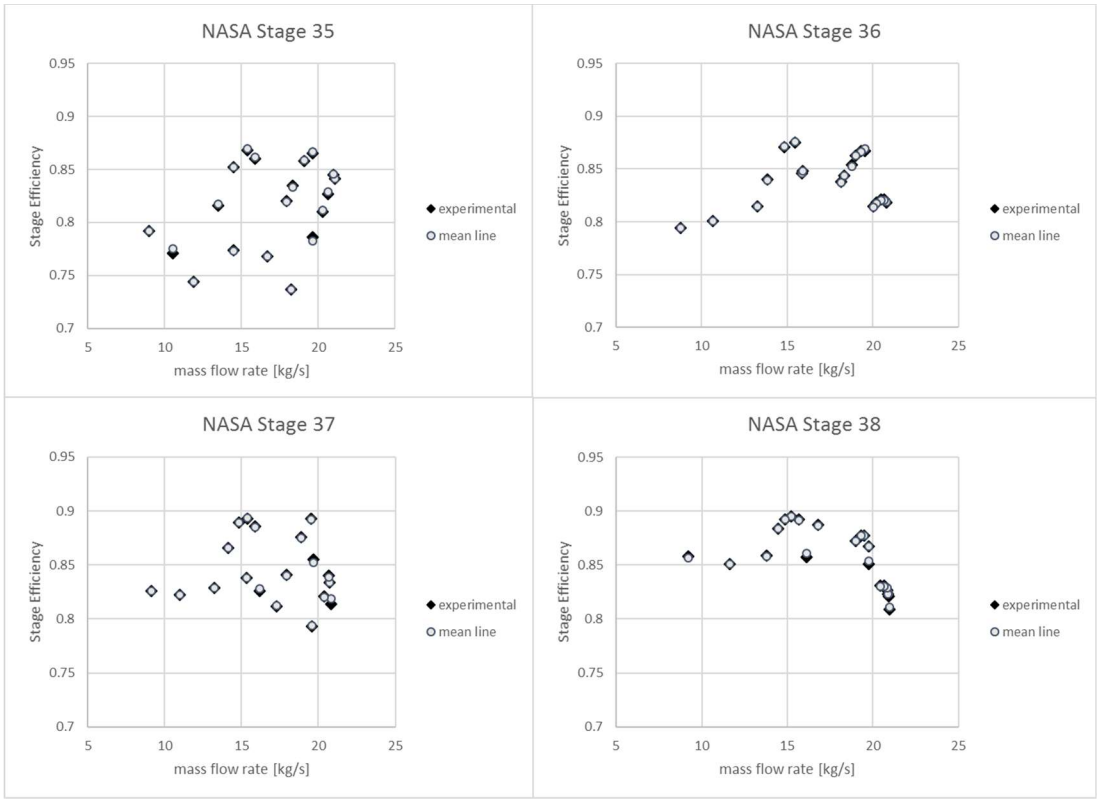

Figure 4-2: Stage Efficiency, off-design mean-line analysis versus experimental results

4.2 Off-design rotor performance

Overall rotor off-design mean-line model prediction: The formulae defining the rotor deviation, inlet blockage factor, total blade row loss, and exit blockage factor were converted and incorporated as a new off-design mean-line code loss model. This loss model was then incorporated into the axial compressor off-design mean-line code, specifically modified for this research, as described in the previous chapter. The results for NASA Rotor 35 at the 100% speed-line, as a *zoomed-in* observation, is shown in Figure 4-3. As it can be seen, the off-design mean-line model results follow closely the trend of the experimental data.

The complete predictive capabilities of the loss model for all four NASA Rotor analysis are shown in Figure 4-4, and its accompanying error analysis is shown in Figure 4-5. As it can be seen, a surprisingly well matched off-design prediction is achieved. The majority of the predicted rotor efficiencies are within the ±0.5% to ±1.0% objective of this investigation.

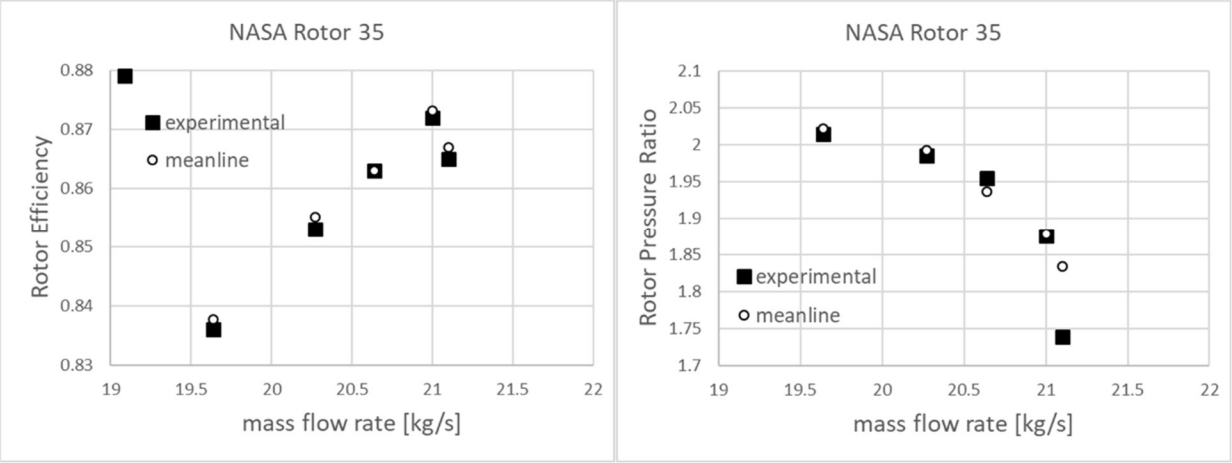

Figure 4-3 : Loss model results for NASA Rotor 35 @ 100% speed-line

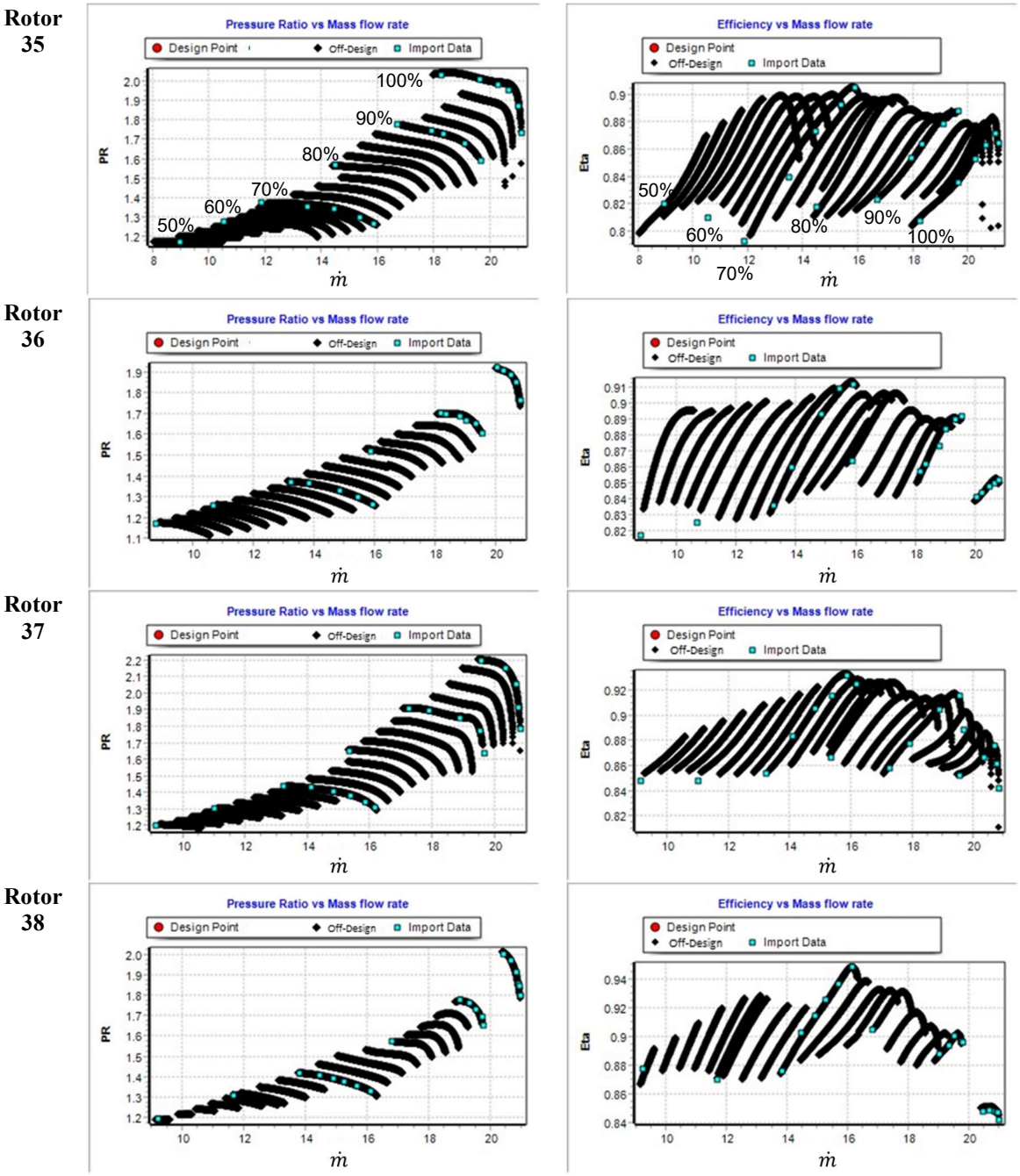

a) PR versus Mass flow rate b) Efficiency versus Mass flow rate

Figure 4-4: Rotor off-design performance chart [Author's software image capture]

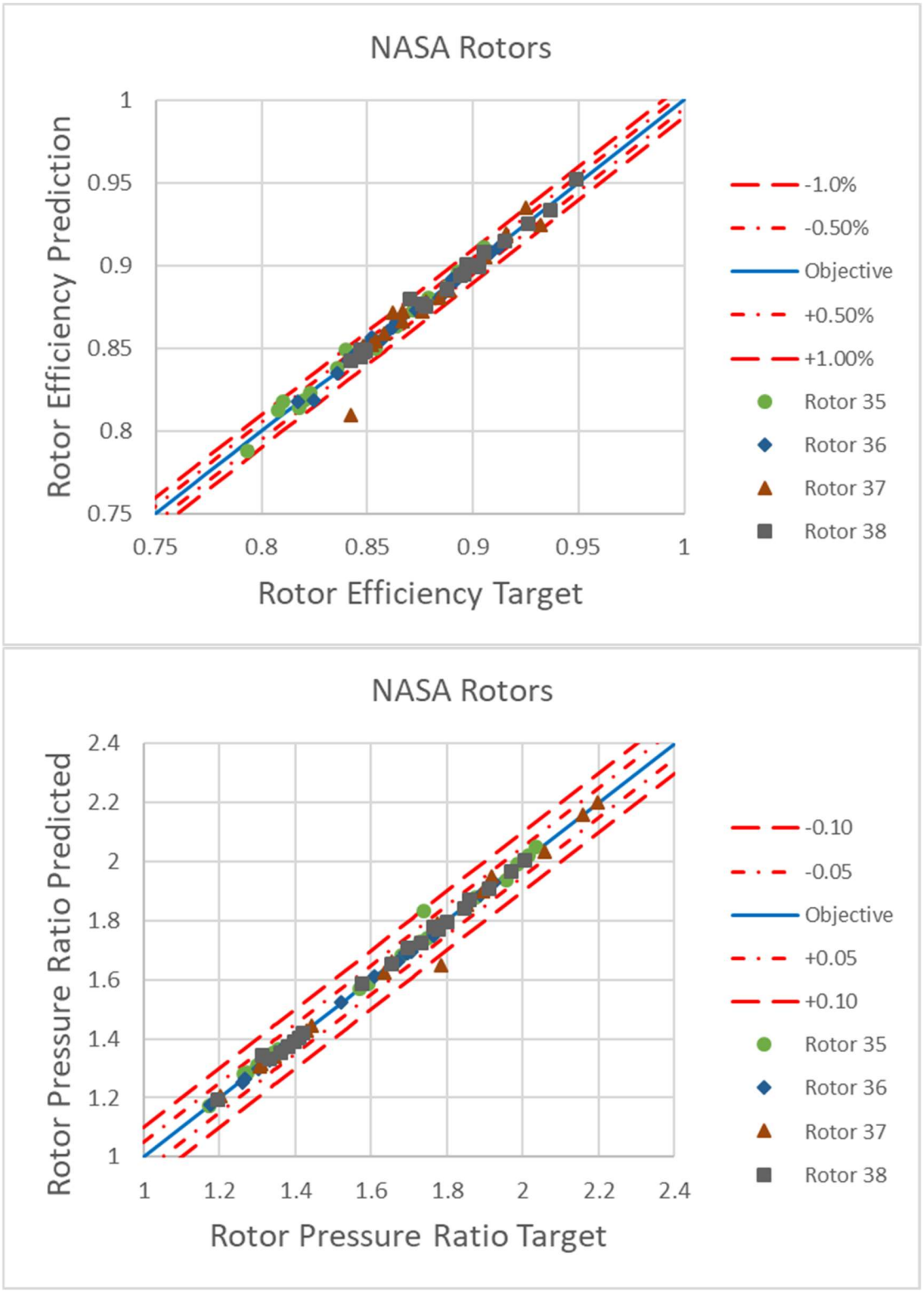

Figure 4-5: Rotor off-design performance prediction error analysis

4.3 Off-design stage performance

Overall stage off-design mean-line model prediction: The formulae defining the stator deviation, inlet blockage factor, total blade row loss, and exit blockage factor were also incorporated into a new off-design loss model in the axial compressor mean-line code. The results for NASA Stage 35 at the 100% speed-line is shown in Figure 4-6. As it can be seen, the off-design mean-line model results follow closely the trend of the experimental data.

The complete predictive capabilities of the loss model for all four NASA Stage analysis are shown in Figure 4-7, and its accompanying error analysis is shown in Figure 4-8. As it can be seen, a surprisingly well matched off-design stage prediction is achieved. The majority of the predicted stage efficiencies are within the ±0.5% to ±1.0% objective of this investigation. There are a few data points that lie outside of the ±1.0% imposed limits of this investigation. These outliers are considered acceptable for the purposes of this investigation.

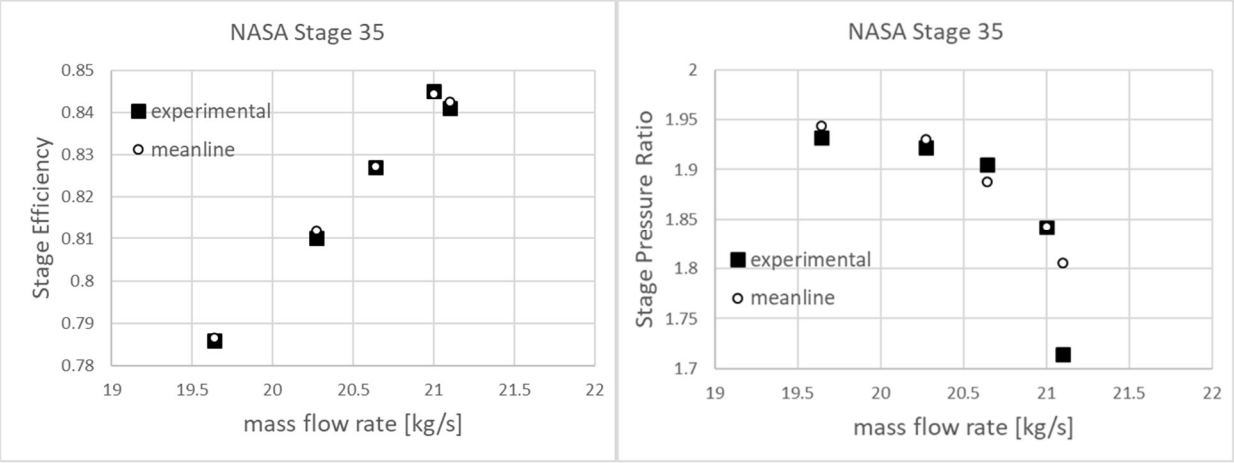

Figure 4-6: Loss model results for NASA Stage 35 @ 100% speed-line

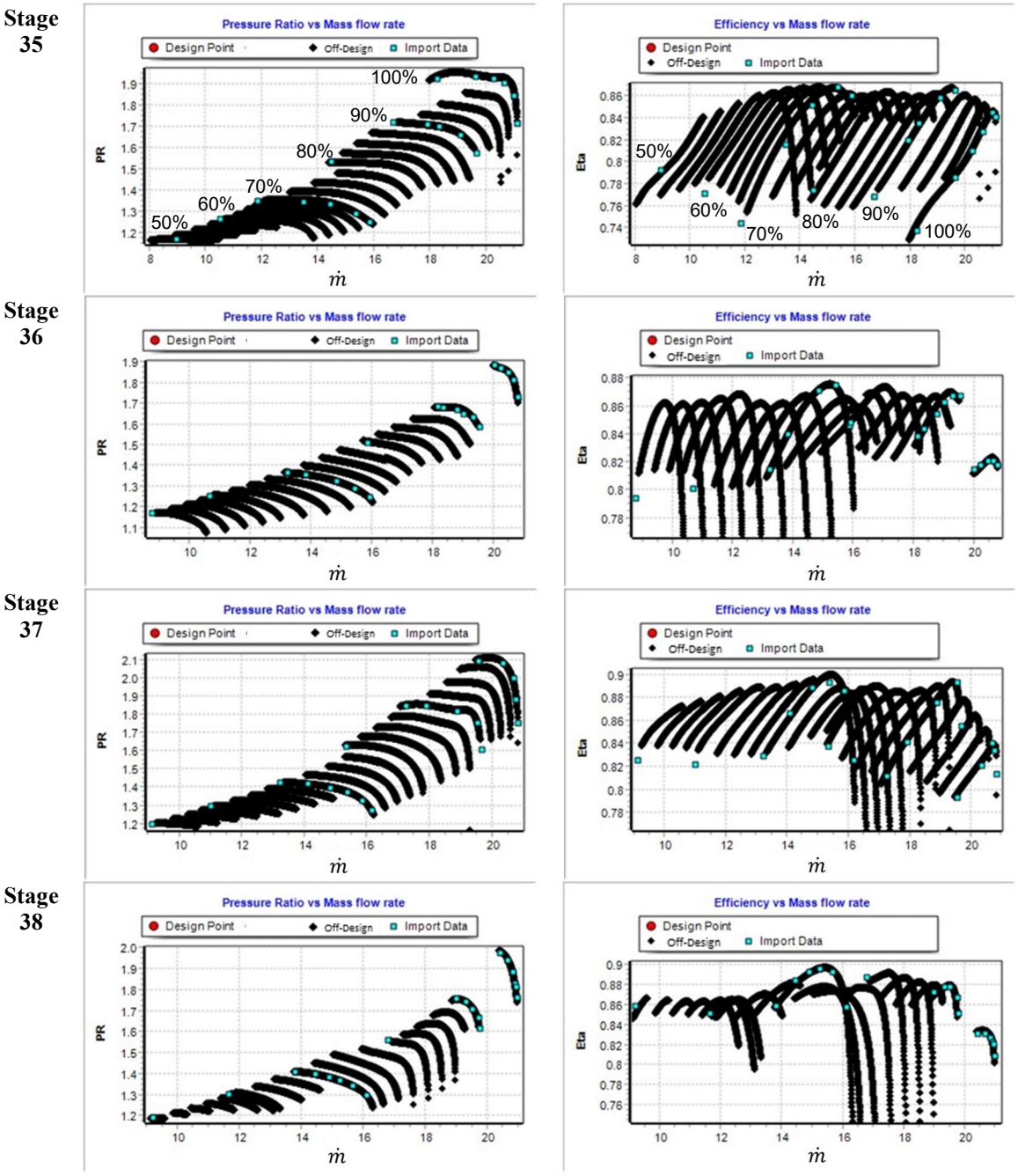

a) PR versus Mass flow rate b) Efficiency versus Mass flow rate

Figure 4-7: Stage performance map [Author's software image capture]

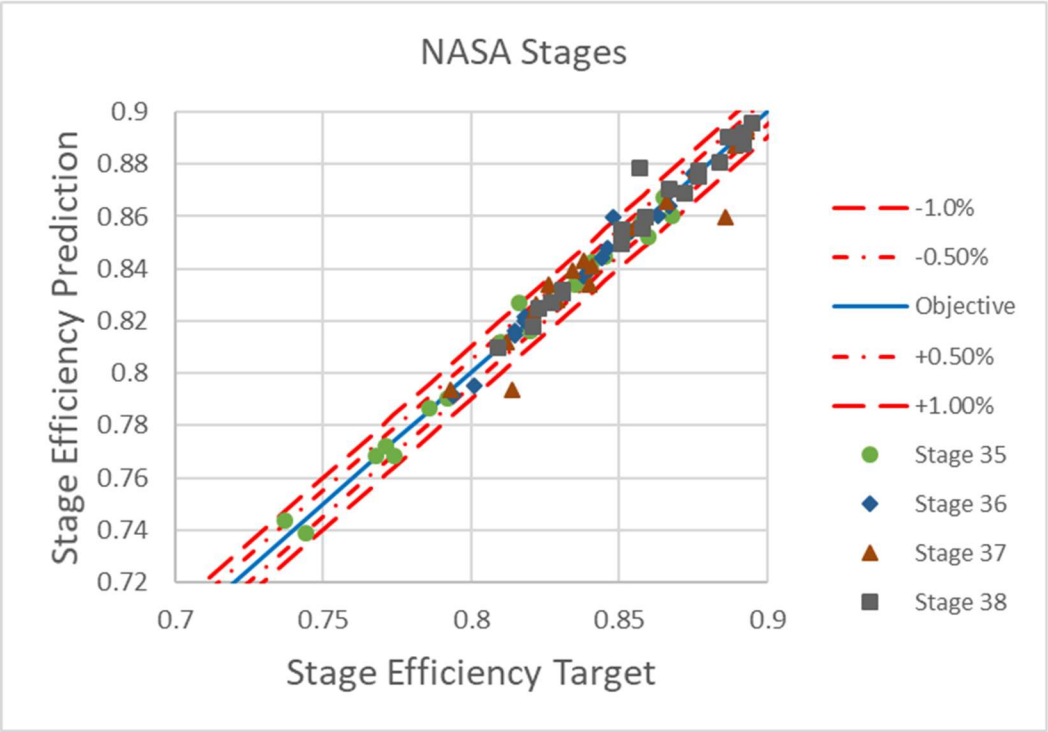

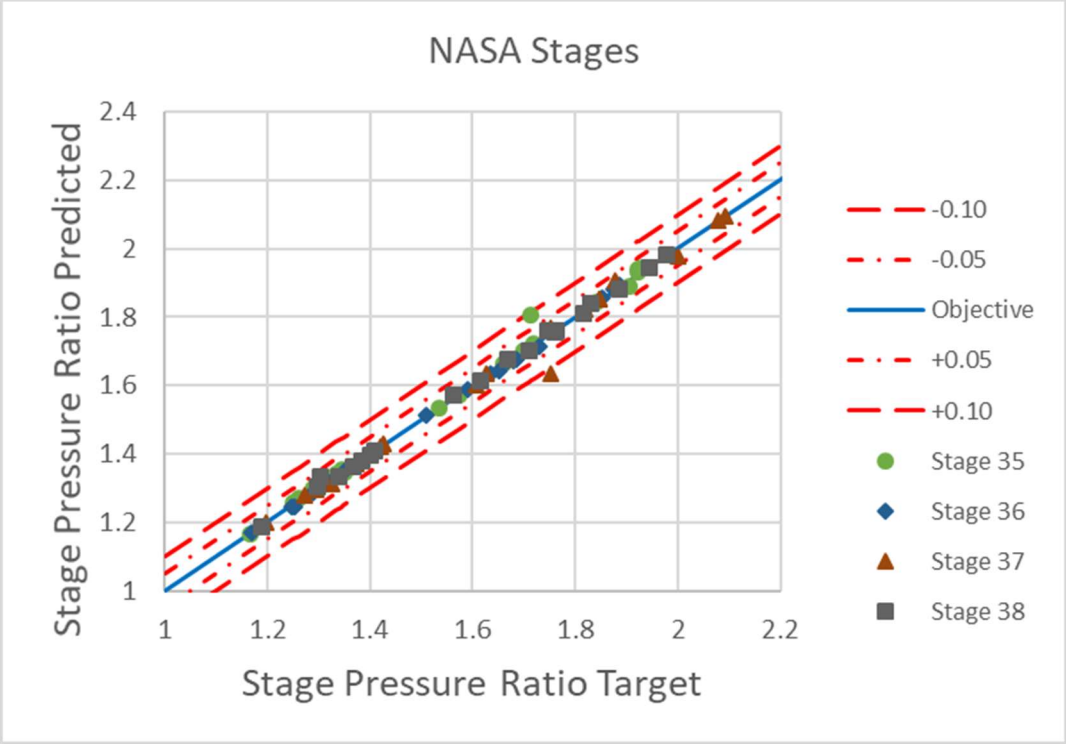

Figure 4-8: Stage prediction error analysis

4.4 Off-design performance modeling using choke criteria

The static pressure ratio based MAMF criteria, introduced in Chapter 3, was incorporated into the axial compressor mean-line model used in this investigation. Off-design speed-line increments of 2.5%, from 50% to 100%, of design-speed were created to show the strengths and weaknesses of the current MAMF criteria when coupled to the generalized loss model also described in Chapter 3. Figures 4-4 and 4-7 respectively describe the rotor and stage off-design performance in terms of pressure ratio versus mass flow rate, and its accompanying efficiency versus mass flow rate.

Rotor performance charts: In Figure 4-4 it can be observed that the identified MAMF conditions closely follow those of the complete data speed-lines of 100%, 90%, and 70% design RPM. The observed premature choking values of the subsonic conditions, those below the 70% design RPM, is due to the extrapolated nature of the generalized loss model[14].

Stage performance charts: In Figure 4-7, it is observed that the applied choke criteria produced similar results as those of the rotor performance charts. The most observable exception is that of the 80% speed-line of Stage 38, where a significant over-estimation exists. This was due to the particular challenge of matching the 80% loss model behavior through a combination of interpolation and best engineering judgment (B.E.J). Unlike the success of the rotor 80% speed-line loss model, the stator was found to be challenging.

As an overall observation, the MAMF criteria, when coupled to a properly tuned loss model, produces a significant improvement in predictive capabilities when compared to other published mean-line model based axial compressor performance maps which employ a constant mas flow convergence criteria or a solution divergence identification.

---

[14] The 50% and 60% loss model formulations were based on a combination of extrapolation and B.E.J. Not many published measured compressor data exist at these levels to give guidance in terms of anticipated blockage, deviation, and loss behaviors.

4.5 Off-design performance modeling using stall criteria

The proposed engineering-based stall criteria was incorporated in the axial compressor mean-line model described in Chapter 3. Off-design speed-lines, from 50% to 100% of design-speed, were created in increments of 2.5%. The results of the engineering-based are presented in Figure 4-4 and 4-7, and Appendix G Tables G-1 to G-4 represent the minimum and maximum mass flow rate values, calculated by both the engineering-based choke criteria and stall criteria, to generate the speed-lines. Respectively, these figures describe the predicted rotor and stage off-design performance against the reported test data.

Rotor performance charts: For all four NASA rotors found in Figure 4-4, it can be observed that the stall point conditions closely follow those of the available test data. The 100% speed-line stall point result for Rotor 35, when compared to the other rotor trends, may be a potential anomaly.

Stage performance charts: In Figure 4-7, it can be clearly observed that the applied stall criteria produce the proper stage stall point trends.

As an overall observation, the proposed novel engineering-based stall criteria, when coupled to a properly matched mean-line loss model as described in Chapter 3, yields predictions that are comparable or better to those that are publicly available through literature, refer to Chapter 2 Figures 2-8 to 2-13. In terms of consistency, the resulting stall lines remain similar in accuracy amongst the four NASA stages under investigation. Figure 4-9 shows the comparison between the results of a NASA based compressor mean-line code, Figure 4-9a [8] and of that generated by the present loss model, Figure 4-9b. As it can be seen in Figure 4-9c, which is a manually superimposed image of the two Stage 37 compressor performance maps, the engineering-based stall criterion results are similar to that of the NASA compressor code, and the speed-line trends using the current loss model show a better match to the experimental test results.

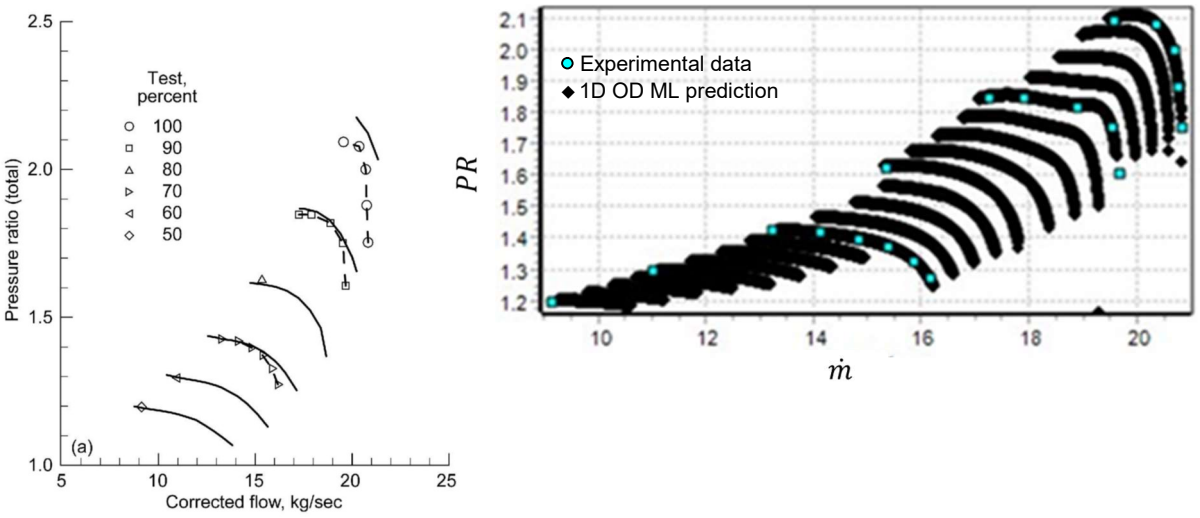

a) Vere's NASA Stage 37 [8] b) Author's NASA Stage 37

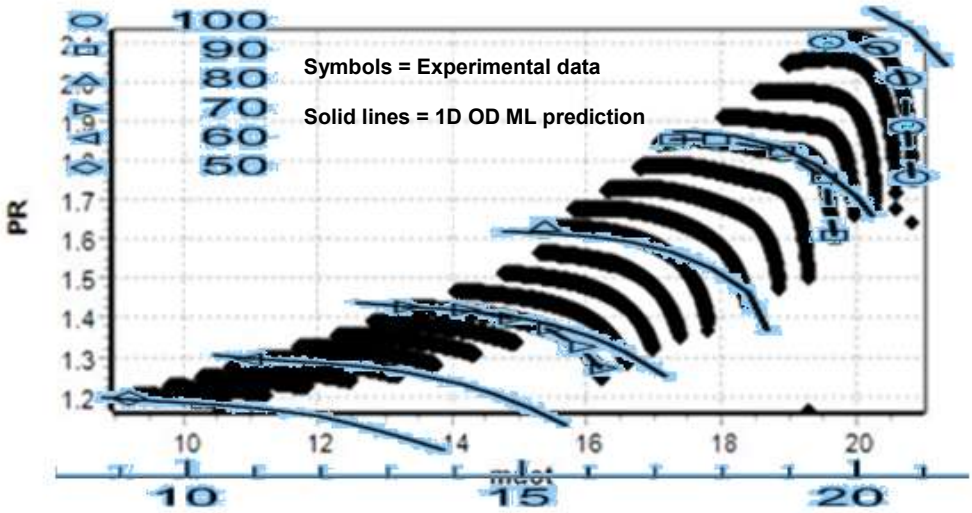

c) Compressor performance maps comparison

Veres-Blue, Kidikian-Black

Figure 4-9: Comparison of Veres' vs current OD results for NASA Stage 37

Additionally, based on the results shown in Tables G-1 to G-4 as found in Appendix G, it is noted that when compared to their experimental counterparts, the predicted stall points are within a maximum error of ±0.65 lbm/sec (±0.29 kg/sec). This error value is surprisingly similar to the reported mass flow error of ±0.66 lbm/sec (±0.3 kg/sec) as described in the respective NASA

reports for Stages 35 to 38. The only significantly noticeable error is that of Stage 35 at the 50% speed-line condition. This can be attributed to the fact that the mean-line loss model, as described in Chapter 3, was developed without test data guidance for the low-end 50 and 60% speed lines.

4.5.1 Stall model comparisons

The proposed simple, novel, and effective stall criteria was shown to be able to predict, within a relatively small error of ±0.65 lbm/sec (±0.29 kg/sec), the onset of the near-stall conditions. The criterion was successful in doing so because the loss model that it was accompanying was properly matched to actual reported data. Furthermore, the blade row loss model constituents of loss, deviation, and inlet & exit blockage factors captured the known physical behaviors described in the various cited literature. Additionally, the complex nature of the rotor-stator interaction which involves boundary layer interaction, secondary vortex interaction, and clearance interaction, was modeled and implicitly captured by casting the stator loss model constituents as a function of the rotor RPM.

With such a simple stall criterion, one may be lead to ask what was missing from the previously cited stall or surge models. First, the fact that the off-design performance charts, presented by the cited authors, did not match or predict with consistency or visual accuracy the various test compressors in their reports. In terms of potential use, each of the cited surge models attempt to compensate for the fact that the loss model that it accompanies did not match the overall speed-line behaviors of the test compressor of interest[15]. For the sake of the *how about* and *what if* curiosity, the commonly cited models of the De Haller value, Lieblein's diffusion factor, and rotor critical incidence were executed to see if there were any potential comparisons to the simple, novel, and effective stall criteria presented.

De Haller value: In Figures 4-10 to 4-13, the off-design de Haller values for the rotor, with the value of 0.72 as a cut-off identifier, and the proposed stall criterion, with its cut-off identifier of 1.0, have been plotted and presented for the 100, 90, 80, 70, 60, and 50% speed-lines. Below the cut-off identifiers stall is considered to occur. For both plot types, the off-design mean-line model

[15] None of the cited authors offered the raw data that they used to create their models for other researchers to corroborate their findings.

with the matched loss model was executed. The off-design de Haller value ($V_{rel,2}$ / $V_{rel,1}$) and the proposed stall criteria formulation (axial velocity vs tangential velocity) was calculated for each speed-line from the MAMF condition until the proposed stall criteria cut-off of 1.0 was achieved.

What the plots reveal is that the de Haller value does not present a cut-off point, nor possesses any peaks, valleys, or asymptotes near the stall conditions. The de Haller value is mainly used as a rule-of-thumb during the conceptual or design-point analysis of compressors. Also, the de Haller value was introduced in 1953 for blade profile shapes that were not of the MCA type. Public literature was not found that shows that the de Haller value has been updated to reflect the various blade profile shapes used since the early 1950's. Furthermore, if the de Haller values were employed as suggested during the creation of the NASA stages, all four stages should have been rejected due to the fact that the 100% mid speed-line mass flow rate was below the classical 0.72 cut-off.

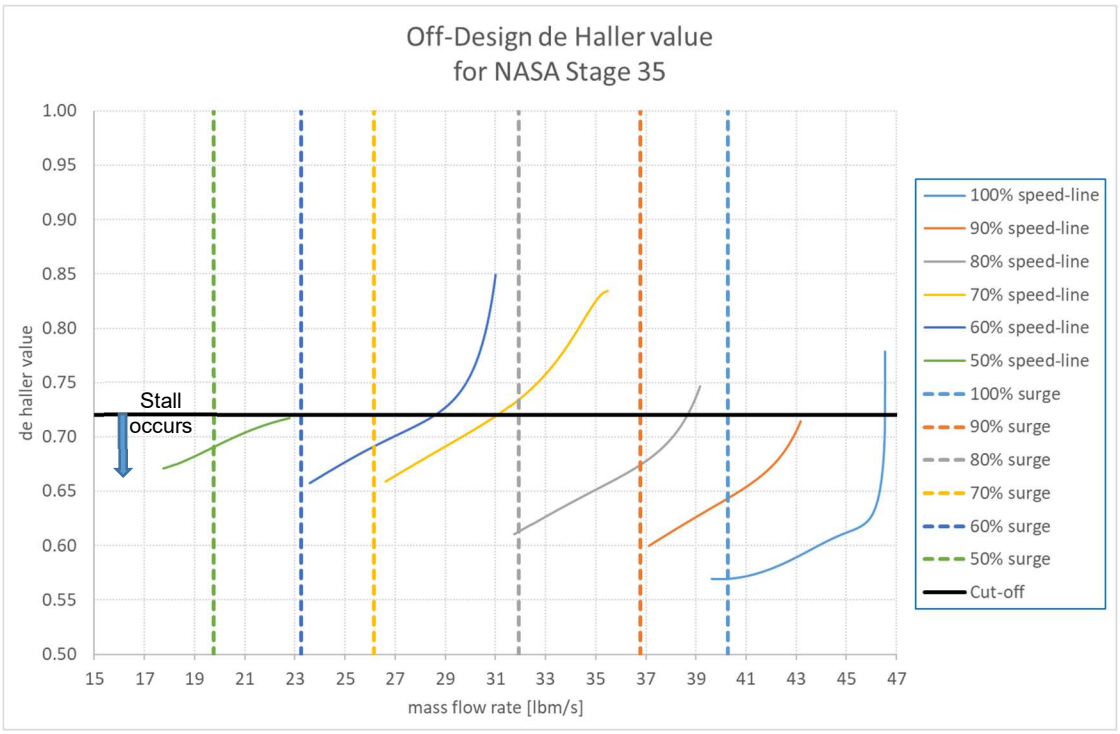

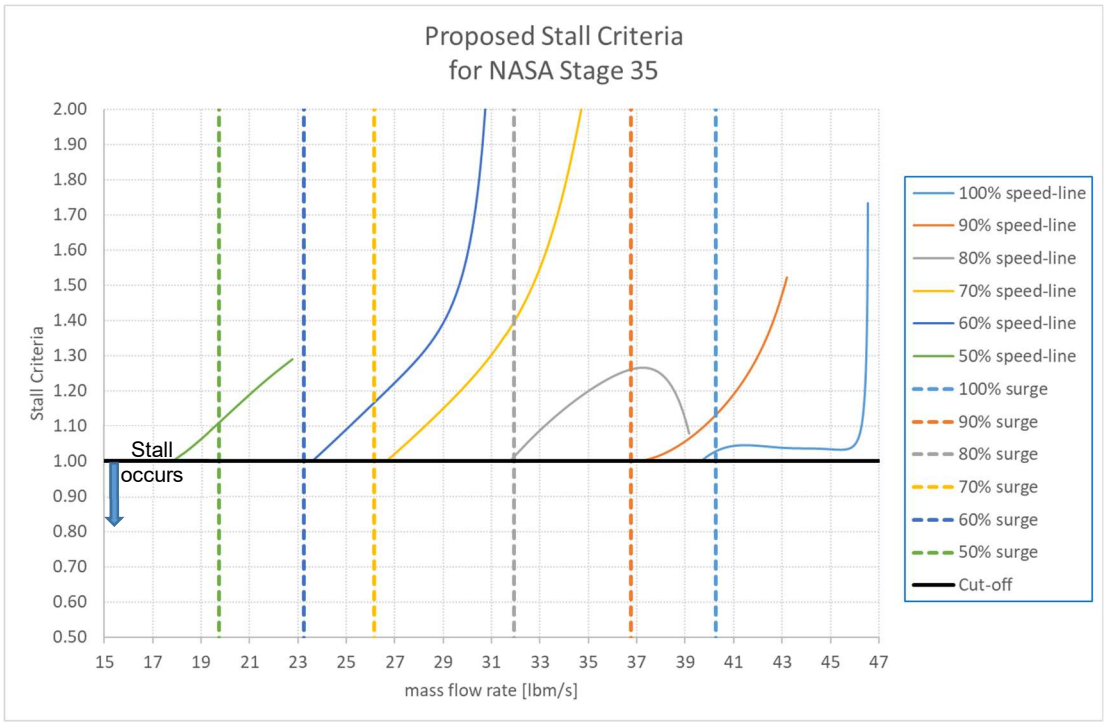

Figure 4-10: Comparison of de Haller value versus proposed stall criteria for NASA Stage 35

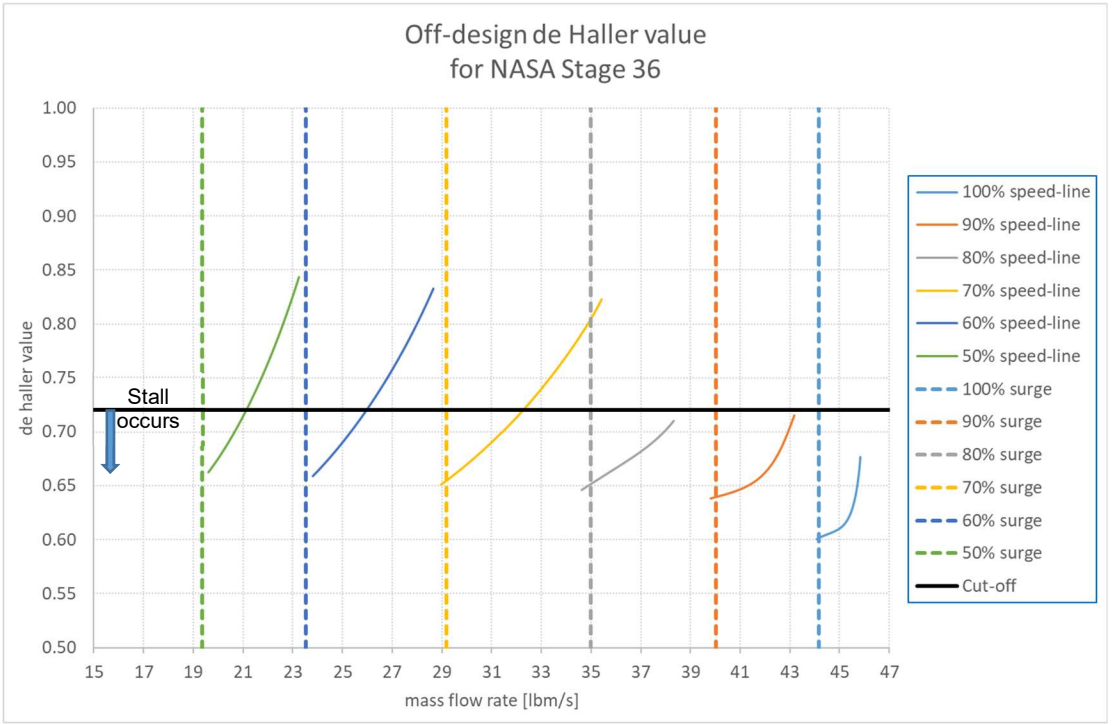

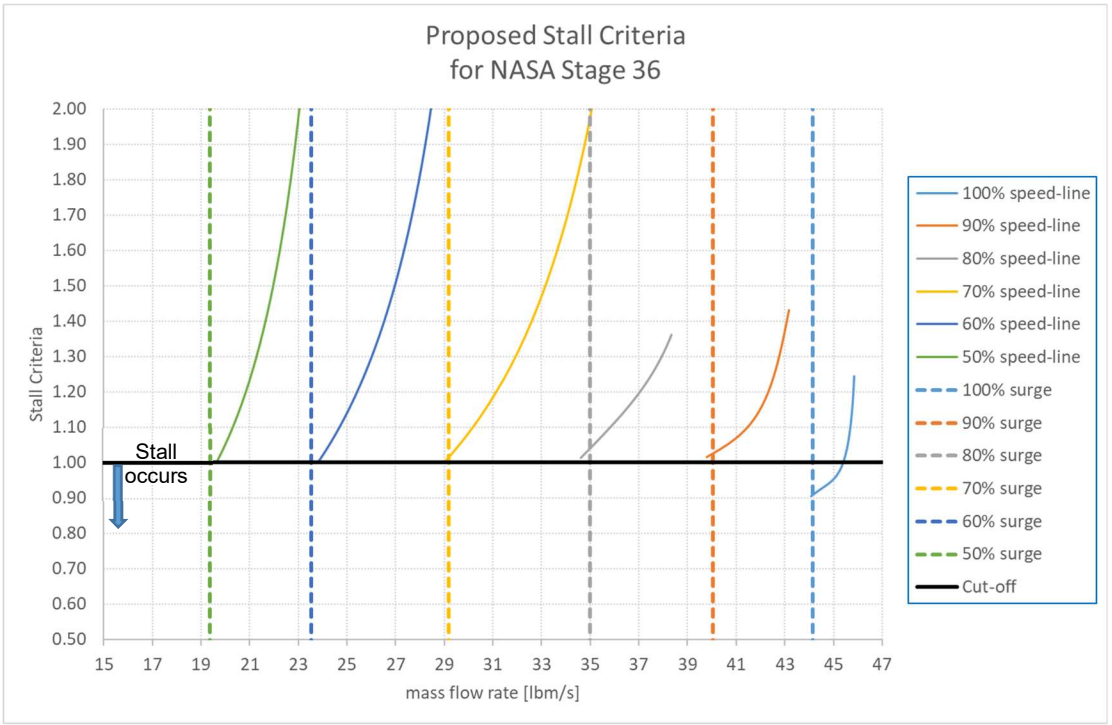

Figure 4-11: Comparison of de Haller value versus proposed stall criteria for NASA Stage 36

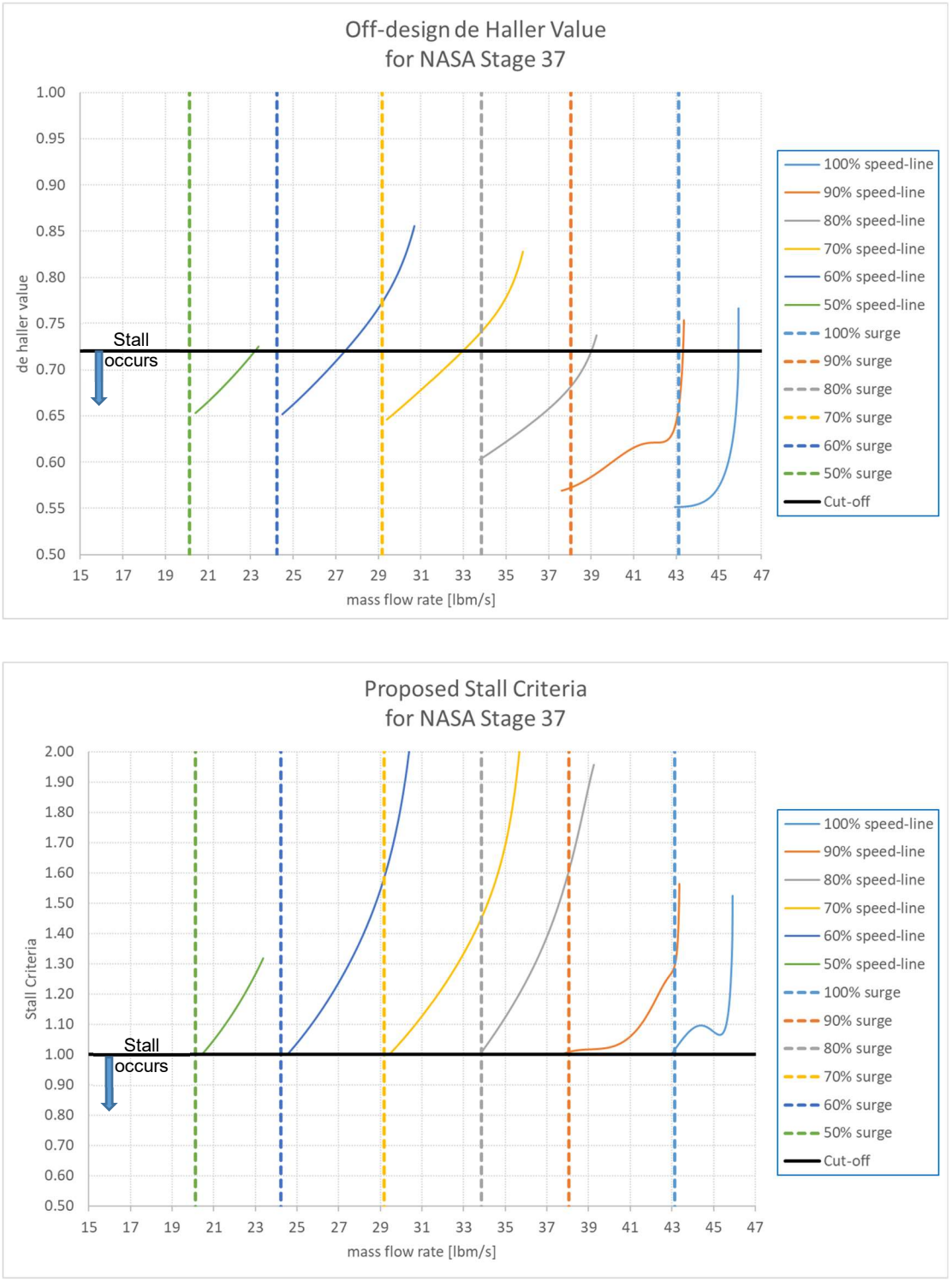

Figure 4-12: Comparison of de Haller value versus proposed stall criteria for NASA Stage 37

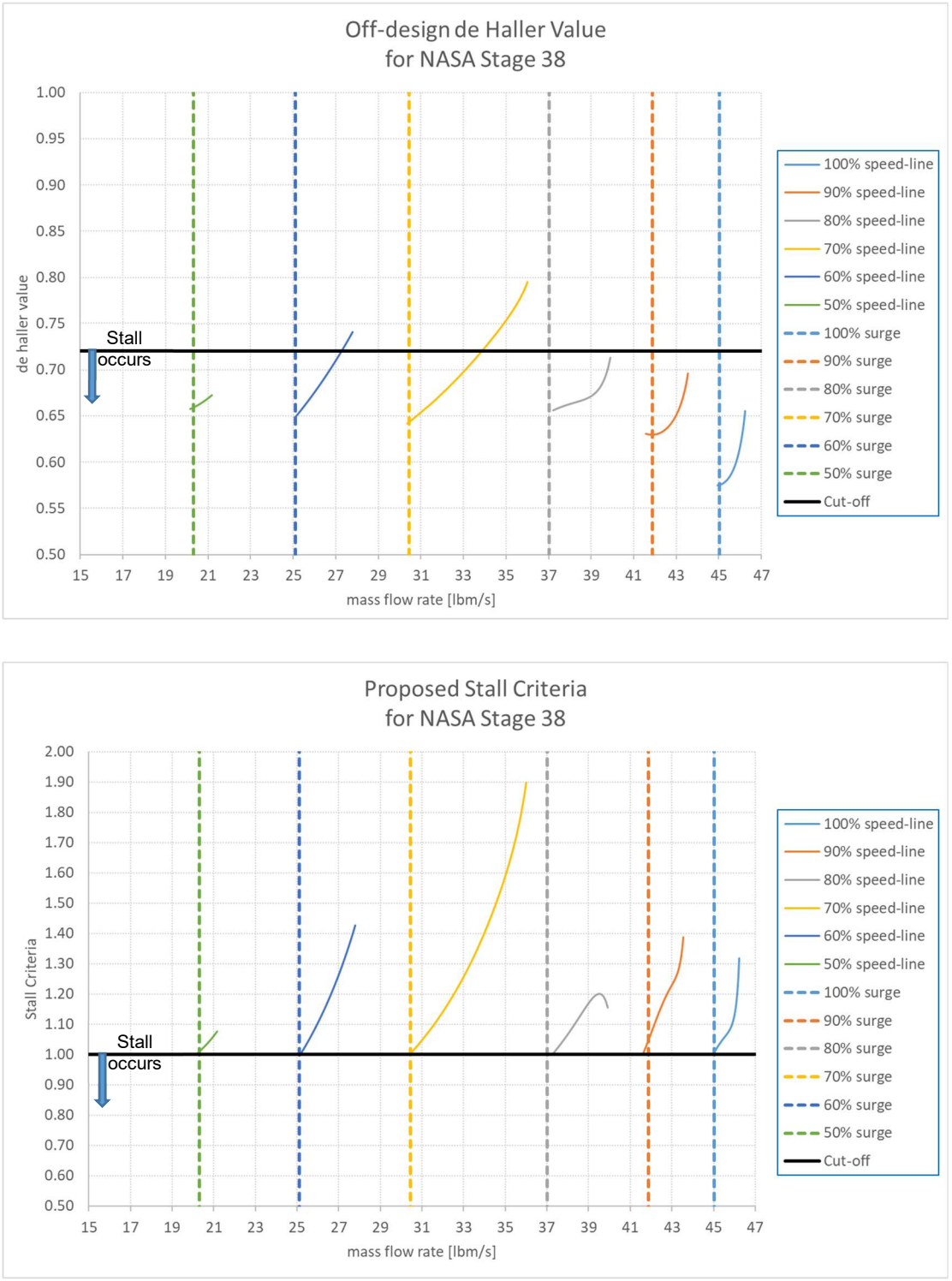

Figure 4-13: Comparison of de Haller value versus proposed stall criteria for NASA Stage 38

Lieblein's Diffusion Factor: Figure 4-14 to 4-17 present the off-design Lieblein Diffusion Factor for rotors and stators. The off-design mean-line model with the matched loss model was executed. The off-design Lieblein Diffusion Factor was calculated for each speed-line from the MAMF condition until the proposed stall criteria cut-off of 1.0 was achieved.

Similar to the de Haller plots, there are no visible peaks, valleys, or asymptotes to be observed near the stall points. Additionally, there are no known cut-off points for the Diffusion Factors (DF). Veres [8] and Barbosa & Figueredo [58] mention a DF value of approximately 0.6. However, if this value is taken into consideration, then the majority of all the rotor DF values calculated will be considered to be in stall or surge, which is not representative for the four NASA stages presented in this investigation.

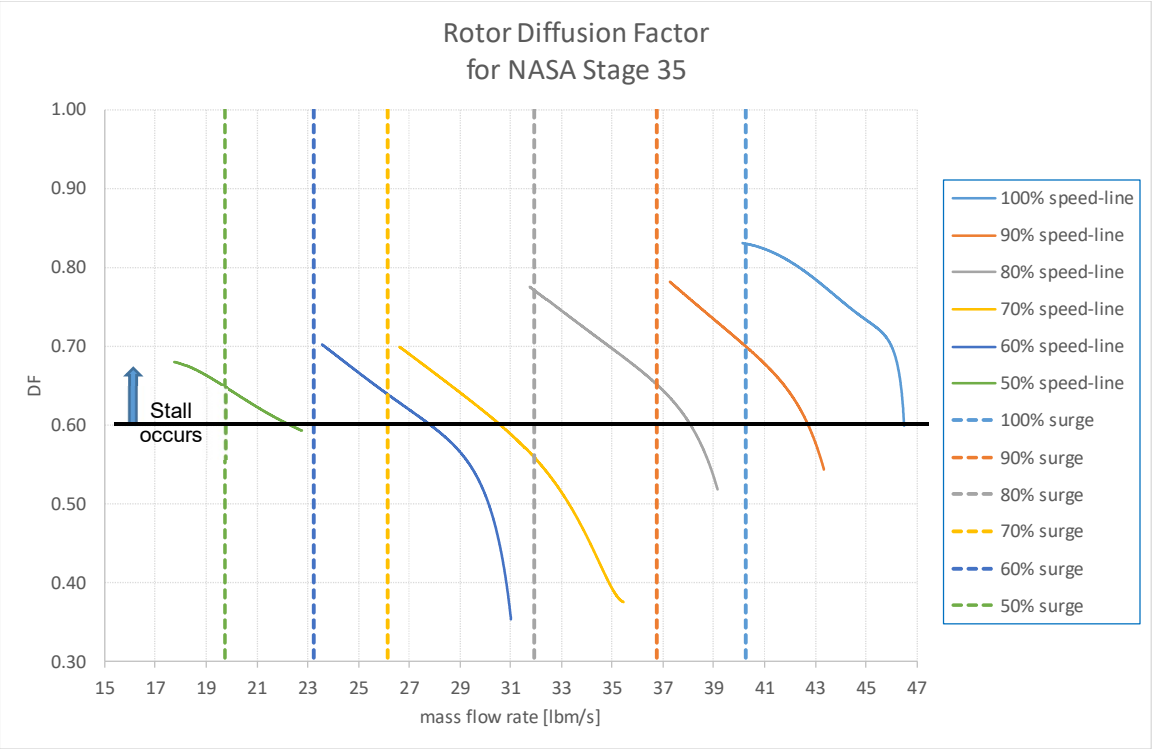

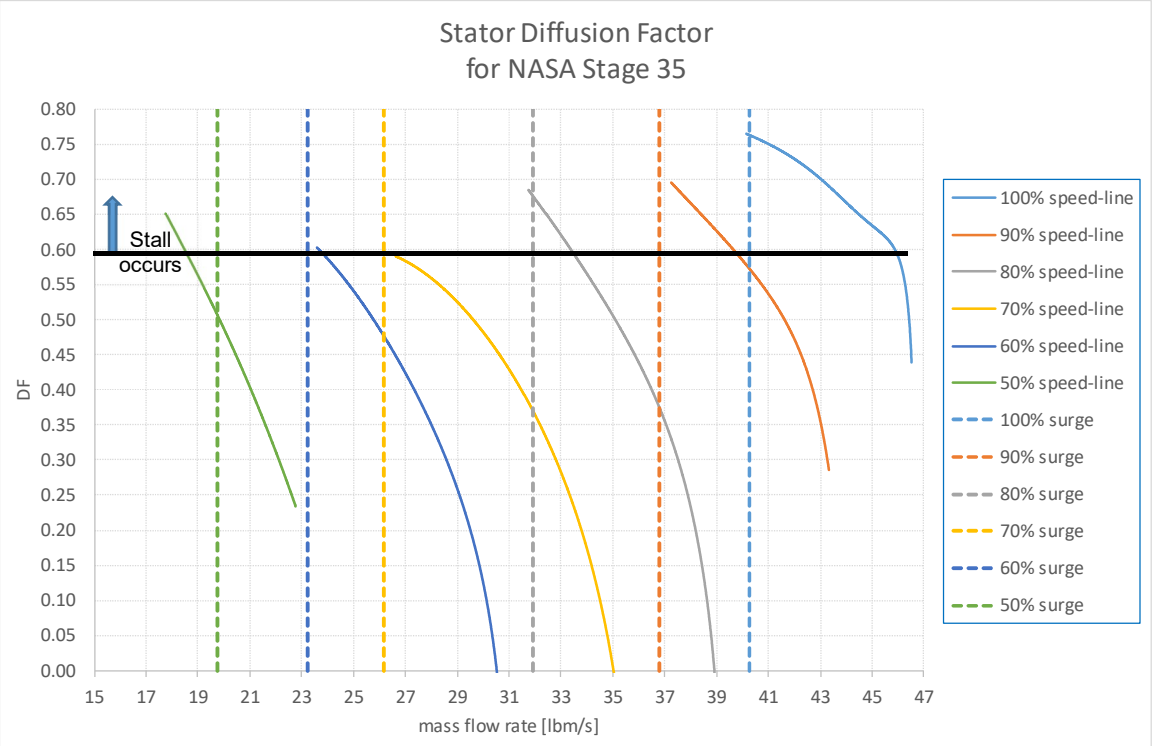

Figure 4-14: Off-design rotor and stator diffusion factors for NASA Stage 35

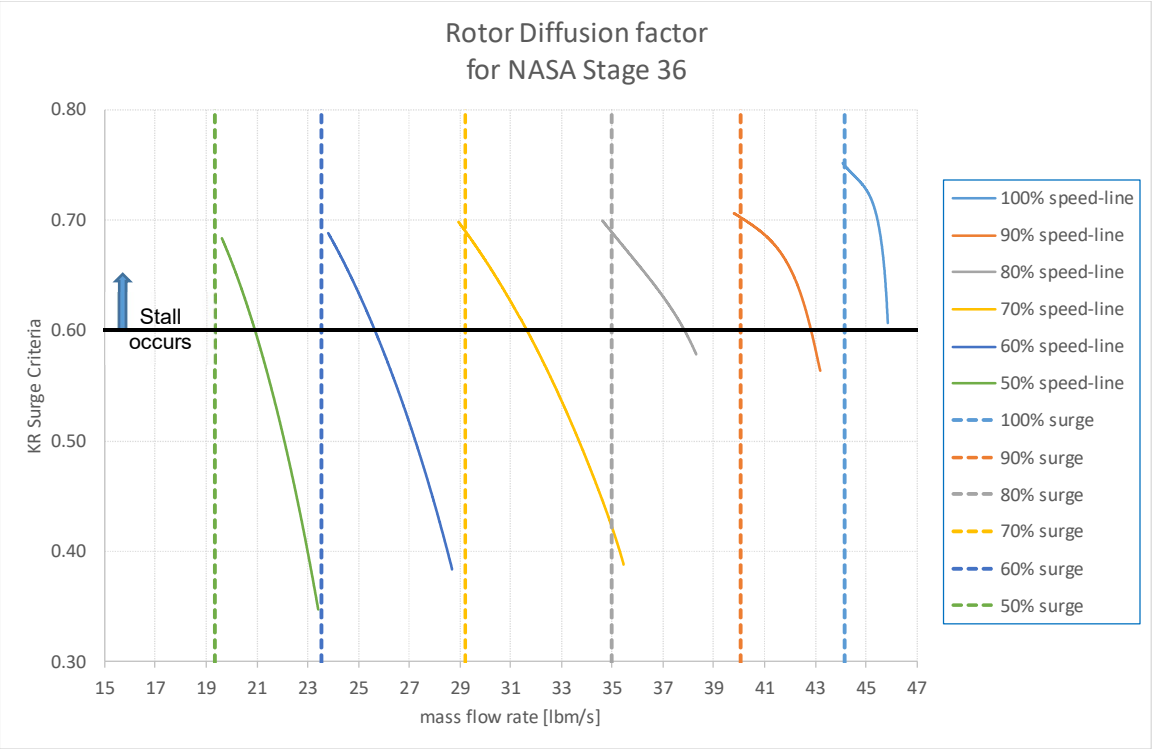

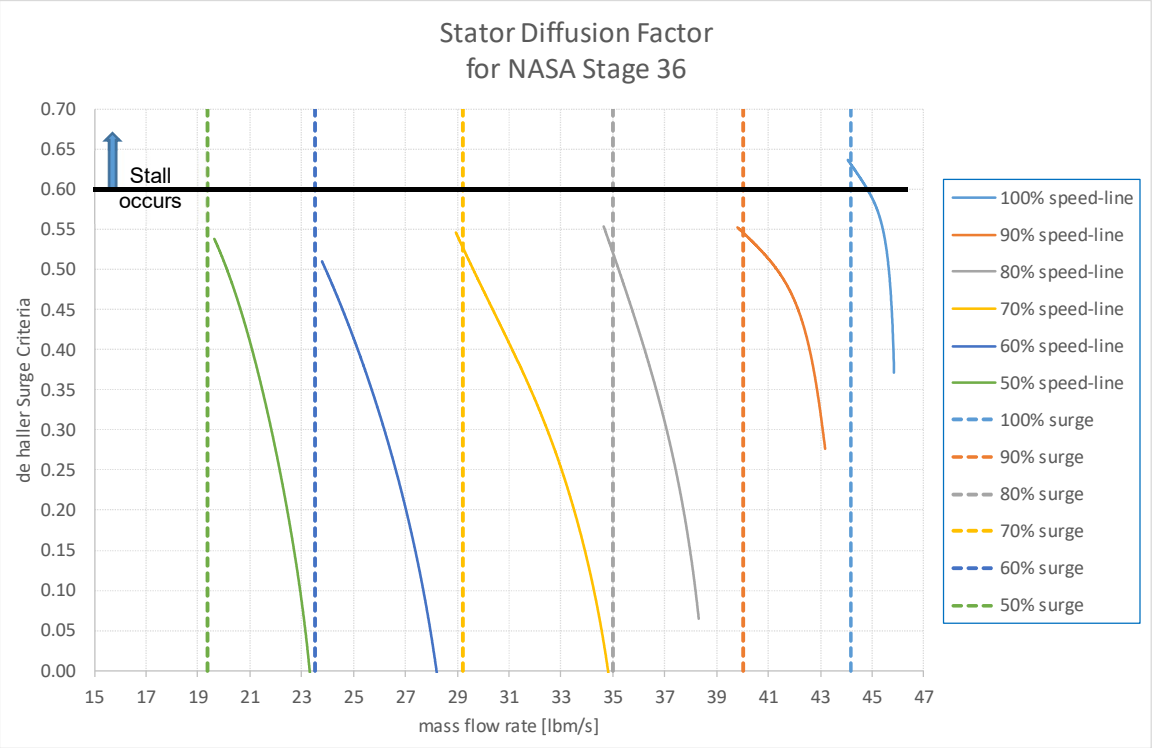

Figure 4-15: Off-design rotor and stator diffusion factors for NASA Stage 36

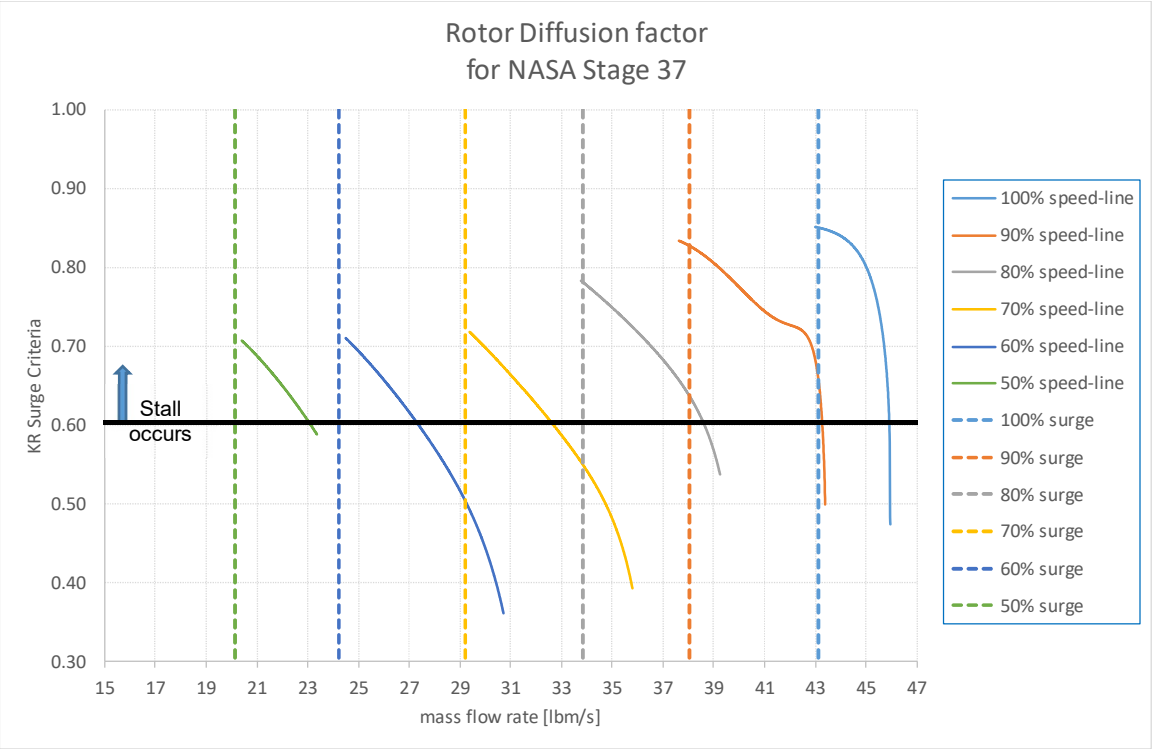

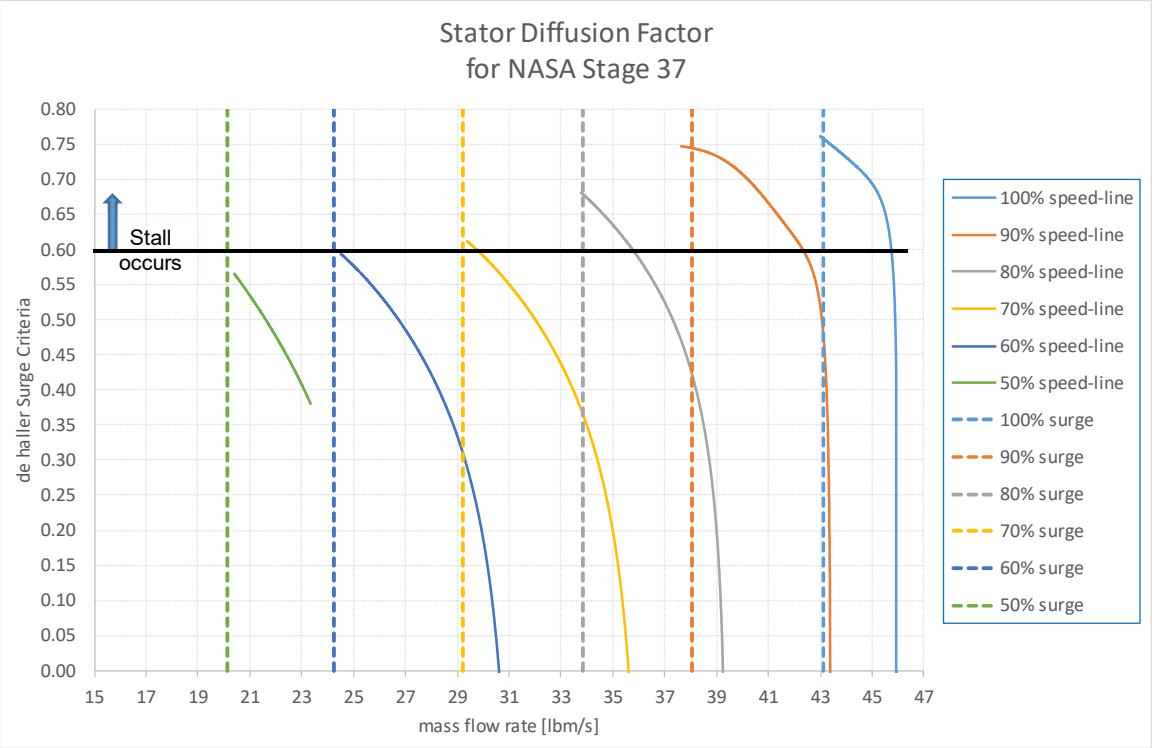

Figure 4-16: Off-design rotor and stator diffusion factors for NASA Stage 37

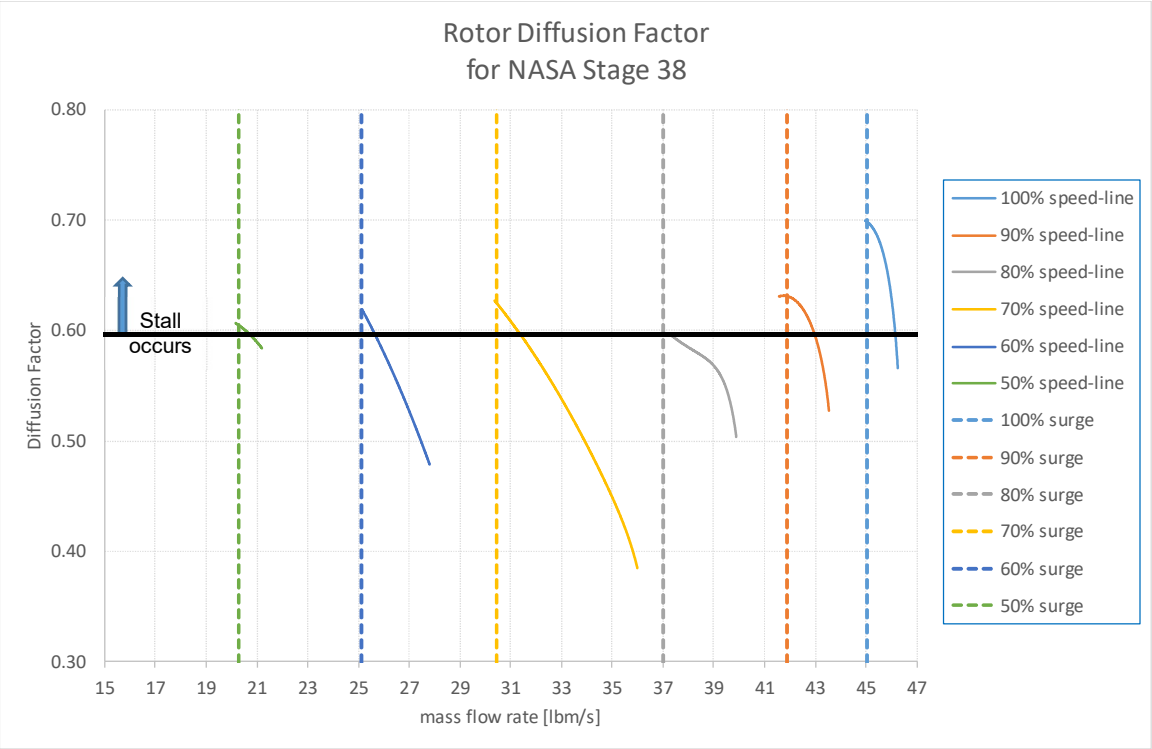

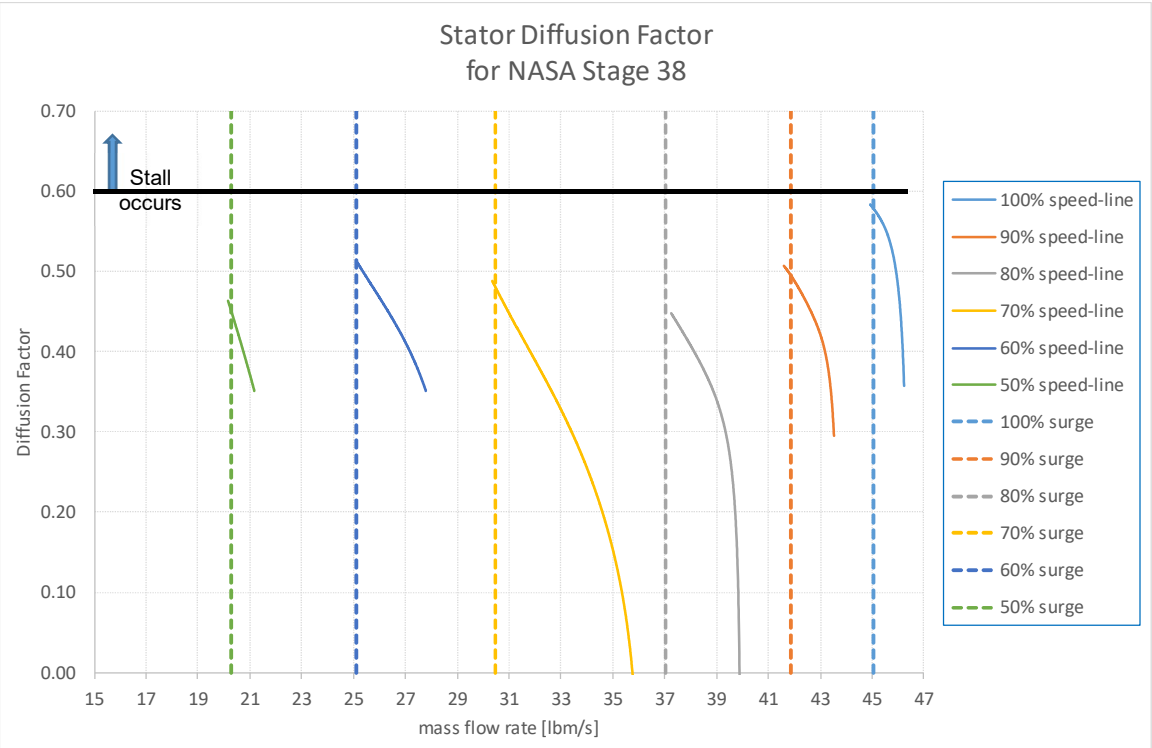

Figure 4-17: Off-design rotor and stator diffusion factors for NASA Stage 38

Rotor Critical Incidence: Another perspective of stall and surge onset comes from the work of Camp & Day [119]. In their 1997 paper they presented the stall and surge measurements of a single stage low-speed compressor and a Cambridge four-stage high-speed axial compressor. They describe two particular phenomenon i) a short length scale disturbance which they named *spike* and driven by 3D effects of high rotor incidence and ii) a long length scale disturbance, which they coined as *modal oscillation*, associated with 2D instability [119]. The information related to the four NASA stages under investigation did not include measurements to be able to detect any *spike* or *modal oscillations*. It was decided to plot the *pressure rise coefficient*, as defined by Camp & Day as $\Delta P_{T\text{-}S} / \frac{1}{2}\rho U^2_{ave}$, against the off-design flow coefficient, V_x / U_{ave}, and the off-design mass flow rate for the 70, 80, 90, and 100% speed-lines of Rotor 35, Figure 4-18. What can be seen from both plots is that there is no indication of a peak pressure rise coefficient during the off-design excursion. Additionally, there seems to be no indication of a cut-off point or an asymptotic behaviour near the stall points.

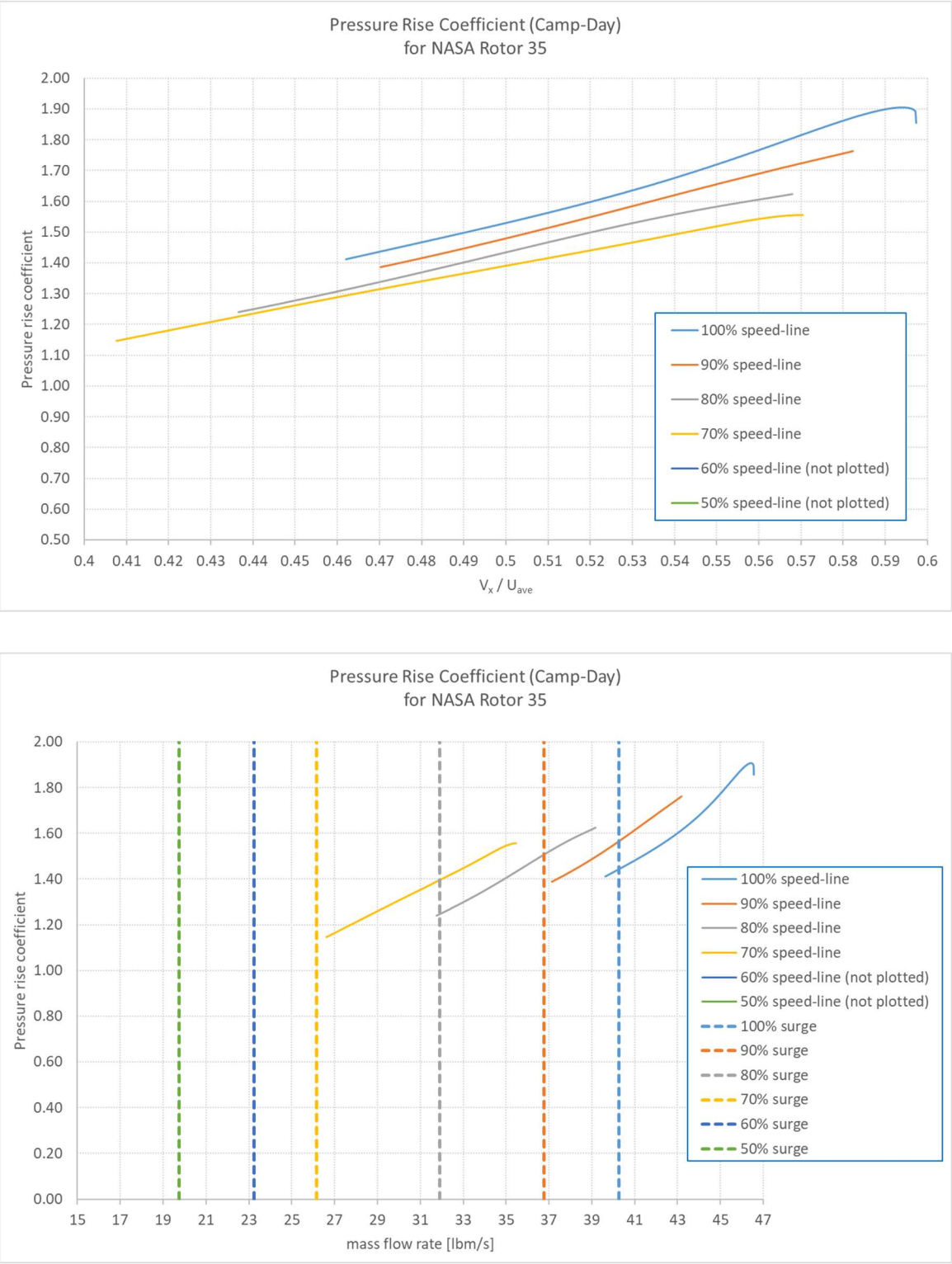

Figure 4-18: Off-design pressure rise coefficient for NASA Stage 35

CHAPTER 5 CONCLUSION AND RECOMMENDATIONS

In this thesis a description of the various obstacles encountered with respect to developing an accurate off-design mean-line methodology based loss model was presented. The lack of quality and systemized test data, coupled with a slew of loss modeling approaches, and differing levels of reported results, creates the fact that 1D off-design mean-line modeling is not to be considered a trivial task, nor should it be considered as a resolved issue in the gas turbine industry. An investigation was undertaken with the scope of trying to match transonic axial compressor test data using an off-design mean-line model. The purpose of the investigation was to replace the compressor map scaling approach with a methodology that is able to predict the missing speed-line data with the added benefit of creating a foundation of loss models, from which improved and accurate loss modeling components may be created. From this research work a mean-line model matching methodology, a generalized loss model creation methodology, an engineering-based choke and a stall onset criterion was proposed. These four aspects, when compared to literature, is new and novel after more than six decades of compressor aerodynamics research. The methodologies presented, and the criteria introduced, have produced a reasonable match between the off-design test data and the mean-line analysis results of the rotor pressure ratio and efficiency, and of the stage pressure ratio and efficiency. In addition, the prediction accuracy of the choke condition may be considered at least equal with the various off-design compressor maps presented in Chapter 2, and the results of the proposed stall criteria may be considered as an improvement when compared to the same compressor maps presented in Chapter 2 and Chapter 4.

As part of the investigation, it was asked if a modified off-design tuning process between a mean-line model and test data was capable of accurately capturing the off-design performance behavior of transonic axial compressors. To obtain a *near-exact* match, between a mean-line model and the reported results of four well documented NASA transonic compressors, required the following changes:

- The rotor inlet blockage factor had to vary significantly from a uniquely imposed value to match the inlet flow angle
- The rotor exit blockage factor had to be modified from a single imposed value to match the rotor temperature ratio

- A non-constant rotor deviation angle had to be employed to properly match the calculated rotor exit flow angles
- The rotor loss had to be adjusted concurrently with the rotor deviation angle and the exit blockage factor to obtain a correct blade row pressure and temperature ratio match
- The stator inlet blockage factor had to be adjusted using non-constant values to match the calculated inlet flow angle
- Only a change in stator loss was required to match the stage pressure and temperature ratio
- A non-constant stator deviation angle was used to match the measured exit flow angle
- And, the stator exit blockage factor was varied to match the exit Mach number

What this tuning process reveals is that, to obtain a proper match between an off-design mean-line model and measured performance data requires the use of inlet & exit blockage factors and deviation angles that vary with the test conditions. This differs from the literature-based procedural assumptions of fixed blockage factors, and the use of a unique deviation angle. Furthermore, it has been shown that there is a strong interdependency between the rotor loss, deviation angle, and blockage factors.

A second mean-line methodology was created to convert the mean-line model tuning factors into a set of loss model curves to be incorporated into an off-design mean-line code. The rotor and stator loss modeling has exposed the fact that a unique formulation does not suffice to match the off-design performance behavior of transonic axial compressors. Contrary to the various approaches described in open literature, the axial compressor loss modelling components should be defined based on the percent RPM speed-lines to be able to mimic the varying rotor trailing edge wake and boundary layer physics, and to capture the implicit tip clearance changes due to the centrifugal forces and thermal expansion. Additionally, since the stator will be exposed to the rotor's complex exit flow conditions, the stator blade row loss modelling itself must also take into account the impact of the rotor's percent RPM speed-lines. It has also been shown that there is a strong interdependency between the blade row loss, deviation angle, and the inlet and exit blockage factors. The results of this generalized loss model creation methodology has produced *near-trend* behavior between the off-design mean-line model and the available experimental test data. The set of correlations presented predict the off-design performance quite accurately and could be further

used to supplement missing speed-line data. Once this approach has been applied to a sufficient number of compressors, and if an institution wishes to do so, analytical formulae may then be developed for specific geometric and flow variables[16]. Table 5-1 is a consolidated view of the eight correlations developed to predict the four NASA transonic axial compressors.

Table 5-1: Consolidated listing of loss model correlations

Loss model for	Input	Correlation
Rotor δ	$\tan(\beta_1)$	$\frac{\tan(inc)}{\tan(\beta_1)}\tan(\beta_1 + inc - \delta) + 0.005$
Stator δ	$\tan(\alpha_3)$	$\tan(\alpha_3 + \delta)$
Rotor C_{Din}	$1/preM_x^{0.5}$	$C_{din}^{0.25} preM_x^{0.5}$
Rotor Loss	$\tan(i)$	$Loss \cdot \tan^3(i) \cdot M_{rel\cdot in}^2$
Rotor C_{Dex}	$\tan(i)$	$C_{Dex} \cdot \tan^3(i) \cdot M_{rel\cdot in}^2$
Stator C_{Din}	$\tan^2(pre\ \alpha_{in})$	$Cd_{in}^{0.25} \tan^3(pre\ \alpha_{in})\, preM_{in}^2$
Stator Loss	$\tan^4(pre\ \alpha_{in})$	$Loss^{0.20} \tan^4(pre\ \alpha_{in})\, preM_{in}^3$
Stator C_{Dex}	$\tan^3(pre\ \alpha_{in})$	$Cd_{ex}^{1.0} \tan^3(pre\ \alpha_{in})\, preM_{in}^2$

The matching (tuning) methodology and the generalized loss model methodology respectively described near-exact and near-trend results between the experimental data and the mean-line model values. This was mainly achieved through the use of deviation angles (δ), and inlet & exit blockage factors (C_{Din} and C_{Dex}), that varied with the off-design conditions for the rotor and stator blade rows. Furthermore, it has been shown that the methodology can be used to predict the off-design

[16] An analytical approach must accurately match a wide range of data. Before such a development is undertaken, semi-empirical formulae or correlations are used to develop an understanding of the dominating parameters.

performance conditions for incomplete and missing speed-lines for the following four NASA transonic axial compressor stages: Stage 35 [88], Stage 36 [90], Stage 37 [91], and Stage 38 [92].

The investigation further included work to understand the ambiguity surrounding the axial compressor choke terminology, and introduced an engineering-based criteria that improves the choke condition prediction. The following has been concluded:

1) choke terminology ambiguity: It was found that the literature between classic fluid mechanics and that of gas turbines, especially those text and research papers that treat the topic, is inconsistent and misleading. Some authors have quoted compressor choke to occur at a Mach number of unity, which may lead the reader to believe that the isentropic choke condition is also valid in cases that involves loss.

2) clarification of compressor choke phenomenon: In this regard, it is recommended that the choke condition should reflect the case for a throat critical Mach number of unity in *1D* flow modelling. The term of *Maximum Attainable Mass Flow* (MAMF) seems adequate to distinguish between the isentropic condition for compressor choking and the non-isentropic condition for MAMF. Another reason to retain the classical isentropic choke definition, independent from the non-isentropic definition, is due to its use in the calculations of axial turbine choke and limit loading; and to take into account and consideration that many a textbook and course notes will need to be updated.

3) an engineering-based criterion for axial compressor choke: In lieu of the procedural use of the *vertical*, or *stone-wall*, mass flow calculation, we propose the use of the static pressure ratio criteria. This criterion follows the comprehension of maximum mass flow condition due to a drop in the stator exit static pressure. This criterion is useful due to its independent nature from geometric parameters, and from the calculation of a modified Mach number as described by Cadrecha et al [61]. Furthermore, as shown in Figures 4-4 and 4-7, this criterion properly predicts the majority of the MAMF conditions for the four NASA transonic axial compressors.

Finally, an investigation was undertaken to understand the stall prediction shortfall, with respect to transonic axial compressors, encountered in a one-dimensional off-design mean-line methodology. The available public literature revealed that the results of the various models were either over- or under- predicting the phenomenon. Additionally, the consistency of the predictive models could be considered questionable; the mean-line model predictions were either dramatically different from

the test results, or the predictions were following a parallel trend at a different absolute value. Inspired by the various models introduced through the decades, the results of the tuned mean-line loss models of the four NASA transonic axial compressors were used to search for an alternative approach to describe the onset of the stall phenomenon.

It was found that, a simple and novel criterion can be employed for the prediction of the onset of stall. Using the mean-line model based mid-span velocities, that stem from properly tuned off-design loss models, it was found that the onset of stall may be identified via the ratio of the mean-line based absolute axial velocity component versus the absolute tangential velocity component. Specifically, two distinct ratios were described, i) for a rotor with a relative subsonic inlet, the ratio is based on the mid-span rotor exit axial velocity versus the mid-span rotor exit tangential velocity, whereas ii) for a rotor with a relative supersonic inlet, the ratio is based on the mid-span stator absolute inlet axial velocity versus the mid-span rotor absolute exit tangential velocity.

The proposed intuitive velocity ratio between axial and tangential velocities, was capable of successfully predicting, or assessing, the stall onset trends of four well known NASA transonic axial compressors. The stall criteria were employed as a cut-off value; once the criteria fell below a value of 1.0 the off-design mean-line model execution was halted. Furthermore, it is assumed that the surge stall can also be employed in a multi-stage compressor environment[17]. Since the performance behavior of each stage, of a multi-stage environment, is consecutively executed during the mass flow iteration, then the stage that first encounters the stall criteria cut-off becomes the stage that is in stall first. Additionally, the stall prediction error was similar to the experimental error with respect to the mass flow rate.

Finally, what this *1D* off-design mean-line model investigation has implicitly and explicitly shown is that, i) to be able to predict the missing data points of a transonic axial compressor, including the prediction of stall, requires the use of a properly tuned off-design loss model, ii) an improved stall prediction is attainable by a simple criterion based on velocity triangle components, iii) the choking condition can be viewed better as a MAMF condition defined by a static pressure ratio check, and

[17] Of course, as an assumption it must be proven, and it will be so at a future date.

iv) the use of the *1D* OD mean-line methodology, for a transonic axial compressor, has not been exhausted to its maximum potential or usefulness.

5.1.1 Limitations and Constraints

Due to the sparse availability of complete and detailed test data, the loss modelling approach and engineering-based criteria, presented in this thesis, was validated against four well-documented NASA transonic axial compressors. As Kacker & Okapuu of the turbine domain, and Aungier of the compressor domain have stated, one can safely assume that a mean-line loss model can predict axial stages that fall within the design space that the model has been based on. As researchers and professional engineers, one must use with caution these models when designing compressors that do not fall within the knowledge base of a particular institutions experience.

The correlations for the rotor loss and exit blockage factor, and the correlations for the stator loss and inlet and exit blockage factors, were developed based on the use of the off-design percent RPM (speed-lines) to implicitly capture the impact of varying off-design tip clearances. These correlations were developed for the specific test conditions executed, and will have to be updated if different compressor cold clearances are used. Furthermore, for these correlations to become generalized correlations, future work is required to develop a proper off-design clearance loss and blockage model.

With respect to the rotor and stator deviation, the correlations were developed manually, by trial-and-error data reduction, by using the mean-line model based flow angles as the main assumption. With hindsight that the blade row exit conditions may be impacted by the inlet Mach number and clearance changes, the rotor deviation angle may be improved by separating the correlation into speed-line based curves. The stator deviation correlation may benefit from the assumption used for the other stator correlations; that rotor exit condition has an impact on the stator. Hence, the stator deviation correlation may also be improved by casting the correlation in terms of the rotor speed-lines.

5.1.2 Recommendations

With respect to existing axial compressor test data, a researcher will come across reports lacking pertinent data. As shown in Chapter 3, Table 3-1, there are quite a few NASA axial compressors to base one's research. However, the detailed radial measurements and tabulated performance data

are missing, and any attempt to create accurate models will be more qualitative than quantitative. It is recommended, and most appreciated, that if the data stills exist to have it released to the public for further research consumption.

For future axial compressor tests, it is highly recommended to have a properly tested single stage compressor. This will include measurements of flow angle and pressure at the rotor leading and trailing edges, and at the stator leading and trailing edges. Knowing that the axial spacing between the rotor and stator of commercial compressors are considered small to fit measuring instruments, it would be recommended to add the appropriate axial spacing for test purposes and for capturing accurate inlet and exit profiles. Additionally, the test cases should also include at least two different compressor cold clearances to capture the impact of clearance penetration depth. Knowing that this recommendation may be considered monetarily expensive, the question should be asked if such test data, which could lead to better predictive capabilities, would be of interest to a commercial institution.

5.1.3 Future Research

This investigation will lead into planned future research. The methodologies and engineering-based criteria introduced will be applied to other publicly available axial compressors tested. Since the methodologies require a set of detailed measurements and calculations, which may not be available for all pre-existing axial compressor performance tests, an investigation will be undertaken to review the methodologies' flexibility to cater for the type of measurements taken and calculation procedures available in the various public reports. Additionally, since the tuning process presented was shown to be procedural, the MDIDS-GT software will be modified to include an automated feature to expedite the tuning process.

Furthermore, this work will be expanded to include multi-stage off-design axial compressor modelling. One must be careful to realize that the methodologies of single-stage axial compressor modelling cannot be blindly extended to multi-stage axial compressor modelling. Despite the fact that a multi-stage axial compressor mean-line model will inherit the routines and methodologies of a single-stage axial compressor mean-line model, there are a few knowledge gaps that need to be analyzed and resolved before implementation. These knowledge gaps, coupled with the fact that there are not many published multi-stage compressor tests that have MCA blade rows, would

require a separate research effort to resolve. An explanation of these knowledge gaps are found in Appendix B.

Additionally, one is now able to investigate the limits and usefulness of potential off-design models that describe deviation, clearance losses, blockage, and rotor-stator interaction. With a properly tuned mean-line model as described in this thesis, any new or old model must be able to create equal or better results. This can be done relatively easy by swapping the presented correlations with the model of interest, and observing the changes in the predictive capabilities.

Another aspect to dwell upon is the potential work involved in comparing *competitor* methodologies to the *1D* off-design mean-line model. Stage-stacking and streamline curvature methods are in many ways the *competitors* to mean-line methods used for off-design prediction during the early stages of compressor design. It will be very interesting to collaborate with experts to see how well these methods predict the four NASA axial compressor stages investigated.

It is hoped that the results presented in this manuscript will invigorate the axial compressor field to further convert available test data into a database of tuned loss models; and, if executed correctly, the industry may see the decommissioning of the compressor map scaling techniques and the dependency reduction of the costly compressor rig test.

Imagine the possibilities.

BIBLIOGRAPHY

1. Kidikian, J. and M. Reggio. *Off-Design Prediction of Transonic Axial Compressors: Part 1—Mean-Line Code and Tuning Factors*. in *ASME Turbo Expo 2018: Turbomachinery Technical Conference and Exposition*. 2018. American Society of Mechanical Engineers.
2. Kidikian, J. and M. Reggio. *Off-Design Prediction of Transonic Axial Compressors: Part 2 — Generalized Mean-Line Loss Modelling Methodology*. in *ASME Turbo Expo 2018: Turbomachinery Technical Conference and Exposition*. 2018. American Society of Mechanical Engineers.
3. Dawes, W.N., et al., *Reducing bottlenecks in the CAD-to-mesh-to-solution cycle time to allow CFD to participate in design.* Journal of Turbomachinery, 2001. **123**(3): p. 552-557.
4. Abate, G., *Aerodynamic optimization of a transonic axial compressor rotor*. 2012, University of Padua.
5. Horlock, J. and J. Denton, *A review of some early design practice using computational fluid dynamics and a current perspective.* Journal of Turbomachinery, 2005. **127**(1): p. 5-13.
6. Song, Y., C.-W. Gu, and Y.-B. Xiao, *Numerical and theoretical investigations concerning the continuous-surface-curvature effect in compressor blades.* Energies, 2014. **7**(12): p. 8150-8177.
7. Koch, C. and L. Smith, *Loss sources and magnitudes in axial-flow compressors.* Journal of Engineering for Power, 1976. **98**(3): p. 411-424.
8. Veres, J.P., *Axial and centrifugal compressor mean line flow analysis method.* NASA Technical Memorandum, 2009(TM-2009-215585).
9. Turner, M.G., A. Merchant, and D. Bruna. *A turbomachinery design tool for teaching design concepts for axial-flow fans, compressors, and turbines*. in *ASME Turbo Expo 2006: Power for Land, Sea, and Air*. 2006. American Society of Mechanical Engineers.
10. Saravanamuttoo, H.I.H., G.F.C. Rogers, and H. Cohen, *Gas turbine theory*. 2001: Pearson Education.
11. de Sousa Júnior, F., et al. *Design Point Efficiency Optimization of a Multi-Stage Axial-Flow Compressor for Aero Application applying a Specially Developed Computer Code*. in *COBEM, 18 th International Congress of Mechanical Engineering, ABCM, Ouro Preto–MG, paper 1802*. 2005.
12. Denton, J.D. *Multall: An Open Source, CFD Based, Turbomachinery Design System*. in *ASME Turbo Expo 2017: Turbomachinery Technical Conference and Exposition*. 2017. American Society of Mechanical Engineers.
13. Klein, C., et al. *A Fully Coupled Approach for the Integration of 3D-CFD Component Simulation in Overall Engine Performance Analysis*. in *ASME Turbo Expo 2017: Turbomachinery Technical Conference and Exposition*. 2017. American Society of Mechanical Engineers.
14. Jones, S.M., *An Introduction to Thermodynamic Performance Analysis of Aircraft Gas Turbine Engine Cycles Using the Numerical Propulsion System Simulation Code.* NASA/TM-2007-214690, 2007.

15. Drummond, C. and C.R. Davison. *Capturing the shape variance in gas turbine compressor maps*. in *2009 ASME Turbo Expo, June 8, 2009 - June 12, 2009*. 2009. Orlando, FL, United states: American Society of Mechanical Engineers.

16. Oztekin, D.E., *The Lattice Boltzmann Methods and Their Applications to Fluid Flows.* 2014.

17. Smith, S.L., *One-Dimensional Mean Line Code Technique to Calculate Stage-by-Stage Compressor Characteristics*. 1999, University of Tennessee - Knoxville.

18. Kacker, S.C. and U. Okapuu, *A mean line prediction method for axial flow turbine efficiency.* Transactions of the ASME. Journal of Engineering for Power, 1982. **104**(1): p. 111-19.

19. Kantrowitz, A., *The supersonic axial-flow compressor.* NACA technical report 974, 1950.

20. Wright, P. and D. Miller. *An improved compressor performance prediction model*. in *IMechE Conference Proceedings CP 1991-3*. 1991. Rolls-Royce plc.

21. Schwenk, F.C., G.W. Lewis, and M.J. Hartmann, *A preliminary analysis of the magnitude of shock losses in transonic compressors.* 1957.

22. Crouse, J.E. and W.T. Gorrell, *Computer Program for Aerodynamic and Blading Design of Multistage Axial-Flow Compressors*. 1981, NATIONAL AERONAUTICS AND SPACE ADMINISTRATION CLEVELAND OH LEWIS RESEARCH CENTER.

23. Yu, X., Z. Zhang, and B. Liu, *The evolution of the flow topologies of 3D separations in the stator passage of an axial compressor stage.* Experimental Thermal and Fluid Science, 2013. **44**: p. 301-311.

24. Bullock, R.O. and I.A. Johnsen, *Aerodynamic Design of Axial Flow Compressors.* NASA report, 1965(SP-36).

25. Carter, A. and H.P. Hughes, *A theoretical investigation into the effect of profile shape on the performance of aerofoils in cascade*. 1950: His Maj. Stat. Office.

26. Barbosa, J., *A Streamline Curvature Computer Programme for Performance Prediction of Axial Compressors*. 1987, Ph. D. Thesis, Cranfield Institute of Technology, England.

27. Bloch, G.S., W.W. Copenhaver, and W.F. O'Brien, *A shock loss model for supersonic compressor cascades.* Journal of turbomachinery, 1999. **121**(1): p. 28-35.

28. Cahill, J.E., *Identification and Evaluation of Loss and Deviation Models for use in Transonic Compressor Stage Performance Prediction*. 1997, Virginia Polytechnic Institute and State University.

29. Ramakdawala, R.R., *Preliminary design code for an axial stage compressor*. 2001, NAVAL POSTGRADUATE SCHOOL MONTEREY CA.

30. Boyer, K.M., *An Improved Streamline Curvature Approach for Off-Design Analysis of Transonic Compression Systems*. 2001, Virginia Polytechnic Institute and State University.

31. Van Antwerpen, W., *Multi-quadrant performance simulation for subsonic axial flow compressors/Werner van Antwerpen*. 2007, North-West University.

32. Falck, N., *Axial Flow Compressor Mean Line Design.* Master's thesis, Lund University, Lund, Sweden, 2008.

33. Benini, E., *Advances in Aerodynamic Design of Gas Turbines Compressors*. 2010: INTECH Open Access Publisher.

34. Steinke, R.J., *STGSTK: A computer code for predicting multistage axial flow compressor performance by a meanline stage stacking method.* 1982.

35. Howell, A. and W. Calvert, *A new stage stacking technique for axial-flow compressor performance prediction.* Journal of Engineering for Power, 1978. **100**(4): p. 698-703.

36. Schobeiri, M., *Advanced compressor loss correlations, part I: theoretical aspects.* International Journal of Rotating Machinery, 1997. **3**(3): p. 163-177.

37. Schobeiri, M., *Advanced Compressor Loss Correlations, Part II: Experimental Verifications.* International Journal of Rotating Machinery, 1997. **3**(3): p. 179-187.

38. Denton, J.D. *Loss mechanisms in turbomachines*. in *ASME 1993 International Gas Turbine and Aeroengine Congress and Exposition*. 1993. American Society of Mechanical Engineers.

39. Cetin, M., et al., *Application of Modified Loss and Deviation Correlations to Transonic Axial Compressors*. 1987, AGARD Report No. 745.

40. Aungier, R., *Axial Flow Compressors-A Strategy for Aerodynamic Design and Analysis.-New York, NY and Bury St. Edmunds, Suffolk: ASME Press and Professional Engineering Publishing Limited.* 2003.

41. Fox, R.W. and A.T. McDonald, *Introduction to fluid mechanics*. 4th ed. 1992: John Wiley & Sons New York.

42. Miller, G.R., G.W. Lewis Jr, and M.J. Hartmann, *Shock losses in transonic compressor blade rows.* 1960.

43. Puterbaugh, S.L. and A.J. Wennerstrom, *Revision of the Shock Loss Re-Estimation Procedure of Program UD0300 Utilizing a Three-Dimensional Shock Model*. 1982, DTIC Document.

44. Freeman, C. and N. Cumpsty. *A method for the prediction of supersonic compressor blade performance*. in *ASME 1989 International Gas Turbine and Aeroengine Congress and Exposition*. 1989. American Society of Mechanical Engineers.

45. Wadia, A. and W. Copenhaver. *An investigation of the effect of cascade area ratios on transonic compressor performance*. in *ASME 1994 International Gas Turbine and Aeroengine Congress and Exposition*. 1994. American Society of Mechanical Engineers.

46. Puterbaugh, S.L., et al. *A three-dimensional shock loss model applied to an aft-swept, transonic compressor rotor*. in *ASME 1996 International Gas Turbine and Aeroengine Congress and Exhibition*. 1996. American Society of Mechanical Engineers.

47. Dunham, J., *Aerodynamic losses in turbomachinery*. 1996, AGARD-CP-571.

48. Boyce, M.P., *Axial-Flow Compressors.* Gas Turbine Engineering Handbook, 2006: p. 274-335.

49. Fruchtman, I. *The Limit Load of Transonic Turbine Blading*. in *ASME 1974 International Gas Turbine Conference and Products Show*. 1974. American Society of Mechanical Engineers.

50. Glassman, A.J., *Estimating turbine limit load.* 1993.

51. Creveling, H. and R. Carmody, *Axial flow compressor computer program for calculating off-design performance*. 1968.

52. Koch, C., *Stalling pressure rise capability of axial flow compressor stages.* ASME J. Eng. Power, 1981. **103**(4): p. 645-656.

53. Miller, D. and D. Wasdell, *Off-design prediction of compressor blade losses.* IMechE Paper, 1987(C279/87).

54. Walsh, P.P. and P. Fletcher, *Gas turbine performance*. second ed. 2004: John Wiley & Sons.

55. Hall, C. and S.L. Dixon, *Fluid mechanics and thermodynamics of turbomachinery*. sixth ed. 2010: Butterworth-Heinemann.

56. Hanlon, P.C., *Compressor handbook McGraw-Hill*. 2001, USA.

57. Boyce, M.P., *Gas turbine engineering handbook*. second ed. 2002: Elsevier.

58. Barbosa, J.R. and J.S. Figueiredo. *SURGING TO CHOKING: A STUDY OF THE AXIAL CHANNEL OF AXIAL COMPRESSORS*. in *Brazilian Congress of Thermal Sciences and Engineering ENCIT*. 2010.

59. Banjac, M., M.V. Petrovic, and A. Wiedermann, *Secondary Flows, Endwall Effects, and Stall Detection in Axial Compressor Design.* Journal of Turbomachinery, 2015. **137**(5): p. 051004.

60. Peyvan, A. and A. Benisi, *Axial-Flow Compressor Performance Prediction in Design and Off-Design Conditions through 1-D and 3-D Modeling and Experimental Study.* Journal of Applied Fluid Mechanics, 2016. **9**.

61. Cadrecha, D., et al. *Robust Method to Solve Meanline Equations for Choked Flows*. in *ASME Turbo Expo 2018: Turbomachinery Technical Conference and Exposition*. 2018. American Society of Mechanical Engineers.

62. Greitzer, E., *Axial compressor stall phenomena.* Journal of Fluids Engineering, 1980. **102**(2): p. 134-151.

63. Nelson, M.L., et al., *The NASA technical report server.* Internet Research, 1995. **5**(2): p. 25-36.

64. Medeiros, A.A., W.A. Benser, and J.E. Hatch, *Analysis of Off-Design Performance of a 16-Stage Axial-Flow Compressor with Various Blade Modifications.* 1953.

65. Johnsen, I.A., *Investigation of a 10-stage Subsonic Axial-flow Research Compressor I: Aerodynamic design.* NACA TN 2589, 1952.

66. Budinger, R.E. and A.R. Thomson, *Investigation of a 10-stage Subsonic Axial-flow Research Compressor II: Preliminary Analysis of Overall Performance.* 1952.

67. Voit, C.H., *Investigation of a high-pressure-ratio eight-stage axial-flow research compressor with two transonic inlet stages I: aerodynamics design.* NACA RM E53I24, 1953.

68. Geye, R.P., C.H. Voit, and R.E. Budinger, *Investigation of a high-pressure-ratio eight-stage axial-flow research compressor with two transonic inlet stages II: preliminary analysis of over-all performance.* 1953.

69. Westphal, W.R. and J.W. Maynard Jr, *Design and tests of a six-stage axial-flow compressor having a tip speed of 550 feet per second and a flat operating characteristic at constant speed.* 1958.

70. Sandercock, D.M., K. Kovach, and S. Lieblein, *Experimental Investigation of a Five-stage Axial-flow Research Compressor with Transonic Rotors in All Stages I: Compressor Design.* NACA EM E54F24, 1954.

71. Kovach, K. and D.M. Sandercock, *Experimental Investigation of a Five-stage Axial-flow Research Compressor with Transonic Rotors in All Stages II: Compressor Over-all Performance.* 1954.

72. Cunnan, W.S., W. Stevans, and D.C. Urasek, *Design and performance of a 427-meter-per-second-tip-speed two-stage fan having a 2.40 pressure ratio.* NASA Technical Paper 1314 (Rotor 67), 1978.

73. Britsch, W.R., W.M. Osborn, and M.R. Laessig, *Effects of diffusion factor, aspect ratio, and solidity on overall performance of 14 compressor middle stages.* NASA-TP-1523, E-9943, 1979.

74. Seyler, D. and L.H. Smith Jr, *Single stage experimental evaluation of high Mach number compressor rotor blading. Part I-Design of rotor blading.* 1967.

75. Reid, L. and E.R. Tysl, *Performance of a transonic compressor rotor with an aspect ratio of 6.5.* 1974.

76. Hager, R.D., D.C. Janetzke, and L. Reid, *Performance of a 1380-foot-per-second-tip-speed axial-flow compressor rotor with a blade tip solidity of 1.3.* 1972.

77. Janetzke, D.C., C.L. Ball, and R.D. Hager, *Performance of 1380-foot-per-second tip-speed axial-flow compressor rotor with blade tip solidity of 1.1.* 1972.

78. Ball, C.L., D.C. Janetzke, and L. Reid, *Performance of 1380 foot per second tip-speed axial-flow compressor rotor blade tip solidity of 1.5.* 1972.

79. Kovich, G. and L. Reid, *Overall and blade-element performance of a multiple-circular-arc bladed transonic compressor rotor with tip speed of 1375 feet per second.* 1973.

80. Kovich, G. and L. Reid, *Overall and blade-element performance of a transonic compressor stage with multiple-circular-arc blades at tip speed of 419 meters per second.* 1973.

81. Osborn, W.M., D.C. Urasek, and R.D. Moore, *Performance of a single-stage transonic compressor with a blade-tip solidity of 1.5 and comparison with 1.3 and 1.7 solidity stages.* 1973.

82. Kovich, G., R.D. Moore, and D.C. Urasek, *Performance of transonic fan stage with weight flow per unit annulus area of 198 kilograms per second per square meter (40.6 (lb/sec)/sq ft).* 1973.

83. Moore, R.D. and L. Reid, *Performance of a single-stage axial-flow transonic compressor stage with a blade tip solidity of 1.7.* 1972.

84. Urasek, D.C. and R.D. Moore, *Performance of a single-stage transonic compressor with a blade-tip solidity of 1.3.* 1972.

85. Moore, R.D., D.C. Urasek, and G. Kovich, *Performance of transonic fan stage with weight flow per unit annulus area of 178 kilograms per second per square meter (6.5 (lb/sec)/(sq ft)).* 1973.

86. Urasek, D.C., G. Kovich, and R.D. Moore, *Performance of transonic fan stage with weight flow per unit annulus area of 208 kilograms per second per square meter (42.6 (lb/sec)/sq ft).* 1973.

87. Lewis Jr, G.W., L. Reid, and E.R. Tysl, *Design and performance of a high-pressure-ratio, highly loaded axial-flow transonic compressor space.* 1974.

88. Reid, L. and R.D. Moore, *Performance of single-stage axial-flow transonic compressor with rotor and stator aspect ratios of 1.19 and 1.26, respectively, and with design pressure ratio of 1.82.* NASA Technical Paper 1338 (stage 35), 1978 November.

89. Reid, L. and R.D. Moore, *Design and overall performance of four highly loaded, high speed inlet stages for an advanced high-pressure-ratio core compressor.* NASA Technical Paper 1337 (stage 35 to 38), 1978 October.

90. Moore, R.D. and L. Reid, *Performance of single-stage axial-flow transonic compressor with rotor and stator aspect ratios of 1.63 and 1.78, respectively, and with design pressure ratio of 1.82.* NASA Technical Paper 1974 (stage 36), 1982 February.

91. Moore, R.D. and L. Reid, *Performance of single-stage axial-flow transonic compressor with rotor and stator aspect ratios of 1.19 and 1.26, respectively, and with design pressure ratio of 2.05.* NASA Technical Paper 1659 (stage 37), 1980 April.

92. Moore, R.D. and L. Reid, *Performance of single-stage axial-flow transonic compressor with rotor and stator aspect ratios of 1.63 and 1.78, respectively, and with design pressure ratio of 2.05.* NASA Technical Paper 2001 (stage 38), 1982 April.

93. Osborn, W.M. and R.J. Steinke, *Performance of a 1.15-pressure-ratio Axial-flow Fan Stage with a Blade Tip Solidity of 0.5.* 1974.

94. Kovich, G. and R.J. Steinke, *Performance of low-pressure-ratio low-tip-speed fan stage with blade tip solidity of 0.65.* 1976.

95. Kovich, G. and R.D. Moore, *Performance of 1.15-pressure-ratio fan stage at several rotor blade setting angles with reverse flow.* 1976.

96. Moore, R.D. and R.J. Steinke, *Aerodynamic Performance of a 1.25-pressure-ratio Axial-flow Fan Stage.* 1974.

97. Osborn, W.M., R.D. Moore, and R.J. Steinke, *Aerodynamic performance of a 1.35-pressure-ratio axial-flow fan stage.* 1978.

98. Lewis Jr, G.W. and R.D. Moore, *Aerodynamic performance of a 1.20-pressure ratio fan stage designed for low noise.* 1976.

99. Moore, R.D., G.W. Lewis Jr, and E.R. Tysl, *Performance of a low-pressure fan stage with reverse flow (Stage 55).* NASA TM X-3349, 1976.

100. Lewis Jr, G.W. and E.R. Tysl, *Overall and blade-element performance of a 1.20-pressure-ratio fan stage at design blade setting angle (Stage 55).* NASA-TM-X-3101, E-7791, 1974.

101. Moore, R.D. and W.M. Osborn, *Aerodynamic performance of 1.38-pressure-ratio, variable-pitch fan stage.* 1979.

102. Moore, R.D. and L. Reid, *Aerodynamic performance of axial-flow fan stage operated at nine inlet guide vane angles*. 1979: National Aeronautics and Space Administration, Scientific and Technical ….

103. Urasek, D.C., R.J. Steinke, and G.W. Lewis Jr, *Performance of inlet stage of transonic compressor (Stage 66).* NASA-TM-X-3345, E-8056, 1976.

104. Urasek, D.C., W.T. Gorrell, and W.S. Cunnan, *Performance of two-stage fan having low-aspect-ratio first-stage rotor blading.* NASA Technical Paper 1493 (Rotor 67), 1979.

105. Steinke, R.J., *Design of 9.271-pressure-ratio five-stage core compressor and overall performance for first three stages (stage 74A).* NASA-TP-2597, E-2589, 1986.

106. Holloway, P., et al., *Energy efficient engine. High pressure compressor detail design report.* NASA-CR-165558, R81AEG710, 1982.

107. Cline, S., et al., *High pressure compressor component performance report.* 1983.

108. Howe, D.C. and R. Marchant, *Energy Efficient Engine: High-pressure compressor test hardware detailed design report.* 1988.

109. Sulam, D., *Single-Stage Evaluation of Highly-Loaded, High-Mach-Number Compressor Stages II, Data and Performance Multiple-Circular-Arc Rotor.* CR-72694, 1970: p. PWA-3772.

110. Wasserbauer, C.A., H.F. Weaver, and R.G. Senyitko, *NASA low-speed axial compressor for fundamental research.* 1995.

111. Copenhaver, W. and W.F. O'Brien, *A Shock Loss Model for Supersonic Compressor Cascades*, in *ASME 1997 International Gas Turbine and Aeroengine Congress and Exhibition, GT 1997*. 1997: Orlando, FL, United states.

112. RDDM *MDIDS-GT Software User Guide. Retrieved from* https://sites.google.com/site/mdidsgt/home/softwareresources. 2017.

113. RDDM, *User Guide for Compressor Only Design Process Including Validation Case Creation.* 2017.

114. Emery, J.C., et al., *Systematic two-dimensional cascade tests of NACA 65-series compressor blades at low speeds.* 1958.

115. Carter, A., *The low speed performance of related aerofoils in cascades*. Vol. 29. 1950: His Maj. Stat. Office.

116. Moeckel, W.E., *Approximate method for predicting form and location of detached shock waves ahead of plane or axially symmetric bodies.* NACA TN 1921, 1949.

117. Lieblein, S. and W.H. Roudebush, *Theoretical loss relations for low-speed two-dimensional-cascade flow.* 1956.

118. Khalid, S.A., *The effects of tip clearance on axial compressor pressure rise*. 1995, Massachusetts Institute of Technology.

119. Camp, T. and I. Day. *A study of spike and modal stall phenomena in a low-speed axial compressor*. in *ASME 1997 International Gas Turbine and Aeroengine Congress and Exhibition*. 1997. American Society of Mechanical Engineers.

120. Vavra, M., *Aero-Thermodynamics and Flow in Turbomachines,(1974), 304.* Robert EK Co.

121. Kurzke, J. *Performance modeling methodology: efficiency definitions for cooled single and multistage turbines*. in *ASME Turbo Expo 2002: Power for Land, Sea, and Air*. 2002. American Society of Mechanical Engineers.

122. Burdsall, E., E. Canal Jr, and K. Lyons, *Core compressor exit stage study. 1: Aerodynamic and mechanical design.* 1979.

123. Suder, K.L. *Blockage development in a transonic, axial compressor rotor*. in *ASME 1997 International Gas Turbine and Aeroengine Congress and Exhibition*. 1997. American Society of Mechanical Engineers.

124. Herrick, G.P., M.D. Hathaway, and J.-P. Chen. *Unsteady full annulus simulations of a transonic axial compressor stage*. in *47th Aerospace Sciences Meeting. AIAA Paper*. 2009.

APPENDIX A – MEAN-LINE MODEL ASSUMPTIONS

A mean-line model (*or methodology*) is the simplest of analytical tools available to the gas turbine designer and engineer. The mean-line model, in itself, is a gross one-dimensional approximation and simplification of the geometry, the physics, and the formulas pertaining to a gas turbine engine and its components. The mean-line model is developed and based on the following fundamental assumptions:

1) A generic mean-line model assumes that the performance of an axial stage and blade row, either that of a compressor or turbine, may be fully described at the geometrical mid-section of the blade row;

   a. One may wish to define the "equal area" mid-section, which is defined as the location where the mass flow is considered equal above and below this mid-section. Neither approach of using the geometrical nor "equal area" mid-section is a "better" representation of physical flow phenomena. The only advice from the author is to be consistent and explicit with which mid-section definition is being used.

   b. It is additionally assumed that the radial profile of all flow parameters is radially constant. For an improved description of the flow field, one may utilize the free-forced vortex equations as described by Vavra [120] to generate a non-constant radial profile. For a more refined radial flow field description, a 2D through-flow approach or 3D CFD should be used.

2) A generic mean-line model assumes that the axial stage is adiabatic; in other words, the complex heat transfer equations of conduction, convection, and radiation are ignored.

   a. The adiabatic assumption is a preliminary, or conceptual, design assumption due to the fact that, during the conceptual design phase, detailed airfoil geometries and materials are yet to be defined. This is an important fact to retain since the material selection will lead to the heat transfer coefficients required for the calculations.

   b. With regards to the adiabatic assumption through a stage, it is additionally assumed that there is no temperature change across a stator blade row.

3) A generic mean-line model assumes that the axial stage is isentropic; this is true when developing the mean-line code with zero loss to verify the success of the numerical schemes employed. The blade row entropy is resolved by specific loss models that are employed to adjust the ideal solution to a closer representation of reality, which is based on test data. It should be noted that the formulation of a loss model is only as complex as the user wishes it to be.

4) A generic mean-line model assumes that the loss through a blade row is instantaneous, hence loss is calculated at the trailing edge. One may wish to split the loss into pre-throat and post-throat losses, however this just adds complexity to the modeling, and requires quality test data that has measured pre- and post- throat flow parameters for a large variety of geometric variations.

5) A generic mean-line model assumes that the work through a blade row is instantaneous; hence calculated at the exit of the rotor trailing edge

6) A generic mean-line model assumes the conservation of rothalpy across a rotor blade row. Even though the conservation of rothalpy is applied to a rotor blade row, it may obviously be used as an assumption for the stator blade row without violating any previously mentioned assumptions.

7) A generic mean-line model assumes the conservation of angular momentum between the trailing edge of one blade row to the leading edge of the subsequent blade row.

8) A generic mean-line model assumes that the throat is described as the minimum "geometric" distance from the leading edge (compressor) or trailing edge (turbine) of one airfoil to the next pitched airfoil surface.

a. The concept of "blockage" is introduced due to the fact that the actual "flow" throat area is considered slightly smaller than the "geometric" throat area.

b. It is additionally assumed that the throat is perpendicular to the design-point inlet flow angle for an axial compressor, or the exit flow angle for an axial turbine.

c. It is additionally assumed that the throat is calculated based on the mean camber of the airfoil, and does not take into consideration the thickness of the airfoil. This leads to the concept of the "ideal" throat area.

9) A generic mean-line model assumes that all flow parameters can be described by the use of the compressible flow equations.

10) A generic mean line model utilizes Euler's turbomachinery equation. Additionally, a mean-line model must show a convergence, or an acceptable error difference, between the Euler work and Enthalpy.

11) A generic mean line, with respect to angles, may assume the following approaches:

a. At the design-point condition the inlet and exit blade row metal angles are equal to the inlet and exit flow angles, or

b. At the design-point condition the inlet and exit blade row metal angles are equal to the inlet and exit flow angles with an additional adjustment for incidence and deviation, respectively.

c. At the off-design condition the exit flow angle is either equal to the blade trailing edge metal angle or adjusted for deviation.

12) A generic mean-line model does not assume that the empirical relations or analytical formulae employed are accurate, realistic, or predictive. That depends on the confidence and opinion of the particular user.

13) A generic mean-line model does not assume that designs outside of its internal loss and geometry database will be predicted accurately or realistically. That depends on the confidence and opinion of the particular user.

14) A generic mean-line model does not assume that it is better than any other sophisticated analytical tool. That depends on the confidence and opinion of the particular user, where it is used, and how it is used.

NOTE: The limitations of a mean-line model are those that are defined by the assumptions used to build a mean-line model.

APPENDIX B – MULTI-STAGE COMPRESSOR KNOWLEDGE GAPS

Multi-stage compressor efficiency formula

The single stage compressor efficiency is based on the assumption that the gas parameters remain constant through the stage blade rows. However, despite being a simplifying assumption for both single- and multi- stage compressors, it is known that the gas properties change due to an increase of the compressor stage static temperature. Therefore, one will need to apply non-constant gas property formulations that are based on the stage or blade row static temperature rise. Additionally, a single stage total-to-total efficiency calculation involves the specific heats ratio, or gamma ($\gamma=c_p/c_v$). This may be considered constant through a stage, however, it does not remain constant through a multi-stage environment due to the increase in static temperature. Therefore, one will need to use an efficiency equation that caters for changes in gamma. A recommended reference paper that discusses the obstacles related to efficiency calculation is that by Kurzke [121].

Work done factor versus blockage factor variation

It is known that through a multi-stage compressor the gas path radial flow profiles do not remain constant. There is an actual boundary layer development across the meridional gas path direction, creating changes in the flow field. There are two approaches that have been identified in literature 1) the use of the work done factor and 2) the use of a multi-stage blockage factor distribution. In the former, a scalar value is applied to the enthalpy work equation to represent the percentage of the total span that does useful work on a compressor blade row [35]. This work done factor decreases as the stage number is increased. The latter is an actual multi-stage blockage factor distribution profile that decreases as the number of stages increase [122]. A study is required to identify which of these approaches best describes the multi-stage compressor environment.

Multi-stage blockage factor variation with off-design conditions

Based on the work to be presented, it is believed that the non-constant blockage factor methodology will resolve the previously mentioned knowledge gap. The work done factor may be excluded from the knowledge gap study. It is most likely that the literature based constant multi-stage blockage factor distribution should be modified to a non-constant multi-stage blockage factor distribution.

APPENDIX C – AXIAL COMPRESSOR CFD

As mentioned in Chapter 1 – Introduction, 3D CFD plays an important role in the overall design life-cycle of gas turbine components. Despite the fact that CFD results and analysis bring insight to the internal flow mechanisms and physics, more realistically than any 1D or 2D methodology can, one must still use such results with caution; it should be noted that both axial compressors and axial turbines share the same limitations, issues, and concerns surrounding the use of such an analysis. Over the years, many attempts of using 3D CFD to predict flow physics have been undertaken. A few of these CFD cases, which are related to this investigation, are mentioned below.

In 1997, Suder reported on detailed laser anemometer measurements for Rotor 37 (the rotor of Stage 37) at the 100%, 85%, 80%, and 60% speed-lines. The results showed that the blockage due to the profile boundary layer growth was sensitive to the inlet Mach number, especially at high Mach number values [123]. Suder also pointed out that Rotor 37 was used as the CFD blind test case study for the 1994 ASME IGTI turbomachinery conference, where the results were based on the at-the-time available CFD models and computers' performance.

The ASME IGTI blind test case was used by various researchers who attempted to predict the flow physics of the NASA Rotor 37 using various CFD packages [123]. It was found that the CFD results did not predict the radial profiles of the actual Rotor 37 test data, and that in general the pressure ratio and temperature ratio were generally predicted higher than what was measured [123]. Suder stated that *"CFD simulation predicted the features and trends of the end-wall flow field but under-predicted the radial penetration of the tip clearance flow. It was surmised that the CFD was under-predicting the blockage in the end-wall region*" [123]

In 2009, Herrick, Hathaway, & Chen released a NASA technical memorandum / AIAA paper describing the full annulus unsteady analysis of the NASA Stage 35. They used a NASA in-house CFD code called *TURBO* [124]. Their results revealed the following about the unsteady CFD analysis:

- The CFD under predicted the PR-vs-mass flow rate levels
- The CFD did not match the measured total PR radial profiles, especially at the end walls
- The CFD did not match the level of the measured stator exit flow angle

What their results showed was that, even if one has the resources to execute an unsteady CFD analysis, the results will not produce values at a level of fidelity where one may replace missing test data measurement with that of CFD data.

The literature research for transonic axial compressor revealed another interesting trend with respect to the CFD analysis of the NASA Rotor 37 executed by other researchers. The importance of NASA Rotor 37 is due to the fact that it was the ASME blind test to benchmark the various CFD predictive capabilities of the mid 1990's. Therefore, one would be lead to think that each research institution is using Rotor 37 as the reference to benchmark their CFD codes. However, the other NASA stages or individual blade rows were not used, or attempted, for comparison purposes.

It was further noticed that some research institutions were reporting the results of Rotor 37 simulation using ANSYS CFX and FLUENT. When the Rotor 37 CFD analysis using ANSYS 16.x TurboGrid (for meshing) and CFX (for 3D simulation) was executed as part of this thesis' preliminary CFD investigation, it was discovered that the NASA Rotor 37 was one of the ANSYS TurboGrid and CFX software demonstration geometries, and, was the user tutorial for an axial compressor CFD case. Furthermore, the literature survey did not reveal if the other researchers were using the provided rotor profile by ANSYS as-is or that they recreated the geometry from the NASA documents. This lead to a subjective opinion that the use of the Rotor 37 axial compressor as part of a CFD analysis has been used more as a convenience due to its availability in the ANSYS software package instead of being recreated manually.

One of the questions raised during this 1D OD ML investigation was *"can we use CFD to supplement missing data?"* To be able to answer this question, a Rotor 37 CFD analysis was executed using ANSYS 16.x Academic TurboGrid and CFX[18]. The purpose was to obtain the off-design performance behaviour of Rotor 37. To do so, the following tasks were executed:

- Recreate the Stage 37 blade rows, rotor and stator, from the NASA documents
- Create speed-line specific mesh with an appropriate off-design tip clearance per speed-line
- Launch and observe the various runs

[18] The CFD analysis was limited to the maximum number of mesh nodes allowed in the ANSYS academic version.

- Post-process the ANSYS CFX CFD cases

Pertinent information with respect to the Rotor 37 ANSYS CFX CFD set-up is presented in Table C-1(5-2).

Table C-1(5-2): ANSYS CFX CFD setup

Parameter	**Value**	**Units**
Blade set number (number of Airfoils)	36	-
Principal Axis	X	-
Coordinates	Cartesian	-
Length units	inch	-
Tip Clearance Geometry		**-**
Tip Option	Normal Distance	-
100% RPM	0.356	mm
90% RPM	0.428 (linearly interpolated)	mm
80% RPM	0.501	mm
70% RPM	0.54 (linearly interpolated)	mm
60% RPM	0.58	mm
50% RPM	0.62 (assumed)	mm
Boundary: R1 Inlet		
Flow Regime		-
Option	Subsonic	-
Mass and Momentum		-
Option	Stat. Frame Tot. Press.	-
Relative pressure	14.613	psi
Flow Direction		-
Option	Normal to Boundary Condition	-
Turbulence		-
Option	Medium (Intensity=5%)	-
Heat Transfer		-
Option	Stat. Frame Tot. Temp.	-
Stat. Frame Tot. Temp.	518.67	Rankine
Boundary: R1 Outlet		
Option	Subsonic	-
Mass and Momentum		-
Option	Average Static pressure	-
Relative Pressure	Refer to the reports for actual BC values imposed	psi
Pre. Profile Blend	0.05	-
Intentionally left blank		

Pressure Averaging		-
Option	Radial Equilibrium	-
Radial Reference Position		-
Option	Minimum Radius (or Pstatic @Hub)	-
Solver Options		
Max iterations	500	-
Residual Target	1e-06	-
Double Precision	**selected**	-
Run mode	Platform MPI local Parallel	-
Turbulence Model		
Rotor Model	K-epsilon	-

The results of the isolated Rotor 37 CFD off-design cases are shown in Figure C5-1. It can be seen that the pressure ratio is following the experimental test data trends, however the rotor efficiency was significantly under-predicted.

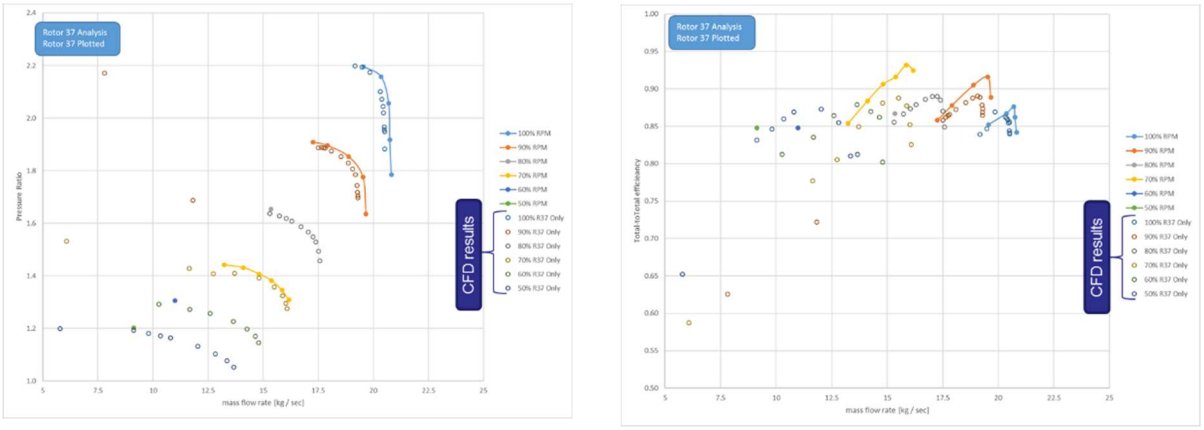

a) Rotor 37 PR versus mass flow rate b) Rotor 37 efficiency versus mass flow rate

Figure C5-1: CFD off-design performance results of Rotor 37 using ANSYS Academic CFX

Furthermore, to aid in the visualization of potential flow field structures, the 50% airfoil span relative Mach number contour plots (Figures C5-2 to C5-7), and exit plane relative Mach number contour plots (Figures C5-8 to C5-11) were captured to give insight with respect to the shock structures and exit blockage variation that one may encounter.

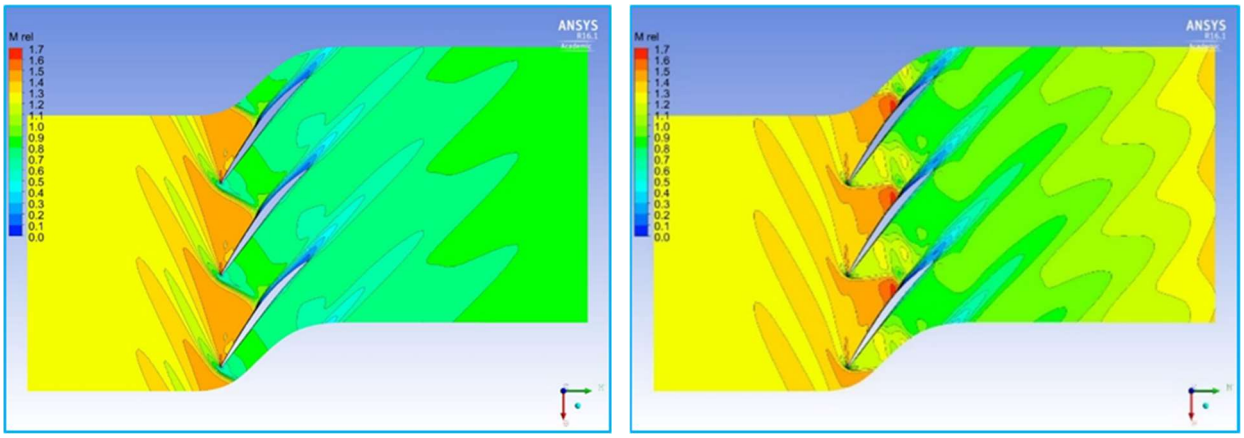

a) low mass flow rate b) high mass flow rate

Figure C5-2: ANSYS CFX results for the 100% speed-line @ 50% span

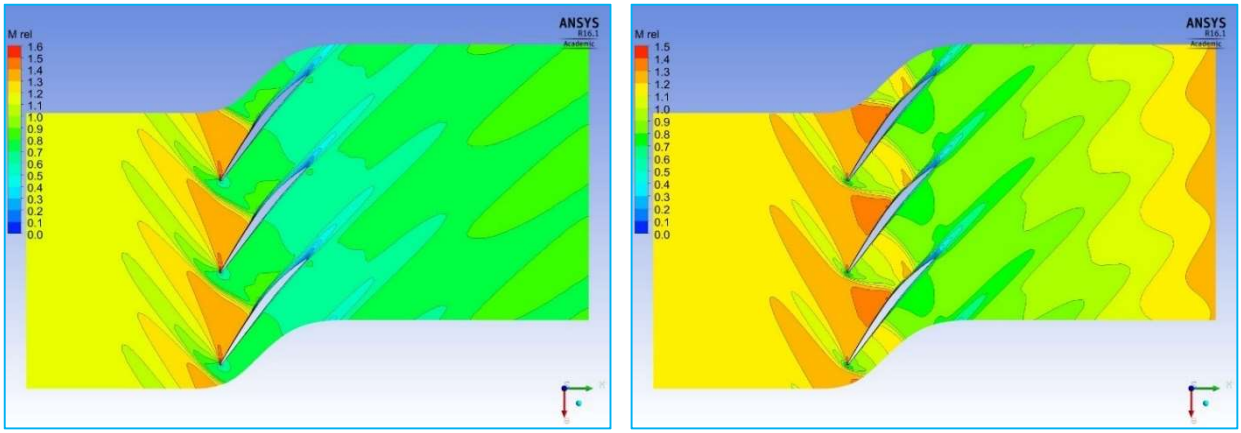

a) low mass flow rate b) high mass flow rate

Figure C5-3: ANSYS CFX results for the 90% speed-line @ 50% span

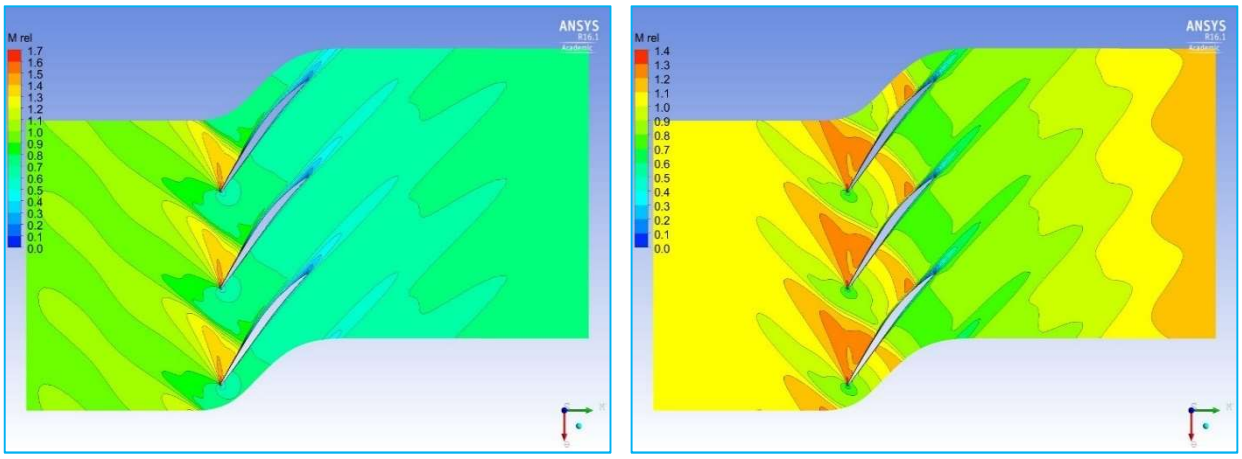

a) low mass flow rate b) high mass flow rate

Figure C5-4: ANSYS CFX results for the 80% speed-line @ 50% span

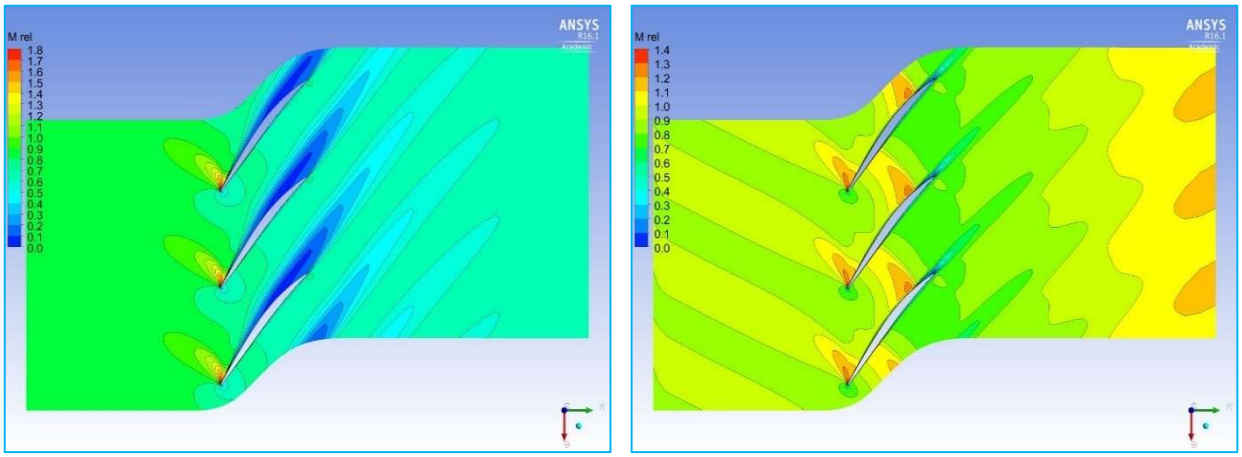

a) low mass flow rate b) high mass flow rate

Figure C5-5: ANSYS CFX results for the 70% speed-line @ 50% span

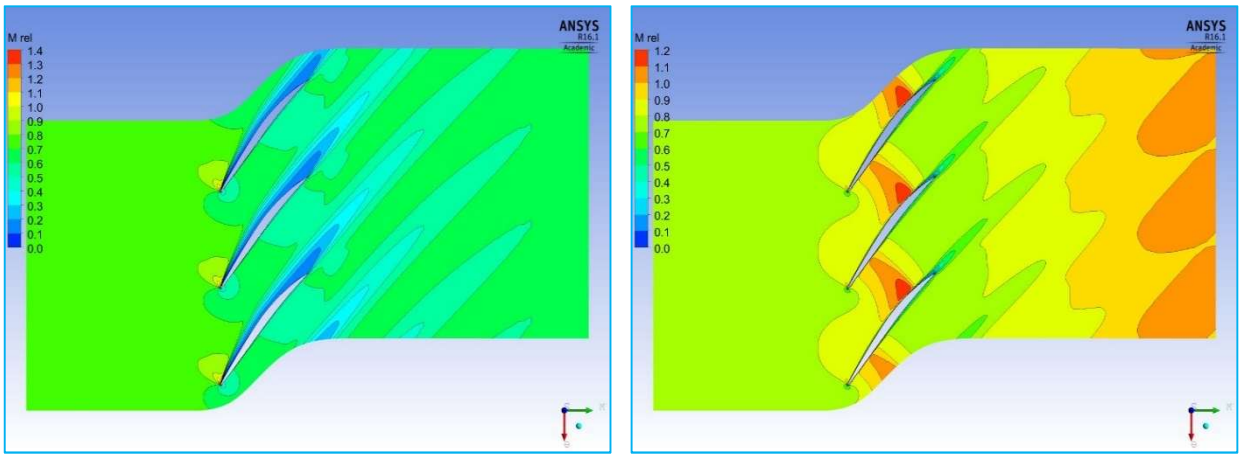

a) low mass flow rate b) high mass flow rate

Figure C5-6: ANSYS CFX results for the 60% speed-line @ 50% span

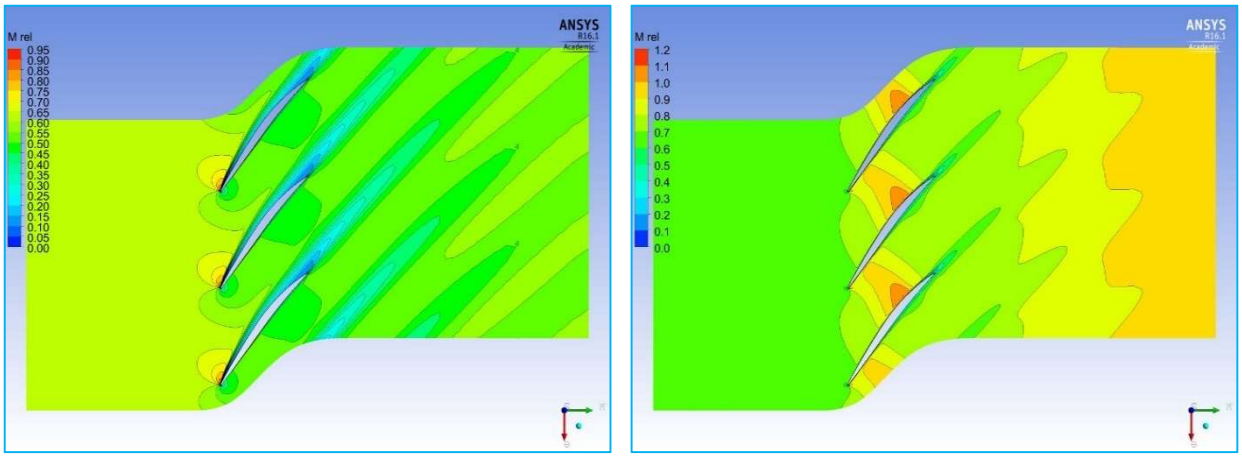

a) low mass flow rate b) high mass flow rate

Figure C5-7: ANSYS CFX results for the 50% speed-line @ 50% span

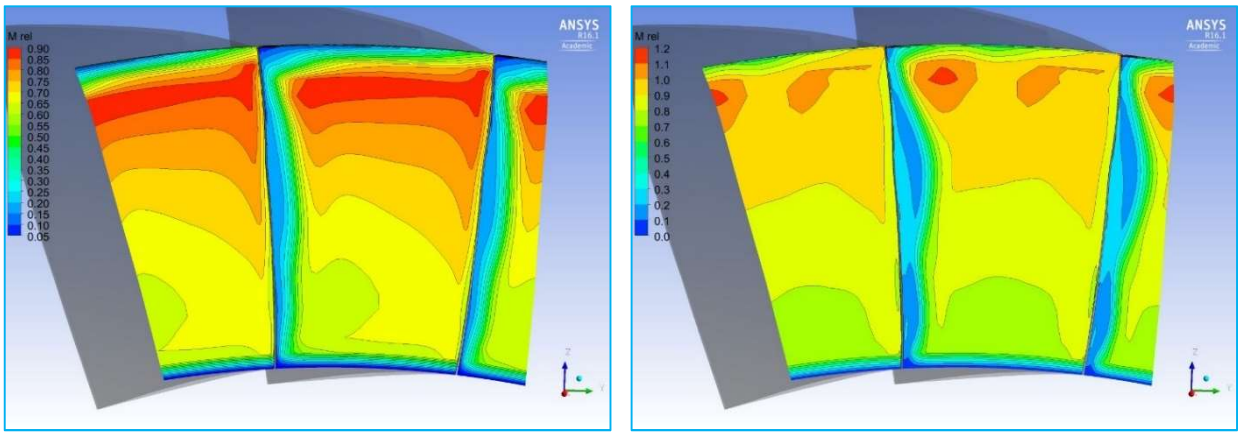

a) low mass flow rate b) high mass flow rate

Figure C5-8: ANSYS CFX results for the 100% speed-line @ TE

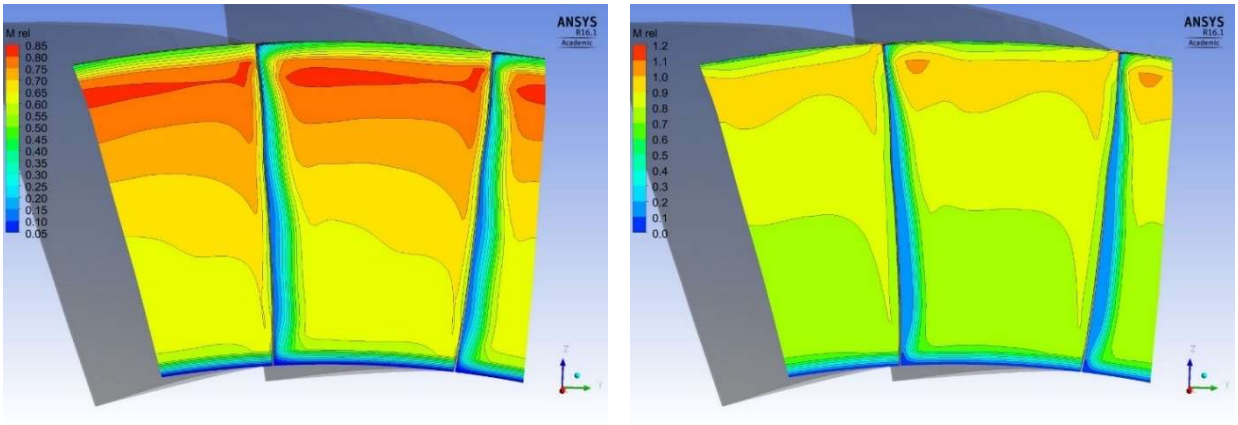

a) low mass flow rate b) high mass flow rate

Figure C5-9: ANSYS CFX results for the 90% speed-line @ TE

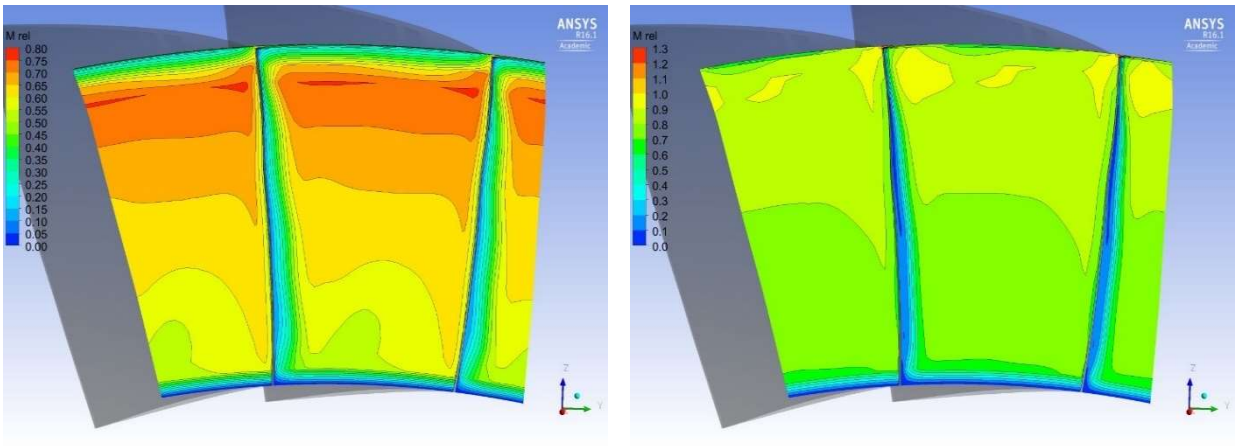

a) low mass flow rate b) high mass flow rate

Figure C5-10: ANSYS CFX results for the 80% speed-line @ TE

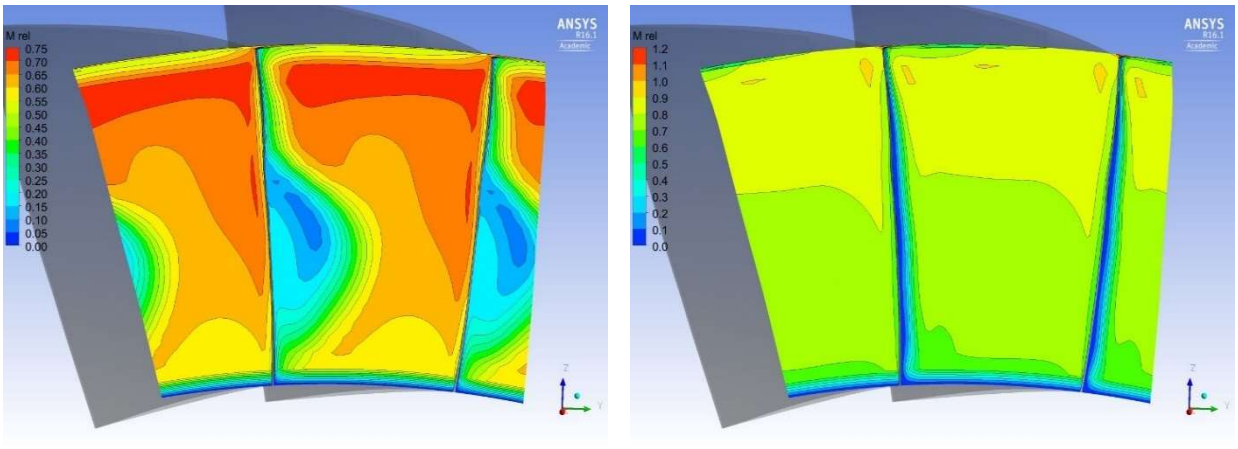

a) low mass flow rate b) high mass flow rate

Figure C5-11: ANSYS CFX results for the 70% speed-line @ TE

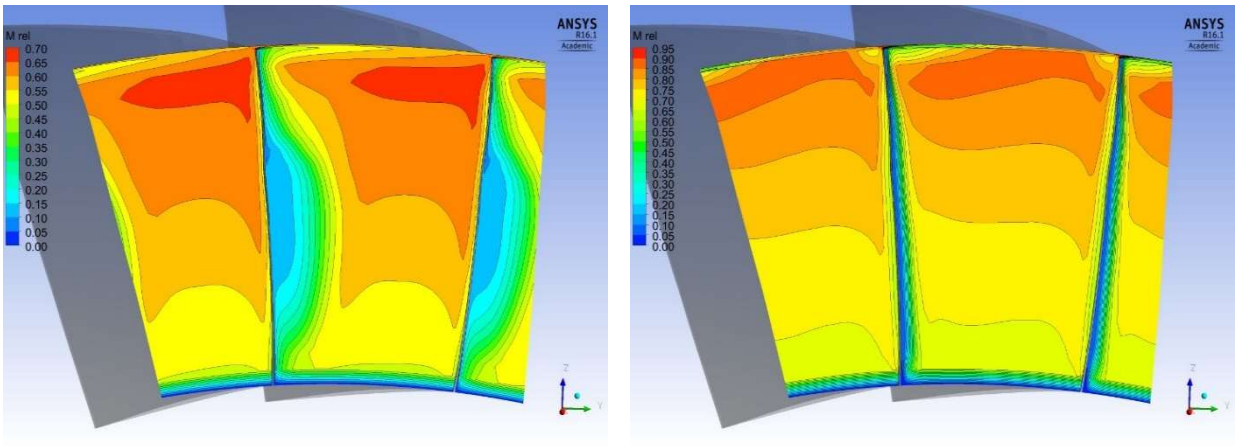

a) low mass flow rate b) high mass flow rate

Figure C5-12: ANSYS CFX results for the 60% speed-line @ TE

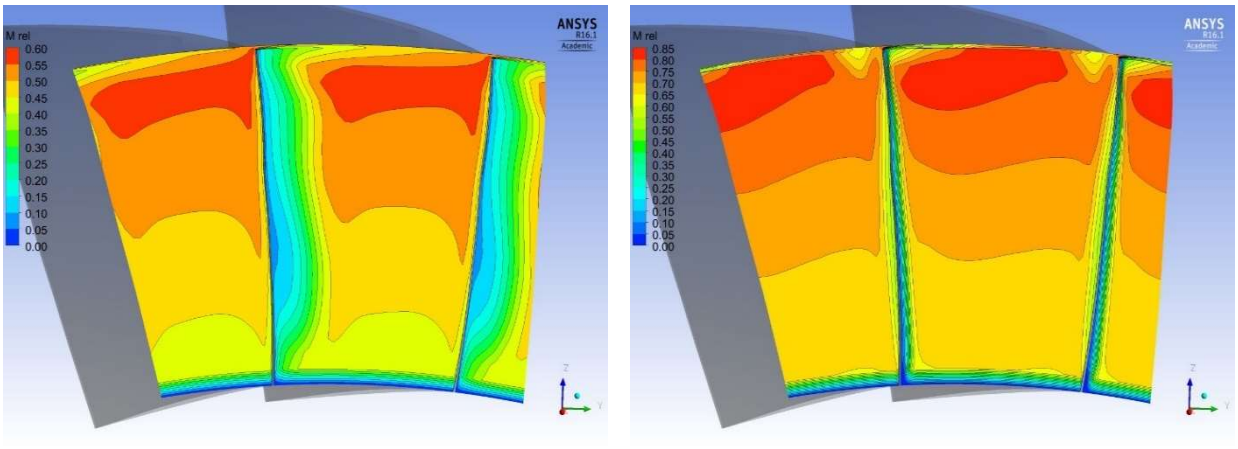

a) low mass flow rate b) high mass flow rate

Figure C5-13: ANSYS CFX results for the 50% speed-line @ TE

A follow-up question could then be raised with the current CFD results, *"why ANSYS CFX did not predict the rotor efficiency of Rotor 37?"* To properly answer this question, one needs to launch an extensive and expensive research program to understand, in this case, ANSYS CFX modeling capabilities, and the required protocols to produce an exact match of the measured test data. It is known that CFD results are dependent on the quality of the geometry being modelled. For example, does it include the blade row fillet radii, does it include bleed flow geometries, are there any

geometric discontinuities. Additionally, CFD results are dependent on the following known aspects:

- **Mesh Quality:** It is known that CFD results are dependent upon the quality of the mesh, and the solution may be grid dependent if proper mesh refinement is not applied. It is CFD best-practice to size the mesh to find a grid independent solution in terms of the various flow parameters, such as pressure loss for example. Nevertheless, grid independent solutions require a large number of nodes that dramatically increase the time to compute and converge a 3D CFD solution.
- **Turbulence Models:** CFD results also depend on the type of turbulence model used. Among them, we distinguish: Baldwin-Lomax, k-omega, k-epsilon, and Menter's Shear Stress Transport (SST). Each turbulence model introduces its own strengths and weaknesses. Furthermore, each turbulence model has tuning factors to aid in the solution matching. One must run all available turbulence models to witness the impact it has on the CFD results.
- **Imposed boundary condition:** Additionally, CFD results are dependent on the imposed inlet and exit boundary conditions. Inlet conditions may be either of the constant profile type, or the parabolic type which includes the effects of the inlet end wall boundary layer thickness. The exit boundary conditions may be based on an average static pressure, imposed at a specific radius, which is used as part of the radial equilibrium calculations to resolve the exit flow field, or it may be based on experimental test data which may include end wall boundary layer thickness.
- **Rotor-Stator interactions:** It is known that an isolated rotor analysis does not produce similar results when compared to a rotor-stator analysis. In a compressor stage, similar to a turbine stage, there is an upstream and downstream impact of the blade rows. For example, the rotor exit flow conditions will have an impact on the downstream stator inlet flow conditions. This is due to the rotor trailing edge wake, boundary layer mixing, deviation angles, and the clearance vortices. The stator itself will have an upstream impact to the rotor due to boundary layer interaction and blockage.
- **Time dependence:** Finally, CFD results differ between the time-invariant (steady-state) and the time-dependent (transient or unsteady case). In the former, the exit condition of one blade row is numerically averaged to a radial profile and used as the inlet condition of the next blade

row. Whereas the latter passes the wake information between blade rows. Furthermore, the computational resources increase as one attempts to model the complete 360-degree case; this is required to avoid the impact of scaling effects when one artificially changes the number of airfoils per blade row to be able to create integer multiples as to minimize the number of CPU to run the CFD case.

APPENDIX D – OFF-DESIGN TUNING FACTORS

Table D-1(5-3): Stage 35 imposed off-design mean-line analysis values

Cond	Rotor Cdin	Rotor δ	Rotor Loss	Rotor Cdex	Stator Cdin	Stator δ	Stator Loss	Stator Cdex
4004	0.9445	3.9659	0.0573	0.9070	0.9593	7.248	0.0535	0.9740
3978	0.9430	3.9626	0.0913	0.9348	0.9680	9.9855	0.0865	0.9750
3977	0.9445	3.6483	0.1410	0.9445	0.9660	9.9389	0.1360	0.9695
3974	0.9420	3.4941	0.1850	0.9382	0.9495	9.9330	0.1720	0.9640
3976	0.9435	3.6754	0.4270	0.9297	0.9275	9.6798	0.3550	0.9310
3975	0.9420	3.3932	0.2600	0.9380	0.9407	9.8836	0.2180	0.9560
3979	0.9410	3.8438	0.0430	0.9502	0.9690	7.4617	0.0435	0.9800
3982	0.9437	3.5099	0.0570	0.9525	0.9689	10.3211	0.0550	0.9800
3983	0.9400	3.3952	0.1050	0.9517	0.9600	9.9395	0.0930	0.9800
3984	0.9385	3.4021	0.1295	0.9517	0.9537	9.9389	0.1210	0.9780
3985	0.9390	3.7354	0.2640	0.9547	0.9357	9.8532	0.2430	0.9680
3987	0.9300	4.0776	0.1950	0.9600	0.9335	9.9102	0.1780	0.9720
3995	0.9395	3.5115	0.0490	0.9410	0.9520	5.6204	0.0458	0.9700
3994	0.9375	3.4129	0.0350	0.9410	0.9357	6.5933	0.0345	0.9750
3993	0.9365	3.4441	0.0430	0.9365	0.9321	7.4443	0.0430	0.9925
3990	0.9415	3.8068	0.0600	0.9289	0.9087	13.5179	0.0620	0.9865
3989	0.9330	5.1948	0.1940	0.9260	0.9019	9.9379	0.1760	0.9590
3997	0.9375	5.1241	0.1190	0.9409	0.8880	9.9430	0.1270	0.9780
4000	0.9395	4.8427	0.0800	0.9550	0.8810	10.2801	0.0780	0.9875

Table D-2(5-4): Stage 36 imposed off-design mean-line analysis values

Cond	Rotor Cdin	Rotor δ	Rotor Loss	Rotor Cdex	Stator Cdin	Stator δ	Stator Loss	Stator Cdex
4273	0.9320	5.9486	0.2590	0.9231	0.9413	7.2351	0.0940	0.9800
4272	0.9315	5.8023	0.3169	0.9423	0.9325	8.0887	0.0970	0.9730
4271	0.9300	5.6916	0.3451	0.9467	0.9250	8.0079	0.0970	0.9680
4270	0.9225	5.6468	0.3779	0.9519	0.9230	7.8965	0.1020	0.9630
4269	0.9300	5.4571	0.4000	0.9480	0.9200	7.8058	0.1050	0.9590
4281	0.9300	2.9829	0.1575	0.8930	0.9337	7.8236	0.0535	0.9650
4280	0.9265	3.1058	0.1835	0.9045	0.9325	7.8538	0.0570	0.9645
4279	0.9275	3.3137	0.2090	0.9110	0.9335	8.2819	0.0550	0.9645
4282	0.9270	3.4677	0.2460	0.9159	0.9277	8.1496	0.0545	0.9645
4284	0.9270	3.6835	0.2860	0.9197	0.9250	8.0712	0.0570	0.9645
4277	0.9260	3.7671	0.3075	0.9213	0.9250	8.0161	0.0630	0.9640
4294	0.9225	4.1742	0.2650	0.9305	0.8970	8.1612	0.0550	0.9670
4301	0.9275	3.2855	0.0760	0.9155	0.8993	5.9709	0.0670	0.9600
4299	0.9260	3.5489	0.0965	0.9211	0.9155	6.9651	0.0470	0.9600
4298	0.9250	3.8434	0.1387	0.9295	0.8675	7.3490	0.0400	0.9660
4297	0.9230	4.4526	0.2403	0.9425	0.8885	7.8305	0.0530	0.9730
4296	0.9210	4.9309	0.3225	0.9487	0.8721	8.1744	0.0650	0.9780
4304	0.9200	6.0436	0.3400	0.9500	0.8210	8.2783	0.0770	0.9800
4309	0.9230	6.6596	0.344	0.9677	0.8487	8.1674	0.0773	0.9950

Table D-3(5-5): Stage 37 imposed off-design mean-line analysis values

Cond	Rotor Cdin	Rotor δ	Rotor Loss	Rotor Cdex	Stator Cdin	Stator δ	Stator Loss	Stator Cdex
4193	0.9395	7.2434	0.2451	0.8810	0.9309	7.6820	0.0800	0.9580
4192	0.9410	6.9231	0.2750	0.8913	0.9329	8.5032	0.1065	0.9630
4182	0.9400	6.6602	0.3000	0.9000	0.9585	10.6990	0.1680	0.9500
4188	0.9395	5.9634	0.4000	0.9221	0.9321	12.1262	0.2475	0.9450
4187	0.9400	5.3272	0.5060	0.9150	0.9139	13.5220	0.3500	0.9370
4209	0.9395	7.3923	0.1660	0.9245	0.9373	7.5305	0.0813	0.9540
4208	0.9375	7.0832	0.1650	0.9405	0.9408	8.2650	0.0730	0.9530
4207	0.9380	5.7466	0.2230	0.9250	0.9430	9.8753	0.1200	0.9540
4205	0.9370	5.3039	0.3440	0.9200	0.9585	12.4091	0.1815	0.9890
4204	0.9350	5.4711	0.4450	0.9250	0.9075	12.4032	0.2500	0.9570
4194	0.9302	5.6705	0.3530	0.9300	0.9165	10.8654	0.1310	0.9670
4202	0.9390	6.3890	0.0700	0.9250	0.9313	7.2758	0.1170	0.9640
4203	0.9365	5.9713	0.0760	0.9250	0.9285	7.3774	0.0735	0.9660
4201	0.9370	5.4595	0.1140	0.9210	0.9185	7.4894	0.0460	0.9700
4198	0.9350	5.3042	0.1480	0.9170	0.9147	7.7117	0.0415	0.9710
4196	0.9320	5.4618	0.2210	0.9210	0.8970	8.1799	0.0553	0.9840
4195	0.9340	6.2178	0.3330	0.9300	0.8897	8.9903	0.0940	0.9820
4215	0.9375	7.1968	0.3350	0.9450	0.8580	8.6645	0.0890	0.9860
4218	0.9345	7.5030	0.3160	0.9600	0.8499	8.3799	0.0710	0.9880

Table D-4(5-6): Stage 38 imposed off-design mean-line analysis values

Cond	Rotor Cdin	Rotor δ	Rotor Loss	Rotor Cdex	Stator Cdin	Stator δ	Stator Loss	Stator Cdex
4129	0.9395	9.5446	0.2970	1.0035	0.9977	7.2164	0.0900	0.9830
4128	0.9395	9.3851	0.3090	1.0065	0.9940	7.3999	0.0820	0.9890
4123	0.9390	9.3694	0.3230	1.0149	0.9963	7.5040	0.0760	0.9880
4121	0.9390	9.1079	0.3510	1.0190	0.9913	7.7841	0.0730	0.9860
4120	0.9385	8.6860	0.3871	1.0210	0.9842	0.2057	0.0695	0.9760
4119	0.9390	8.3148	0.4169	1.0195	0.9647	8.9603	0.0720	0.9690
4140	0.9400	5.4715	0.1619	0.9475	0.9839	6.9960	0.0955	0.9775
4139	0.9390	5.4819	0.1765	0.9550	0.9755	7.0916	0.0730	0.9810
4133	0.9370	5.5106	0.1877	0.9645	0.9857	7.3329	0.0645	0.9750
4132	0.9355	5.5573	0.2179	0.9700	0.9797	7.5378	0.0510	0.9720
4131	0.9345	5.6432	0.2457	0.9730	0.9701	7.7102	0.0530	0.9790
4093	0.9355	5.9231	0.1877	0.9895	0.9765	7.4439	0.0520	0.9910
4097	0.9360	5.5702	0.0553	0.9750	0.9535	6.7338	0.1170	0.9815
4098	0.9345	5.6921	0.0810	0.9843	0.9543	6.8387	0.0737	0.9890
4099	0.9345	5.8578	0.1090	0.9915	0.9685	6.9364	0.0597	0.9895
4100	0.9315	6.0110	0.1390	0.9980	0.9565	7.0181	0.0510	0.9900
4101	0.9300	6.2663	0.1770	1.0030	0.9450	7.1493	0.0480	0.9950
4095	0.9310	6.8365	0.2600	1.0143	0.9420	7.4889	0.0542	1.0050
4104	0.9300	7.8046	0.2650	1.0143	0.9189	7.4291	0.0580	1.0000
4102	0.9345	8.6107	0.2410	1.0460	0.8823	7.2271	0.0610	1.0020

APPENDIX E – NASA STAGE MEAN-LINE MODEL PARAMETERS

Table E-1(5-7): NASA stage design-point definition

	Stage 35	Stage 36	Stage 37	Stage 38	Units
RPM	17188.7	17188.7	17188.7	17188.7	Rev/min
Tip Speed	454.456	455.233	454.136	455	m/sec
Tip Speed	**1490.9974**	**1493.5466**	**1489.9476**	**1492.7822**	ft/sec
Flow	20.188	20.188	20.188	20.188	Kg/sec
Flow	**44.5069**	**44.5069**	**44.5069**	**44.5069**	lbs/sec
TR-rotor	1.2250	1.2270	1.2700	1.2690	-
PR-rotor	1.865	1.863	2.106	2.105	-
PR-stg	1.82	1.82	2.05	2.05	-
ETA-rotor	0.865	0.858	0.877	0.878	-
ETA-stg	0.828	0.822	0.842	0.844	-
To-in	288.2	288.2	288.2	288.2	Kelvin
To-in	**518.7600**	**518.7600**	**518.7600**	**518.7600**	Rankine
Po-in	10.14	10.14	10.14	10.14	N/cm2
Po-in	**14.7068**	**14.7068**	**14.7068**	**14.7068**	PSI
Y-rotor	0.116	0.123	0.12	0.12	-
Y-stator	0.079	0.08	0.081	0.082	-

Table E-2(5-8): NASA stage rotor and stator mean-line geometry

Rotor	Stage 35	Stage 36	Stage 37	Stage 38	Units
AF Type	MCA	MCA	MCA	MCA	-
NOA	36	48	36	48	-
AR	1.19	1.63	1.19	1.63	-
Axial chord	3.4211	2.5300	3.505	2.5969	[cm]
Axial chord	**1.3469**	**0.9961**	**1.3799**	**1.0224**	**[in]***
Aero Chord	5.572	4.209	5.570	4.208	[cm]
True Chord	**2.1937**	**1.6570**	**2.1929**	**1.6566**	**[in]***
Pitch	3.7828	2.8400	3.7865	2.8410	[cm]
Pitch	**1.4893**	**1.1181**	**1.4907**	**1.1185**	**[in]***
Solidity	1.473	1.482	1.471	1.481	
Pitch / Chord	0.6788	0.6747	0.6798	0.6752	-
Pitch / Ax Chord	1.1057	1.1224	1.0802	1.0940	-
LE Thickness (TI)	0.037	0.029	0.037	0.029	[cm]
Max Thickness (TM)	0.304	0.239	0.303	0.239	[cm]
TE Thickness (TO)	0.038	0.030	0.038	0.030	[cm]
LE metal angle	56.16	56.54	56.53	56.51	Deg
TE metal angle	44.26	46.11	38.87	41.52	Deg
Total Camber	11.91	10.43	17.66	14.99	Deg
Setting Angle	52.3	53.22	51.16	52.04	Deg
Tip clearance	unknown	unknown	Partial info	unknown	[cm]

Stator	Stage 35	Stage 36	Stage 37	Stage 38	Units
AF Type	MCA	MCA	MCA	MCA	-
NOA	46	62	46	62	-
AR	1.26	1.78	1.26	1.77	-
Axial chord	3.812	2.819	3.739	2.759	[cm]
Axial chord	**1.5008**	**1.1098**	**1.4720**	**1.0862**	**[in]***
True Chord	**1.5937**	**1.1873**	**1.5949**	**1.6099**	**[in]***
Pitch	**1.1584**	**0.8596**	**1.1586**	**1.1586**	**[in]***
Pitch / Chord	0.7268	0.7240	0.7264	0.7197	-
Pitch / Ax Chord	0.7718	0.7745	0.7871	1.066	-
LE metal angle	35.72	37.28	42.12	43.93	Deg
TE metal angle	3.11	3.86	2.54	3.23	Deg
Total Camber	32.61	33.41	39.58	40.70	Deg
Setting Angle	19.66	20.81	22.64	23.89	Deg
Hub clearance	none	none	none	none	[cm]

APPENDIX F – OFF-DESIGN USER INTERFACE DEVELOPMENT

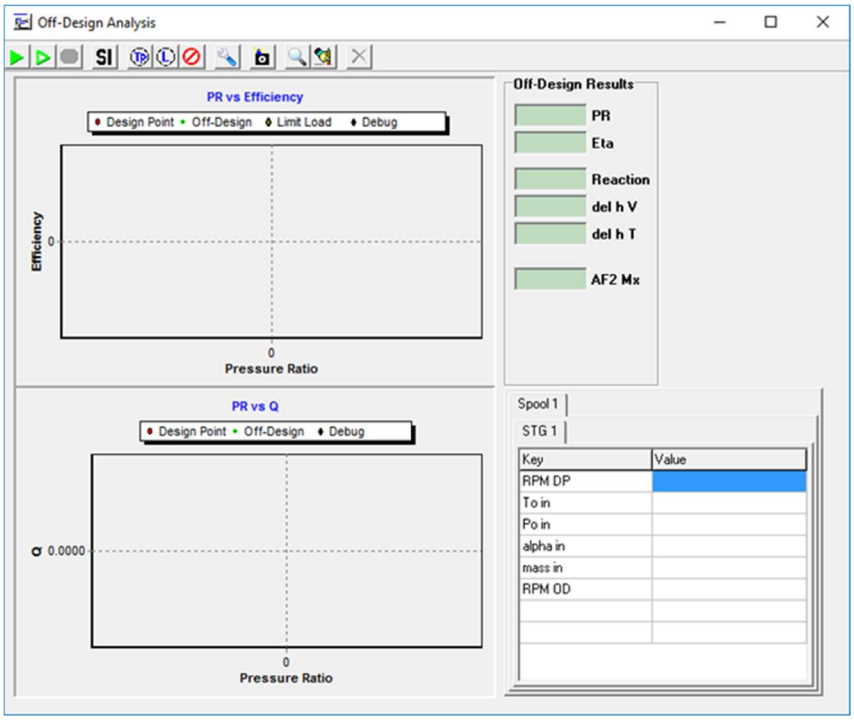

2014

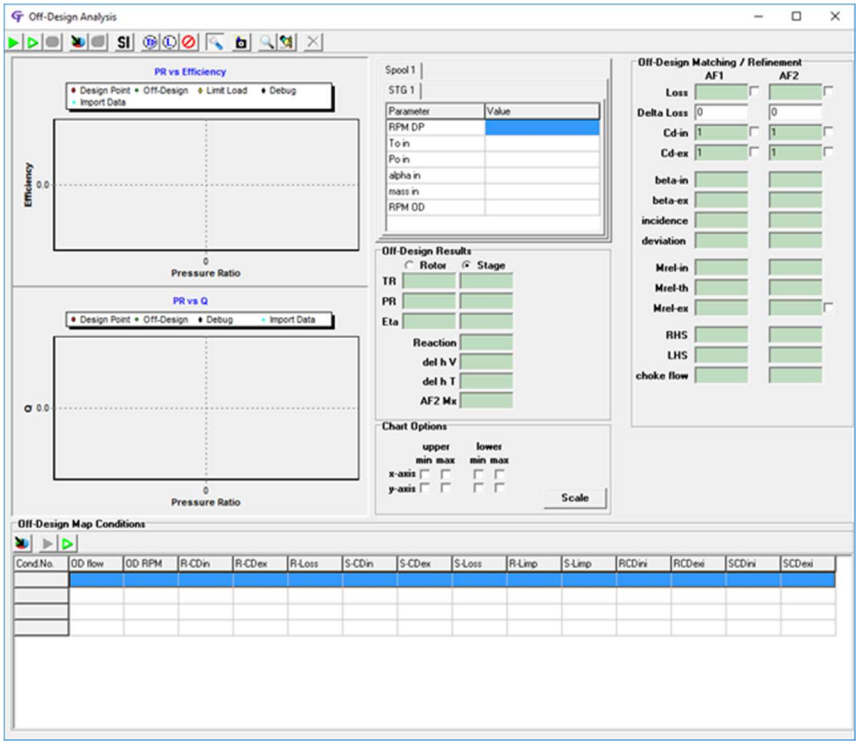

2016

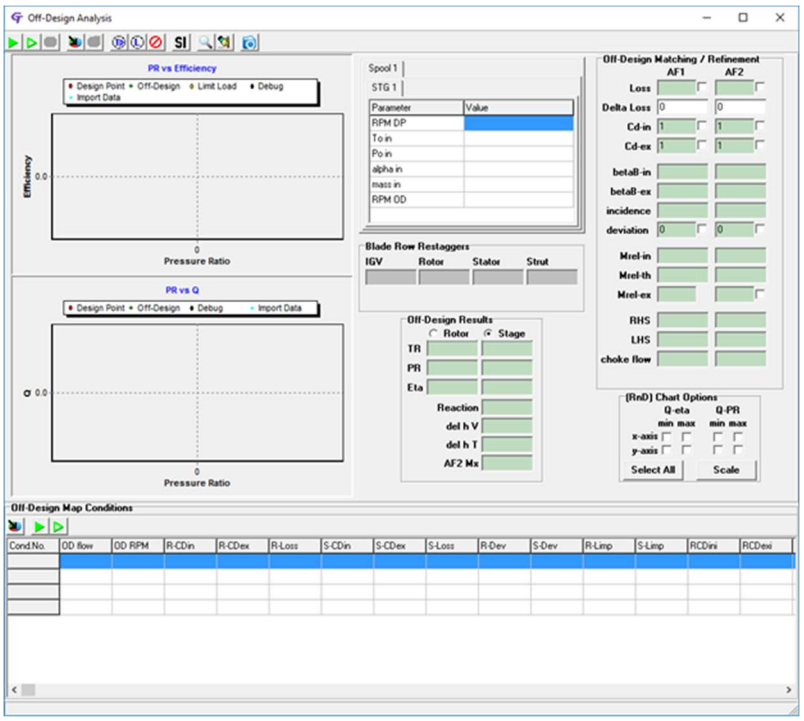

2017

Figure F5-14: Off-design user interface evolution

APPENDIX G – OFF-DESIGN MINIMUM AND MAXIMUM FLOW RATES

Table G-1(5-9): Stage 35 speed-line mass flow rates and surge prediction versus test results

RPM%	RPM	Mass Max	Mass Ave	Mass min	Prediction	Abs % diff	Abs diff
100.0	17188.70	46.55	43.41	40.26	39.63	1.56%	0.63
97.5	16758.98	45.91	42.65	39.39	42.47	7.82%	
95.0	16329.26	45.27	41.89	38.51	40.52	5.22%	
92.5	15899.50	44.37	41.00	37.64	39.00	3.61%	
90.0	15469.83	43.19	39.98	36.77	37.12	0.95%	0.35
87.5	15040.11	42.83	39.20	35.56	35.13	1.21%	
85.0	14610.39	41.58	37.96	34.34	33.96	1.11%	
82.5	14180.68	40.34	36.74	33.13	32.83	0.91%	
80.0	13750.96	39.16	35.54	31.92	31.74	0.56%	0.18
77.5	13321.24	38.08	34.28	30.48	32.43	6.40%	
75.0	12891.52	37.09	33.06	29.03	30.61	5.44%	
72.5	12461.81	36.14	31.87	27.59	28.70	4.02%	
70.0	12032.09	35.47	30.81	26.15	26.63	1.8%	0.48
67.5	11602.37	34.10	29.77	25.43	25.99	2.20%	
65.0	11172.66	32.94	28.82	24.70	25.28	2.35%	
62.5	10742.94	31.77	27.87	23.97	24.48	2.13%	
60.0	10313.22	30.99	27.12	23.24	23.89	2.8%	0.65
57.5	9883.50	27.67	25.02	22.37	22.48	0.50%	
55.0	9453.79	25.98	23.74	21.50	21.21	1.35%	
52.5	9024.06	24.52	22.58	20.63	19.72	4.41%	
50.0	8594.35	22.78	21.27	19.75	17.9	9.37%	1.85

Table G-2(5-10): Stage 36 speed-line mass flow rates and surge prediction versus test results

RPM%	RPM	Mass Max	Mass Ave	Mass min	Prediction	Abs % diff	Abs diff
100.0	17188.70	45.84	45.00	44.16	44.07	0.20%	0.09
97.5	16758.98			43.13			
95.0	16329.26			42.10			
92.5	15899.50			41.07			
90.0	15469.83	43.17	41.61	40.04	39.80	0.60%	0.24
87.5	15040.11	42.40	40.59	38.78	38.25	1.37%	
85.0	14610.39	41.48	39.50	37.51	36.91	1.60%	
82.5	14180.68	40.19	38.22	36.25	35.69	1.54%	
80.0	13750.96	38.33	36.66	34.99	34.59	1.14%	0.40
77.5	13321.24	37.95	35.74	33.54	32.92	1.85%	
75.0	12891.52	37.03	34.56	32.09	31.66	1.34%	
72.5	12461.81	36.22	33.43	30.64	30.34	0.98%	
70.0	12032.09	35.43	32.31	29.19	28.96	0.79%	0.23
67.5	11602.37	33.73	30.75	27.77	27.72	0.18%	
65.0	11172.66	32.05	29.20	26.35	26.45	0.38%	
62.5	10742.94	30.36	27.65	24.94	25.15	0.84%	
60.0	10313.22	28.67	26.10	23.52	23.80	1.19%	0.28
57.5	9883.50	27.40	24.94	22.48	22.86	1.69%	
55.0	9453.79	26.07	23.76	21.44	21.85	1.88%	
52.5	9024.06	24.71	22.56	20.41	20.77	1.76%	
50.0	8594.35	23.42	21.39	19.36	19.70	1.76%	0.34

Table G-3(5-11): Stage 37 speed-line mass flow rates and surge prediction versus test results

RPM%	RPM	Mass Max	Mass Ave	Mass min	Prediction	Abs % diff	Abs diff
100.0	17188.70	45.93	44.53	43.12	42.95	0.39%	0.17
97.5	16758.98	45.42	43.64	41.85	41.83	0.05%	
95.0	16329.26	44.75	42.67	40.58	40.90	0.79%	
92.5	15899.50	44.04	41.68	39.32	39.72	1.02%	
90.0	15469.83	43.37	40.71	38.05	37.63	1.10%	0.42
87.5	15040.11	42.55	39.78	37.00	36.99	0.03%	
85.0	14610.39	41.59	38.77	35.95	35.94	0.03%	
82.5	14180.68	40.49	37.69	34.89	34.84	0.14%	
80.0	13750.96	39.26	36.79	33.84	33.78	0.18%	0.06
77.5	13321.24	38.32	35.50	32.68	33.74	3.24%	
75.0	12891.52	37.44	34.48	31.52	32.57	3.33%	
72.5	12461.81	36.57	33.47	30.36	30.99	2.08%	
70.0	12032.09	35.78	32.49	29.19	29.39	0.69%	0.20
67.5	11602.37	32.92	30.44	27.95	28.28	1.18%	
65.0	11172.66	31.60	29.16	26.71	27.10	1.46%	
62.5	10742.94	30.31	27.89	25.47	25.85	1.50%	
60.0	10313.22	30.70	27.47	24.23	24.48	0.21%	0.25
57.5	9883.50	27.53	25.37	23.21	23.62	1.03%	
55.0	9453.79	26.09	24.14	22.18	22.66	2.16%	
52.5	9024.06	24.71	22.93	21.15	21.60	2.13%	
50.0	8594.35	23.37	21.08	20.13	20.43	1.50%	0.30

Table G-4(5-12): Stage 38 speed-line mass flow rates and surge prediction versus test results

RPM%	RPM	Mass Max	Mass Ave	Mass min	Prediction	Abs % diff	Abs diff
100	17188.70	46.23	45.64	45.04	44.95	0.20%	0.09
97.5	16758.98			44.25			
95.0	16329.26			43.46			
92.5	15899.50			42.66			
90	15469.83	43.54	42.71	41.87	41.58	0.69%	0.29
87.5	15040.11	42.50	41.58	40.66	40.26	0.98%	
85.0	14610.39	41.86	40.67	39.45	39.12	0.84%	
82.5	14180.68	40.90	39.57	38.24	38.12	0.31%	
80	13750.96	39.91	38.47	37.02	37.23	0.57%	0.21
77.5	13321.24	38.87	37.13	35.38	35.19	0.54%	
75.0	12891.52	37.80	35.77	33.74	33.15	1.75%	
72.5	12461.81	36.75	34.42	32.09	31.81	0.87%	
70	12032.09	36.00	33.23	30.45	30.37	0.26%	0.08
67.5	11602.37	32.22	30.75	29.27	28.96	1.06%	
65.0	11172.66	30.91	29.50	28.08	27.58	1.78%	
62.5	10742.94	29.38	28.14	26.89	26.22	2.50%	
61.8	10621.20	28.91	26.89	25.84	-	-	
60	10313.22	27.78	26.45	25.11	25.14	0.12%	0.03
57.5	9883.50	26.09	25.22	24.35	24.13	0.90%	
55.0	9453.79	24.38	23.69	23.00	23.02	0.09%	
52.5	9024.06	22.74	22.20	21.65	21.77	0.55%	
50	8594.35	21.18	20.74	20.30	20.16	0.07%	0.14